
# *SOLUTION PROCESSABLE CARBON NANOTUBE DEVICES: FROM OPTOELECTRONICS TO BIOSENSING*

Xinzhao Xu

Supervised by Dr Matteo Palma

School of Biological and Chemical Sciences

Queen Mary University of London

September 2020

# Statement of Originality

I, Xinzhao Xu, confirm that the research included within this thesis is my own work or that where it has been carried out in collaboration with, or supported by others, that this is duly acknowledged below and my contribution indicated. Previously published material is also acknowledged below.

I attest that I have exercised reasonable care to ensure that the work is original, and does not to the best of my knowledge break any UK law, infringe any third party's copyright or other Intellectual Property Right, or contain any confidential material.

I accept that the College has the right to use plagiarism detection software to check the electronic version of the thesis.

I confirm that this thesis has not been previously submitted for the award of a degree by this or any other university.

The copyright of this thesis rests with the author and no quotation from it or information derived from it may be published without the prior written consent of the author.

Signature: Xinzhao Xu

Date: 28-09-2020

# Publications

1. **X. Xu**, P. Clement, J. Eklöf, N. Loughnane, K. Moth-Poulsen, J. L. Chávez, M. Palma "Reconfigurable carbon nanotube multiplexed sensing devices" *Nano Lett.* **2018**,18, 4130.

2. P. Clement*, **X. Xu***, C. T. Stoppiello, G. A. Rance, A. Attanzio, J. N. O'Shea, R. H. Temperton, A. N. Khlobystov, K. R. J. Lovelock, J. M. Seymour, R. M. Fogarty, A. Baker, R. A. Bourne, B. Hall, T. W. Chamberlain, M. Palma "Direct synthesis of multiplexed metal nanowire based devices using carbon nanotubes as vector templates" *Angew. Chem. Int. Ed.* **2019**, 58, 9928. (***** Equal Authorship)

3. H. Zhang, H. Giddens, Y. Yue, **X. Xu**, V. Araullo-Peters, V. Koval, M. Palma, I. Abrahams, H. Yan, Y. Hao "Polar nano-clusters in nominally paraelectric ceramics demonstrating high microwave tunability for wireless communication" *J. Eur. Ceram. Soc.* **2020**, 40, 3996.

4. **X. Xu**, B. J. Bowen, R. Gwyther, M. Freeley, B. Grigorenko, A. V. Nemukhin, J. Eklöf-Österberg, K. Moth-Poulsen, D. D. Jones, M. Palma "Tuning electrostatic gating of semi-conducting carbon nanotubes by controlling protein orientation in biosensing devices", Submitted

5. **X. Xu**, Z. Mukadam, Q. Ye, M. Palma "Directed assembly of single chirality carbon nanotubes: from individual devices to photodetectors", In preparation

6. Q. Ye, **X. Xu**, M. Palma "Directed assembly of metal sulfide-carbon nanotube hybrids for multiplexed photodetection", In preparation

# Abstract

Single Walled Carbon nanotubes (SWCNTs) have attracted substantial attention due to their unique properties, such as one-dimensional architecture, excellent electrical properties, chemical stability for different modification and the easy integration into electronic circuits, which allows for the potential applications in field effect transistors, biosensors and optoelectronics. Despite these considerable achievements, it is still challenging to fabricate SWCNTs devices with low-cost processability and multipurpose capability. Herein, we propose facile, low cost, and solution processable strategies for the fabrication of SWCNT devices, which broaden the application of SWCNTs in different fields.

In this work, DNA-wrapped SWCNTs were functionalised with specific and distinct aptamer sequences which were used as selective receptors to bio-analytes. These distinct SWCNT-aptamer hybrids were immobilised onto pre-patterned electrodes via dielectrophoresis (DEP) on the same chip into device configurations, forming multiplexed sensing devices. Multiplexed detection of three different analytes was successfully performed and real time detection was achieved in serum.

Moreover, we reported the fabrication of protein-based biosensors, where the β-lactamase binding proteins (BLIP2) were engineered with phenylazide handles at defined sites, which allowed us to control the orientations of BLIP attached to SWCNTs. Therefore, we can control the local electrostatic surface presented within the Debye length when TEM β-lactamase was binding to BLIP2, thus modulating the conductance gating effect. The devices gave distinct responses depending on TEM presenting either negative or positive local charge patches. This indicates that local electrostatic properties act as the key driving force for electrostatic gating.

Due to their nanoscale one dimensional (1D) architecture, we used SWCNTs as vector templates to fabricate devices with multiplexed metal wires. Since metal precursors were encapsulated inside the SWCNT templates, we were able to precisely control their size, shape and orientation via DEP. Multiscale characterization of the different fabrication steps revealed details of the structure and charge transfer between the material encapsulated and the carbon nanotube. Electrical measurements further demonstrated the successful fabrication of metal nanowire devices.

Finally, we performed the separation of single chirality SWCNTs. By immobilised the separated (6,5), (7,5) and metallic tubes on the same chip, we demonstrated the fabrication of multiplexed single chirality SWCNT devices. Additionally, mixed chirality and single chirality SWCNTs were used to synthesize CdS-SWCNT hybrids for photodetection. The results showed that single chirality devices were more sensitive to green laser.

Overall, we immobilised SWCNTs to fabricate nanoscale devices via a solution processable method. This makes the fabrication of devices processing multipurpose capability and easy processing possible, which is of importance for broadening the application of SWCNTs. We also demonstrated the applications of SWCNTs in electronics and biosensors. I hope our work can inspire others to develop SWCNT devices from theoretical research to practical applications.

# Acknowledgements

First of all, I would like to thank my supervisor, Dr Matteo Palma for giving me the opportunity to work with him. His professional knowledge inspires me a lot and sparks my interest in nanoelectronics. In the past four years, when I encountered problems, he always patiently listened to my complaints, encouraged me and provided useful suggestions. His kindness and patience make working in the group an absolute pleasure. Secondly, I would like to thank my second supervisor, Professor William Gillin. I have benefited a lot from his sophisticated knowledge in physics and semiconductors.

I have to thank all of my colleagues and friends in Palma's research group. Dr Pierrick Clement has taught me a lot about nanofabrication. Dr Jingyuan Zhu has shared his knowledge in nanoelectronics and atomic force microscopy. Mark Freeley has shared his experience in chemical modification with me. I would also like to thank Giuseppe Amoroso and Zamaan Mukadam for preparing single chirality SWCNTs for me. I would like to thank Qingyu Ye for patiently explaining fundamentals in physics to me. I would also like to thank Dr Da Huang, Dr. Antonio Attanzio, Dr William Hawkes, Dr Alessandro Cecconello and Sandra Perez Garrido for their kind help.

I would also like to thank our collaborators. Dr Jorge Chavez-Benavides and Dr Nancy Kelley-Loughnane provided information about aptamers and biomarkers, which was very helpful for our research. Also, thanks to Dr Kasper Moth-Poulsen and Dr Johnas Victor Roland Eklöf from Chalmers University of Technology for their contribution in nanofabrication. I would like to thank Prof Dafydd Jones from Cardiff University and his group member, Ben Bowen, for their contribution in protein engineering as well as useful information on protein interactions.

I would like to thank Dr Ken Scott and Geoff Gannaway for their help in electrical measurement and nanofabrication. I would also like to thank Maurizio Leo for helping

me to perform annealing treatment.

I would like to thank my friends, Pengfei Liu, Le Fang, Wei Song, Xiaoshuai Zhang, Zhaoyang Xu for making my time in QMUL all the better. It is always enjoyable to have a hotpot together, especially in a traditional festival.

I would like to thank my parents and my sisters for supporting me in chasing my dreams.

Finally, I would like to thank my girlfriend, Nai, for her patience and support.

# Table of Contents

# List of Figures

# List of Acronyms and Abbreviations

| | |
|---|---|
| 1D | One-dimensional |
| AFM | Atomic force microscopy |
| AzF | *p*-Azido-L-phenylalanine |
| BCN | Bicyclo[6.1.0]non-4-yn-9-ylmethyl |
| BLIP2 | β-lactamases inhibitor protein-II |
| bp | Base pair |
| CNT | Carbon nanotube |
| $Cu(acac)_2$ | Copper precursor |
| $Cu(acac)_2$@SWCNT | Copper precursor filled single walled carbon nanotube |
| DBCO | Dibenzocyclooctyne |
| DEP | Dielectrophoresis |
| DHEAS | Dehydroepiandrosterone sulfate |
| DMSO | Dimethylsulphoxide |
| DMF | Dimethylformamide |
| DNA | Deoxyribonucleic acid |
| DPBS | Dulbecco's phosphate-buffered saline |
| dsDNA | Double stranded DNA |
| EDX | Energy-dispersive X-ray spectroscopy |
| FET | Field effect transistor |
| HPLC | High performance liquid chromatography |
| HRTEM | high-resolution transition electron microscopy |
| $M(acac)_2$ | Metal precursor |
| $M(acac)_2$@SWCNT | Metal precursor filled single walled carbon nanotube |

| | |
|---|---|
| MWCNT | Multi-walled carbon nanotube |
| NHS | N-hydroxysuccinimide |
| NPY | Neuropeptide Y |
| PEG | Polyethylene glycol |
| $Pt(acac)_2$ | Platinum precursor |
| $Pt(acac)_2$@SWCNT | Platinum precursor filled single walled carbon nanotube |
| QD | Quantum dot |
| RT | Room temperature |
| SDS | Sodium dodecyl sulfate |
| SDC | Sodium deoxy- cholate |
| SEC | Size exclusion chromatography |
| SEM | Scanning electron microscopy |
| SPM | Scanning probe microscopy |
| SPAAC | Strain promoted azide–alkyne cycloaddition |
| ssDNA | Single stranded DNA |
| STM | Scanning tunneling microscopy |
| SWCNT | Single walled carbon nanotube |
| TEM | Transmission electron microscopy |
| TEM-1 | TEM beta-lactamase |
| UV-vis | Ultraviolet-visible spectroscopy |
| WT | Wild type |

# Chapter 1 Introduction

Nanomaterials, in general, refer to materials of which the size of a single unit is in the range of 1-100 nm in at least one dimension.[1,2] The ultra-small dimensional size imparts unique properties to nanomaterials: due to quantum mechanical effects and quantum confinement effects, nanomaterials exhibit superior optical and electronic properties compared to bulk materials;[1,3] moreover, the large specific surface area of nanomaterials enables immobilisation of more functional units on their surface, resulting in high sensitivity to changes in the surrounding environment.[4]

Nanomaterials have found important applications in the semiconductor industry. To achieve devices with superior performance, increased density and energy efficiency, integrated circuit technologies have been developing and the node size of electronic devices have shrunk dramatically.[5,6] However, the conventional techniques for the fabrication of silicon-based electronics have nearly reached their miniaturization limitation.[7–9] In this regard, nanomaterials, such as graphene, nanowires and nanotubes, have emerged as promising candidates to replace silicon in nanoelectronics due to their nanoscale architecture and outstanding electronic properties.[10–16] Integrating nanomaterials into electronic circuits paves the way for the fabrication of functional electronics.

Nanomaterials have also attracted tremendous interest in the field of biological sensing. The high surface to volume ratio offers nanomaterials high sensitivity to the surrounding environment, and since the size scale of nanomaterials is comparable to that of biomolecules, biomolecules can be seamlessly interfaced with

nanomaterials.[4,12,17–19] Furthermore, biomolecules are natural nanomachines and many biological processes occur at the nanoscale. Monitoring these processes at the scale at which they occur allows scientists to better understand the nature of processes and fundamental biology.[20–22] Therefore, the integration of biomolecules with nanomaterials opens up new opportunities and frontiers for the next generation biosensors.

Various techniques have been presented to precisely manipulate the assembly of nanomaterials for functional devices; these can be mainly divided into two categories: top-down and bottom-up approaches.[23,24] In top-down approaches, bulk materials are broken down and the components are externally controlled to direct their morphology. Lithography (e-beam and photo) is a typical example of top-down approach for the fabrication of nanoscale devices. In contrast, bottom-up approaches take advantage of the chemical properties of molecules to cause single molecules to (self-)assemble into functional configurations. A common example of bottom-up methods is chemical vapor deposition (CVD). However, practical application of lithography and CVD are still limited since these strategies are time-consuming, expensive and require skilled operators.[24]

In particular, solution processable assembly of nanomaterials is an attractive bottom-up method for the fabrication of nanoscale devices in which nanomaterials are directly assembled from solution into defined configurations. This strategy have many advantages over general lithography and CVD, such as its ease of processability, low cost of fabrication and biocompatibility.[25] This thesis will focus on the assembly of a class of one-dimensional (1D) carbon nanomaterials, namely single walled carbon nanotubes (SWCNTs), into functional electronic devices via solution processable strategies. SWCNTs are 1D hollow cylinders of rolled up graphene sheets,[26] and have

been recognised as next generation building blocks for ultra-sensitive biosensing systems.[27,28] Compared with other nanostructured materials, such as graphene, silicon nanowires, SWCNTs not only exhibit excellent mechanical, electronic and optical properties and high specific surface area,[29] but also have comparable size to that of biomolecules which makes SWCNTs suitable for biosensing.[27] Additionally, SWCNTs are ideal templates for the encapsulation of nanomaterials as well as for the investigation of new material phases caused by 1D confinement since they are 1D hollow and chemically stable.[30]

Although tremendous achievements have been obtained in SWCNT devices fabricated via a combination of photolithography (or e-beam lithography) and CVD strategies,[31–34] challenges still remain in terms of fabrication and power costs, as well as complexity of processability.[35,36] In this regard, we immobilised SWCNTs from solution into device configurations via a solution-processable strategy, namely dielectrophoresis, which shows potential application for fabrication of SWCNTs devices with low cost processability and multipurpose analysis capability. Furthermore, we controlled the interfacing of SWCNTs with either biomolecules, like DNA and proteins, or metal precursors. These SWCNT hybrids were then assembled between prepatterned electrodes, into field effect transistor configuration. We demonstrated the potential applications of these nanoscale devices in various fields, such as biosensing and photodetection.

Chapter 1 Introduction

## 1.1 Carbon Nanotubes

### 1.1.1 Properties of Carbon Nanotubes

Carbon atoms can form many allotropes due to their specific atomic valency, including fullerene, nanotube, graphene, graphite and diamond[37] (Figure 1.1). Carbon nanotubes (CNTs) are one dimensional allotropes of carbon, which can have an aspect ratio as large as 132,000,000.[38] They can be regarded as hollow cylinders of rolled-up graphene sheets with dimeters in range of 1-100 nm. Depending on the layers of graphene sheets, CNTs can be divided into two types: single walled CNTs (SWCNTs) containing a single graphene layer and multi-walled CNTs (MWCNTs) consisting of multi-layers of graphene sheets.[39] The diameters of SWCNTs are in the range of 1-2 nm, while MWCNTs have diameters up to 100 nm with an interlayer spacing. This thesis will focus on the investigation and application of SWCNTs due to their 1D architecture and excellent electronic properties.

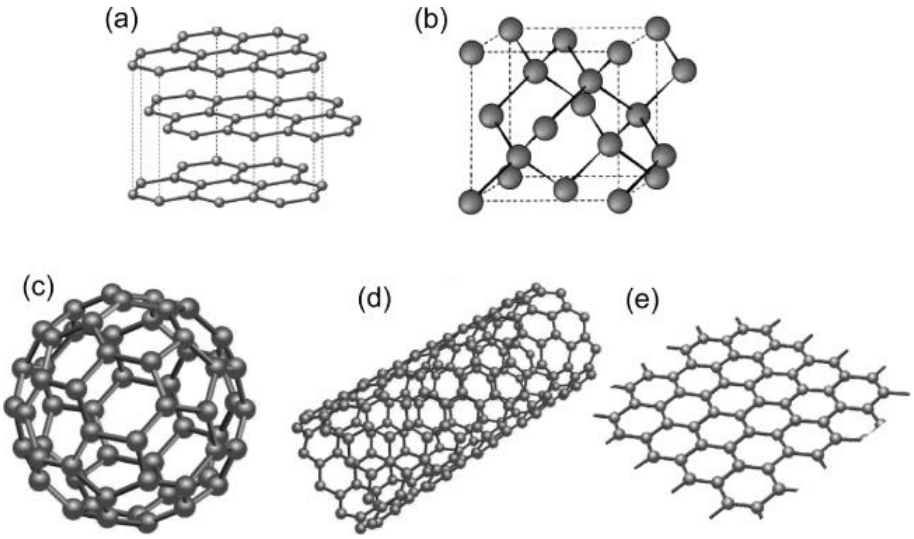


**Figure 1.1** Allotropes of Carbon (a) 3D Graphite (b) 3D Dimond (c) 0D buckminsterfullerene (d) 1D nanotube (e) 2D graphene.[37]

Depending on the angles at which graphene sheets are rolled up, SWCNTs can present

distinct structures and properties. Therefore, a chirality vector, $\overrightarrow{C_h}$, is introduced to define the atomic structure of SWCNTs, which is given by:

$$\overrightarrow{C_h} = n \times \overrightarrow{a_1} + m \times \overrightarrow{a_2} \quad (1)$$

The integers (n,m) describe the chirality of SWCNTs, which correspond to the number of steps along the unit vectors ($\overrightarrow{a_1}$ and $\overrightarrow{a_2}$) of the hexagonal lattice (Figure 1.2). Particularly, if $n = m$, the tubes are called "armchair". If $m = 0$, the tubes are called "zigzag". We can estimate the diameter $d$ of a SWCNTs, which is given by:

$$d = \frac{|\overrightarrow{C_h}|}{\pi} = \frac{a}{\pi}\sqrt{n^2 + nm + m^2} \quad (2)$$

where $a$ is the lattice constant of the hexagonal structure: $a \approx 2.46\ \dot{A}$.[37]

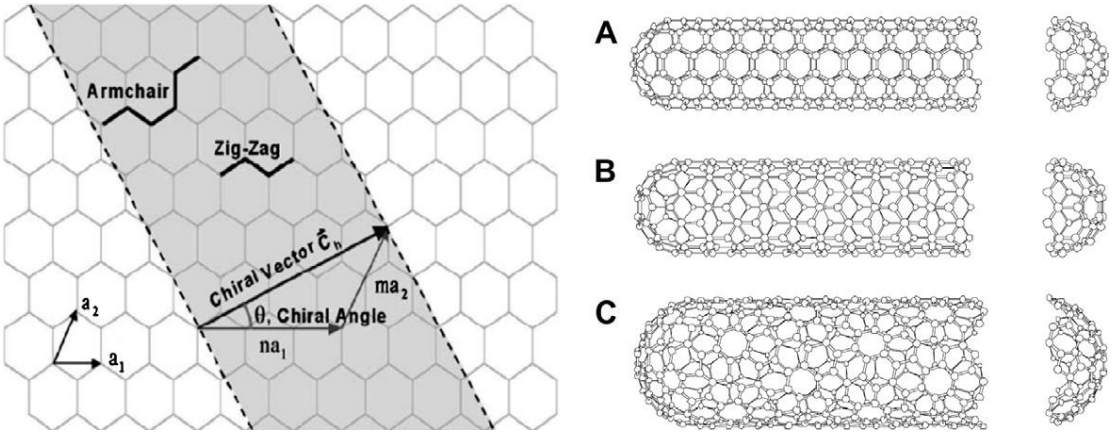


**Figure 1.2** Schematic diagram showing how a hexagonal sheet of graphene is rolled to form a CNT with different chiralities (A: armchair; B: zigzag; C: chiral).[40]

SWCNTs possess excellent electronic properties and they can be either semiconducting or metallic, depending on their chiralities. Generally, $(n, n)$ armchair SWCNTs are always metallic due to their intrinsic symmetry. The band structure and electronic densities of states of CNTs can be studied and calculated resulting from the honeycomb graphene structure. Figure 1.3a shows the band structure and the corresponding density of states of graphene. Since a CNT is a rolled-up graphene sheet, a periodic boundary is imposed onto the system, given by:[41]

$$\overrightarrow{C_h} \times \vec{k} = 2\pi q$$

where $\overrightarrow{C_h}$ is the chirality vector and $q$ is a nonzero integer. Consequently, wave vector $\vec{k}$ is quantized and only certain set of graphene states are allowed. This leads to the formation of a series of subbands, which is represented by the yellow lines in Figure 1.3b and 1.3c. Therefore, the electronic properties of the CNTs are defined by the position of the allowed states: for (n,m) tubes, if $n - m = 3q$, the electronic states passing through a Fermi level point are allowed and hence the nanotubes are metallic; on the other hand, if $n - m = 3q \pm 1$, there is a gap of forbidden states at the Fermi level and hence the nanotube is semiconducting. Similarly, Figure 1.3d shows the corresponding density of states for the conduction and valence bands of graphene and metallic CNTs.

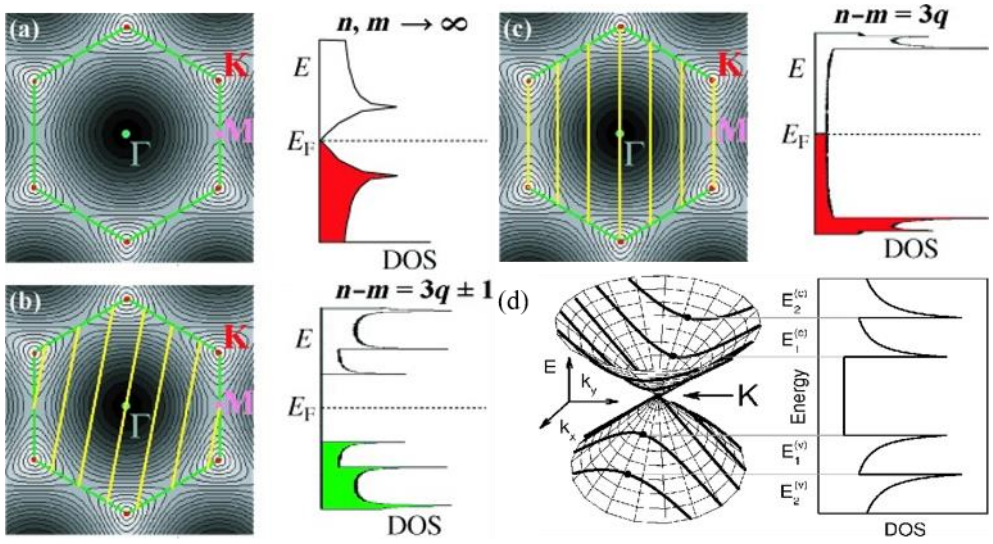


**Figure 1.3** (a-c) Band structures (left) and electronic densities of states (right) of: (a) graphene; (b) semiconducting single-wall carbon nanotubes; (c) metallic single-wall carbon nanotubes. (d) The density of 5 states (DOS) for the conduction and valence bands (graphene (left) and metallic CNT (right)).[41,42]

### 1.1.2 Synthesis of Carbon Nanotubes

Various methods have been reported for the massive production of CNTs. The first reported method is based on arc-discharge technique, in which carbon atoms are

evaporated though applying a high voltage between two graphite electrodes.[43,44] Metal catalysts, e.g. Fe or Co, are required in the process for the production of SWCNTs, otherwise fullerenes and MWCNTs will be synthesized.[44] This method yields around 30% by weight and produces both SWCNTs and MWCNTs with few structural defects. However, it is difficult to control the size and orientation of CNTs in this method.[45]

Laser ablation is another well-studied method.[46,47] In a laser ablation process, a laser beam vaporizes a graphite-metal target which is placed in a tube-furnace at 1200 $^{o}$C while an insert gas is bled into the chamber, resulting in the formation of CNTs on the cooler surfaces of the furnace. The yield of this method is up to 70% and produces primarily SWCNTs with a controllable diameter. However, due to the expensive lasers, this method is more costly than other methods.[45]

Chemical vapour deposition (CVD) is a popular strategy for the bulk production of CNTs. In a CVD process, a substrate embedded with metal catalyst nanoparticles is heated to 600-700 $^{o}$C, while a gaseous carbon source is bled into the chamber to initiate the growth of CNTs. CNTs are grown directly on the substrate since the growth of CNTs are determined by the sites of the metal catalysts.[48,49] This methods can produce large quantities of nanotubes with controlled diameter and orientation.[50–53] The growth of ultralong SWCNTs over 18 cm has been reported by Wang *et al.* in which they used ethanol or methane as the feed gas, Fe-Mo as the catalyst, and a CNT film as the catalyst supporting frame.[38] CNTs grown via CVD method can also be transferred onto transparent and flexible plastic substrates. The formed devices not only showed excellent electrical properties, but also possessed optical transparency and mechanical bendability.[54,55]

Particularly, high-pressure carbon monoxide disproportionation (HiPCO) is a more advanced CVD strategy since it allows for continuous growth of CNTs. In a HiPCO

process, carbon monoxide (CO) is used as the gaseous carbon source while iron serves as the catalyst in the condition of high pressure (30-50 bar) and high temperature (900-1100 $^{o}$C). The formation of $Fe(CO)_5$ starts when Fe is added to CO gas flow. Subsequently, large Fe clusters are formed due to the thermal decomposition of $Fe(CO)_5$ caused by the high temperature, which catalyse the disproportionation of CO and thus induce the nucleation and growth of SWCNTs.[56] HiPCO strategy can produce high purity SWCNTs (no more than 7% iron impurities) in high quantity (up to 450 mg/h), which makes CNTs more commercially available. However, the major issue of CVD method is that different types of CNTs (different chirality) are simultaneously grown on the same substrate, which requires further purification.[57,58]

Considerable efforts have been dedicated to control the growth of CNT through optimising the composition or shape of the catalyst particles used in the CVD process, which have significant influence on CNT nucleation and growth.[59–63] Zhang *et al* demonstrated CVD growth of high quality semiconducting CNTs with a narrow band gap distribution.[64] Partially carbon-coated cobalt nanoparticles with a uniform size and structure were used as the catalyst for CNT growth, in which the inner cobalt nanoparticle acted as active catalytic phase for carbon nanotube growth, while the outer carbon layer prevented the aggregation of cobalt nanoparticles and ensures a perpendicular growth mode. The grown CNTs have a very narrow diameter distribution, as well as a small band gap difference of 0.08V. Yang *et al* demonstrated the direct growth of single chirality CNTs, (12,6), where tungsten-based bimetallic alloy nanocrystals were used as the catalyst.[65] The selective growth of (12,6) tubes was attributed to the high melting points and unique atomic arrangements of tungsten-based bimetallic alloy nanoparticles.[65] Another example is the application of molecular precursors for controlled growth of single chirality (6,6) tubes.[66] The molecular

precursors can be easily converted into (6,6) tube seeds via cyclodehydrogenation, which would facilitate the growth of (6,6) tubes via epitaxial elongation.[66]

Although the purity and quantity of synthesised CNTs have been dramatically improved owing to the efforts made by researchers,[60-62] chemical impurity and structural defects still exist in the CNTs synthesised via the aforementioned methods. General chemical impurities include residues of primary materials used for the CNT production, such as graphite from arc discharge or catalyst particles from CVD, as well as by products like amorphous carbon or fullerenes.[58,67–69] Vacancies and interstitials are the main structural defects in CNTs, which have significant effects on the helicity and the electronic structure of CNTs.[70–73] Therefore, purification is essential in the production process, hence obtaining CNTs with better mechanical and electronic properties. Acid treatment using HCl, $HNO_3$ and/or $H_2SO_4$ is the most used method to dissolve chemical residues, i.e. metal catalysts, and carbon materials, i.e. amorphous carbon and graphite.[68,74,75]

Furthermore, various approaches have been developed to obtain CNTs with uniform lengths, diameters as well as uniform chiralities. Duesberg *et al.* demonstrated the efficient purification of both MWCNTs and SWCNTs via size exclusion chromatography (SEC).[76,77] They not only successfully removed chemical impurities, like metal particles and amorphous carbon, but also obtained length sorted CNTs. Gel chromatography is an effective method for single chirality separation of SWCNTs.[57,78] Liu *et al.* reported the separation of 13 different (n,m) species via gel chromatography.[57] SWCNTs can also be purified and separated into single chirality species via density gradient ultracentrifugation.[58,79]

### 1.1.3 Dispersion of Carbon Nanotubes

Due to the strong van der Waals attraction which is attributed to their 1D nanostructure and high surface area, CNTs tend to assemble and entangle into bundles or ropes.[47,80] Therefore, it is hard to dissolve or disperse pristine CNTs in aqueous solution, which limits their practical applications. In the literature, various dispersion approaches have been reported to separate CNT bundles into homogeneous dispersions, including covalent functionalisation, non-covalent adsorption of surfactants and DNA.

Ultrasonication is extensively applied to disperse and exfoliate nanoparticles into aqueous dispersion. CNTs can be effectively separated into small bundles or even individual CNTs by ultrasonication.[81,82] However, ultrasonication causes defects in CNT structures,[83] and with increased energy, CNTs are fragmented into shorter length. Moreover, due to the strong van der Waals attraction, the separated CNTs can easily agglomerate into big bundles again when ultrasonication is removed, resulting in unstable dispersion of CNTs. Therefore, ultrasonication is generally combined with other dispersion methods to improve the stability of CNT dispersion.

Covalent functionalisation is an efficient strategy for stable CNT dispersions, since introduction of polar groups onto the carbon scaffold of CNTs can decease the attraction between CNTs, hence separating them into small bundles or even individual ones. Polar groups can also help CNTs to be dispersed into polar media like water. Hydrophilic oxygen-containing groups, e.g. carboxylic and hydroxyl groups, were introduced on the surface of MWCNTs via UV/ozone treatment. Results from UV-vis spectroscopy confirmed that the dispersion of functionalised MWCNTs was more stable than that of pristine MWCNTs in polar solvents.[84] Inorganic acids, including $HNO_3$, $H_2SO_4$, HCl, were also widely used to functionalise CNTs with carboxylic and hydroxyl groups. [85–87] The acid treated SWCNTs can be individually dispersed in acetone and water since

the repulsion induced by the charged polar groups overcome the van der Waals attraction hence keeping CNTs individually dispersed.[86] Functionalisation of CNTs with other chemicals, such as iodine-doping[88], sodium metal–ammonia[89], can also improve the stability of the dispersion.

However, the introduction of functional groups, especially when heavy chemical functionalisation is performed, might induce structural defects, which can be detrimental to the electronic properties of CNTs.[90] Non-covalent strategies take advantage of physical adsorption of various of molecules onto the sidewall, hence retaining the electronic structure of CNTs. Generally, the molecules consist of two parts: one is hydrophobic and the other is hydrophilic. The hydrophobic parts are absorbed onto the surface of CNTs via van der Waals forces, π-π staking or CH-π bonding while the hydrophilic parts provide aqueous solubility and electrostatic repulsion.[89,91]

One of the most used non-covalent strategies is to disperse CNTs with surfactants combined with ultrasonication. Ultrasonication provides local shear, especially to the ends of CNT bundles, causing spaces and gaps. This induces further adsorption of surfactants, eventually separating the bundles into individual CNTs.[92] In the literature, the most used surfactants for SWCNT dispersion in aqueous solution are sodium dodecyl sulphate[93] and sodium deoxycholate.[94]

Particularly, Deoxyribonucleic acid (DNA) has been demonstrated to be effective materials for the dispersion and separation of CNTs.[95] Zheng *et al.* found that by sonicating SWCNTs with single strand DNA, SWCNTs can be individually dispersed in aqueous solution. Molecular modelling revealed that DNA helically wrapped around SWCNTs through π-π stacking between the aromatic bases in DNA and the sidewall of SWCNTs (Figure 1.4). Subsequently, they demonstrated the purification of more than 20 single-chirality semiconducting species via ion exchange chromatography using

these DNA wrapped SWCNTs.[96] They also demonstrated that specific sequences of homochiral DNA can be used to differentiate the handedness and helicity of SWCNTs via polymer aqueous two phase separation.[97] This is the first comprehensive method for simultaneous handedness and helicity enrichment for three electronic types of SWCNTs.

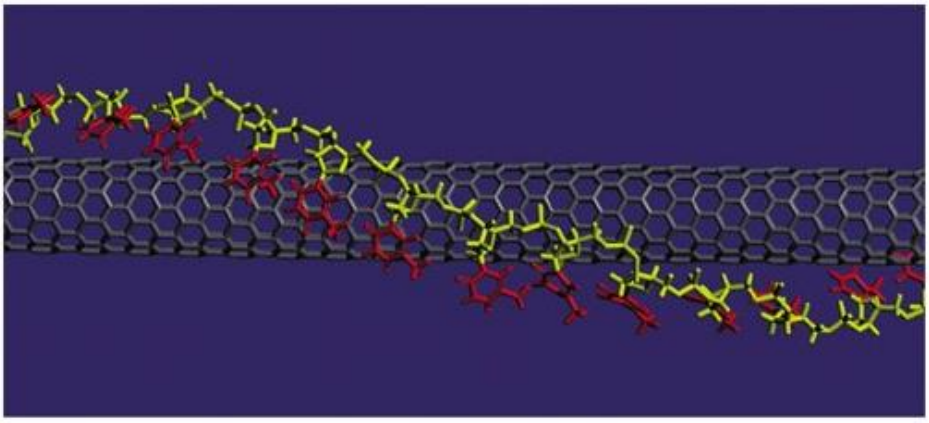

**Figure 1.4** Binding model of a (10,0) SWCNT wrapped with DNA.[95]

## 1.2 Dielectrophoresis

A variety of applications of SWCNTs have been proposed due to their unique properties. For example, due to their 1D hollow structure, SWCNTs can be used as templates for synthesis of 1D nanoscale materials.[98,99] Since SWCNTs are able to penetrate into cells, it is possible to use them for drug delivery.[100] Among these, field effect transistors based on SWCNTs have been recognised to be a promising platform for the next generation of nanoscale electronics due to their outstanding electronic properties. This leads to considerable applications of SWCNTs in the field of photodetection[101,102] and biosensrnsing.[103,104] However, the issues of device fabrication inhibits the commercialization of CNT devices. The most common methods for the assembly of CNTs into device configuration are the strategy combining chemical modification of the substrate with spin-coating and direct growth via CVD.[29] But these techniques are

not suitable for large-scale device fabrication and cannot precisely control the location and orientation of CNTs.[105]

Dielectrophoresis (DEP) appears to be an ideal strategy for device fabrication. CNTs can be precisely positioned between prepatterned metal electrodes via DEP. Therefore, these CNTs are directly integrated into electrical circuits at defined location with controlled orientation. Moreover, CNTs can be assembled at different locations to fabricate many devices simultaneously and reproducibly on a single chip. By controlling the DEP parameters, it is possible to control the assembly of CNTs from dense arrays to individual CNT devices.

### 1.2.1 What is Dielectrophoresis?

Under the influence of an electrical field, charged particles dispersed in a fluid undergo an electrical force, of which the phenomenon is called electrophoresis. In contrast, dielectrophoresis (DEP) describes a phenomenon in which dielectric particles undergo a force when an inhomogeneous electric field is applied. All particles which are charged or not exhibit dielectrophoretic activity to some extent in the presence of an electric field. The electric field polarizes the particles, inducing dipoles in the particles. The dipoles experience either attractive or repulsive force depending on the orientation of the dipoles. Due to the non-uniform nature of the electric field, one end of the dipole will experience a greater force, hence resulting in the alignment and motion of the particles. The relative polarizability of the particles and the fluid medium are the main factors determining the polarization and the orientation of the DEP force, i.e. the direction of the force depends on field gradient rather than field direction. In a non-uniform electric field, particles moving in the direction of increasing field experience positive DEP, while particles moving towards the direction of decreasing field experience negative DEP.[106,107]

### 1.2.2 Dielectrophoresis Force

Theoretical models have been built to investigate the DEP force exerted on particles or long rods suspended in a fluid medium.[108] For homogeneous particles of radius $r$ suspended in a fluid medium, the DEP force ($F_{DEP}$) they experience is given by[108]:

$$F_{DEP} = 2\pi r^3 \varepsilon_m Re\left(\frac{\varepsilon_p^* - \varepsilon_m^*}{\varepsilon_p^* + 2\varepsilon_m^*}\right)\nabla E^2 \quad (3)$$

$$\varepsilon^* = \varepsilon - \frac{i\sigma}{\omega} \quad (4)$$

In the equations, $\varepsilon_p^*$ and $\varepsilon_m^*$ refer to the complex dielectric constants of the particles and the medium. $\varepsilon$ and $\sigma$ are the corresponding dielectric constant and the electrical conductivity. $E$ and $\omega$ are the strength and the frequency of the electric field. $i$ is the imaginary unit.

For more general field-aligned long rods, e.g. nanowires, carbon nanotubes, of radius $r$ and length $l$, the DEP force is given by[108]:

$$F_{DEP} = \frac{1}{8}\pi r^2 l \varepsilon_m Re\left(\frac{\varepsilon_p^* - \varepsilon_m^*}{\varepsilon_m^* + (\varepsilon_p^* - \varepsilon_m^*)L}\right)\nabla E^2 \quad (5)$$

$$\varepsilon^* = \varepsilon - \frac{i\sigma}{\omega} \quad (6)$$

$L$ is the depolarization factor of the rods. Therefore, the strength of the DEP force is strongly dependent on the electrical properties and the size of particles, and the electrical properties of the media, and the strength and the frequency of the electrical field. According to Equation (5) and (6), the direction of DEP force acting on particles or rods is dependent on the frequency of the electric field. In practical experiments, it has also been observed that DEP force acting on some particles or tubes may experience a crossover from positive DEP to negative DEP in electric field at a specific frequency. [109] This specific frequency is termed as crossover frequency ($\omega_c$). If the frequency

applied is higher than the crossover frequency, the particles will experience positive DEP force. If the frequency applied is lower than the crossover frequency, the particles will experience negative DEP force (Figure 1.5).

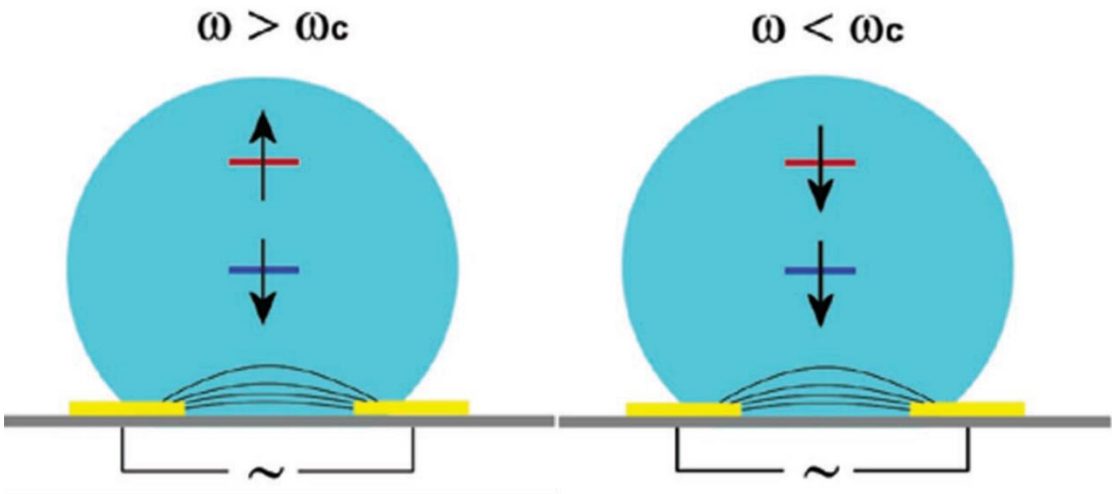


**Figure 1.5** Schematic cross section of the experimental setup during DEP. The lines illustrate the electric field during deposition when a drop of suspended SWCNTs is applied to the surface (cyan). Metallic SWCNTs (blue) and semiconducting SWCNTs (red) interact with the ac field with positive dielectrophoresis (↑) or negative dielectrophoresis (↓) depending on the frequency ω.[109]

DEP has been applied in the manipulation, transportation, deposition and separation of different types of particles. Pommer *et al.* reported the direct separation of platelets from diluted whole blood in microfluidic channels with cell-sorters taking advantage of DEP.[109] By combined DEP with impedance spectroscopy, Constantinou *et al.* demonstrated simultaneous and direct selection and deposition of semiconducting silicon nanowires. This strategy led to the controlled deposition of high quality, defectless nanowires between prepatterned electrodes.[110] In another experiment, gold nanowires have been directly assembled and the electrical transport property of the nanowires has been studied.[111]

### 1.2.3 Dielectrophoresis of Carbon nanotubes

Since the Nakayama group first reported the immobilisation of CNTs from solution via DEP,[112] it has been widely applied in the deposition of CNTs due to its striking advantages, such as ease of processing at room temperature, selection of electrical properties, precisely positioning between predefined electrodes, highly preferential orientation, controllable density of CNTs and multiplexed deposition of various types of CNTs on the same chip. The scheme of the set-up for DEP is shown in Figure 1.6. CNTs dispersed in fluid were drop-cast onto pre-patterned metal electrodes with a gap of hundreds nanometers. Alternating current voltage was applied between source and drain electrodes, inducing an inhomogeneous electric field between the gap of the electrodes. After a duration of a few minutes, CNTs were aligned and deposited between the electrodes. In general, four DEP parameters influence the immobilisation of CNTs between electrodes: namely, amplitude and frequency of the electric field, duration of DEP, concentration of CNT solution.[113-116] The amplitude of the electric field, the duration of DEP and concentration of CNT solution determine the number of CNTs immobilised between electrodes: increases in these parameters would result in increases in the number of CNTs immobilised. On the other hand, the frequency of the electric field detemines the types of CNTs immobilised between electrodes, for instance, both semiconducting and metalic CNTs can be immobilised between electrodes when the frequency is on the order of the magnitude of 100KHz, while only metallic tube can be immobilised when the frequency is higher than 5MHz.[105,113]

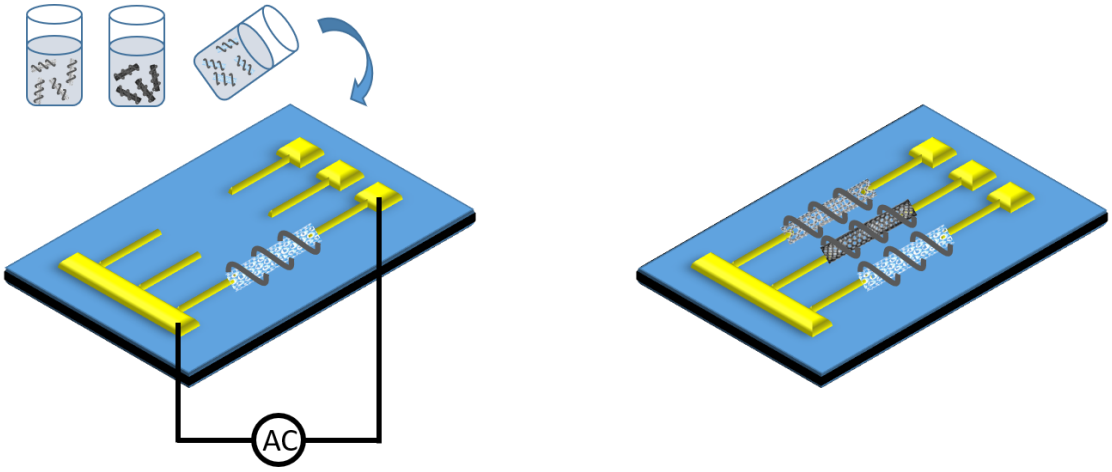


**Figure 1.6** Scheme of the set-up for the deposition of CNTs via DEP

Calculation based on Equation (5) was performed to understand how a non-uniform electric field influence the motion and deposition of CNTs. Due to the mobile carriers, the dielectric constant of metallic nanotubes should be very large. It has been reported that the polarizability of metallic CNTs is effectively infinite.[114,115] Therefore, positive DEP force is exerted on metallic CNTs in water at any frequency. Theoretically, semiconducting CNTs should undergo negative DEP in water at any frequency since the dielectric constant of semiconducting CNTs ranges from 2 to 5 while that of water ranges from 75 to 85.[115,116] This led to the separation of metallic CNTs from mixed CNTs from solution by Krupke *et al.*.[114,117] Furthermore, single bundles of metallic CNTs were simultaneously and site-selectively deposited on pre-patterned electrodes, which allowed for the investigation of the electrical properties of metallic CNTs.[117] However, they observed a crossover from positive to negative DEP for semiconducting CNTs.[109] They assembled CNTs via DEP at various electric field frequency and solvent conductivities, finding that the deposition of metallic CNTs was independent on the frequency and the solvent conductivity, while a crossover frequency for semiconducting CNTs did exist. At low frequency ($\omega < \omega_c$), both metallic and

semiconducting CNTs can be deposited, while only metallic CNTs can be deposited at high frequency ($\omega > \omega_c$) (Figure 1.4). This crossover has been attributed to the surface effect that the dielectric properties of semiconducting CNTs are modified by the electrical double layer at the solid-liquid interface.[109]

A further attempt was to scale up the separation of metallic CNTs at high frequency (10MHz) through applying a large electric field. This led to the formation of a thick CNTs film, composed of highly aligned metallic CNTs and randomly oriented semiconducting CNTs.[118] Simulations revealed that metallic CNTs were aligned and attracted towards the substrate along the electric field lines both horizontally and vertically (Figure 1.7a and b). However, the DEP forces exerted on semiconducting CNTs were repulsive in the horizontal direction (Figure 1.7c) but attractive in the vertical direction (Figure 1.7d). This was attributed to that at large fields, the transverse polarizability of semiconducting CNTs played important roles in the DEP processing, resulting in them being attracted towards electrodes vertically. Eventually, these semiconducting CNTs would collapse onto the substrate in random orientations.

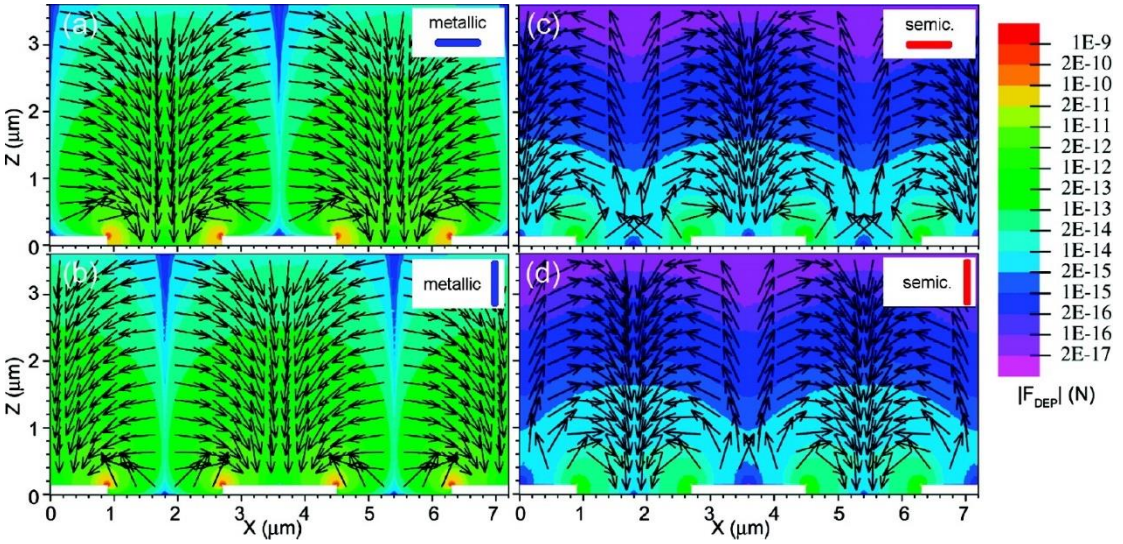


**Figure 1.7** Simulation of the dielectrophoretic force fields exerted on (a and b) metallic CNTs and (c and d) semiconducting CNTs at horizontal and vertical orientations.[118]

The Nojeh group studied the influence of solution conductivity on the deposition of CNTs via DEP, in which the conductivity of the solution was controlled with surfactants.[119] In their experiment, solution with higher concentration of surfactants had higher conductivity. The experimental results showed that without surfactants (hence low conductivity), CNTs were deposited well between electrodes. The presence of surfactant increased the conductivity of the solution as well as the Joule heating effect.[120–122] The resulting electrothermal force adversely interfered with the DEP force, influencing the motion and deposition of CNTs. Therefore, fewer CNTs were deposited between electrodes when the concentration of surfactants was higher (Figure1.8).

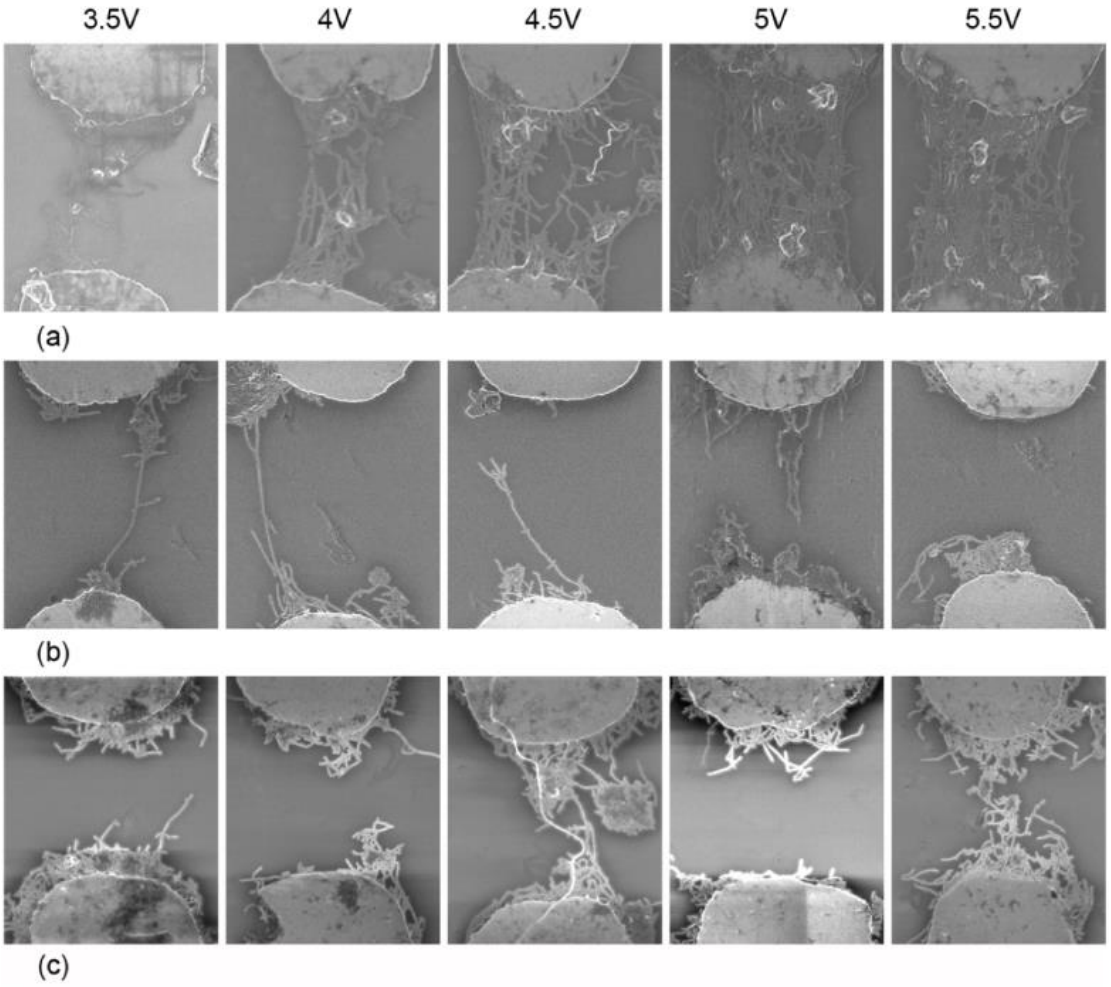


**Figure 1.8** Scanning electron micrographs of the devices made from solutions with (a) 0, (b) 0.5 and (c) 1 wt% surfactant, at voltages ranging from 3.5 to 5.5 V.[119]

When the contacts between metal electrodes and CNTs are made, Schottky barriers arise due to the mismatch between the Fermi level of the metal and the valence (conduction) band of CNTs.[123] Schottky barriers for either holes or electrons significantly influence the transport characterisation of the CNT devices: a high Schottky barrier not only leads to high contact resistance but also results in low on/off ratio. Hence, for transistor applications, a low Schottky barrier is preferable. However, Schottky barrier effects are one of the most relevant mechanisms underlying biosensing.[34,124] Therefore, in this thesis, gold electrodes are chosen since gold electrodes are chemically stable and the Schottky barrier between gold and CNTs is suitable for biosensing.[124]

One of the practical applications of DEP is to fabricate CNTs devices since CNTs can be precisely aligned and placed from solution onto predefined electrodes via DEP.[35,125,126] By optimising the parameters of DEP, such as strength and frequency of the electric field, duration of DEP, concentration of CNT solution, Stokes and Khondaker were able to control the assembly of CNTs from dense arrays to individual devices.[113] The electrical properties of both individual metallic and semiconducting CNT devices were investigated. Field effect transistors fabricated from semiconducting CNTs showed typical p-type transfer characteristics and perfect electrical performance. Vijayaraghavan *et al.* presented a strategy for ultra large scale deposition of individual CNT devices.[105] In this strategy, AC voltage was applied between the common electrode and the underlying silicon gate electrode, while floating electrodes were capacitively coupled to the gate electrode, resulting in inhomogeneous electric field between the common electrode and the floating electrodes. Since hundreds of floating electrodes can be biased by capacitive coupling simultaneously, this strategy allowed for the fabrication of numbers of CNT devices with identical conditions.

DEP can also be performed to immobilise DNA-wrapped CNTs, which was reported by the Lee group.[127] Both SDS dispersed CNTs and DNA wrapped CNTs were immobilised between electrodes and the electrical properties were studied. They found that the presence of water can activate a transition of DNA-CNT devices from metallic to semiconducting, while SDS-CNT devices were not sensitive to the presence of water.

## 1.3 Carbon Nanotubes Biosensors

Since the discovery of CNTs, they have quickly been applied in different areas due to their excellent properties. Researchers found that CNTs are sensitive to the changes in the environment surrounding CNTs, which causes measurable electrical or optical signals in CNTs. The high specific surface area of CNTs allows for ultrafast detections of biological species at very low concentrations. Additionally, the diameters of CNTs are comparable to the size of single molecules. Therefore, CNT-based biosensors are recognized to be a next generation building block for ultra-sensitive biosensing systems. This leads to considerable investigations of using CNTs as sensing elements for biosensors.

In general, biosensors consist of at least two units: receptors which can selectively interact with biological targets and transducers which can convert the biological recognition events into measurable physical signals, e.g. currents, absorbance, for testing and detecting. Due to the semiconducting nature of CNTs, they are be directly used as transducing elements in biosensing systems.

### 1.3.1 Functionalisation of Carbon nanotubes

In order to use CNTs for biosensing, surface modification and functionalization are performed to attach biological receptors to CNTs. In the literature, various methods

have been reported, which can generally be divided into two categories: covalent modification and noncovalent modification.

For covalent modification, functional groups, such as carboxylic, hydroxyl, are created onto the terminals or the defect sites of CNTs by high concentration acid treatment or plasma treatment.[128,129] Subsequently, moieties with different functionalities can be introduced onto CNTs via covalent reactions (e.g. amidation, esterification, alkylation reaction and cycloaddition) to meet specific requirements of different applications.[130] For example, Williams *et al.* demonstrated covalent coupling of SWCNTs to peptide nucleic acid (PNA).[131] They performed acid treatment to create carboxylic groups on SWCNTs. Subsequently, these SWCNTs were activated in buffer solutions containing standard amide coupling and activating agents. This allowed PNA terminated with amine groups to be attached onto the SWCNTs.

Another typical example is reported by our group. Acid treated SWCNTs were wrapped with ssDNA, hence soluble in aqueous solution. The ssDNA also protected the sidewall of SWCNTs, leaving only carboxylic groups at the ends available for chemical reactions. Molecules containing two or more amine groups were used as linkers for the formation of end to end SWCNT junctions via amidation reaction.[132,133] Taking advantage of this strategy, Jingyuan *et al.* used metallic SWCNTs as nanoelectrodes to fabricate molecular transport junctions.[132] This strategy also have been employed for the covalent formation of SWCNT-protein hybrids[134], SWCNT-DNA hybrids[135] and SWCNT-QDs hybrids.[136]

Although covalent attachment of biomolecules is more stable, to a certain extent, it impairs the electronic structure of CNTs, hence impairing the performance of CNT biosensors. Instead, non-covalent modification can preserve the electronic structure and properties of CNTs since moieties with functionalities are introduced via π-π non-

covalent bonding. Molecules containing π electrons can easily bind onto the sidewall of CNTs thanks to the delocalised π electron via $sp^2$ hybridisation.[137,138] Among these conjugated molecules, ssDNA[139–141] and Pyrene derivatives [142–144] are the most used linkers for the noncovalent functionalisation of SWCNT devices.

### 1.3.2 Carbon Nanotube Optical Biosensors

Semiconducting SWCNTs exhibit fluorescent behaviour in near infrared (NIR, 800-1600) due to their electronic band-gap between valence and conduction band[145] and their optical emission is sensitive to molecular adsorption in close proximity.[146] This offers potential applications of using SWCNTs as transduction units to detect analyte adsorption via fluorescent emission.[147] Additionally, optical properties of SWCNTs are dependent on their electronic structures, i.e. SWCNTs of different (n, m) species exhibit distinct optical emission.[148] Therefore, mixed (n, m) species can be used for multiplexed optical detection as every (n, m) specie can be treated as an individual sensor.[149] Another beneficial property of SWCNTs is that their fluorescence is extremely photostable, showing no blinking or photobleaching after long time exposure to excitation,[150,151] which makes SWCNTs ideal materials for long term sensing applications. Since living tissue and biological media are transparent in the NIR emission region of SWCNTs[17,150] and physical connection is not needed for optical sensors, optical sensors based on SWCNTs are more suitable for in-vivo applications.[152]

The Strano group first demonstrated the fabrication of SWCNT based optical sensors, which was used to detect DNA hybridisation through the modulation of SWCNT fluorescence with a detection limit of 6 nM.[153] Single stranded DNA (probe DNA) was assembled on the surface of SWCNTs and subsequently exposed to its complementary

DNA, which induced an energy shift of 2meV. Modelling suggested that the shift resulted from the increased coverage of DNA from 25% to 50% on the SWCNT surface due to DNA hybridisation. This was further confirmed by Forster resonance energy transfer assay.

They also exposed these SWCNTs decorated with probe DNA to single nucleotide polymorphism DNA (SNP, complementary DNA with one base mismatched).[154] They monitored the fluorescence energy every 3 minutes for 8 hours and also found an energy increase of 0.8meV. In contrast, under same conditions, adding the complementary DNA (cDNA) to the samples can induce an energy increase of 1.2meV. This suggested that SWCNT based optical sensors were sensitive enough to detect and differentiate hybridisation of probe DNA to SNP DNA or full complement through energy shift. Studies of the hybridisation kinetics of these samples showed that the hybridisation kinetics of free DNA in solution were faster than that of DNA adsorbed to SWCNTs, while the kinetics for SNP DNA were lower than that of complementary DNA.[155] (Figure 1.9)

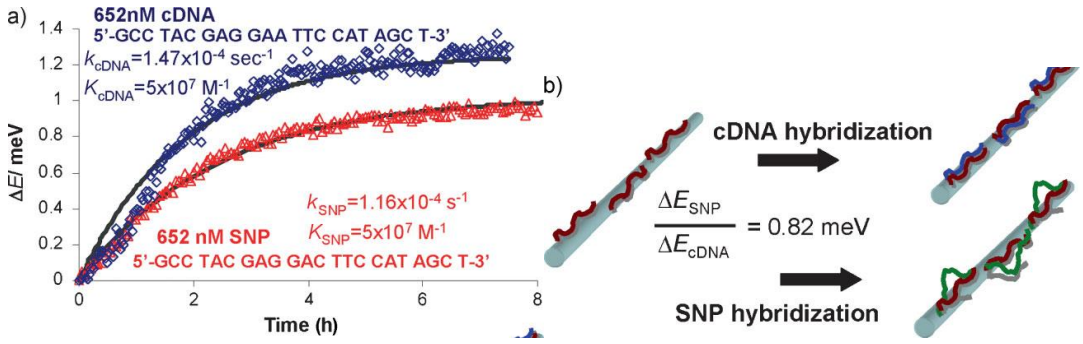


**Figure 1.9** The presence of SNP in the complement results in incomplete hybridization on the nanotube surface and a smaller surface coverage. (a) Energy shifts of the transient detection for cDNA and SNP were fitted with a two-step model of adsorption followed by hybridization of the cDNA or SNP. While the equilibrium constants are the same, the partial hybridization of SNP comes to steady state slower than cDNA

hybridization. b) Diagram showing the different nanotube coverage that can result from cDNA and cDNA containing a SNP.[154]

Optical biosensors based on DNA wrapped SWCNTs can be used to detect miRNA hybridisation transiently and in vivo (Figure 1.10).[139] The ssDNA used to wrap SWCNTs consists of two domains: one to wrap around SWCNTs and a second one complementary to target miRNA. Photoluminescence spectroscopy (PL) measurement showed that the addition of target oligonucleotide induced blue shift in both the emission peak and the excitation peak ($E_{22}$) of SWCNTs. Experiments and simulations revealed that the mechanism resulted from competitive effects of displacement of oligonucleotide charged groups and water. These sensors also allowed for multiplexed detection by using different nanotube chiralities. Moreover, the authors demonstrated in vivo optical detection of target DNA and miRNA by implanting the sensors into live mice.

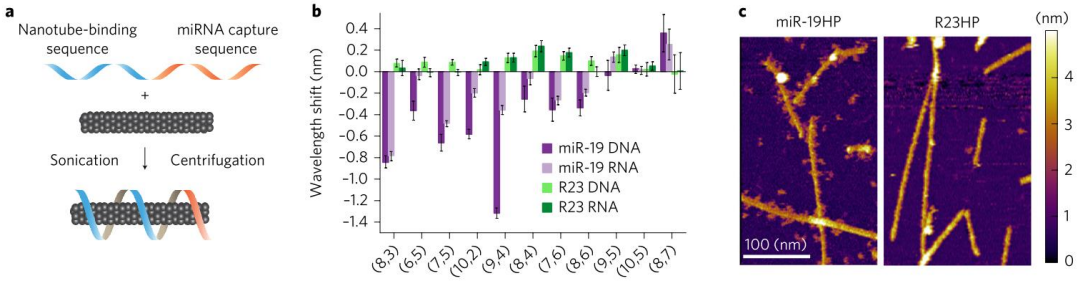


**Figure 1.10** Carbon nanotube sensor for the detection of miRNA hybridization events. (a) Construction scheme of the miRNA sensor complex, consisting of a single DNA oligonucleotide containing a nanotube-binding sequence (blue) and a miRNA capture sequence (orange) that is non-covalently bound to the carbon nanotube surface. (b) Response of the sensor to analyte DNA or RNA or a control sequence for each nanotube chirality (n,m). (c) AFM images of the sensor complex on incubation with non-complementary or complementary hairpin DNA.[139]

These SWCNT devices based on near-infrared photoluminescence (NIR PL) also have been extended for protein detection.[140,141] Williams *et al.* demonstrated the detection of

protein-protein interaction by using fluorescent SWCNT sensors.[141] The SWCNTs were wrapped with ssDNA terminated with amine groups which was conjugated to antibodies. Thus, these SWCNT-protein hybrids can selectively bind to the target antigens. NIR PL emission measurement showed that the binding of the antigens induced a red shifting in fluorescence emission and SWCNTs of different (n, m) species gave different red shifting: (9,4) chirality up to 1.6 nm, (8,6) up to 4.2 nm and (8,7) up to 3.1 nm. This red shifting was attributed to the increase in local electrostatic charge density on SWCNTs caused by the binding of the antigens.

Since SWCNTs possess specific spectral features and high Raman scattering cross sections, they are ideal materials for Raman labels for protein detection. Compared with conventional fluorescence methods, Raman detection provides ultra-sensitive detection with high signal-to-noise ratios thanks to the sharp scattering peaks of SWCNTs. Chen *et al.* demonstrated the highly sensitive, multiplexed protein detection using functionalised SWCNTs as Raman labels.[156] Antibodies were conjugated to SWCNTs functionalised with PEGylated phospholipids, which were used as multi-color Raman labels to detect proteins. Combined with Raman enhancing surfaces, this platform provided sensitive and reproducible protein detection down to 1fM of the target. They further applied this strategy to the clinically relevant detection of an autoimmune disease biomarker, aPR3 in native serum. In all cases, the detection based on SWCNT Raman presented better results than conventional fluorescence assays.

Although SWCNT based optical sensors provide sensitive and reliable detections of biomolecules, challenges still remain due to the complexity of optical detection. Firstly, preparative steps and multiple reagents are required for optical measurements. Secondly, SWCNTs have different chiralities, length and impurities, which might influence the sensitivity and selectivity of the detections. Additionally, the data analysis

of optical detection is quite complicated.[157] Therefore, electrical detection is a more promising alternative for the direct detection of biomolecules since most biological processes involve electrostatic interactions and charge transfer, which can be directly detect by electronic circuits.[158,159]

### 1.3.3 Carbon Nanotube Field Effect Transistors Biosensors

In a CNT FET sensor, metal electrodes are generally deposited on the surface of silicon substrate coated with silicon dioxide layer, serving as the source and drain electrode. SWCNTs (single or bundles) are connected between metal electrodes to act as conductive channel, forming field effect transistors. A liquid gate or back gate electrode is created to import gate voltage to control the conduction of the FET.[160] (Figure 1.11)

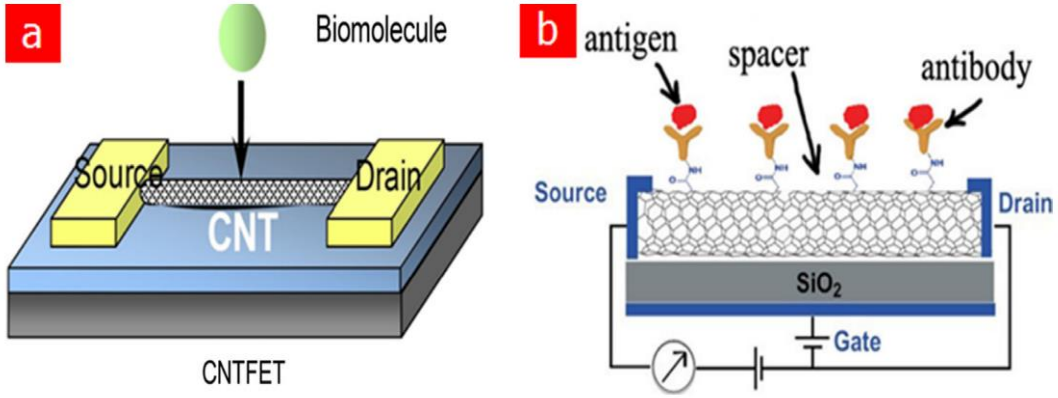


**Figure 1.11** (a) Exhibiting a structural model, CNTs is acted as conductive channel between the two electrodes to absorb biomolecules. (b) A schematic illustrates the working principle of CNTFET.[160]

Among nanoscale devices for electrical detection, SWCNT based devices offer many advantages. Due to the intrinsic 1D structure, the diameter of SWCNTs is around 1 nm, which is exactly comparable to the size of biomolecules and to the electronic screening length.[161] The large surface area of SWCNTs allows for the conjugation of biomolecules and every single carbon atom in SWCNT surface can directly contact

with the environment, optically interacting with nearby biomolecules.[124] Additionally, SWCNTs have a rather low charge carrier density, which is comparable to that of proteins.[124] These unique advantages make SWCNT FETs suitable for electronic detection dependent on electrostatic interaction.

Various SWCNT FETs have been developed for detections in different areas. For example, Zhao *et al.* decorated SWCNT devices with cyclodextrins, which can capture small organic molecules into their cavity. This enabled the modified devices to detect small organic molecules.[162] Ordinario *et al.* covalently modified metallic SWCNTs with amino-substituted phenyl radicals, which functioned as pH-dependent carrier scattering sites.[161] Thus, they demonstrated a novel pH sensor, in which the conductance of the modified SWCNTs varied as a function of pH.

SWCNT FETs are popular in the field of DNA detection. Martínez *et al*. used streptavidin as a linker to attach probe DNA to SWCNT FETs for the electronic detection of DNA hybridisation.[163] The streptavidin also prevented nonspecific adsorption of biomolecules onto SWCNTs, thus reducing noise in electrical detection. The devices showed high sensitivity and specificity of DNA hybridisation. In another experiment, Ordinario *et al.* showed the electrical monitoring of protein-DNA interactions using SWCNT FETs.[164] Pyrene modified DNA Duplexes were self-assembled on the devices, which would be cut by the restriction enzyme at specific sites. The DNA duplexes acted as sensitive recognition elements to transduce the biochemical events into electrical signals. Taking advantage of the sensitivity of SWCNTs to the electrostatic environment, the devices showed sequence specific detection of the enzyme.

Protein detection based on SWCNT FETs is one of the major focuses of research towards biosensing. Studies shows that many proteins can strongly adsorb onto the

exterior surface of SWCNTs via non-specific adsorption. The early work on electrical detection of proteins takes advantage of the non-specific adsorption, which results in a decrease in the conductance of the devices.[124,165,166] However, the selectivity of these devices is limited since proteins adsorb onto the SWCNT surface without any preference.[167] Moreover, impurities in solutions can also be adsorbed via nonspecific adsorption, which will cause electrical noise in the detection.[13,168] Therefore, passivation and specific receptors are required for electrical detections with high selectivity. Therefore, antibodies, aptamers have been widely used as receptors for protein detections.[104,142,168,169]

### 1.3.4 Sensing Mechanism of Electrical Detection

Since carbon nanotube transistors are a promising platform for the next generation of biosensors, tremendous efforts have been made to understand the nature of the interaction between SWCNTs and biomolecules, which facilitate to fully explore potential applications of these biosensors. Depending on analytes and the corresponding receptors, various mechanisms have been proposed to explain how SWCNTs transduce biological events into measurable electronic signals.

In a typical process of electrical detection, adding analytes to the devices causes changes or shifts in current since the analyte molecules approaching the surface of SWCNTs may change their charge carrier density, thereby effecting their conductance. Charge transfer is a common mechanism which can be used to explain the interaction of SWCNTs with analytes. Bradley *et al.* reported the detection of ammonia in aqueous solution and attributed the shift of current to charge transfer from ammonia to SWCNTs.[170] The study of interactions of aromatic compounds with SWCNTs also revealed that the gate voltage shift was the result of charge transfer between the

SWCNTs and the aromatic molecules adsorbed.[171] SWCNTs with zinc porphyrin derivatives were used to directly investigate photoinduced electron transfer, in which SWCNTs acted as the electron donor and the porphyrin molecules as the electron acceptor.[172]

Electrostatic gating is another reason why charged molecules can also induce changes in the conductance of SWCNTs. Upon binding of analytes, their charges modulate the surface potential of the nanotubes, causing accumulation or depletion of carriers in the FET channel. Therefore, the current through the FETs is affected by the binding of analytes. Artyukhin *et al.* assembled either positively or negatively charged polymers onto SWCNT devices and found that the regular oscillations of the transistor threshold voltage were dependent on the polarity of the outer polymer layer in the multilayer film. This phenomenon was addressed with a simple electrostatic model in which the potential change at the tubes caused by the alternating oppositely charged layers was taken into account.[173]

Schottky barrier effects may also account for the current changes in SWCNT devices. To investigate where proteins were adsorbed can induce conductance change, Chen *et al.* designed devices of which selected parts were blocked for protein adsorption, self-assembled monolayers (SAMs) of methoxy(poly(ethylene glycol))thiol (mPEG-SH) on the metal electrodes and PEG-containing surfactants on the nanotubes.[165] The results showed that the conductance change caused by protein adsorption originated from the metal-tube contact region, i.e. Schottky barrier modulation is likely dominant in the conductance change. Similar experiment was reported in which DNA hybridisation was detected. In this case, the conductance change was mainly induced by DNA hybridisation on gold electrodes, instead of on SWCNT sidewalls, since the formation of double stranded DNA lowered the work function of gold, inducing energy level

alignment between SWCNT and gold contact.[174]

In general, the mechanism in most electrical sensing is a combination of electrostatic gating and Schottky barrier effects. However, electrostatic gating is more consistent and more reproducible than the Schottky barrier effect at the contact. Therefore, devices with passivation of metal-SWCNT contacts can produce more reliable results for biosensing, since passivation of contacts inhibits signals caused by metal work function modulation.[124]

In aqueous solution, due to electrostatic interactions, charged biomolecules would be surrounded by dissolved solution counterions. On a certain length scale, the number of net positive charges would equal the number of net negative charges.[175] The screening effect is that the electrostatic potential caused by charged biomolecules decays exponentially toward zero with distance.[176] This length is termed Debye length ($\lambda_D$), which is given by:

$$\lambda_D = \frac{1}{\sqrt{4\pi l_B \sum_i \rho_i z_i^2}} \tag{7}$$

in which $l_B$ is the Bjerrum length (0.7 nm), and $\rho_i$ and $z_i$ are the density and the valent of ion species $i$.[176] Therefore, Debye length is dependent on the ionic solution (ionic strength): higher ionic strength results in shorter Debye length. In a biosensor, Debye length determines how close biomolecules to the biosensor can modulate the conductance of the biosensor. If biomolecules are far away from the devices ($>\lambda_D$), the effects of charged biomolecules on the conductance of SWCNTs are negligible, since the charges on biomolecules are screened; if biomolecules enter in the region of SWCNTs within Debye length ($<\lambda_D$), the charges can effectively modulate the conductance of the devices.

The influence of Debye length on biomolecule detection was first demonstrated using

silicon nanowire-based devices for specific detection of an avidin ligand.[175] The devices were functionalised with biotin molecules as receptors, which can selectively bind to streptavidin. Electrical detection of streptavidin was performed in three buffer solutions with different salt concentration, corresponding to Debye length of 0.7 nm, 2.3 nm, 7.3 nm, respectively. The results showed that a significant increase in current was observed when the Debye length was 7.3 nm, while the change in current was negligible when the Debye length was 0.7 nm since the charges on streptavidin were screened. This suggested that increasing buffer salt concentration resulted in decreasing device sensitivity for recognition. (Figure 1.12)

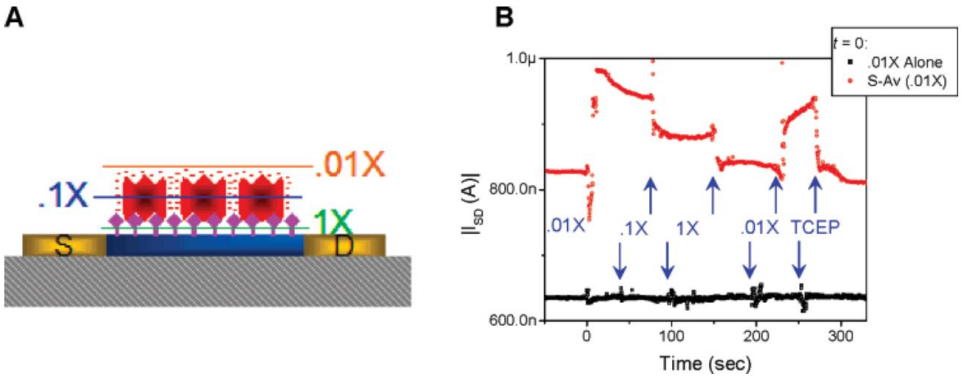


**Figure 1.12** Impact of Debye screening on streptavidin sensing. (a) Schematic showing Debye length from the device surface. (b) Biotin-functionalized sensor response to varying buffer ionic concentrations with (red) and without (black) streptavidin addition at time = 0.[175]

In another experiment, antibodies were attached onto silicon nanowires by different termini as receptors, resulting in antibodies either "standing" or "lying" on the biosensor with different distances of sensor to antigen binding site (Figure 1.13). The influence of charge screening on biosensing was studied through electrical detection of the corresponding antigen in different buffer solution. The results showed that the sensitivity of biosensors was dependent on the orientation of receptors.[177] The influence of Debye length on biosensing have been also observed in SWCNT devices.[144,178]

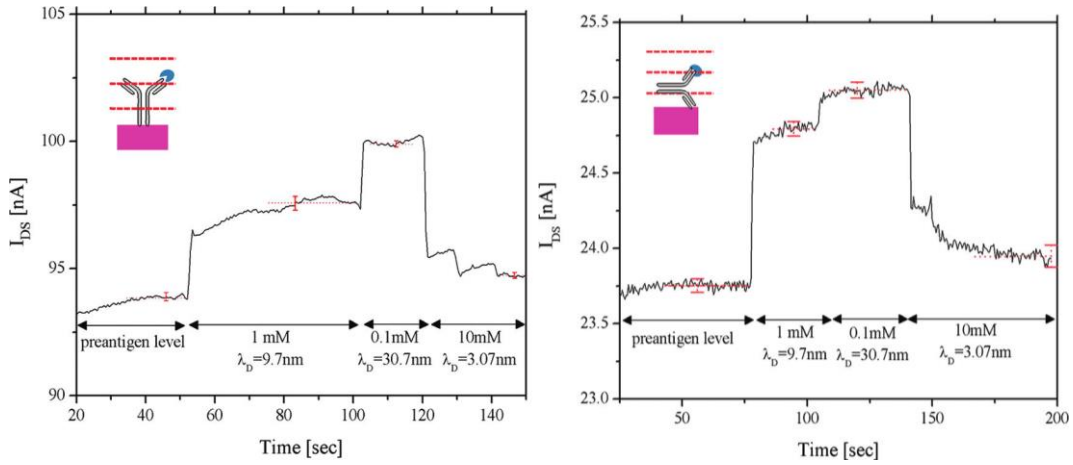


**Figure 1.13** Debye length modulation. Time domain device response after antigen injection, followed by a buffer exchange (top) "standing" or (bottom) "lying". Insets show nonlinear fit of device signal change versus the Debye length.[177]

In the literature, both "increasing" and "decreasing" signals are experimentally observed in response to the binding of bio-analytes.[103,104,179–181] The explanation is based on a single charge model: the direction of the signal is dependent on the net charge of the analyte, taking into account whether the FETs are p-type or n-type. Since semiconducting SWCNTs are intrinsically p-type, negatively charged biomolecules will induce an increase in conductance[103,104], while positively charged biomolecules will induce a decrease in conductance[169,181]. This assumption works satisfactorily in many simple cases, especially for small biomolecules and large Debye length.

However, the practical situation is more complicated as most proteins have an inhomogeneous charge distribution. The charged groups distributed throughout the protein may be subject to different screening effects. Screening modelling was performed mimicking a negatively charged proteins possessing a positively charged region.[182] The results suggested that the partial positive charges closer to the biosensor were dominant in the conductance modulation of the biosensor when the Debye length was limited (0-1.8 nm). When the Debye length was large enough (>1.8 nm), opposite signal would be observed since the negative charges dominated the biosensing. (Figure

1.14)

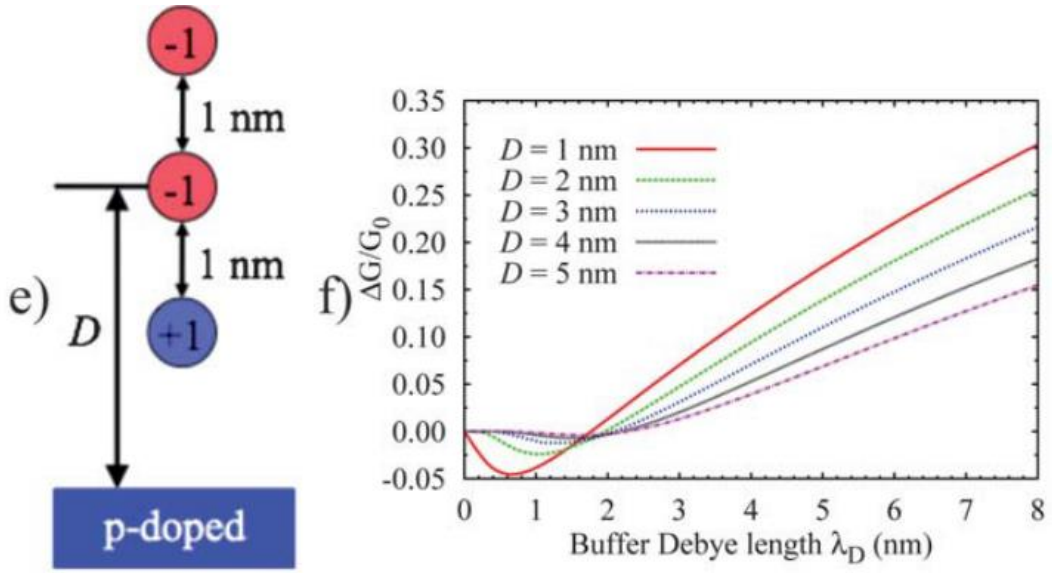


**Figure 1.14** Dependence of the conductance sensitivity of a p-type doped nano-BioFET on the Debye length: a negatively charged proteins possessing a positive region and its predicted signal.[182]

## 1.4 Thesis aims

In this thesis, we controlled the interfacing of SWCNTs with either biomolecules, like DNA and proteins, or metal precursors and assembled them between prepatterned electrodes, into field effect transistor configuration. We demonstrated the potential applications of these nanoscale devices in various fields, such as biosensing and photodetection.

In chapter 2, we summarise all the techniques applied in this thesis. In the next four chapters, we present our research results in the application of SWCNTs for biosensing (Chapter 3 and 4), for the fabrication of metal nanowire devices (Chapter 5), and in photo-responsive devices (Chapter 6).

In detail, in chapter 3, we will demonstrate the fabrication of multiplexed sensing devices based on DNA wrapped CNTs. We functionalised DNA-wrapped CNTs with specific and distinct aptamer sequences which were used as selective receptors to bio-

analytes. These distinct CNTs were immobilised from solution onto pre-patterned electrodes via DEP on the same chip. Multiplexed detection of three different analytes was successfully performed and real time detection was achieved in serum. This strategy can be applied to develop the next generation portable diagnostic assays for the simultaneous monitoring of different health parameters.

In chapter 4, we discuss how to control the orientation of proteins attached onto SWCNTs via click reaction. β-lactamase binding proteins (BLIP2) were engineered with phenylazide handles at defined sites, which allowed us to control the orientations of BLIP attached to CNTs. Hence, we could control the local electrostatic surface presented within the Debye length when TEM β-lactamase was binding to BLIP2, modulating the conductance gating effect. The devices gave distinct responses depending on TEM presenting either negative or positive local charge patches. This indicates that local electrostatic properties act as the key driving force for electrostatic gating. This in turn can improve our ability to build label-free directly gated electrical biosensors.

In chapter 5, we show the assembly of SWCNTs encapsulated with metal precursors between electrodes. Since metal precursors were encapsulated inside the CNT templates, we were able to precisely control their size, shape and orientation via DEP. Multiscale characterization of the different fabrication steps revealed details of the structure and charge transfer between the material encapsulated and the carbon nanotube. Electrical measurements further demonstrated the successful fabrication of metal nanowire devices. The strategy presented allows facile, low-cost and direct synthesis of multiplexed metal nanowire devices for nanoelectronic applications.

In Chapter 6, we show how individual SWCNTs of single chirality can be immobilised between electrodes. Additionally, we demonstrate the directed assembly of CdS-

SWCNT hybrids for photodetection. Moreover, we successfully sorted single chirality SWCNTs, following a published protocol; this allowed us to then fabricate individual CNT devices of single chirality via DEP. Subsequently, the electrical properties of these devices were studied, including multiplexed devices containing semiconducting and metal CNTs. The sorted CNTs were used as templates to fabricate photodetectors, which exhibited photo response. This study shows the potential application of single chirality CNT in nanoscale photodetectors. Finally, in the last chapter, the thesis is summarised and concluded, and future challenges and outlook are discussed.

References

(1) Borm, P. J. A.; Robbins, D.; Haubold, S.; Kuhlbusch, T.; Fissan, H.; Donaldson, K.; Schins, R.; Stone, V.; Kreyling, W.; Lademann, J.; Krutmann, J.; Warheit, D. B.; Oberdorster, E. *The Potential Risks of Nanomaterials: A Review Carried out for ECETOC*; 2006; Vol. 3. https://doi.org/10.1186/1743-8977-3-11.

(2) Buzea, C.; Pacheco, I. I.; Robbie, K. Nanomaterials and Nanoparticles: Sources and Toxicity. *Biointerphases* **2007**, *2* (4), MR17–MR71. https://doi.org/10.1116/1.2815690.

(3) Roduner, E. Size Matters: Why Nanomaterials Are Different. *Chem. Soc. Rev.* **2006**, *35* (7), 583–592. https://doi.org/10.1039/b502142c.

(4) Holzinger, M.; Goff, A. Le; Cosnier, S. Nanomaterials for Biosensing Applications: A Review. *Front. Chem.* **2014**, *2* (AUG), 1–10. https://doi.org/10.3389/fchem.2014.00063.

(5) Kanjolia, R. New Materials In Semiconductor Fabrication : An Evolutionary Process; 2007.

(6) Xiang, D.; Wang, X.; Jia, C.; Lee, T.; Guo, X. Molecular-Scale Electronics :

From Concept to Function. **2016**. https://doi.org/10.1021/acs.chemrev.5b00680.

(7) Karthäuser, S. Control of Molecule-Based Transport for Future Molecular Devices. *J. Phys. Condens. Matter* **2011**, *23* (1). https://doi.org/10.1088/0953-8984/23/1/013001.

(8) Damle, P.; Rakshit, T.; Paulsson, M.; Datta, S. Current-Voltage Characteristics of Molecular Conductors: Two versus Three Terminal. *IEEE Trans. Nanotechnol.* **2002**, *1* (3), 145–152. https://doi.org/10.1109/TNANO.2002.806825.

(9) Jia, C.; Ma, B.; Xin, N.; Guo, X. Carbon Electrode-Molecule Junctions: A Reliable Platform for Molecular Electronics. *Acc. Chem. Res.* **2015**, *48* (9), 2565–2575. https://doi.org/10.1021/acs.accounts.5b00133.

(10) Gui, E. L.; Li, L.; Zhang, K.; Xu, Y.; Dong, X.; Ho, X.; Lee, P. S.; Kasim, J.; Shen, Z. X.; Rogers, J. A. DNA Sensing by Field-Effect Transistors Based on Networks of Carbon Nanotubes. **2007**, 14427–14432. https://doi.org/10.1021/ja075176g.

(11) Oikonomou, A.; Clark, N.; Heeg, S.; Kretinin, A.; Varey, S.; Yu, G.; Vijayaraghavan, A. Scalable Bottom-up Assembly of Suspended Carbon Nanotube and Graphene Devices by Dielectrophoresis. *Phys. Status Solidi - Rapid Res. Lett.* **2015**, *9* (9), 539–543. https://doi.org/10.1002/pssr.201510177.

(12) Gao, Z.; Xia, H.; Zauberman, J.; Tomaiuolo, M.; Ping, J.; Zhang, Q.; Ducos, P.; Ye, H.; Wang, S.; Yang, X.; Lubna, F.; Luo, Z.; Ren, L.; Johnson, A. T. C. Detection of Sub-FM DNA with Target Recycling and Self-Assembly Amplification on Graphene Field-Effect Biosensors. *Nano Lett.* **2018**, *18* (6), 3509–3515. https://doi.org/10.1021/acs.nanolett.8b00572.

(13) Tran, T. T.; Mulchandani, A. Carbon Nanotubes and Graphene Nano Field-

Effect Transistor-Based Biosensors. *TrAC - Trends Anal. Chem.* **2016**, *79*, 222–232. https://doi.org/10.1016/j.trac.2015.12.002.

(14) Candini, A.; Klyatskaya, S.; Ruben, M.; Wernsdorfer, W.; Affronte, M. Graphene Spintronic Devices with Molecular Nanomagnets. *Nano Lett.* **2011**, *11* (7), 2634–2639. https://doi.org/10.1021/nl2006142.

(15) Cao, Q.; Han, S.; Tulevski, G. S. Fringing-Field Dielectrophoretic Assembly of Ultrahigh-Density Semiconducting Nanotube Arrays with a Self-Limited Pitch. *Nat. Commun.* **2014**, *5*, 5071. https://doi.org/10.1038/ncomms6071.

(16) Park, S. H.; Kang, Y. J.; Majd, S. A Review of Patterned Organic Bioelectronic Materials and Their Biomedical Applications. *Adv. Mater.* **2015**, *27* (46), 7583–7619. https://doi.org/10.1002/adma.201501809.

(17) Amiot, C. L.; Xu, S.; Liang, S.; Pan, L.; Zhao, J. X. Near-Infrared Fluorescent Materials for Sensing of Biological Targets. *Sensors* **2008**, *8* (5), 3082–3105. https://doi.org/10.3390/s8053082.

(18) Spinato, C.; Perez Ruiz De Garibay, A.; Kierkowicz, M.; Pach, E.; Martincic, M.; Klippstein, R.; Bourgognon, M.; Wang, J. T. W.; Ménard-Moyon, C.; Al-Jamal, K. T.; Ballesteros, B.; Tobias, G.; Bianco, A. Design of Antibody-Functionalized Carbon Nanotubes Filled with Radioactivable Metals towards a Targeted Anticancer Therapy. *Nanoscale* **2016**, *8* (25), 12626–12638. https://doi.org/10.1039/c5nr07923c.

(19) Yang, W.; Thordarson, P.; Gooding, J. J.; Ringer, S. P.; Braet, F. Carbon Nanotubes for Biological and Biomedical Applications. *Nanotechnology* **2007**, *18* (41), 412001. https://doi.org/10.1088/0957-4484/18/41/412001.

(20) Manjasetty, B.; Nair, T.; Ramaswamy, Y. Nano-Biotechnology: Structure and Dynamics of Nanoscale Biosystems. *arXiv Prepr. arXiv1001.3529* **2010**, No. c,

22–26.

(21) Wang, J. Can Man-Made Nanomachines Compete with Nature Biomotors? *ACS Nano* **2009**, *3* (1), 4–9. https://doi.org/10.1021/nn800829k.

(22) Chan, W. C. W. Bionanotechnology Progress and Advances. *Biol. Blood Marrow Transplant.* **2006**, *12* (SUPPL. 1), 87–91. https://doi.org/10.1016/j.bbmt.2005.10.004.

(23) Sandoval, S.; Pach, E.; Ballesteros, B.; Tobias, G. Encapsulation of Two-Dimensional Materials inside Carbon Nanotubes: Towards an Enhanced Synthesis of Single-Layered Metal Halides. *Carbon N. Y.* **2017**, *123*, 129–134. https://doi.org/10.1016/j.carbon.2017.07.031.

(24) Biswas, A.; Bayer, I. S.; Biris, A. S.; Wang, T.; Dervishi, E.; Faupel, F. Advances in Top-down and Bottom-up Surface Nanofabrication: Techniques, Applications & Future Prospects. *Adv. Colloid Interface Sci.* **2012**, *170* (1–2), 2–27. https://doi.org/10.1016/j.cis.2011.11.001.

(25) Stokes, P.; Silbar, E.; Zayas, Y. M.; Khondaker, S. I. Solution Processed Large Area Field Effect Transistors from Dielectrophoreticly Aligned Arrays of Carbon Nanotubes. *Appl. Phys. Lett.* **2009**, *94* (11). https://doi.org/10.1063/1.3100197.

(26) Dai, H. Carbon Nanotubes: Synthesis, Integration, and Properties. *Acc. Chem. Res.* **2002**, *35* (12), 1035–1044. https://doi.org/10.1021/ar0101640.

(27) Guo, X. Single-Molecule Electrical Biosensors Based on Single-Walled Carbon Nanotubes. *Adv. Mater.* **2013**, *25* (25), 3397–3408. https://doi.org/10.1002/adma.201301219.

(28) Kim, S. N.; Rusling, J. F.; Papadimitrakopoulos, F. Carbon Nanotubes for Electronic and Electrochemical Detection of Biomolecules. *Adv. Mater.* **2007**,

*19* (20), 3214–3228. https://doi.org/10.1002/adma.200700665.

(29) Banerjee, S.; White, B.; Huang, L.; Rego, B. J.; O'Brien, S.; Herman, I. P. Precise Positioning of Carbon Nanotubes by Ac Dielectrophoresis Using Floating Posts. *Appl. Phys. A Mater. Sci. Process.* **2007**, *86* (4), 415–419. https://doi.org/10.1007/s00339-006-3787-6.

(30) Medeiros, P. V. C.; Marks, S.; Wynn, J. M.; Vasylenko, A.; Ramasse, Q. M.; Quigley, D.; Sloan, J.; Morris, A. J. Single-Atom Scale Structural Selectivity in Te Nanowires Encapsulated Inside Ultranarrow, Single-Walled Carbon Nanotubes. *ACS Nano* **2017**, *11* (6), 6178–6185. https://doi.org/10.1021/acsnano.7b02225.

(31) Liu, S.; Zhang, X.; Luo, W.; Wang, Z.; Guo, X.; Steigerwald, M. L.; Fang, X. Single-Molecule Detection of Proteins Using Aptamer-Functionalized Molecular Electronic Devices. *Angew. Chemie - Int. Ed.* **2011**, *50* (11), 2496–2502. https://doi.org/10.1002/anie.201006469.

(32) Guo, X.; Small, J. P.; Klare, J. E.; Wang, Y.; Purewal, M. S.; Tam, I. W.; Hong, B. H.; Caldwell, R.; Huang, L.; Brien, S. O.; Yan, J.; Breslow, R. Covalently Bridging Gaps in with Conducting Molecules. *Science (80-. ).* **2011**, *356* (2006), 356–360. https://doi.org/10.1126/science.1120986.

(33) Guo, X.; Huang, L.; O'Brien, S.; Kim, P.; Nuckolls, C. Directing and Sensing Changes in Molecular Conformation on Individual Carbon Nanotube Field Effect Transistors. *J. Am. Chem. Soc.* **2005**, *127* (43), 15045–15047. https://doi.org/10.1021/ja054335y.

(34) Guo, X. Single-Molecule Electrical Biosensors Based on Single-Walled Carbon Nanotubes. *Adv. Mater.* **2013**, *25* (25), 3397–3408. https://doi.org/10.1002/adma.201301219.

(35) Sorgenfrei, S.; Meric, I.; Banerjee, S.; Akey, A.; Rosenblatt, S.; Herman, I. P.; Shepard, K. L. Controlled Dielectrophoretic Assembly of Carbon Nanotubes Using Real-Time Electrical Detection. *Appl. Phys. Lett.* **2009**, *94* (5), 92–95. https://doi.org/10.1063/1.3077620.

(36) Kuzyk, A. Dielectrophoresis at the Nanoscale. *Electrophoresis* **2011**, *32* (17), 2307–2313. https://doi.org/10.1002/elps.201100038.

(37) Scarselli, M.; Castrucci, P.; De Crescenzi, M. Electronic and Optoelectronic Nano-Devices Based on Carbon Nanotubes. *J. Phys. Condens. Matter* **2012**, *24* (31). https://doi.org/10.1088/0953-8984/24/31/313202.

(38) Wang, X.; Li, Q.; Xie, J.; Jin, Z.; Wang, J.; Li, Y.; Jiang, K.; Fan, S. Fabrication of Ultralong and Electrically Uniform Single-Walled Carbon Nanotubes on Clean Substrates. *Nano Lett.* **2009**, *9* (9), 3137–3141. https://doi.org/10.1021/nl901260b.

(39) Iijima, S. © 19 9 1 Nature Publishing Group 그라첼꺼. *Nature* **1991**, *354*, 56–58.

(40) Ma, P. C.; Siddiqui, N. A.; Marom, G.; Kim, J. K. Dispersion and Functionalization of Carbon Nanotubes for Polymer-Based Nanocomposites: A Review. *Compos. Part A Appl. Sci. Manuf.* **2010**, *41* (10), 1345–1367. https://doi.org/10.1016/j.compositesa.2010.07.003.

(41) Joselevich, E. Electronic Structure and Chemical Reactivity of Carbon Nanotubes: A Chemist's View. *ChemPhysChem* **2004**, *5* (5), 619–624. https://doi.org/10.1002/cphc.200301049.

(42) Samsonidze, G. G.; Saito, R.; Jorio, A.; Pimenta, M. A.; Souza Filho, A. G.; Grüneis, A.; Dresselhaus, G.; Dresselhaus, M. S. The Concept of Cutting Lines in Carbon Nanotube Science. *J. Nanosci. Nanotechnol.* **2003**, *3* (6), 431–458.

https://doi.org/10.1166/jnn.2003.231.

(43) Kiang, C. H.; Devries, M. S.; Gorman, G.; Savoy, R.; Bethune, D. S.; Klang, C. H.; de-Vries, M. S.; Vazquez, J.; Beyers, R. Cobalt-Catalysed Growth of Carbon Nanotubes with Single-Atomic-Layer Walls. *Nature* **1993**, *363* (6430), 605–607.

(44) Journet, C.; Maser, W. K.; Bernier, P.; Loiseau, A.; Lamy de la Chapelle, M.; Lefrant, S.; Deniard, P.; Lee, R.; Fischer, J. E. Large-Scale Production of Single-Walled Carbon Nanotubes by the Electric-Arc Technique. *Nature* **1997**, *388* (6644), 756–758. https://doi.org/10.1038/41972.

(45) Avouris, P. Nanotubes Electronics. *Sci. Am.* **2000**, *283* (December), 62–69.

(46) Scott, C. D.; Arepalli, S.; Nikolaev, P.; Smalley, R. E. Growth Mechanisms for Single-Wall Carbon Nanotubes in a Laser-Ablation Process. *Appl. Phys. A Mater. Sci. Process.* **2001**, *72* (5), 573–580. https://doi.org/10.1007/s003390100761.

(47) Thess, A.; Lee, R.; Nikolaev, P.; Dai, H.; Petit, P.; Robert, J.; Xu, C.; Lee, Y. H.; Kim, S. G.; Rinzler, A. G.; Colbert, D. T.; Scuseria, G. E.; Tománek, D.; Fischer, J. E.; Smalley, R. E. Crystalline Ropes of Metallic Carbon Nanotubes. *Science (80-. ).* **1996**, *273* (5274), 483–487. https://doi.org/10.1126/science.273.5274.483.

(48) Nikolaev, P.; Bronikowski, M. J.; Bradley, R. K.; Rohmund, F.; Colbert, D. T.; Smith, K. A.; Smalley, R. E. Gas-Phase Catalytic Growth of Single-Walled Carbon Nanotubes from Carbon Monoxide. *Chem. Phys. Lett.* **1999**, *313* (1–2), 91–97. https://doi.org/10.1016/S0009-2614(99)01029-5.

(49) Ishigami, N.; Ago, H.; Imamoto, K.; Tsuji, M.; Iakoubovskii, K.; Minami, N. Crystal Plane Dependent Growth of Aligned Single-Walled Carbon Nanotubes on Sapphire. *J. Am. Chem. Soc.* **2008**, *130* (30), 9918–9924. https://doi.org/10.1021/ja8024752.

(50) Ren, Z. F.; Huang, Z. P. Synthesis of Large Arrays of Well-Aligned Carbon Nanotubes on Glass. *Science (80-. ).* **1998**, *282* (5391), 1105–1107. https://doi.org/10.1126/science.282.5391.1105.

(51) Neupane, S.; Lastres, M.; Chiarella, M.; Li, W.; Su, Q.; Du, G. Synthesis and Field Emission Properties of Vertically Aligned Carbon Nanotube Arrays on Copper. *Carbon N. Y.* **2012**, *50* (7), 2641–2650. https://doi.org/10.1016/j.carbon.2012.02.024.

(52) Fan, S.; Chapline, M. G.; Franklin, N. R.; Tombler, T. W.; Cassell, A. M.; Dai, H. Self-Oriented Regular Arrays of Carbon Nanotubes and Their Field Emission Properties. *Science (80-. ).* **1999**, *283* (5401), 512–514. https://doi.org/10.1126/science.283.5401.512.

(53) Takeuchi, K.; Hayashi, T.; Kim, Y. A.; Fujisawa, K.; Endo, M. The State-of-the-Art Science and Applications of Carbon Nanotubes. *Наносистемы: Физика, Химия, Математика* **2014**, *5* (1), 15–24.

(54) Cao, Q.; Hur, S. H.; Zhu, Z. T.; Sun, Y.; Wang, C.; Meitl, M. A.; Shim, M.; Rogers, J. A. Highly Bendable, Transparent Thin-Film Transistors That Use Carbon-Nanotube-Based Conductors and Semiconductors with Elastomeric Dielectrics. *Adv. Mater.* **2006**, *18* (3), 304–309. https://doi.org/10.1002/adma.200501740.

(55) Anggraini, A. R.; Oliver, J. 済無No Title No Title. *J. Chem. Inf. Model.* **2019**, *53* (9), 1689–1699. https://doi.org/10.1017/CBO9781107415324.004.

(56) Bronikowski, M. J.; Willis, P. A.; Colbert, D. T.; Smith, K. A.; Smalley, R. E. Gas-Phase Production of Carbon Single-Walled Nanotubes from Carbon Monoxide via the HiPco Process: A Parametric Study. *J. Vac. Sci. Technol. A Vacuum, Surfaces, Film.* **2001**, *19* (4), 1800–1805.

https://doi.org/10.1116/1.1380721.

(57) Liu, H.; Nishide, D.; Tanaka, T.; Kataura, H. Large-Scale Single-Chirality Separation of Single-Wall Carbon Nanotubes by Simple Gel Chromatography. *Nat. Commun.* **2011**, *2* (1). https://doi.org/10.1038/ncomms1313.

(58) Ghosh, S.; Bachilo, S. M.; Weisman, R. B. Advanced Sorting of Single-Walled Carbon Nanotubes by Nonlinear Density-Gradient Ultracentrifugation. *Nat. Nanotechnol.* **2010**, *5* (6), 443–450. https://doi.org/10.1038/nnano.2010.68.

(59) Liu, J.; Wang, C.; Tu, X.; Liu, B.; Chen, L.; Zheng, M.; Zhou, C. Chirality-Controlled Synthesis of Single-Wall Carbon Nanotubes Using Vapour-Phase Epitaxy. *Nat. Commun.* **2012**, *3*, 1–7. https://doi.org/10.1038/ncomms2205.

(60) Bachilo, S. M.; Balzano, L.; Herrera, J. E.; Pompeo, F.; Resasco, D. E.; Weisman, R. B. Narrow (n,m)-Distribution of Single-Walled Carbon Nanotubes Grown Using a Solid Supported Catalyst. *J. Am. Chem. Soc.* **2003**, *125* (37), 11186–11187. https://doi.org/10.1021/ja036622c.

(61) An, L.; Owens, J. M.; McNeil, L. E.; Liu, J. Synthesis of Nearly Uniform Single-Walled Carbon Nanotubes Using Identical Metal-Containing Molecular Nanoclusters as Catalysts. *J. Am. Chem. Soc.* **2002**, *124* (46), 13688–13689. https://doi.org/10.1021/ja0274958.

(62) Zhou, W.; Han, Z.; Wang, J.; Zhang, Y.; Jin, Z.; Sun, X.; Zhang, Y.; Yan, C.; Li, Y. Copper Catalyzing Growth of Single-Walled Carbon Nanotubes on Substrates. *Nano Lett.* **2006**, *6* (12), 2987–2990. https://doi.org/10.1021/nl061871v.

(63) Liu, B.; Ren, W.; Li, S.; Liu, C.; Cheng, H. M. High Temperature Selective Growth of Single-Walled Carbon Nanotubes with a Narrow Chirality Distribution from a CoPt Bimetallic Catalyst. *Chem. Commun.* **2012**, *48* (18), 2409–2411. https://doi.org/10.1039/c2cc16491d.

(64) Zhang, F.; Hou, P. X.; Liu, C.; Wang, B. W.; Jiang, H.; Chen, M. L.; Sun, D. M.; Li, J. C.; Cong, H. T.; Kauppinen, E. I.; Cheng, H. M. Growth of Semiconducting Single-Wall Carbon Nanotubes with a Narrow Band-Gap Distribution. *Nat. Commun.* **2016**, *7*. https://doi.org/10.1038/ncomms11160.

(65) Yang, F.; Wang, X.; Zhang, D.; Yang, J.; Luo, D.; Xu, Z.; Wei, J.; Wang, J. Q.; Xu, Z.; Peng, F.; Li, X.; Li, R.; Li, Y.; Li, M.; Bai, X.; Ding, F.; Li, Y. Chirality-Specific Growth of Single-Walled Carbon Nanotubes on Solid Alloy Catalysts. *Nature* **2014**, *510* (7506), 522–524. https://doi.org/10.1038/nature13434.

(66) Sanchez-Valencia, J. R.; Dienel, T.; Gröning, O.; Shorubalko, I.; Mueller, A.; Jansen, M.; Amsharov, K.; Ruffieux, P.; Fasel, R. Controlled Synthesis of Single-Chirality Carbon Nanotubes. *Nature* **2014**, *512* (1), 61–64. https://doi.org/10.1038/nature13607.

(67) Monthioux, M.; Smith, B. W.; Burteaux, B.; Claye, A.; Fischer, J. E.; Luzzi, D. E. Sensitivity of Single-Wall Carbon Nanotubes to Chemical Processing: An Electron Microscopy Investigation. *Carbon N. Y.* **2001**, *39* (8), 1251–1272. https://doi.org/10.1016/S0008-6223(00)00249-9.

(68) Saito, Y.; Mizushima, R.; Tanaka, T.; Tohji, K.; Uchida, K.; Yumura, M.; Uemura, S. Synthesis, Structure and Field Emission of Carbon Nanotubes. *Fuller. Sci. Technol.* **1999**, *7* (4), 653–664. https://doi.org/10.1080/10641229909351368.

(69) Dillon, A. C.; Gennett, T.; Jones, K. M.; Alleman, J. L.; Parilla, P. A.; Heben, M. J. Simple and Complete Purification of Single-Walled Carbon Nanotube Materials. *Adv. Mater.* **1999**, *11* (16), 1354–1358. https://doi.org/10.1002/(SICI)1521-4095(199911)11:16<1354::AID-ADMA1354>3.0.CO;2-N.

(70) Gómez-Navarro, C.; De Pablo, P. J.; Gómez-Herrero, J.; Biel, B.; Garcia-Vidal,

F. J.; Rubio, A.; Flores, F. Tuning the Conductance of Single-Walled Carbon Nanotubes by Ion Irradiation in the Anderson Localization Regime. *Nat. Mater.* **2005**, *4* (7), 534–539. https://doi.org/10.1038/nmat1414.

(71) Sgobba, V.; Guldi, D. M. Carbon Nanotubes—Electronic/Electrochemical Properties and Application for Nanoelectronics and Photonics. *Chem. Soc. Rev.* **2009**, *38* (1), 165–184. https://doi.org/10.1039/b802652c.

(72) Louie, S. G. Electronic Properties, Junctions, and Defects of Carbon Nanotubes BT - Carbon Nanotubes: Synthesis, Structure, Properties, and Applications; Dresselhaus, M. S., Dresselhaus, G., Avouris, P., Eds.; Springer Berlin Heidelberg: Berlin, Heidelberg, 2001; pp 113–145. https://doi.org/10.1007/3-540-39947-X_6.

(73) Fan, Y.; Goldsmith, B. R.; Collins, P. G. Identifying and Counting Point Defects in Carbon Nanotubes. *Nat. Mater.* **2005**, *4* (12), 906–911. https://doi.org/10.1038/nmat1516.

(74) Li, Y.; Zhang, X.; Luo, J.; Huang, W.; Cheng, J.; Luo, Z.; Li, T.; Liu, F.; Xu, G.; Ke, X.; Lin, L.; Geise, H. J. Purification of CVD Synthesized Single-Wall Carbon Nanotubes by Different Acid Oxidation Treatments. *Nanotechnology* **2004**, *15* (11), 1645–1649. https://doi.org/10.1088/0957-4484/15/11/047.

(75) Martínez, M. T.; Callejas, M. A.; Benito, A. M.; Cochet, M.; Seeger, T.; Ansón, A.; Schreiber, J.; Gordon, C.; Marhic, C.; Chauvet, O.; Maser, W. K. Modifications of Single-Wall Carbon Nanotubes upon Oxidative Purification Treatments. *Nanotechnology* **2003**, *14* (7), 691–695. https://doi.org/10.1088/0957-4484/14/7/301.

(76) S. Duesberg, G.; Burghard, M.; Muster, J.; Philipp, G. Separation of Carbon Nanotubes by Size Exclusion Chromatography. *Chem. Commun.* **1998**, No. 3,

435–436. https://doi.org/10.1039/A707465D.

(77) Duesberg, G. S.; Muster, J.; Krstic, V.; Burghard, M.; Roth, S. Chromatographic Size Separation of Single-Wall Carbon Nanotubes. *Appl. Phys. A Mater. Sci. Process.* **1998**, *67* (1), 117–119. https://doi.org/10.1007/s003390050747.

(78) Tanaka, T.; Jin, H.; Miyata, Y.; Fujii, S.; Nishide, D.; Kataura, H. Mass Separation of Metallic and Semiconducting Single-Wall Carbon Nanotubes Using Agarose Gel. *Phys. Status Solidi Basic Res.* **2009**, *246* (11–12), 2490–2493. https://doi.org/10.1002/pssb.200982313.

(79) Arnold, M. S.; Green, A. A.; Hulvat, J. F.; Stupp, S. I.; Hersam, M. C. Sorting Carbon Nanotubes by Electronic Structure Using Density Differentiation. *Nat. Nanotechnol.* **2006**, *1* (1), 60–65. https://doi.org/10.1038/nnano.2006.52.

(80) Girifalco, L. A.; Hodak, M.; Lee, R. S. Carbon Nanotubes, Buckyballs, Ropes, and a Universal Graphitic Potential. *Phys. Rev. B - Condens. Matter Mater. Phys.* **2000**, *62* (19), 13104–13110. https://doi.org/10.1103/PhysRevB.62.13104.

(81) Caneba, G. T.; Dutta, C.; Agrawal, V.; Rao, M. Novel Ultrasonic Dispersion of Carbon Nanotubes. *J. Miner. Mater. Charact. Eng.* **2010**, *09* (03), 165–181. https://doi.org/10.4236/jmmce.2010.93015.

(82) Yasumitsu, T.; Liu, G.; Leveque, J. M.; Aonuma, S.; Duclaux, L.; Kimura, T.; Komatsu, N. A Rosette Cooling Cell: More Effective Container for Solubilization of Single-Walled Carbon Nanotubes under Probe-Type Ultrasonic Irradiation. *Ultrason. Sonochem.* **2013**, *20* (1), 37–39. https://doi.org/10.1016/j.ultsonch.2012.06.009.

(83) Lu, K. L.; Lago, R. M.; Chen, Y. K.; Green, M. L. H.; Harris, P. J. F.; Tsang, S. C. Mechanical Damage of Carbon Nanotubes by Ultrasound. *Carbon N. Y.* **1996**, *34* (6), 814–816. https://doi.org/10.1016/0008-6223(96)89470-X.

(84) Kim, S.; Lee, Y. I.; Kim, D. H.; Lee, K. J.; Kim, B. S.; Hussain, M.; Choa, Y. H. Estimation of Dispersion Stability of UV/Ozone Treated Multi-Walled Carbon Nanotubes and Their Electrical Properties. *Carbon N. Y.* **2013**, *51* (1), 346–354. https://doi.org/10.1016/j.carbon.2012.08.062.

(85) Singh, J.; Kothiyal, N. C.; Pathania, D. Synthesis of Highly Dispersed Single Walled Carbon Nanotubes from Furnace Oil and Light Diesel Oil by Modified Chemical Vapour Deposition Method. *Int. J. Theor. Appl. Sci.* **2011**, *3* (2), 15–20.

(86) Yu, A.; Su, C. C. L.; Roes, I.; Fan, B.; Haddon, R. C. Gram-Scale Preparation of Surfactant-Free, Carboxylic Acid Groups Functionalized, Individual Single-Walled Carbon Nanotubes in Aqueous Solution. *Langmuir* **2010**, *26* (2), 1221–1225. https://doi.org/10.1021/la902341w.

(87) Farbod, M.; Tadavani, S. K.; Kiasat, A. Surface Oxidation and Effect of Electric Field on Dispersion and Colloids Stability of Multiwalled Carbon Nanotubes. *Colloids Surfaces A Physicochem. Eng. Asp.* **2011**, *384* (1–3), 685–690. https://doi.org/10.1016/j.colsurfa.2011.05.041.

(88) Song, H.; Ishii, Y.; Al-Zubaidi, A.; Sakai, T.; Kawasaki, S. Temperature-Dependent Water Solubility of Iodine-Doped Single-Walled Carbon Nanotubes Prepared Using an Electrochemical Method. *Phys. Chem. Chem. Phys.* **2013**, *15* (16), 5767–5770. https://doi.org/10.1039/c3cp50506e.

(89) Dyke, C. A.; Tour, J. M. Unbundled and Highly Functionalized Carbon Nanotubes from Aqueous Reactions. *Nano Lett.* **2003**, *3* (9), 1215–1218. https://doi.org/10.1021/nl034537x.

(90) Hilding, J.; Grulke, E. A.; Zhang, Z. G.; Lockwood, F. Dispersion of Carbon Nanotubes in Liquids. *J. Dispers. Sci. Technol.* **2003**, *24* (1), 1–41.

https://doi.org/10.1081/DIS-120017941.

(91) Shvartzman-Cohen, R.; Levi-Kalisman, Y.; Nativ-Roth, E.; Yerushalmi-Rozen, R. Generic Approach for Dispersing Single-Walled Carbon Nanotubes: The Strength of a Weak Interaction. *Langmuir* **2004**, *20* (15), 6085–6088. https://doi.org/10.1021/la049344j.

(92) Strano, M. S.; Moore, V. C.; Miller, M. K.; Allen, M. J.; Haroz, E. H.; Kittrell, C.; Hauge, R. H.; Smalley, R. E. The Role of Surfactant Adsorption during Ultrasonication in the Dispersion of Single-Walled Carbon Nanotubes. *J. Nanosci. Nanotechnol.* **2003**, *3* (1–2), 81–86. https://doi.org/10.1166/jnn.2003.194.

(93) Hodge, S. A.; Bayazit, M. K.; Coleman, K. S.; Shaff, M. S. P.; Hodge, S. A.; Bayazit, M. K.; Coleman, S.; Shaffer, M. S. P.; Hodge, S. A. Chem Soc Rev Single-Walled Carbon Nanotube Molecular Structures and Their Chemical Reactivity. **2012**, *41* (12). https://doi.org/10.1039/c2cs15334c.

(94) Streit, J. K.; Fagan, J. A.; Zheng, M. A Low Energy Route to DNA-Wrapped Carbon Nanotubes via Replacement of Bile Salt Surfactants. *Anal. Chem.* **2017**, *89* (19), 10496–10503. https://doi.org/10.1021/acs.analchem.7b02637.

(95) Zheng, M.; Jagota, A.; Semke, E. D.; Diner, B. A.; McLean, R. S.; Lustig, S. R.; Richardson, R. E.; Tassi, N. G. DNA-Assisted Dispersion and Separation of Carbon Nanotubes. *Nat. Mater.* **2003**, *2* (5), 338–342. https://doi.org/10.1038/nmat877 M4 - Citavi.

(96) Tu, X.; Manohar, S.; Jagota, A.; Zheng, M. DNA Sequence Motifs for Structure-Specific Recognition and Separation of Carbon Nanotubes. *Nature* **2009**, *460* (7252), 250–253. https://doi.org/10.1038/nature08116.

(97) Ao, G.; Streit, J. K.; Fagan, J. A.; Zheng, M. Differentiating Left- and Right-

Handed Carbon Nanotubes by DNA. *J. Am. Chem. Soc.* **2016**, *138* (51), 16677–16685. https://doi.org/10.1021/jacs.6b09135.

(98) Han, W.; Fan, S.; Li, Q.; Gu, B.; Zhang, X.; Yu, D. Synthesis of Silicon Nitride Nanorods Using Carbon Nanotube as a Template. *Appl. Phys. Lett.* **1997**, *71* (16), 2271–2273. https://doi.org/10.1063/1.120550.

(99) Satishkumar, B. C.; Govindaraj, A.; Nath, M.; Rao, C. N. R. Synthesis of Metal Oxide Nanorods Using Carbon Nanotubes as Templates. *J. Mater. Chem.* **2000**, *10* (9), 2115–2119. https://doi.org/10.1039/b002868l.

(100) Hilder, T. A.; Hill, J. M. Carbon Nanotubes as Drug Delivery Nanocapsules. *Curr. Appl. Phys.* **2008**, *8* (3–4), 258–261. https://doi.org/10.1016/j.cap.2007.10.011.

(101) Zhang, T. F.; Li, Z. P.; Wang, J. Z.; Kong, W. Y.; Wu, G. A.; Zheng, Y. Z.; Zhao, Y. W.; Yao, E. X.; Zhuang, N. X.; Luo, L. B. Broadband Photodetector Based on Carbon Nanotube Thin Film/Single Layer Graphene Schottky Junction. *Sci. Rep.* **2016**, *6* (December), 1–8. https://doi.org/10.1038/srep38569.

(102) Park, S.; Kim, S. J.; Nam, J. H.; Pitner, G.; Lee, T. H.; Ayzner, A. L.; Wang, H.; Fong, S. W.; Vosgueritchian, M.; Park, Y. J.; Brongersma, M. L.; Bao, Z. Significant Enhancement of Infrared Photodetector Sensitivity Using a Semiconducting Single-Walled Carbon Nanotube/C60 Phototransistor. *Adv. Mater.* **2015**, *27* (4), 759–765. https://doi.org/10.1002/adma.201404544.

(103) Lo, Y. S.; Nam, D. H.; So, H. M.; Chang, H.; Kim, J. J.; Kim, Y. H.; Lee, J. O. Oriented Immobilization of Antibody Fragments on Ni-Decorated Single-Walled Carbon Nanotube Devices. *ACS Nano* **2009**, *3* (11), 3649–3655. https://doi.org/10.1021/nn900540a.

(104) Kim, J. P.; Lee, B. Y.; Lee, J.; Hong, S.; Sim, S. J. Enhancement of Sensitivity

and Specificity by Surface Modification of Carbon Nanotubes in Diagnosis of Prostate Cancer Based on Carbon Nanotube Field Effect Transistors. *Biosens. Bioelectron.* **2009**, *24* (11), 3372–3378. https://doi.org/10.1016/j.bios.2009.04.048.

(105) Vijayaraghavan, A.; Oron-Carl, M.; Blatt, S.; Vijayaraghavan, A.; Blatt, S.; Weissenberger, D.; Weissenberger, D.; Oron-Carl, M.; Hennrich, F.; Hennrich, F.; Gerthsen, D.; Hahn, H.; Gerthsen, D.; Hahn, H.; Krupke, R.; Krupke, R. Ultra-Large-Scale Directed Assembly of Single-Walled Carbon Nanotube Devices. Supporting Information. *Nano Lett.* **2007**, *7* (6), 1556–1560. https://doi.org/10.1021/nl0703727.

(106) Pohl, H. A. The Motion and Precipitation of Suspensoids in Divergent Electric Fields. *J. Appl. Phys.* **1951**, *22* (7), 869–871. https://doi.org/10.1063/1.1700065.

(107) Pohl, H. A. Some Effects of Nonuniform Fields on Dielectrics. *J. Appl. Phys.* **1958**, *29* (8), 1182–1188. https://doi.org/10.1063/1.1723398.

(108) Dielectrophoresis and Magnetophoresis. In *Electromechanics of Particles*; Jones, T. B., Ed.; Cambridge University Press: Cambridge, 1995; pp 34–82. https://doi.org/DOI: 10.1017/CBO9780511574498.005.

(109) Krupke, R.; Hennrich, F.; Kappes, M. M.; Löhneysen, H. V. Surface Conductance Induced Dielectrophoresis of Semiconducting Single-Walled Carbon Nanotubes. *Nano Lett.* **2004**, *4* (8), 1395–1399. https://doi.org/10.1021/nl0493794.

(110) Constantinou, M.; Rigas, G. P.; Castro, F. A.; Stolojan, V.; Hoettges, K. F.; Hughes, M. P.; Adkins, E.; Korgel, B. A.; Shkunov, M. Simultaneous Tunable Selection and Self-Assembly of Si Nanowires from Heterogeneous Feedstock. *ACS Nano* **2016**, *10* (4), 4384–4394. https://doi.org/10.1021/acsnano.6b00005.

(111) Venkatesh, R.; Kundu, S.; Pradhan, A.; Sai, T. P.; Ghosh, A.; Ravishankar, N. Directed Assembly of Ultrathin Gold Nanowires over Large Area by Dielectrophoresis. *Langmuir* **2015**, *31* (33), 9246–9252. https://doi.org/10.1021/acs.langmuir.5b01986.

(112) Yamamoto, K.; Akita, S.; Nakayama, Y. Orientation and Purification of Carbon Nanotubes Using Ac Electrophoresis. *J. Phys. D. Appl. Phys.* **1998**, *31* (8). https://doi.org/10.1088/0022-3727/31/8/002.

(113) Stokes, P.; Khondaker, S. I. Directed Assembly of Solution Processed Single-Walled Carbon Nanotubes via Dielectrophoresis: From Aligned Array to Individual Nanotube Devices. *J. Vac. Sci. Technol. B Microelectron. Nanom. Struct.* **2010**, *28* (6), C6B7. https://doi.org/10.1116/1.3501347.

(114) Separation of Metallic from Semiconducting Single-Walled Carbon Nanotubes Author ( s ): Ralph Krupke , Frank Hennrich , Hilbert V . Löhneysen and Manfred M . Kappes Published by : American Association for the Advancement of Science Stable URL : Http://Www. **2016**, *301* (5631), 344–347.

(115) Bond, V. Theories of Covalent Bonding. **1995**, *2* (11), 8541–8549.

(116) Vijayaraghavan, A. Bottom-up Assembly of Nano-Carbon Devices by Dielectrophoresis. *Phys. Status Solidi Basic Res.* **2013**, *250* (12), 2505–2517. https://doi.org/10.1002/pssb.201300565.

(117) Krupke, R.; Hennrich, F.; Weber, H. B.; Kappes, M. M.; Löhneysen, H. V. Simultaneous Deposition of Metallic Bundles of Single-Walled Carbon Nanotubes Using Ac-Dielectrophoresis. *Nano Lett.* **2003**, *3* (8), 1019–1023. https://doi.org/10.1021/nl0342343.

(118) Blatt, S.; Hennrich, F.; Löhneysen, H. Influence of Structural and Dielectric Anisotropy on the Dielectrophoresis of Single-Walled Carbon Nanotubes.

*Nano …* **2007**.

(119) Naieni, A. K.; Nojeh, A. Effect of Solution Conductivity and Electrode Shape on the Deposition of Carbon Nanotubes from Solution Using Dielectrophoresis. *Nanotechnology* **2012**, *23* (49). https://doi.org/10.1088/0957-4484/23/49/495606.

(120) Ramos, A.; Morgan, H.; Green, N. G.; Castellanos, A. Ac Electrokinetics: A Review of Forces in Microelectrode Structures. *J. Phys. D. Appl. Phys.* **1998**, *31* (18), 2338–2353. https://doi.org/10.1088/0022-3727/31/18/021.

(121) Green, N. G.; Ramost, A.; González, A.; Castellanos, A.; Morgan, H. Electric Field Induced Fluid Flow on Microelectrodes: The Effect of Illumination. *J. Phys. D. Appl. Phys.* **2000**, *33* (2). https://doi.org/10.1088/0022-3727/33/2/102.

(122) Green, N. G.; Ramos, A.; González, A.; Castellanos, A.; Morgan, H. Electrothermally Induced Fluid Flow on Microelectrodes. *J. Electrostat.* **2001**, *53* (2), 71–87. https://doi.org/10.1016/S0304-3886(01)00132-2.

(123) Svensson, J.; Campbell, E. E. B. Schottky Barriers in Carbon Nanotube-Metal Contacts. *J. Appl. Phys.* **2011**, *110* (11). https://doi.org/10.1063/1.3664139.

(124) Heller, I.; Janssens, A. M.; M??nnik, J.; Minot, E. D.; Lemay, S. G.; Dekker, C. Identifying the Mechanism of Biosensing with Carbon Nanotube Transistors. *Nano Lett.* **2008**, *8* (2), 591–595. https://doi.org/10.1021/nl072996i.

(125) Shekhar, S.; Stokes, P.; Khondaker, S. I. Ultrahigh Density Alignment of Carbon Nanotube Arrays by Dielectrophoresis. *ACS Nano* **2011**, *5* (3), 1739–1746. https://doi.org/10.1021/nn102305z.

(126) Monica, A. H.; Papadakis, S. J.; Osiander, R.; Paranjape, M. Wafer-Level Assembly of Carbon Nanotube Networks Using Dielectrophoresis. *Nanotechnology* **2008**, *19* (8). https://doi.org/10.1088/0957-4484/19/8/085303.

(127) Cha, M.; Jung, S.; Cha, M. H.; Kim, G.; Ihm, J.; Lee, J. Reversible Metal− Semiconductor Transition of SsDNA-Decorated Single-Walled Carbon Nanotubes. *Nano Lett.* **2009**, *9* (4), 1345–1349.

(128) Campidelli, S.; Klumpp, C.; Bianco, A.; Guldi, D. M.; Prato, M. Functionalization of CNT: Synthesis and Applications in Photovoltaics and Biology. *J. Phys. Org. Chem.* **2006**, *19* (8–9), 531–539. https://doi.org/10.1002/poc.1052.

(129) Balasubramanian, K.; Burghard, M. Biosensors Based on Carbon Nanotubes. *Anal. Bioanal. Chem.* **2006**, *385* (3), 452–468. https://doi.org/10.1007/s00216-006-0314-8.

(130) Bottini, M.; Rosato, N.; Bottini, N. PEG-Modified Carbon Nanotubes in Biomedicine: Current Status and Challenges Ahead. *Biomacromolecules* **2011**, *12* (10), 3381–3393. https://doi.org/10.1021/bm201020h.

(131) Carbon Nanotubes with DNA Recognition. **2002**, *548* (2000), 2002.

(132) Zhu, J.; McMorrow, J.; Crespo-Otero, R.; Ao, G.; Zheng, M.; Gillin, W. P.; Palma, M. Solution-Processable Carbon Nanoelectrodes for Single-Molecule Investigations. *J. Am. Chem. Soc.* **2016**, *138* (9), 2905–2908. https://doi.org/10.1021/jacs.5b12086.

(133) Palma, M.; Wang, W.; Penzo, E.; Brathwaite, J.; Zheng, M.; Hone, J.; Nuckolls, C.; Wind, S. J. Controlled Formation of Carbon Nanotube Junctions via Linker-Induced Assembly in Aqueous Solution. *J. Am. Chem. Soc.* **2013**, *135* (23), 8440–8443. https://doi.org/10.1021/ja4018072.

(134) Freeley, M.; Worthy, H. L.; Ahmed, R.; Bowen, B.; Watkins, D.; Macdonald, J. E.; Zheng, M.; Jones, D. D.; Palma, M. Site-Specific One-to-One Click Coupling of Single Proteins to Individual Carbon Nanotubes: A Single-Molecule

Approach. *J. Am. Chem. Soc.* **2017**, *139* (49), 17834–17840. https://doi.org/10.1021/jacs.7b07362.

(135) Freeley, M.; Attanzio, A.; Cecconello, A.; Amoroso, G.; Clement, P.; Fernandez, G.; Gesuele, F.; Palma, M. Tuning the Coupling in Single-Molecule Heterostructures: DNA-Programmed and Reconfigurable Carbon Nanotube-Based Nanohybrids. *Adv. Sci.* **2018**, *5* (10). https://doi.org/10.1002/advs.201800596.

(136) Attanzio, A.; Sapelkin, A.; Gesuele, F.; van der Zande, A.; Gillin, W. P.; Zheng, M.; Palma, M. Carbon Nanotube-Quantum Dot Nanohybrids: Coupling with Single-Particle Control in Aqueous Solution. *Small* **2017**, *13* (16), 1–5. https://doi.org/10.1002/smll.201603042.

(137) Feng, W.; Ji, P. Enzymes Immobilized on Carbon Nanotubes. *Biotechnol. Adv.* **2011**, *29* (6), 889–895. https://doi.org/10.1016/j.biotechadv.2011.07.007.

(138) Tuncel, D. Non-Covalent Interactions between Carbon Nanotubes and Conjugated Polymers. *Nanoscale* **2011**, *3* (9), 3545–3554. https://doi.org/10.1039/c1nr10338e.

(139) Harvey, J. D.; Jena, P. V.; Baker, H. A.; Zerze, G. H.; Williams, R. M.; Galassi, T. V.; Roxbury, D.; Mittal, J.; Heller, D. A. A Carbon Nanotube Reporter of MicroRNA Hybridization Events in Vivo. *Nat. Biomed. Eng.* **2017**, *1* (4), 0041. https://doi.org/10.1038/s41551-017-0041.

(140) Landry, M. P.; Ando, H.; Chen, A. Y.; Cao, J.; Kottadiel, V. I.; Chio, L.; Yang, D.; Dong, J.; Lu, T. K.; Strano, M. S. Single-Molecule Detection of Protein Efflux from Microorganisms Using Fluorescent Single-Walled Carbon Nanotube Sensor Arrays. *Nat. Nanotechnol.* **2017**, *12* (4), 368–377. https://doi.org/10.1038/nnano.2016.284.

(141) Williams, R. M.; Lee, C.; Heller, D. A. A Fluorescent Carbon Nanotube Sensor Detects the Metastatic Prostate Cancer Biomarker UPA. *ACS Sensors* **2018**, *3* (9), 1838–1845. https://doi.org/10.1021/acssensors.8b00631.

(142) Choi, Y. Single-Molecule Lysozyme Dynamics. *Science (80-. ).* **2012**, *319* (January), 319–325. https://doi.org/10.1126/science.1214824.

(143) Hatada, M.; Tran, T. T.; Tsugawa, W.; Sode, K.; Mulchandani, A. Affinity Sensor for Haemoglobin A1c Based on Single-Walled Carbon Nanotube Field-Effect Transistor and Fructosyl Amino Acid Binding Protein. *Biosens. Bioelectron.* **2019**, *129* (June 2018), 254–259. https://doi.org/10.1016/j.bios.2018.09.069.

(144) Kase, H.; Negishi, R.; Arifuku, M.; Kiyoyanagi, N.; Kobayashi, Y. Biosensor Response from Target Molecules with Inhomogeneous Charge Localization. *J. Appl. Phys.* **2018**, *124* (6). https://doi.org/10.1063/1.5036538.

(145) O'Connell, M. J.; Bachilo, S. H.; Huffman, C. B.; Moore, V. C.; Strano, M. S.; Haroz, E. H.; Rialon, K. L.; Boul, P. J.; Noon, W. H.; Kittrell, C.; Ma, J.; Hauge, R. H.; Weisman, R. B.; Smalley, R. E. Band Gap Fluorescence from Individual Single-Walled Carbon Nanotubes. *Science (80-. ).* **2002**, *297* (5581), 593–596. https://doi.org/10.1126/science.1072631.

(146) Strano, M. S.; Huffman, C. B.; Moore, V. C.; O'Connell, M. J.; Haroz, E. H.; Hubbard, J.; Miller, M.; Rialon, K.; Kittrell, C.; Ramesh, S.; Hauge, R. H.; Smalley, R. E. Reversible, Band-Gap-Selective Protonation of Single-Walled Carbon Nanotubes in Solution. *J. Phys. Chem. B* **2003**, *107* (29), 6979–6985. https://doi.org/10.1021/jp027664a.

(147) Barone, P. W.; Baik, S.; Heller, D. A.; Strano, M. S. Near-Infrared Optical Sensors Based on Single-Walled Carbon Nanotubes. *Nat. Mater.* **2005**, *4* (1),

86–92. https://doi.org/10.1038/nmat1276.

(148) Bachilo, S. M.; Strano, M. S.; Kittrell, C.; Hauge, R. H.; Smalley, R. E.; Weisman, R. B. Structure-Assigned Optical Spectra of Single-Walled Carbon Nanotubes. *Science (80-. ).* **2002**, *298* (5602), 2361–2366. https://doi.org/10.1126/science.1078727.

(149) Heller, D. A.; Jin, H.; Martinez, B. M.; Patel, D.; Miller, B. M.; Yeung, T. K.; Jena, P. V.; Höbartner, C.; Ha, T.; Silverman, S. K.; Strano, M. S. Multimodal Optical Sensing and Analyte Specificity Using Single-Walled Carbon Nanotubes. *Nat. Nanotechnol.* **2009**, *4* (2), 114–120. https://doi.org/10.1038/nnano.2008.369.

(150) Heller, D. A.; Baik, S.; Eurell, T. E.; Strano, M. S. Single-Walled Carbon Nanotube Spectroscopy in Live Cells: Towards Long-Term Labels and Optical Sensors. *Adv. Mater.* **2005**, *17* (23), 2793–2799. https://doi.org/10.1002/adma.200500477.

(151) Cherukuri, P.; Bachilo, S. M.; Litovsky, S. H.; Weisman, R. B. Near-Infrared Fluorescence Microscopy of Single-Walled Carbon Nanotubes in Phagocytic Cells. *J. Am. Chem. Soc.* **2004**, *126* (48), 15638–15639. https://doi.org/10.1021/ja0466311.

(152) Kruss, S.; Hilmer, A. J.; Zhang, J.; Reuel, N. F.; Mu, B.; Strano, M. S. Carbon Nanotubes as Optical Biomedical Sensors. *Adv. Drug Deliv. Rev.* **2013**, *65* (15), 1933–1950. https://doi.org/10.1016/j.addr.2013.07.015.

(153) Jeng, E. S.; Moll, A. E.; Roy, A. C.; Gastala, J. B.; Strano, M. S. Detection of DNA Hybridization Using the Near-Infrared Band-Gap Fluorescence of Single-Walled Carbon Nanotubes. *Nano Lett.* **2006**, *6* (3), 371–375. https://doi.org/10.1021/nl051829k.

(154) Jeng, E. S.; Nelson, J. D.; Prather, K. L. J.; Strano, M. S. Detection of a Single Nucleotide Polymorphism Using Single-Walled Carbon-Nanotube near-Infrared Fluorescence. *Small* **2010**, *6* (1), 40–43. https://doi.org/10.1002/smll.200900944.

(155) Jeng, E. S.; Barone, P. W.; Nelson, J. D.; Strano, M. S. Hybridization Kinetics and Thermodynamics of DNA Adsorbed to Individually Dispersed Single-Walled Carbon Nanotubes. *Small* **2007**, *3* (9), 1602–1609. https://doi.org/10.1002/smll.200700141.

(156) Chen, Z.; Tabakman, S. M.; Goodwin, A. P.; Kattah, M. G.; Daranciang, D.; Wang, X.; Zhang, G.; Li, X.; Liu, Z.; Utz, P. J.; Jiang, K.; Fan, S.; Dai, H. Protein Microarrays with Carbon Nanotubes as Multicolor Raman Labels. *Nat. Biotechnol.* **2008**, *26* (11), 1285–1292. https://doi.org/10.1038/nbt.1501.

(157) Gruner, G. Carbon Nanotube Transistors for Biosensing Applications. *Anal. Bioanal. Chem.* **2006**, *384* (2), 322–335. https://doi.org/10.1007/s00216-005-3400-4.

(158) Come, T. H. Ech Ight. *Science (80-. ).* **2002**, *296* (April), 64–65.

(159) Allen, B. L.; Kichambare, P. D.; Star, A. Carbon Nanotube Field-Effect-Transistor-Based Biosensors. *Adv. Mater.* **2007**, *19* (11), 1439–1451. https://doi.org/10.1002/adma.200602043.

(160) Yang, N.; Chen, X.; Ren, T.; Zhang, P.; Yang, D. Carbon Nanotube Based Biosensors. *Sensors Actuators, B Chem.* **2015**, *207* (PartA), 690–715. https://doi.org/10.1016/j.snb.2014.10.040.

(161) Maroto, A.; Balasubramanian, K.; Burghard, M.; Kern, K. Functionalized Metallic Carbon Nanotube Devices for PH Sensing. *ChemPhysChem* **2007**, *8* (2), 220–223. https://doi.org/10.1002/cphc.200600498.

(162) Zhao, Y.-L.; Hu, L.; Stoddart, J. F.; Grüner, G. Pyrenecyclodextrin-Decorated

Single-Walled Carbon Nanotube Field-Effect Transistors as Chemical Sensors. *Adv. Mater.* **2008**, *20* (10), 1910–1915. https://doi.org/10.1002/adma.200702804.

(163) Martínez, M. T.; Tseng, Y. C.; González, M.; Bokor, J. Streptavidin as CNTs and DNA Linker for the Specific Electronic and Optical Detection of DNA Hybridization. *J. Phys. Chem. C* **2012**, *116* (42), 22579–22586. https://doi.org/10.1021/jp306535d.

(164) Ordinario, D. D.; Burke, A. M.; Phan, L.; Jocson, J.-M.; Wang, H.; Dickson, M. N.; Gorodetsky, A. A. Sequence Specific Detection of Restriction Enzymes at DNA-Modified Carbon Nanotube Field Effect Transistors. *Anal. Chem.* **2014**, *86* (17), 8628–8633. https://doi.org/10.1021/ac501441d.

(165) Chen, R. J.; Choi, H. C.; Bangsaruntip, S.; Yenilmez, E.; Tang, X.; Wang, Q.; Chang, Y. L.; Dai, H. An Investigation of the Mechanisms of Electronic Sensing of Protein Adsorption on Carbon Nanotube Devices. *J. Am. Chem. Soc.* **2004**, *126* (5), 1563–1568. https://doi.org/10.1021/ja038702m.

(166) Byon, H. R.; Choi, H. C. Network Single-Walled Carbon Nanotube-Field Effect Transistors (SWNT-FETs) with Increased Schottky Contact Area for Highly Sensitive Biosensor Applications. *J. Am. Chem. Soc.* **2006**, *128* (7), 2188–2189. https://doi.org/10.1021/ja056897n.

(167) Balavoine, F.; Schultz, P.; Richard, C.; Mallouh, V.; Ebbesen, T. W.; Mioskowski, C. Helical Crystallization of Proteins on Carbon Nanotubes: A First Step towards the Development of New Biosensors. *Angew. Chemie - Int. Ed.* **1999**, *38* (13–14), 1912–1915. https://doi.org/10.1002/(SICI)1521-3773(19990712)38:13/14<1912::AID-ANIE1912>3.0.CO;2-2.

(168) So, H. M.; Won, K.; Kim, Y. H.; Kim, B. K.; Ryu, B. H.; Na, P. S.; Kim, H.; Lee, J. O. Single-Walled Carbon Nanotube Biosensors Using Aptamers as

Molecular.Pdf. *J. Am. Chem. Soc.* **2005**, *127* (34), 11906–11907. https://doi.org/10.1021/ja053094r.

(169) Khosravi, F.; Loeian, S. M.; Panchapakesan, B. Ultrasensitive Label-Free Sensing of IL-6 Based on PASE Functionalized Carbon Nanotube Micro-Arrays with RNA-Aptamers as Molecular Recognition Elements. *Biosensors* **2017**, *7* (2). https://doi.org/10.3390/bios7020017.

(170) Bradley, K.; Gabriel, J. C. P.; Briman, M.; Star, A.; Grüner, G. Charge Transfer from Ammonia Physisorbed on Nanotubes. *Phys. Rev. Lett.* **2003**, *91* (21), 1–4. https://doi.org/10.1103/PhysRevLett.91.218301.

(171) Star, A.; Han, T. R.; Gabriel, J. C. P.; Bradley, K.; Grüner, G. Interaction of Aromatic Compounds with Carbon Nanotubes: Correlation to the Hammett Parameter of the Substituent and Measured Carbon Nanotube FET Response. *Nano Lett.* **2003**, *3* (10), 1421–1423. https://doi.org/10.1021/nl0346833.

(172) Hecht, D. S.; Ramirez, R. J. A.; Briman, M.; Artukovic, E.; Chichak, K. S.; Stoddart, J. F.; Grüner, G. Bioinspired Detection of Light Using a Porphyrin-Sensitized Single-Wall Nanotube Field Effect Transistor. *Nano Lett.* **2006**, *6* (9), 2031–2036. https://doi.org/10.1021/nl061231s.

(173) Artyukhin, A. B.; Stadermann, M.; Friddle, R. W.; Stroeve, P.; Bakajin, O.; Noy, A. Controlled Electrostatic Gating of Carbon Nanotube FET Devices. *Nano Lett.* **2006**, *6* (9), 2080–2085. https://doi.org/10.1021/nl061343j.

(174) Tang, X.; Bansaruntip, S.; Nakayama, N.; Yenilmez, E.; Chang, Y. I.; Wang, Q. Carbon Nanotube DNA Sensor and Sensing Mechanism. *Nano Lett.* **2006**, *6* (8), 1632–1636. https://doi.org/10.1021/nl060613v.

(175) Stern, E.; Wagner, R.; Sigworth, F. J.; Breaker, R.; Fahmy, T. M.; Reed, M. A. Importance of the Debye Screening Length on Nanowire Field Effect Transistor

Sensors. *Nano Lett.* **2007**, *7* (11), 3405–3409. https://doi.org/10.1021/nl071792z.

(176) Israelachvili, J. N. Intermolecular and Surface Forces . 2nd ed. Academic : London 1992.

(177) Vacic, A.; Criscione, J. M.; Rajan, N. K.; Stern, E.; Fahmy, T. M.; Reed, M. A. Determination of Molecular Configuration by Debye Length Modulation. *J. Am. Chem. Soc.* **2011**, *133* (35), 13886–13889. https://doi.org/10.1021/ja205684a.

(178) Maehashi, K.; Katsura, T.; Kerman, K.; Takamura, Y.; Matsumoto, K.; Tamiya, E. Label-Free Protein Biosensor Based on Aptamer-Modified Carbon Nanotube Field-Effect Transistors. *Anal. Chem.* **2007**, *79* (2), 782–787. https://doi.org/10.1021/ac060830g.

(179) Wasik, D.; Mulchandani, A.; Yates, M. V. A Heparin-Functionalized Carbon Nanotube-Based Affinity Biosensor for Dengue Virus. *Biosens. Bioelectron.* **2017**, *91* (November 2016), 811–816. https://doi.org/10.1016/j.bios.2017.01.017.

(180) Tan, F.; Saucedo, N. M.; Ramnani, P.; Mulchandani, A. Label-Free Electrical Immunosensor for Highly Sensitive and Specific Detection of Microcystin-LR in Water Samples. *Environ. Sci. Technol.* **2015**, *49* (15), 9256–9263. https://doi.org/10.1021/acs.est.5b01674.

(181) Tung, N. T.; Tue, P. T.; Thi, T.; Lien, N.; Ohno, Y. Peptide Aptamer-Modified Single- Walled Carbon Nanotube-Based Transistors for High-Performance Biosensors. **2017**, No. September, 1–9. https://doi.org/10.1038/s41598-017-18169-1.

(182) De Vico, L.; Iversen, L.; Sørensen, M. H.; Brandbyge, M.; Nygård, J.; Martinez, K. L.; Jensen, J. H. Predicting and Rationalizing the Effect of Surface Charge Distribution and Orientation on Nano-Wire Based FET Bio-Sensors. *Nanoscale*

**2011**, *3* (9), 3635–3640. https://doi.org/10.1039/c1nr10316d.

# Chapter 2 Experimental Techniques

## 2.1 Materials

2-[Methoxy(polyethyleneoxy)6-9propyl]trimethoxysilane (PEG-silane) was purchased from Fluorochem. Ltd. Steroid free serum was purchased from MP Biomedicals, Inc. Dulbecco's phosphate buffered saline (DPBS) was purchased from Thermo Scientific. All DNA sequences were obtained from Integrated DNA Technologies. Cortisol binding aptamer, Neuropeptide Y (NPY) binding aptamer and dehydroepiandrosterone sulfate (DHEAS) binding aptamer were already functionalized with an azide group on the 5' terminal position (via N-hydroxysuccinimide ester reaction). The final sequences of the three aptamers are:

Cortisol aptamer: 5'-azide-GGA ATG GAT CCA CAT CCA TGG ATG GGC AAT GCG GGG TGG AGA ATG GTT GCC GCA CTT CGG CTT CAC TGC AGA CTT GAC GAA GCT T-3'

NPY aptamer: 5'-azide-AGC AGC ACA GAG GTC AGA TGC AAA CCA CAG CCT GAG TGG TTA GCG TAT GTC ATT TAC GGA CCT ATG CGT GCT ACC GTG AA-3'

DHEAS aptamer: 5'-azide-CTG CTC TCG GGA CGT GGA TTT TCC GCA TAC GAA GTT GTC CCG AG-3'

The sequence of the DNA complementary to cortisol aptamer is 5'-AAG CTT CGT CAA GTC TGC AGT GAA GCC GAA GTG CGG CAA CCA TTC TCC ACC CCG CAT TGC CCA TCC ATG GAT GTG GAT CCA TTC C-3'.

For the non-complementary control experiment, the sequence of the non-

complementary DNA is 5'-GAT TCA GCA ATT AAG CTC TAA GCG ATC CGC AAC ACT GAC CTC TTA TCA AAA GGA GCA ATT AAA GGT ACT CTC TAA TCC TGA CGG G -3'.

Metallic SWCNTs and 95% semiconducting SWNCTs were purchased from NanoIntegris. Dextran (DX), polyethylene glycol (PEG), and poly-vinylpyrrolidone (PVP) were purchased from Alfa Aesar. Qdot 585 Streptavidin Conjugates (streptavidin-wrapped QDs) were obtained from Thermo Scientific. Au/Cr Nanoelectrodes on silicon wafers, patterned with via electron beam lithography, were purchased from Con-Science. HiPco SWCNTs, CoMoCAT SWCNT, (7,6), (6,5) enriched SWCNTs and other chemicals were purchased from Sigma-Aldrich.

## 2.2 Spectroscopic Techniques

### 2.2.1 Ultraviolet-visible Spectroscopy

Ultraviolet-visible Spectroscopy was performed using an Agilent Cary 100 UV-Vis. Generally, 50 μL solution samples were placed in a Hellma quartz cuvette with a light path of 3×3mm.

### 2.2.2 High Performance Liquid Chromatography

High performance liquid chromatography was performed using an Agilent 1100 series. Modified DNA (in Chapter 3) was purified with a Water XBrige Oligonucleotide BEH C18 Column in triethylammonium acetate buffer and acetonitrile.

## 2.3 Chemical Techniques

### 2.3.1 Carbon Nanotube Dispersion

To prepare SWCNT devices via solution processable methods, I needed to prepare

SWCNT solutions first. In Chapter 3 and 6, DNA-wrapped SWCNTs were used. In Chapter 4 and 5, SWCNTs were dispersed in SDS solution. All the SWCNTs I used in this thesis are commercially available, hence reducing the costs of the experiments.

Wrapping SWCNT with DNA, hence making them water-soluble, is an established procedure[1]. Briefly, 1mg of (7,6) enriched ((6,5) enriched) SWCNT was suspended in 1mL of 1mg/mL aqueous DNA solution (the DNA sequence is $(GTT)_3G$, $(GTT)_3G$ terminated with amine groups ($(GTT)_3G$-amine) or $(GT)_{20}$, 0.1M NaCl). The mixture was sonicated in an ice water bath for 60 minutes at a power of 3W (*Sonics, VC130PB*). Subsequently, the solution was centrifuged for 60 minutes at 13K rpm (*Eppendorf 5415C*) to precipitate undispersed SWCNTs. The supernatant was collected and stored as the stock SWCNT solution (labelled with DNA-(7,6) CNT).

SDS is an optimal surfactant which helps disperse SWCNTs in water. Generally, 0.1 mg of 95% semiconducting SWCNT was suspended in 0.5 mL of 1wt% SDS solution. The mixture was sonicated for 60 minutes in an ice water bath. After sonication, the mixture was centrifuged for 60 minutes to remove undispersed SWCNTs. The supernatant was collected and stored as the stock SWCNT solution (labelled with SDS-95S).

### 2.3.2 Carbon nanotube-aptamer Hybrids Formation

In chapter 3, I prepared SWCNT-aptamer hybrids. In detail, 1.0 mg (1R,8S,9s)-Bicyclo[6.1.0]non-4-yn-9-ylmethyl N-succinimidyl carbonate (BCN-NHS) was dissolved in 42 µL dimethyl sulfoxide (DMSO), then diluted with 225 µL phosphate buffer (0.1 M, pH 9). 12 µL of 25 mg/mL of $(GTT)_3G$-amine was added to the solution, and additional water (*MilliQ*) was added to get the total volume of 300 µL. After overnight incubation at room temperature, ethanol precipitation was used to remove

free BCN-NHS. 30 µL NaCl (3 M) and 825 µL ethanol (95%) were added to the mixture, kept in the freezer for 2 h and then centrifuged at 13 K rpm for 30 mins. The precipitation was washed with 70% cold ethanol (-20 ℃). After being dried, the modified DNA ($(GTT)_3$G-BCN) was re-dissolved in 0.1 M NaCl. Subsequently, 3 KDa Amicon filter (*Millipore*) was used to further remove free BCN-NHS by centrifugation at 13K rpm for 10 mins three times. The final solution was diluted with 0.1 M NaCl and the volume was kept to 300 µL.

0.2 mg (7,6) enriched SWCNTs were dispersed into the as prepared $(GTT)_3$G-BCN solution (300 µL) by sonication for 30 mins. The mixture was centrifuged at 13K rpm for 30 mins to remove unwrapped SWCNTs.

For the functionalization of SWCNT with aptamers, typically, 6 µL of as prepared SWCNT solution was mixed with 2 µL aptamer solution (100 µM) and 12 µL DPBS was added to the mixture. Then, the mixture was incubated at 37 ℃ overnight. After the reaction, the mixture was dialysed against water using Slide-A-Lyzer™ MINI Dialysis Devices with a 20 kDa cut-off (purchased from Thermo Scientific) overnight to remove free aptamers.

### 2.3.3 Attachment of Proteins to Carbon Nanotube Devices

In chapter 4, proteins were attached to SWCNT devices. In detail, 0.4 mg pyrene-NHS and 0.5 mg DBCO-amine were dissolved and mixed in 200 µL DMF to give a solution containing 5 mM of pyrene-NHS and 9mM of DBCO-amine. The mixture was placed on a shaker overnight at room temperature to form DBCO-pyrene. Subsequently, 10 µL ethanol-amine was added to the mixture to block unreacted NHS groups.

The prepared devices were immersed in the mixture solution for 1h. DBCO-pyrene would be immobilised onto the sidewall of SWCNT bundles via π-π stacking between

pyrene and SWCNTs. The devices were rinsed with iso-propanol and DPBS buffer after incubation. Subsequently, 20 μL azide modified BLIP variants (200 nM, in DPBS) were cast on the devices. After overnight incubation, the devices were rinsed with water and blown dried with nitrogen gas for atomic force microscopy (AFM) imaging.

### 2.3.4 Synthesis of Metal Precursor Filled SWCNTs

Our collaborator, the Thomas group, synthesized the metal precursor filled SWCNTs ($M(acac)_2$@SWCNT) for this experiment. In a general method, metal precursor ($M(acac)_2$, 90 mg, where M = Pt, Cu or a mixture of Pt:Cu in a 1:1 ratio of atomic %) and freshly opened SWCNTs (25 mg) were sealed together under vacuum (10-3 mbar) in a Pyrex ampoule and heated at 150 $^{o}$C for 3 days to ensure penetration of the SWCNTs by the $M(acac)_2$. The ampoule was cooled rapidly in ice-water and repetitive washing with dichloromethane (4×25 mL) was performed, followed by filtration to remove any excess material from the exterior of the SWCNT, forming $M(acac)_2$@SWCNT. Under an atmosphere of argon, $M(acac)_2$@SWCNT (10 mg) was heated at 500 $^{o}$C for 1 h and allowed to cool down slowly forming M@SWCNT.

### 2.3.5 Separation of Single Chirality SWCNTs

My colleagues, Zamaan and Giuseppe performed the separation of single chirality SWCNTs following a previously published strategy.[2] SWCNT mixture wrapped with DNA sequence ($(CCG)_2CC$) was added to a polyethylene glycol/dextran (PEG/DX) ATP system. After vortex and centrifuge, (6,5) species was enriched in the DX-rich bottom phase. The DX-rich bottom phase and SWCNTs residing in it were collected as the starting materials for further purification. A blank PEG/DX was added to the bottom phase, forming a new ATP system. Poly(vinylpyrrolidone) (PVP) serving as a

modulating agent was added to the ATP system to further facilitate the separation. After repeating the purification process, highly enriched (6,5) species was obtained.

(7,5) species was separated and purified via a similar process. Briefly, the SWCNT mixture was initially wrapped with DNA sequence $(ATT)_4$. Subsequently, the DNA wrapped SWCNT mixture was subsequently added to a (PEG + poly(ethylene glycol) diamine (PEG-DA))/DX system. After vortex and centrifuge, DX-rich bottom phase, in which (7,5) species was enriched, was collected as the starting materials for further purification. By repeating the purification process, highly enriched (7,5) species was obtained.

## 2.4 Sample deposition

### 2.4.1 Deposition of Carbon Nanotubes

To deposit samples on a mica substrate, a mica disc was freshly cleaved three to five times with sticky tape and 50 μL of 1M $MgSO_4$ was cast on the substrate. After a few minutes incubation, the mica was blown dried with compressed air. Subsequently, 20 μL of the SWCNT solution was cast on the mica and incubated for 20 minutes. The substrate was then rinsed with water and dried with compressed air.

For deposition on a silicon substrate, a silicon wafer was diced into 1×1 $cm^2$ chips. These chips were immersed in acetone and sonicated for 10 minutes, followed by rinsing with ethanol and water and blown dried with compressed air. Subsequently, these chips were exposed to oxygen plasma for 5 minutes on high power. 20 μL of the SWCNT solution was cast on the chips and incubated for 20 minutes. The substrate was then rinsed with water and dried with compressed air.

### 2.4.2 Immobilisation of Carbon Nanotubes Between Electrodes

Dielectrophoresis (DEP) was performed to immobilise SWCNTs between prepatterned gold electrodes by applying an alternating current (AC) voltage between the electrode pairs after having cast the SWCNT solution on the electrodes. Gold is chosen since it is chemically stable, hence I can perform chemical reactions on these electrodes. Cr is the adhesion layer to increase the affinity between gold and the silicon substrate.

By tuning the parameters of DEP, such as the amplitude and frequency of the AC voltage, the duration of DEP and the concertation of the SWCNT solution, I can control the immobilization between one to few tens of CNTs bridging the electrodes. The frequency of the AC voltage mainly determines the type of CNTs (semiconducting or metallic) immobilised between electrodes. Therefore, AC voltage of $f$ = 400 or 500 KHz was used to immobilise a mixture of semiconducting and metallic tubes while AC voltage of $f$ = 5 MHz was used to immobilise metallic tubes. To simplify the process of DEP optimisation, the AC voltage was set in the range of 2-6 V, and the duration of DEP was set in the range of 20-60 s. AFM was used to check the results of DEP (whether CNTs were immobilised or how large the CNT bundles are). Therefore, to optimise DEP parameters is to control the concentration of CNT solution: if there are no CNTs immobilised (the number of CNTs are not enough), I would increase the concentration of CNT solution; if there are big bundles of CNTs, I would decrease the concentration of CNT solution. Similarly, I can also increase the AC voltage or duration of DEP to immobilise more CNTs.

In Chapter 3, I used DNA wrapped SWCNTs and I preferred semiconducting SWCNTs bridging the gap. Therefore, the frequency of the generator was switched onto typically $V_{p\text{-}p}$ = 3V at $f$ = 400 KHz; a drop of CNT-aptamer hybrids solution (5 µL, ~100 ng/mL) was cast to the chip with a pipette. After a delay of typically 30 seconds, the substrate

was washed with water and blown gently with nitrogen gas.

In chapter 4, 95% semiconducting SWCNTs were dispersed in SDS aqueous solution. To immobilise a small bundle of SWCNTs between electrodes, DEP was performed by applying an AC voltage between electrodes after SDS-dispersed SWCNT solution was cast on the electrodes. Typically, the frequency of the generator was switched onto $V_{p-p}$ = 3 V at $f$ = 400 KHz. The as prepared CNT solution was diluted by 100-fold and cast onto the chip with a pipette (5 μL). After a delay of 10 seconds, the substrate was washed carefully with water to remove SDS and blown gently with nitrogen gas. Electrical measurement was performed to confirm the immobilisation of SWCNTs between electrodes.

In Chapter 5, the copper precursor filled SWCNTs ($Cu(acac)_2$@SWCNT) were dispersed in aqueous SDS solution (1wt%). To immobilise an individual $Cu(acac)_2$@SWCNT via DEP, the stock solution was diluted 40-fold and cast on electrodes with a pipette. The frequency of the AC voltage was switched to typically $V_{p-p}$ = 3 V at $f$ = 500 KHz. After 20 seconds duration, the chip was washed with water and blown gently with nitrogen gas. To immobilize a bundle of $Cu(acac)_2$@SWCNT via DEP, the stock solution was diluted 15-fold and cast onto the electrodes. The frequency of the generator was switched onto typically $V_{p-p}$ = 3 V at $f$ = 500 KHz. After a delay of typically 25 seconds, the substrate was washed with water and blown gently with nitrogen gas.

The method to prepare platinum precursor-filled CNT ($Pt(acac)_2$@SWCNT) (and [$Pt(acac)_2$ + $Cu(acac)_2$]@SWCNT) solution is similar to the method above. However, the final concentration of this SWCNT solution was lower than that of the $Cu(acac)_2$@SWCNT solution after centrifugation. The original solution of $Pt(acac)_2$@SWCNT was diluted 20-fold and cast on electrodes with a pipette to

immobilize an individual SWCNT. The frequency of the generator was switched onto typically $V_{p-p}$ = 3 V at *f* = 500 KHz. After a delay of typically 15 seconds, the substrate was washed with water and blown gently with nitrogen gas. To immobilize a bundle of CNT filled with platinum precursor via DEP, the original solution was diluted 10-fold and cast onto electrodes. After a delay of typically 20 seconds, the substrate was washed with water and blown gently with nitrogen gas.

In chapter 6, I demonstrated the immobilisation of individual SWCNTs. My colleagues, Zamaan and Giuseppe, performed the separation of single chirality semiconducting (6, 5) and (7, 5) species from a mixture. Subsequently, these (6, 5) and (7, 5) were centrifuged against a filter with a 100 KDa cut-off to remove organic polymers dissolved in the solutions.

To immobilise an individual (6, 5) species, the AC voltage of the generator was switched onto typically $V_{p-p}$ = 2 V at *f* = 400 KHz. The as-prepared solution was diluted 100-fold and drop-cast onto the prepatterned electrode pairs with a pipette. After a duration of 15 seconds, the samples were rinsed with water and blow-dried gently with nitrogen gas.

To immobilise an individual (7, 5) species, the AC voltage of the generator was switched onto typically $V_{p-p}$ = 2 V at *f* = 400 KHz. The as-prepared solution was diluted 10-fold and drop-cast onto the prepatterned electrode pairs with a pipette. After a duration of 10 seconds, the samples were rinsed with water and blow-dried gently with nitrogen gas.

To immobilise a metallic SWCNTs, the AC voltage of the generator was switched onto typically $V_{p-p}$ = 2.5 V at *f* = 5 MHz. The as-prepared solution was diluted 80-fold and drop-cast onto the prepatterned electrode pairs with a pipette. After a duration of 10 seconds, the samples were rinsed with water and blow-dried gently with nitrogen gas.

AFM was used to check the diameters of the immobilised SWCNT. If the diameter was in the range of 1-2 nm, we considered this as an individual SWCNT.

Generally, the resistance of the devices containing individual DNA wrapped SWCNTs is very high and we cannot measure the current through these devices. Therefore, to measure the conductance, annealing treatment is required.

I also immobilised metal sulfide-SWCNT (CdS-SWCNT and PbS-SWCNT) hybrids between electrodes for photodetection, which were prepared by my colleague, Qingyu. The hybrids solution was dialysed against water against water using Slide-A-Lyzer™ MINI Dialysis Devices with a 20kDa cut-off to remove ions in solution. Subsequently, the solution was diluted for 5-fold and drop-cast onto the electrodes. AC voltage of $V_{p\text{-}p}$ = 5 V at $f$ = 400 KHz was applied to the electrodes. After a delay of typically 20 seconds, the substrate was washed with water and blown gently with nitrogen gas. Electrical measurement was performed to confirm the deposition of the hybrids.

### 2.4.3 Annealing Treatment

Annealing treatment was performed in a tube furnace under the protection of nitrogen gas at a flow rate of 500 mL/min. The temperature was set to be 200 ℃ with an increase rate of 10 ℃ per minute. After a duration of 1h at 200 ℃, the samples were cooled down to room temperature under the protection of nitrogen gas.

### 2.4.4 Oxygen Plasma Treatment

Oxygen plasma treatment was performed to remove SWCNTs in the samples with a Harrick oxygen plasma cleaner (PDC-32G-2, 18 W).

In chapter 5, I exposed the devices to oxygen plasma to remove SWCNT templates. In detail, I exposed these samples for 10 seconds, and checked their conductivities

afterwards, and repeated this process until the source-drain current ($I_{sd}$) was independent on the gate voltage ($V_g$) (generally, I repeated this process 5-6 times, and the final resistance of the devices was around 10 MΩ). I also immobilized SWCNT bundles (without any precursors) between electrodes as a control experiment. The nanotubes can be easily removed in 20-30 seconds when they were exposed to oxygen plasma.

To reuse the chips patterned with electrodes where SWCNTs had been deposited, I employed sonication combined with oxygen plasma. The chips were immersed in acetone and experienced sonication for 2 mins. This can remove the majority of SWCNTs, but a few residues remained in the gaps. Subsequently, the chips were exposed to oxygen plasma to remove the remaining residues.

## 2.5 Atomic Force Microscopy Techniques

Atomic force microscopy (AFM) is a high-resolution type of scanning probe microscopy (SPM). Using a mechanical probe, AFM allows the scanning of the morphology of surfaces and interfaces with high resolution: vertical resolution on the order of fractions of a nanometer and lateral resolution of a few nanometers.[3]

A typical AFM configuration is shown in Figure 2.1. AFM scans the specimen surface by using a cantilever with a sharp tip (probe) of which the tip radius is usually on the order of nanometers.[4] The cantilever is flexible with a sensitive spring constant. When the tip is approaching the surface, forces between the tip and the sample occur and lead to a deflection of the cantilever, according to Hooke's law.[5] This deflection is monitored by the laser beam, which causes measurable signals in the photodetector. Thus, the deflection of the cantilever can be measured and in turn the force between the tip and the surface. By measuring the force, AFM can provide a 3D profile of the surface at

nanoscale.

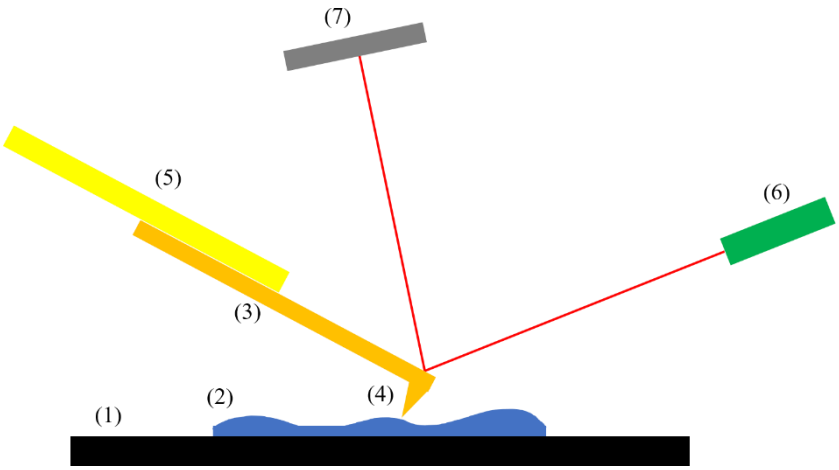


**Figure 2.1** Typical AFM configuration: (1) stage, (2) sample to be measured, (3) cantilever, (4) tip, (5) piezoelectric element (to oscillate cantilever at its frequency), (6) laser beam and (7) photodetector of the deflection and motion of the cantilever.

Different types of forces can be measured in AFM, including mechanical contact force, van der Waals forces, electrostatic forces, magnetic forces and chemical bonding: hence AFM can provide information about various properties of the samples. Herein, we only focus on the measurement based on van der Waals forces.

Generally, the tip-surface interaction is described by the Lennard-Jones potential[6]:

$$U_{LJ} = U_0 \left[ (\frac{r_0}{r})^{12} - 2(\frac{r_0}{r})^6 \right] \quad (1)$$

where $r$ is the tip-surface distance, $r_0$ is the tip-surface distance at which the potential reaches its minimum, and $U_0$ is the minimal value of the potential. Based on the equation, the tip-surface force as a function of distance is shown in Figure 2.2. $(\frac{r_0}{r})^{12}$ can be attributed to the short range repulsive forces, while $(\frac{r_0}{r})^6$ can be attributed to the long range attractive forces. When the tip is in very close proximity to the surface (a few angstrom), a strong repulsive force occurs, which is attributed to the exchange interactions caused by the overlap of the electronic orbitals at atomic distances. When

the tip is moving away from the surface, an attractive force occurs mainly due to van der Waals force.

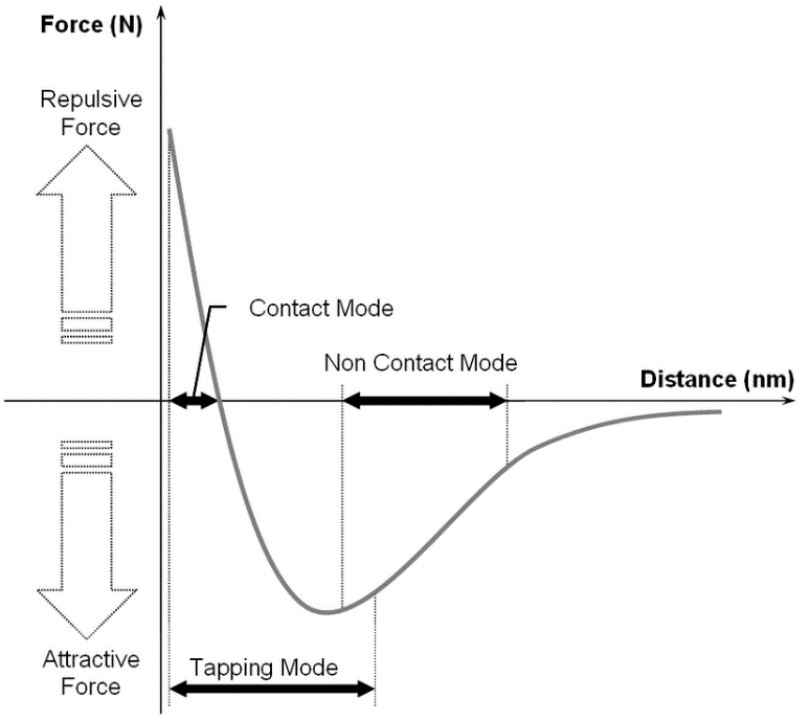


**Figure 2.2** Tip-surface force as a function of distance.[7]

Based on the nature of the tip motion, the AFM working modes can be classified into three types: contact mode, non-contact mode and tapping mode. In contact mode, the tip is kept constant on the surface in the repulsive zone and the contours of the surface are commonly measured using the feedback signal required to keep the cantilever at a constant position. In non-contact mode, the tip does not contact the surface, but instead oscillates at the resonant frequency in the attractive zone. When the tip is approaching the surface, the van der Waals forces cause decrease in the resonance frequency of the cantilever. This decrease combined with the feedback loop system maintains the constant oscillation amplitude by adjusting the tip-to-sample distance. Thus, topographic images of the sample surface can be constructed by measuring the tip-to-sample distance.

Tapping mode is the most frequently used AFM mode. In tapping mode, the cantilever is driven to oscillate up and down at or near its resonance frequency. The frequency and amplitude of the driving signal are kept constant, resulting in a constant amplitude of the cantilever oscillation as long as there is no interaction between the tip and surface. When the tip is approaching the surface, the force between the tip and surface cause decreases in the oscillation amplitude. This amplitude is used as the parameter to control the distance of the cantilever to the surface to maintain the cantilever oscillation amplitude. Therefore, an AFM image can be produced by imaging the force of the intermittent contacts between the tip and the surface. Thanks to the oscillating contact, tapping mode can achieve a higher lateral resolution compared to non-contact mode, and does not damage "soft" surfaces which may occur in contact mode.

Figure 2.3 shows a typically graph of tip-surface force as a function of time at a pixel.[8] When the tip is approaching the surface, attractive force dominates and reaches the peak at point B. As the tip continues approaching, attractive force decreases while repulsive force starts to dominate and reaches the peak at point C. Similar phenomena can be observed when the tip is withdrawing from the surface. The force at point D is larger than that at point B due to the adhesion of the tip to the surface before being withdrawn.

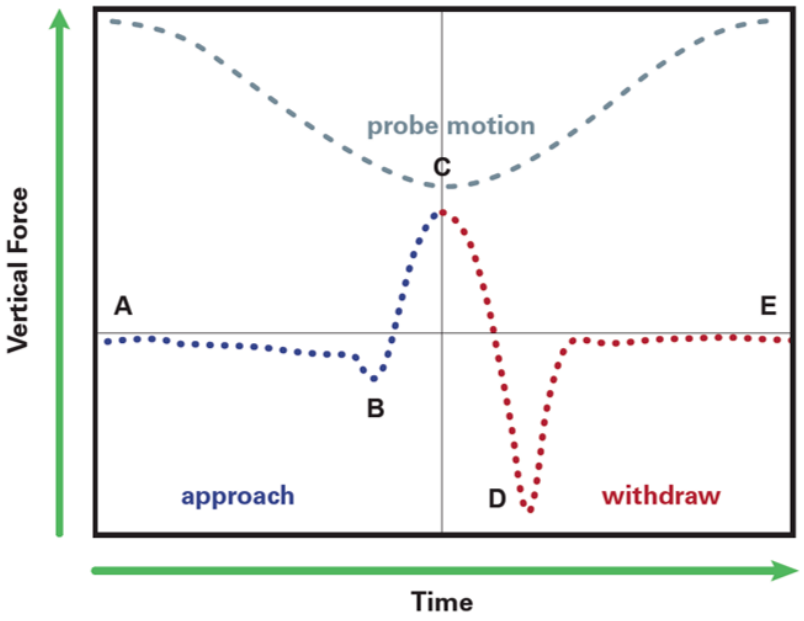


**Figure 2.3** Tip-surface force as a function of time of An AFM tip approaching and withdrawing from the surface: A and E refer to the force at approach and withdraw, B represents the initial contact with the surface, C denotes the peak force and D denotes the adhesion of the tip to the surface before being withdrawn.[8]

In this work, Peak Force Tapping was the main approach to image AFM samples, in which the peak force for each measurement is used as the feedback signal to create the AFM image. A "setpoint" is defined to tell the feedback loop what amplitude to maintain during scanning. Peak Force Tapping is particularly useful since the force can be precisely controlled which allows lower forces to be used compared to standard tapping mode, hence allowing the higher resolution scanning of more delicate samples. In this work, the topographic analysis of the electrodes and the SWCNT samples was performed with a Bruker Dimension Icon atomic force microscope (AFM) (Figure 2.4). For measurements in air, silicon nitride ScanAsyst probes with a spring constant of 0.4 N/m from Bruker were used. Generally, the frequency of the sample scanning was around 1 Hz per line with a setpoint of 0.03 V.

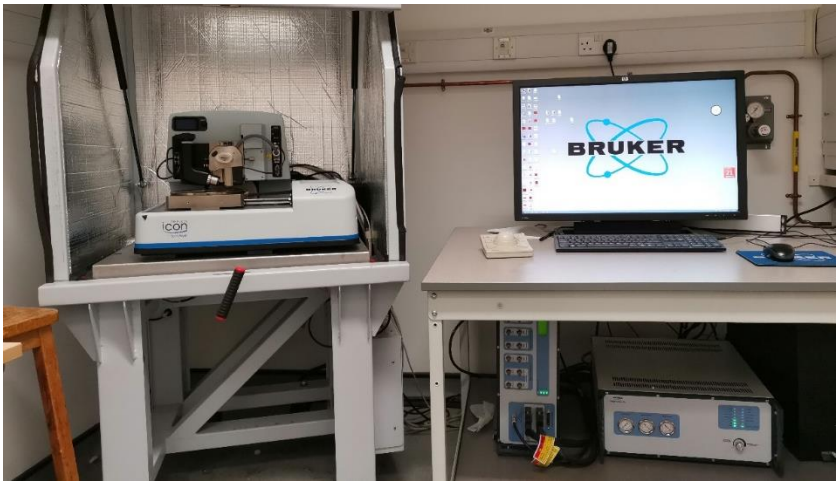


**Figure 2.4** Image of the Bruker Dimension Icon AFM system

## 2.6 Electrical Measurements

Electrical measurements were performed using a probe station (PS-100, Lakeshore) equipped with a semiconducting parameter analyser (Keithley, 4200SCS) at room temperature (Figure 2.5). The semiconductor parameter analyser can measure and analyse electrical characteristic of different types of semiconductors, electronic devices and materials since it integrates multiple measurement and analysis capabilities. In this work, I used the analyser to perform the current-voltage (I-V) measurement, transfer characteristics (source-drain current versus gate voltage, $I_{sd}$-$V_g$) measurement, and Current-time ($I_{sd}$-t) measurement.

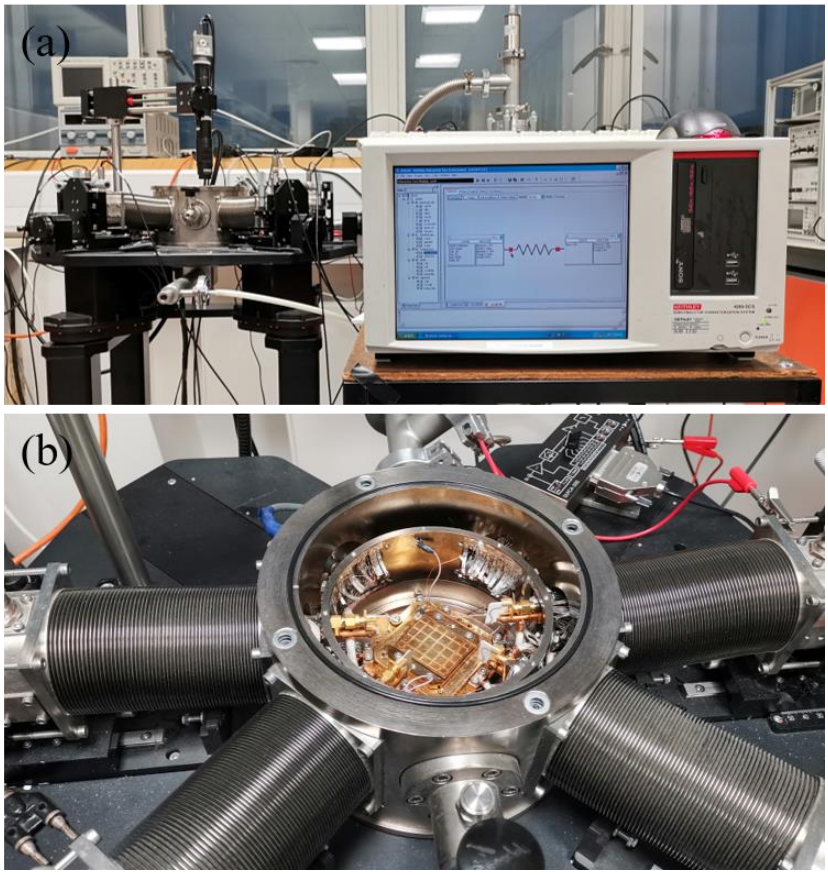


**Figure 2.5** Image of (a) the semiconducting parameter analyser and (b) the probe station.

### 2.6.1 Current versus Voltage Measurement

To measure the current through CNT devices as a function of voltage, two terminals mode was chosen. Devices were placed in the chamber of the probe station and linked to the analyser though cables. Generally, Probe 1 was linked to the separate electrode of the devices while Probe 4 was linked the common electrode of the devices. Probe 1 was set to bias sweeping mode (-1V to 1V) at a step of 0.05 V while Probe 4 was grounded.

### 2.6.2 Transfer Characteristics Measurement

To measure the transfer characteristic of CNT devices, three terminals mode was

chosen. Similarly, devices were placed in the chamber of the probe station and linked to the analyser though cables. I scratched a small area of the surface of the devices to remove the layer of $SiO_2$, which would be used as the backgate electrode. Generally, Probe 1 was set as the source electrode where a fixed voltage was applied (0.1V) and Probe 4 was grounded. Probe 3 was linked to the backgate electrode with a bias sweeping mode from -15V to 15V.

### 2.6.3 Current as a Function of Time Measurement

To measure the I-t trace of CNT devices, three terminals mode was chosen. I linked Probe 1 to the separate electrode and Probe 4 to the common electrode. Probe 1 was set as source electrode where a fixed voltage was applied (0.1V) and Probe 4 was grounded. Probe 2 was linked to the backgate of the substrate and grounded.

In the real time detections in chapter 3 and 4, analyte solutions were added to the devices when the analyser was recording the current through the devices. In the photodetection in chapter 6, lasers of different wavelength (typically, red, green and blue) were shined to the devices when the analyser was recording the current through the devices.

## References

(1) Zheng, M.; Jagota, A.; Semke, E. D.; Diner, B. A.; McLean, R. S.; Lustig, S. R.; Richardson, R. E.; Tassi, N. G. DNA-Assisted Dispersion and Separation of Carbon Nanotubes. *Nat. Mater.* **2003**, *2* (5), 338–342.

(2) Pam, P. E. G. DNA-Controlled Partition of Carbon Nanotubes in Polymer Aqueous Two-Phase Systems. **2014**.

(3) Note, M.; Resolution, U.; The, A. Ultimate Resolution of AFM in Air (2005-10-

26).Pub. *100*, 1–2.

(4) Markiewicz, P.; Goh, M. C. Atomic Force Microscopy Probe Tip Visualization and Improvement of Images Using a Simple Deconvolution Procedure. *Langmuir* **1994**, *10* (1), 5–7.

(5) Cappella, B.; Dietler, G. Force-Distance Curves by Atomic Force Microscopy. *Surf. Sci. Rep.* **1999**, *34* (1–3), 1–3. https://doi.org/10.1016/S0167-5729(99)00003-5.

(6) Mironov, V. L. Fundamentals of Scanning Probe Microscopy. *Russ. Acad. Sci. Inst. Phys. Microstruct.* **2004**, 1–95.

(7) You, L.; You, L.; Ramonda, M. M. Es Optimisation de La Mesure Du Travail de Sortie Par Microscopie à Sonde Locale Sous Vide : Application Aux Dispositifs Avancés. **2013**.

(8) Bruker. PeakForce Tapping PeakForce Tapping How AFM Should Be — for 10 Years and Counting. **2019**.

# Chapter 3 Reconfigurable Carbon Nanotube Multiplexed Sensing Devices

## 3.1 Introduction

In this chapter, we present a facile strategy for the fabrication of reconfigurable and solution processable nanoscale biosensors for the detection of biomarkers with multi-sensing capability. Biomarkers play important roles in the early detection of disease and physiological dysfunction.[1–4] In this context, miniaturized/portable sensing apparatuses for biomarkers allow for continuous functionality in diagnostic or treatment.[5] Developing a platform for achieving this is of importance to both fundamental biology and practical point of care and home diagnosis, where low-cost processability and multipurpose analysis capability are among the most sort-out features that sensing devices would need to possess.

Many detection methods have been employed so far, from the use of enzymes, to nanoparticles, nanopores, as well as electrochemical and mechanical strategies.[6–13] Notably, biosensing platforms that allow for the simultaneous detection of several types of biotargets on a single platform have been fabricated;[14–17] while these results are promising, challenges still remain in terms of fabrication and power costs, as well as biochip size, mainly due to the top-down fabrication methods employed.

In this regard, electrical detection methodologies based on nanomaterials can offer unique advantages, such as simplicity, low-cost fabrication, and label-free real-time electrical detection in a non-destructive manner,[18,19] as well as the ability to be

effectively merged with miniaturized hardware.[20–24] In particular, there has been great interest in the use of one-dimensional nanostructured materials,[25–28] and single walled carbon nanotubes (SWCNTs) emerged as strong candidates.[29–36] It has been demonstrated that target biomolecules in close proximity to SWCNTs can alter their electronic properties via various mechanisms;[37–45] additionally, the application of SWCNTs ensures appropriate size compatibility with biological analytes.[19,31]

The application of nucleic acid aptamers as the sensing moieties on SWCNT electrical platforms has emerged of particular interest due to: i) aptamers' high affinity and specificity (comparable with those of antibodies); ii) little or no batch-to-batch variation in their production (unlike antibodies); and iii) the easiness in their design and engineering.[46,47,56,48–55] Nevertheless, the fabrication of these sensing platforms is still costly and time-consuming, typically involving numerous fabrication steps, from chemical vapor deposition of the CNTs, to lithographic patterning. Moreover, and most importantly, the SWCNT-aptamer biosensing devices so far presented do not allow for multi-sensing capability nor low-cost processability (ideally from solution).

Here we present a strategy for the facile fabrication of reconfigurable and solution processable nanoscale multiplexed biosensors, based on SWCNTs. DNA-wrapped (hence water-soluble) SWCNTs[57] functionalized with specific nucleotide sequences were employed as selective recognition elements. Distinct SWCNT-aptamer hybrids were then immobilized on the same chip from solution onto pre-patterned electrodes via dielectrophoresis (DEP). This allowed us to fabricate a multisensing platform for the simultaneous electrical detection of different biomarkers. As a proof-of-concept, we employed our devices for both the selective detection of ss-DNA (i.e. hybridization events) and, most notably, the label-free multiplexed sensing of cortisol,[58,59] neuropeptide Y (NPY),[60,61] and dehydroepiandrosterone-sulfate (DHEAS),[62,63] due to

the roles of these biomarkers in various physiological processes such as energy metabolism, blood pressure regulation, cognitive function, post-traumatic stress disorder and traumatic brain injury.[59,61] We demonstrate the real-time detection of these hormones at their physiological relevant concentrations, from pM to µM; additionally, we show how the platform developed is reconfigurable and reusable via a simple cleaning procedure.

## 3.2 Formation of SWCNT-aptamer hybrids

In order to tether aptamers to SWCNTs, and form SWCNT-aptamer hybrids, we modified wrapping DNA sequences ($(GTT)_3$G-amine) with (1R,8S,9s)-Bicyclo[6.1.0]non-4-yn-9-ylmethyl (BCN) groups (see section 2.2.1 and 2.2.2). N-hydroxysuccinimide esters (NHS) can easily react with amine groups. This allowed us to covalently functionalise DNA with BCN groups (see Figure 3.1).

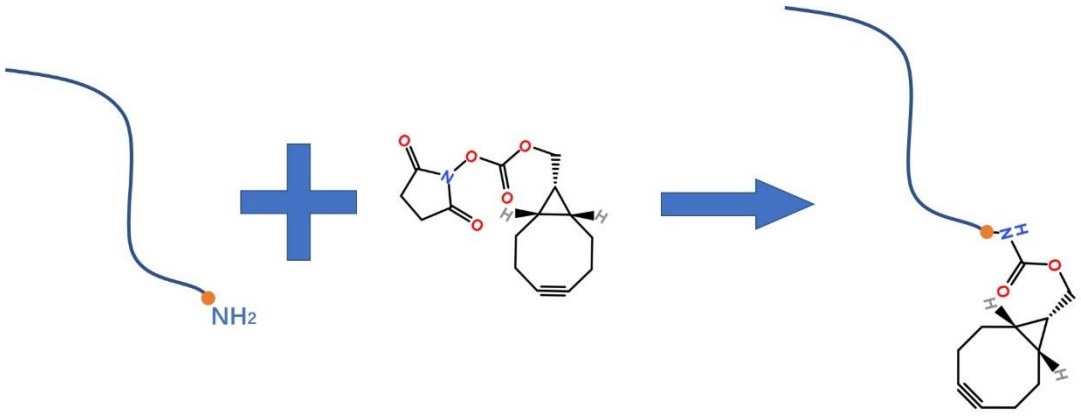


**Figure 3.1** Scheme for the modification of $(GTT)_3$G-amine with BCN groups.

To demonstrate the successful modification of $(GTT)_3$G-amine with BCN group, we analysed $(GTT)_3$G-BCN and $(GTT)_3$G-amine samples with HPLC (High Performance Liquid Chromatography, Agilent LC 1100, XBridge Column Reversed-Phase 2.5 µm, 4.6 mm × 50 mm) (see section 2.1.2). As shown in Figure 3.2, HPLC analysis of the

BCN-ssDNA compared to the amine-ssDNA shows a shift in the retention time of the more hydrophobic BCN-ssDNA, suggesting the successful BCN functionalization of the DNA following the BCN-NHS chemistry on the amine-terminated DNA.

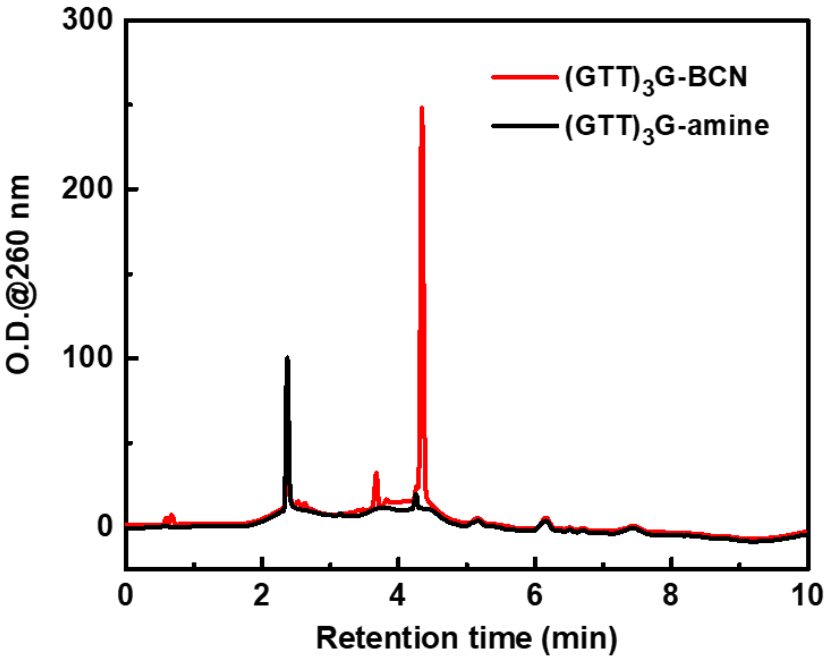


**Figure 3.2** HPLC analysis of the chemical modification of $(GTT)_3G$-amine to $(GTT)_3G$-BCN.

Subsequently, BCN-functionalised DNA was used to wrap (7,6) enriched SWCNTs (BCN-SWCNT) (see section 2.2.1). Single-stranded DNA would tightly bind onto the sidewall of CNTs via π-π stacking, making SWCNTs soluble in aqueous solution, while BCN groups were still available for chemical reaction. Aptamers terminated with azide groups were then used to react with BCN-SWCNT via a simple copper-free cycloaddition (click reaction), directly in solution and without altering the electronic properties of the nanotubes by covalent attachment, forming SWCNT-aptamer hybrids (see Figure 3.3).[64] The yield of the click reaction is more than 70%.

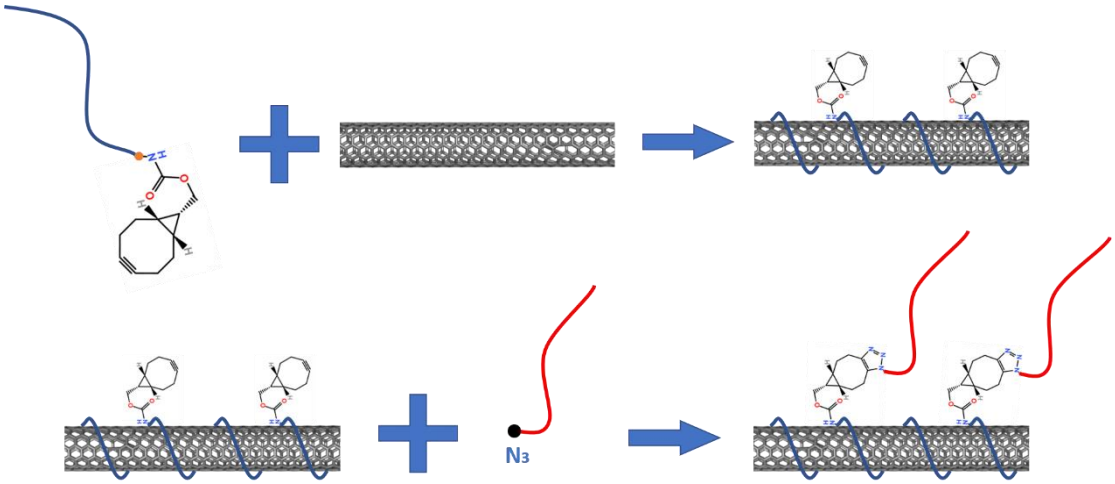


**Figure 3.3** Scheme for the tethering of SWCNTs with aptamers on the sidewall.

Notably, the reaction of different azide-terminated aptamers to separate solutions of BCN-SWCNT permits the preparation of distinct aptamer-functionalized SWCNTs solutions. We employed this strategy to produce three different solutions of SWCNTs, each functionalized with a distinct aptamer selective to a specific biomarker, namely cortisol, NPY, and DHEAS: the schematic in Figure 3.4 outlines this approach.

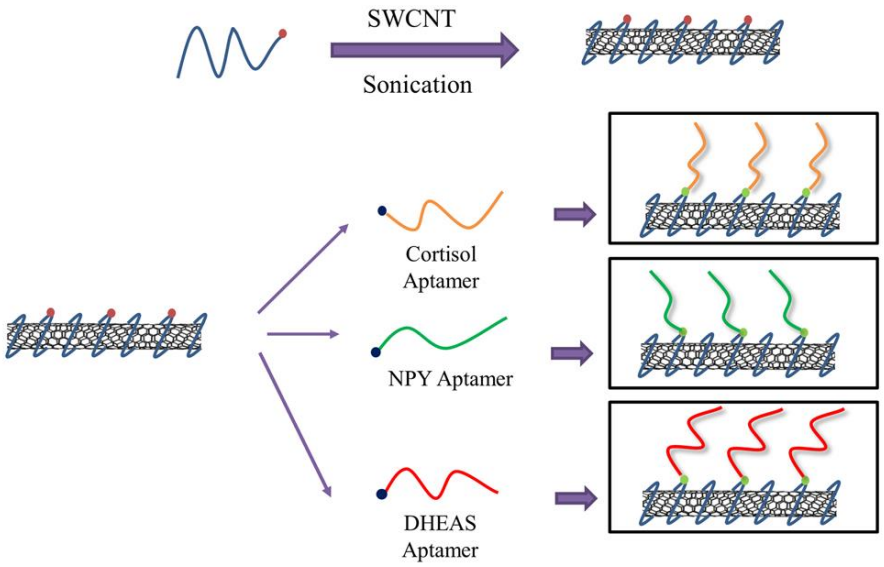


**Figure 3.4** DNA-wrapping of the SWCNTs and tethering of different aptamers: cortisol (orange), NPY (green) and DHEAS (red) binding aptamers.

In order to verify the successful functionalization of DNA wrapped SWCNTs with the employed aptamers, we hybridized cortisol aptamer-functionalized nanotubes with complementary ss-DNA directly in solution, then cast these on muscovite mica substrates and imaged them with AFM (see section 2.3.1 and 2.4). Figure 3.5 shows representative AFM images of the SWCNT-aptamer hybrids before and after hybridisation with the complementary strands. Before DNA hybridisation (Figure 3.5a), ss-DNA (cortisol aptamers) around SWCNTs are not visible in the AFM image since ss-DNA are flexible and not rigid enough, hence randomly distributed. After hybridisation (Figure 3.5b), the double stranded (ds) DNA portion protruding out of the nanotubes is clearly visible in the samples that were exposed to the aptamer's complementary sequence, demonstrating that the functionalization strategy was successful. These AFM images also demonstrate that the nucleic acid aptamers are present on the SWCNTs and are accessible to other biomolecules, ss-DNA in this case (an important feature for the subsequent use of these hybrids as selective recognition elements in a device). From the analysis of AFM images of multiple nanotubes in different samples, we determined the height of the ds-DNA was about 1nm and the length of ds-DNA was about 20 nm. We also determined that each SWCNT exhibited on average 4 ± 2 aptamers per 100 nm, and that these are available for hybridization. Additionally, it is reasonable to assume that the tens of nm distance between the aptamers on each nanotube will prevent potential detrimental crowding effects on the biosensing properties of these hybrids once immobilized in a device.

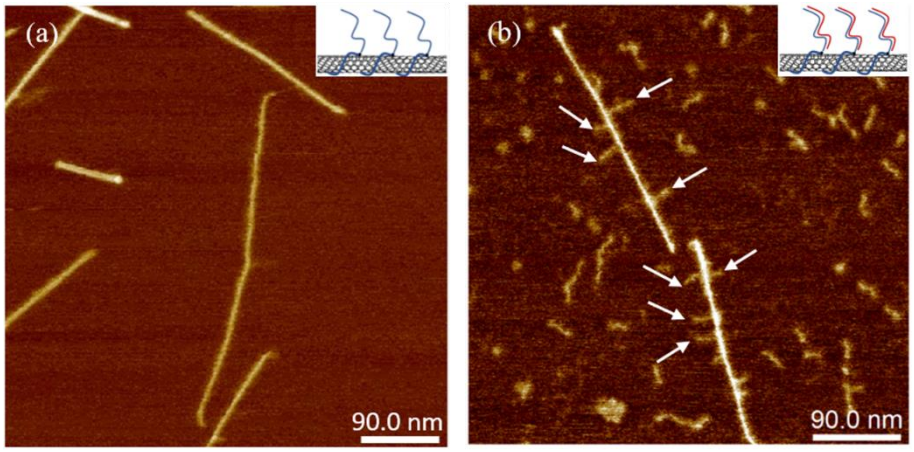


**Figure 3.5** AFM images, and cartoon insets, of aptamer-functionalized SWCNTs (a) without and (b) with hybridized ss-DNA sequences. The yellow arrows show the hybridized aptamers along the nanotubes. Z-scales = 2.5 nm

To further demonstrate the successful functionalisation, we labelled aptamers with quantum dots (QDs, Qdot 585 streptavidin conjugate, with a diameter of about 10 nm). As shown in Figure 3.6, complementary ss-DNA terminated with biotin groups was used to hybridise the aptamer sequence in the SWCNT-aptamer heterostructures. As a control experiment, we also hybridised complementary ss-DNA without biotin groups with the SWCNT-aptamer hybrids. Subsequently, streptavidin functionalised QDs were added to these samples since streptavidin can easily bind to biotin groups. After incubation, the samples were deposited on a mica substrate and scanned with AFM.

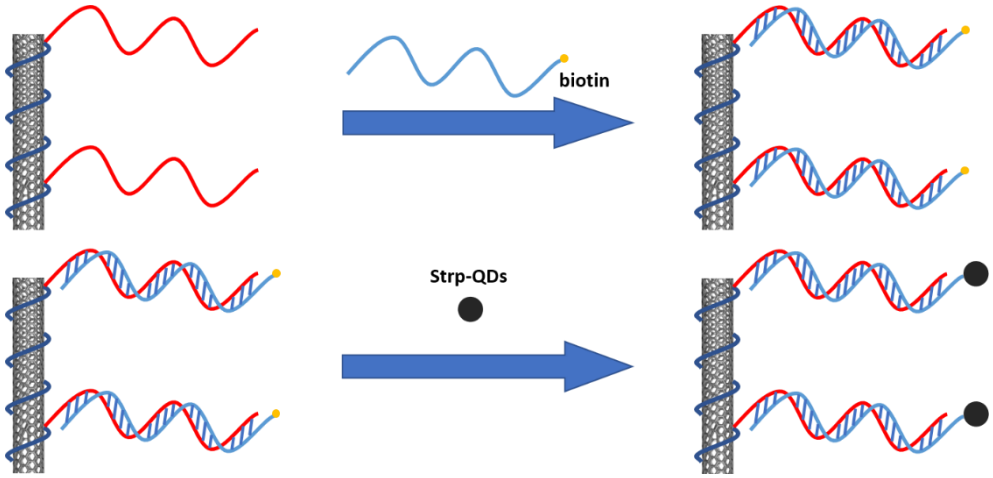


**Figure 3.6** Scheme for the formation of SWCNT-QDs hybrids.

It can be clearly seen that in Figure 3.7a, when the complementary ss-DNA is terminated with biotin groups, QDs are attached onto the sidewall of SWCNTs. Due to the large difference in the height between QDs (c.a.10nm) and ds-DNA (c.a. 1nm), we can observe QDs attached on the sidewall of SWCNTs in AFM images. In the control experiment in which complementary ss-DNA without biotin groups (Figure 3.7b), QDs and SWCNTs are randomly distributed on the mica substrate. This demonstrates that the attachment of QDs to SWCNTs results from biotin-streptavidin interaction, further confirming the successful hybridisation between aptamers and the complementary DNA sequences.

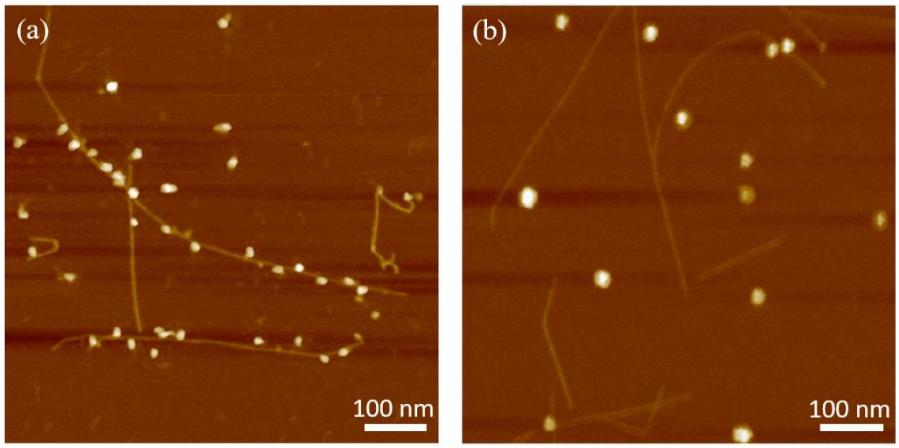


**Figure 3.7** AFM images of the formation of SWCNT-QDs hybrids (a) with biotin groups and (b) without biotin groups.

## 3.3 Fabrication of SWCNT-aptamer devices and electrical detection of DNA hybridisation

The CNT-aptamer hybrids prepared as described in the previous section (3.2), were immobilised between pre-patterned gold electrodes via DEP. With optimised parameters, we were able to immobilise a small bundle of CNT-aptamer hybrids between electrodes (see section 2.3.2). Figure 3.8 shows the schematic of the strategy

utilised, as well as a representative AFM image of CNT-aptamer hybrids aligned between two pre-patterned electrodes. As DEP strategy is a well-developed technique, the yield of CNT-aptamer devices is more than 90%.

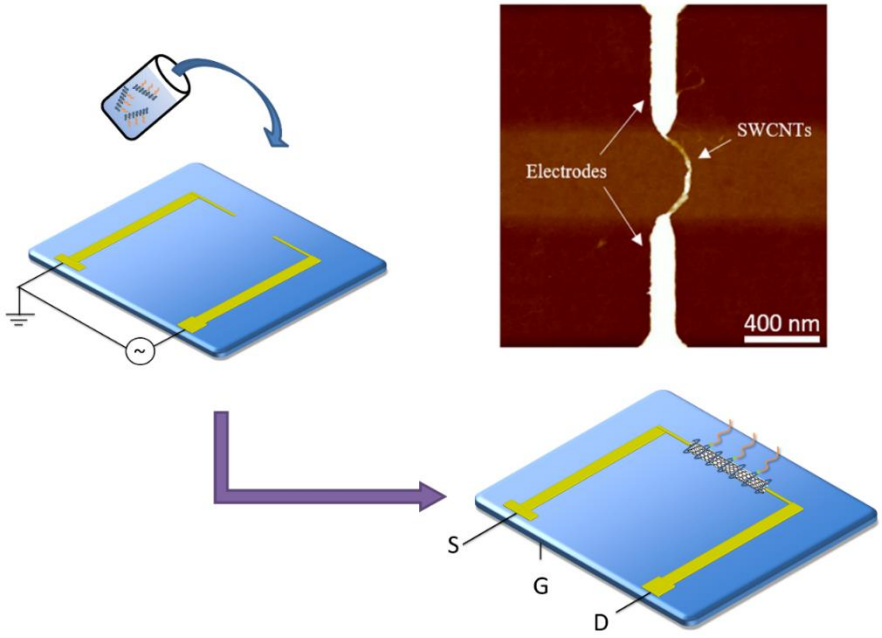


**Figure 3.8** DEP of SWCNT-aptamer hybrids with the corresponding AFM picture. S, D and G indicate respectively the source, drain and gate (electrodes). Z scales = 10 nm.

To confirm the accessibility of the nucleotide recognition element within the SWCNT-aptamer hybrids immobilized in the device configuration, we performed in-situ DNA hybridization experiments exposing the chip to the cortisol aptamer's complementary ss-DNA, and recording the electrical response of the device in dry condition (in air) when the ds-DNA (double-stranded) was formed (see section 2.5). Figure 3.9 shows a representative electrical response of the SWCNT-aptamer field effect transistor (FET), before and after DNA hybridization. After the first formation of ds-DNA (red curve), the source-drain current through the FET increased significantly, while after denaturation (blue curve), the current recovered to the initial level. This suggests that the CNT-aptamer devices can be used to detect DNA hybridisation. Moreover, we were

able to use the same chip to perform a second detection of DNA hybridisation (green curve), suggesting that the devices are reusable, which is an ideal feature of biosensors.

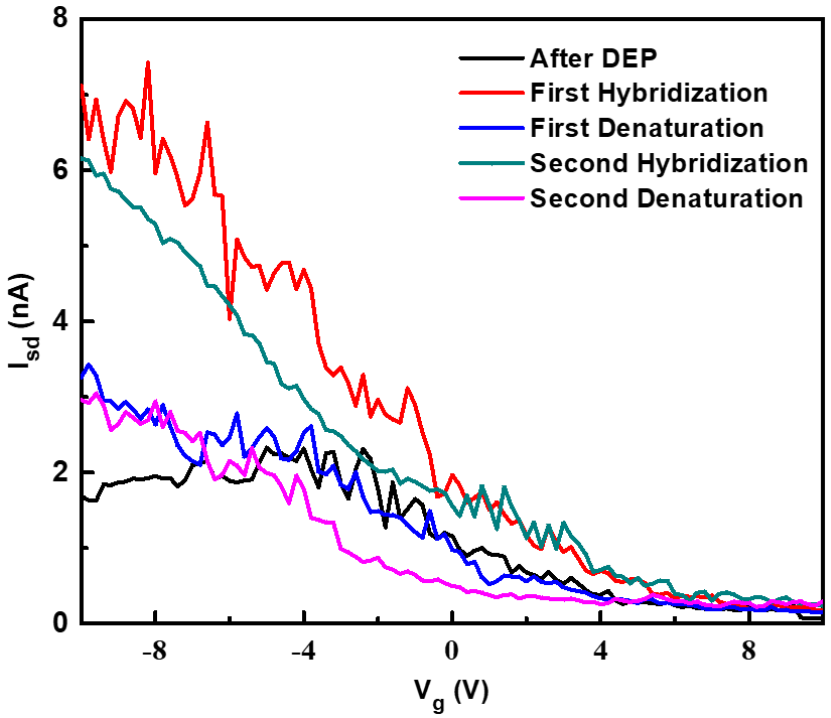


**Figure 3.9** Electrical response of the SWCNT-aptamer field effect transistor, before (black) and after DNA hybridization (red) and DNA denaturation (blue), and an additional cycle of DNA hybridization (green) and DNA denaturation (purple). $V_{sd}$ = 100 mV.

Control experiments were carried out to further demonstrate that the change in current comes from the occurred recognition of the complementary ss-DNA to the aptamer in the SWCNT-based devices. Another CNT device where DNA wrapped SWCNTs (without aptamers) were immobilised were exposed to the complementary ss-DNA and the electrical response was recorded, as shown in Figure 3.10. Obviously, there is no significant change in current in these devices, confirming that only devices functionalised with aptamers can give a response to complementary ss-DNA.

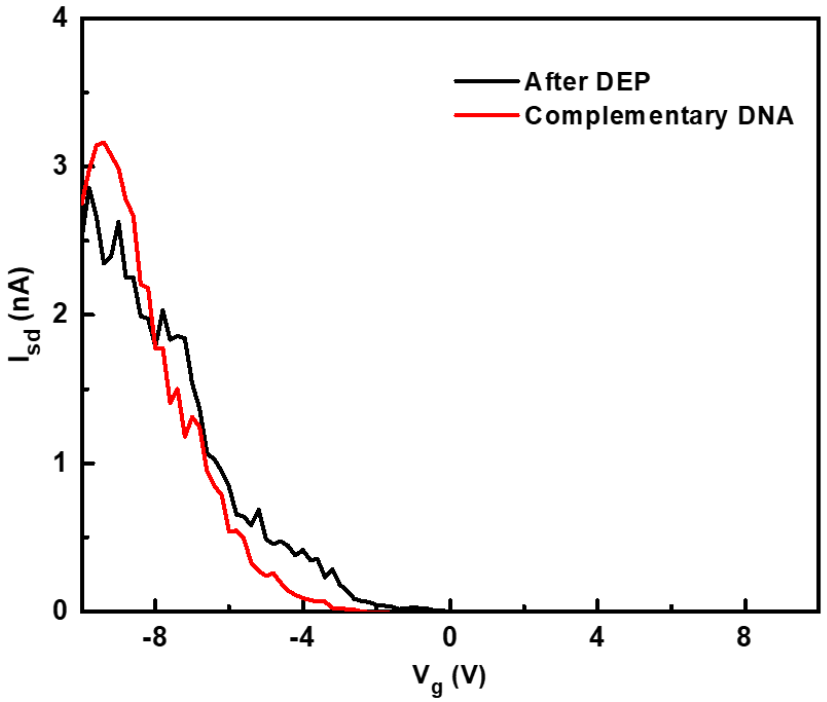


**Figure 3.10** $I_{sd}$ vs $V_g$ characterization of the non-functionalized device before and after exposure to the ssDNA, $V_{sd}$ = 100 mV.

We also performed experiments to demonstrate the selectivity of the SWCNT-aptamer devices. Figure 3.11 shows a representative electrical response of a CNT-aptamer device when it was exposed to complementary and non-complementary ss-DNA. As shown in the figure, there was no significant change in current when the device was exposed non-complementary ss-DNA (red curve). However, subsequent exposure of the device to complementary ss-DNA induced an increase in current (blue), demonstrating that the device is selective to specific DNA sequences. We also denatured the formed ds-DNA using formamide solution, without affecting the electrical properties of the SWCNT-aptamer hybrids,[65] which induced a recovery of the current to initial state (green curve). Second hybridisation was performed by exposing the same device to complementary ss-DNA, which induced an increase in current as shown in purple curve. This further demonstrates that the device is reconfigurable and reusable. The observed change in current can be attributed to a potential scattering

mechanism occurring upon the rearrangement of the aptamer's conformation due to DNA hybridization.[66]

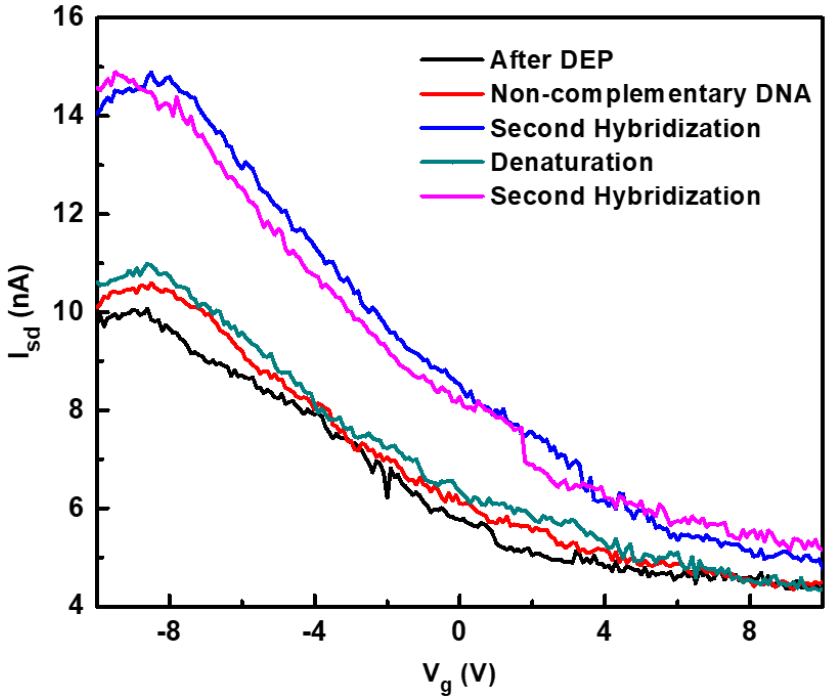


**Figure 3.11** $I_{sd}$ vs $V_g$ characterization of the device functionalized with cortisol aptamer before (black) and after exposure to non-complementary DNA (red), after exposure to complementary DNA (blue), after DNA denaturation (green) and a second hybridization with the complementary DNA (purple). $V_{sd}$ = 100 mV.

## 3.4 Multiplexed detection of three analytes

In order to use the devices for multipurpose analysis, we assembled SWCNT-aptamer hybrids exhibiting distinct bio-recognition elements at different locations on the same chip. One of the attractive features of DEP strategy is that CNT-aptamer hybrids can only be immobilised between electrodes where voltage is applied. Therefore, by separately addressing distinct electrodes pairs it is possible to immobilise, via DEP, n aptamer-functionalised SWCNTs between n different electrode pairs. The organisation of distinct SWCNT-aptamer hybrids from solution to surfaces in parallel 2D device configurations on the same chip can then allow for the fabrication of multifunctional, high-throughput bio-electronic devices with parallel multi-purpose sensing capability

(see Figure 3.12). The electronic devices prepared in this way should indeed withstand and respond to various environmental changes on the same substrates, depending on the different aptamers employed: upon recognition of an analyte, the specific aptamer will undergo a structural rearrangement and induce a change in the electrical response (resistance) of the CNT embedded in the device.[67,68]

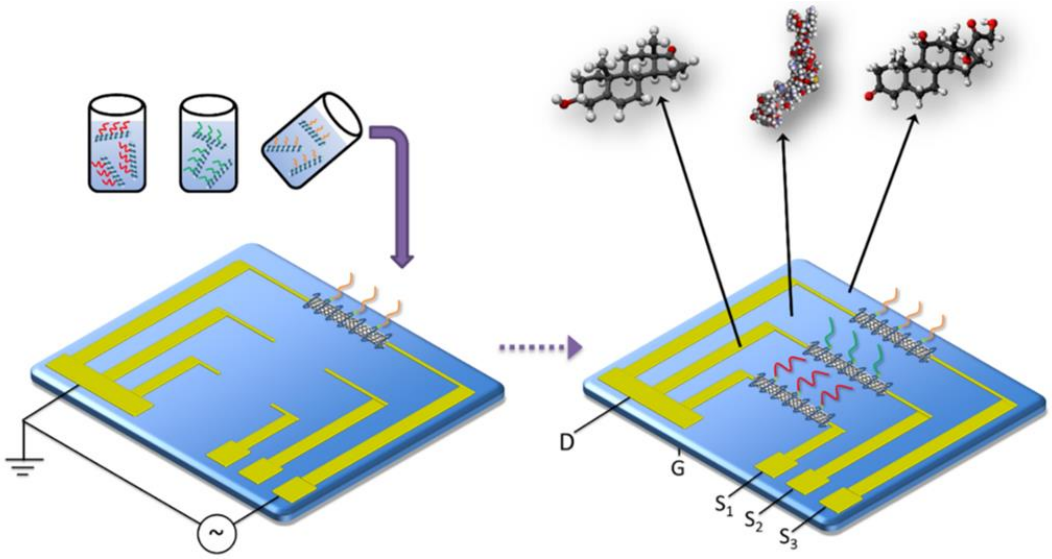


**Figure 3.12** Schematic of the DEP strategy employed for the fabrication of multi-sensing devices.

we immobilized two distinct SWCNT-aptamer hybrids on separate electrode pairs on the same chip. The aptamers target the aforementioned biomarkers indicative of stress and neuro-trauma conditions, namely, cortisol and NPY. This step is marked as "after DEP" in the curves shown in Figure 3.13. We performed subsequent detection experiments on the same chip, employing different solutions containing either one, two biomarkers and recorded the electrical response of the device in dry condition (in air). As shown in Figure 3.13, after immersing the devices into a solution only containing cortisol solution, only devices with cortisol aptamers (cortisol sensor) gave a significant response in current, while there was no change in current in devices with NPY aptamers (NPY sensor). The devices can be easily cleaned with urea solution,[69] and the current

recovered to the initial state (see the curves in black after cleaning). An opposite response was observed when the devices were immersed in a solution only containing NPY. After being cleaning with urea, the devices were immersed in a solution containing both cortisol and NPY, which induced a significant decrease in current in both cortisol and NPY sensors. This suggests that we are able to perform multiple detection tests on the same chip, without any crosstalk between the different devices selective to the other analytes, nor any false-positive signals.

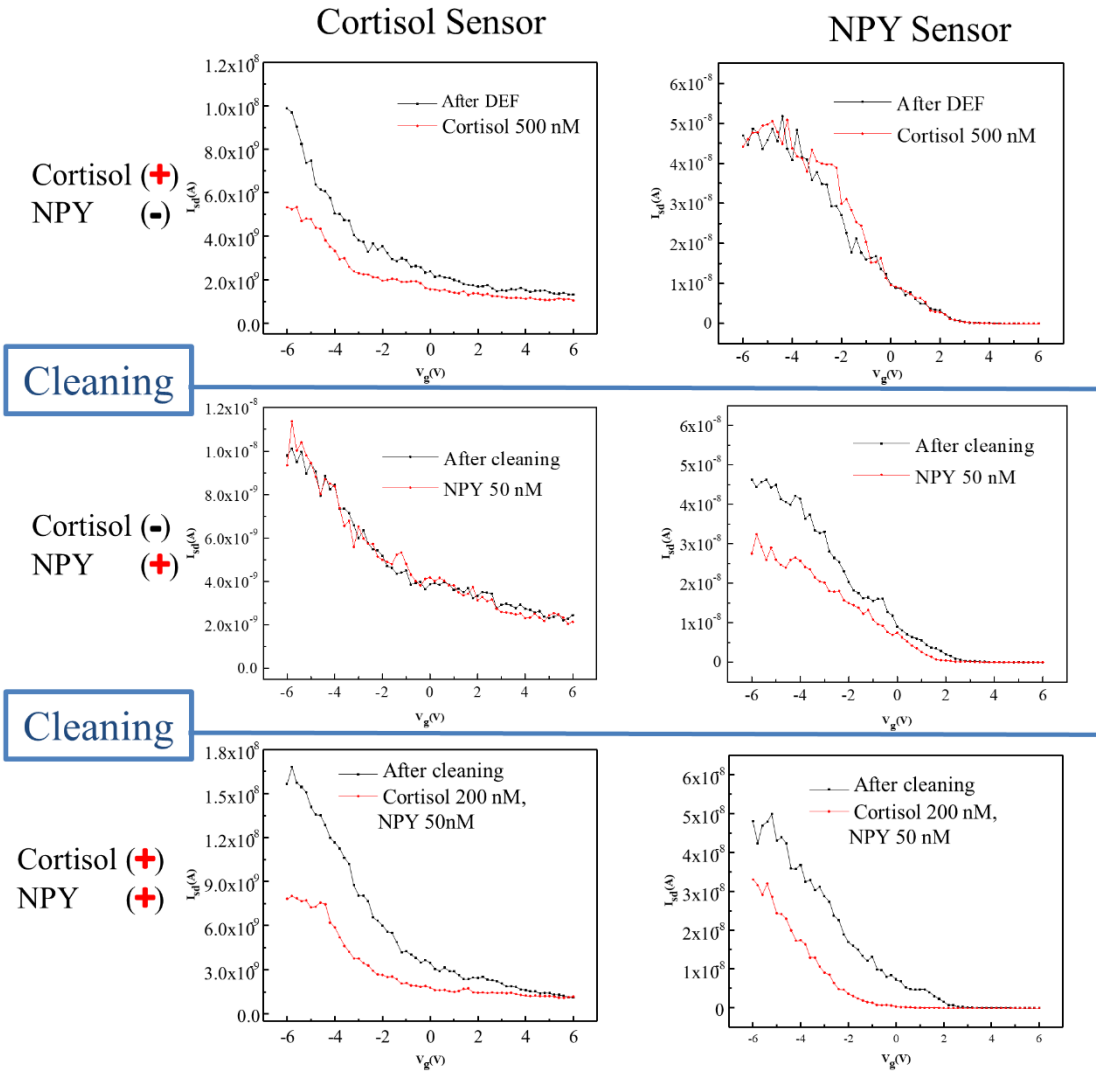


**Figure 3.13** Electrical responses of Cortisol and NPY biosensors on the same chip ($V_{sd}$ =100 mV): the + sign indicates the addition/presence of the analyte of interest; the "cleaning step" indicates the addition of 8M of urea in order to regenerate the sensor after each detection; "after cleaning" indicates the measurements performed after this step.

Similarly, three distinct SWCNT-aptamer hybrids (i.e. cortisol, NPY and DHEAS) were immobilised between separate electrode pairs, on the same chip. We also performed subsequent detection experiments on the same chip, employing different solutions containing either one, two or all three biomarkers. Similarly, upon selective binding of a analyte to the specific aptamer tethered to the SWCNTs, we observed a reduction in the current response only for the corresponding device on the chip, again without any crosstalk between the different devices selective to the other analytes, nor any false-positive signals (see Figure 3.14). Notably, each distinct nanoscale device on the chip could be reversed to its initial state by removing the analyte bound to the aptamer by immersing the devices into a urea solution ("cleaning" in Figure 3.14). We performed multiple detection tests on the same chip, and successfully demonstrated the multiplexed electrical detection of the three biomarkers of interest.

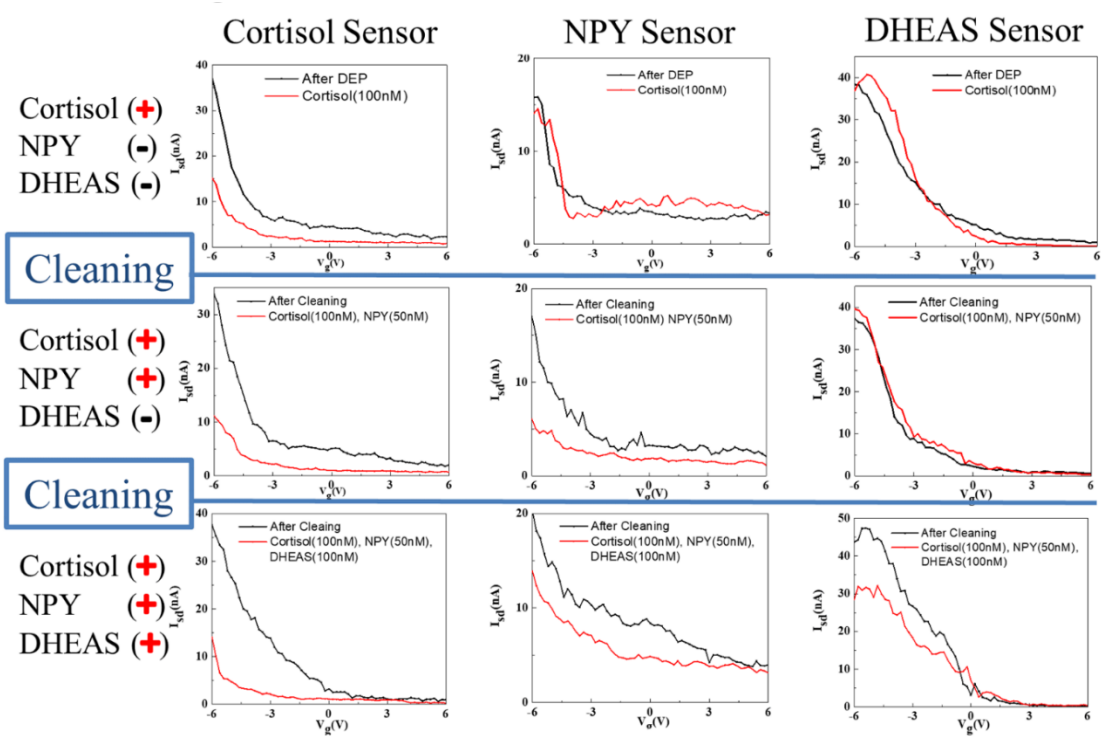


**Figure 3.14** Multiplexed sensing: electrical responses of the different biosensors on the same chip($V_{sd}$ =100 mV): the + sign indicates the addition/presence of the analyte of interest; the "cleaning step" indicates the addition of 8M of urea in order to regenerate

the sensor after each detection; “after cleaning” indicates the measurements performed after this step.

We further investigated the real-time detection of cortisol, DHEAS, and NPY, at their relevant physiological concentrations in serum, i.e. from 100 pM to 1 µM. The devices were first immersed in serum and the electrical response was recorded simultaneously; subsequently, different concentrations of each biomarker were added to the devices at different time intervals, which induced decease in current (see Figure 3.15). This is in line with previous electrical detection (see Figure 3.14). The electrical response increased with the change in concentration; we detected in real-time concentrations of cortisol, DHEAS and NPY down to ca 50 nM, 10 nM and 500 pM respectively (Figure 3.15). The drop in $I_{sd}$-$V_g$ is likely due to a screening charge in the CNTs induced by the change in conformation of the aptamer upon analyte binding, as previously observed for ss-DNA folding in CNT-DNA devices. Figure 3.15 shows that CNT devices functionalised with different aptamers exhibit different sensitivities to their corresponding analytes, which might result from their specific configurations caused by the binding between aptamers and their corresponding analytes.

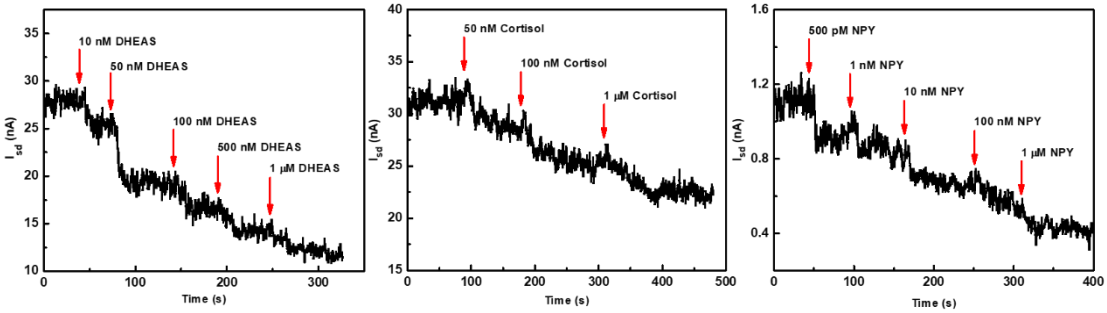


**Figure 3.15** Real time detection of (a) cortisol (from 50 nM to 1 µM), (b) DHEAS (from 10 nM to 1 µM) and (c) NPY (from 500 pM to 1 µM) at various concentrations, in serum ($V_{sd}$ = 100 mV, $V_g$ = –2V).

To demonstrate that the change in current comes from the binding of aptamer to its corresponding analyte, control experiment was performed. Devices, where the

nanotubes were not functionalized with any aptamers, did not exhibit any change in their electrical reponse upon the additon of the aformentioned biomarkers (see Figure 3.16), suggesting that only devices functionalised with apatamers can give a response in current to the corresponding analytes. This also confirms the selectivity and biosensing nature of the devices presented here.

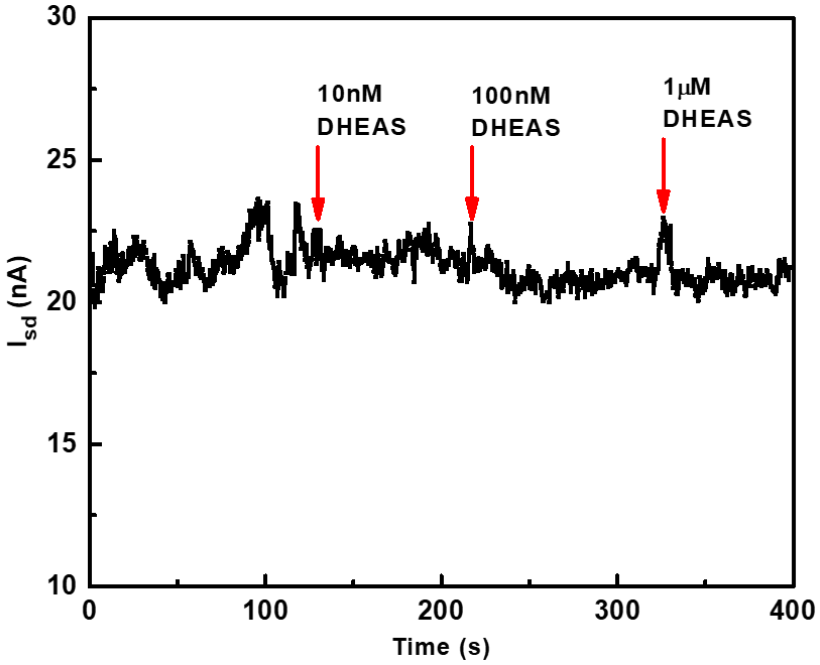


**Figure 3.16** Real time response of a non-functionalized CNT-device upon addition of DHEAS at different concentrations (from 10 nM to 1 μM).

To further demonstrate the selectivity of the fabricated multiplexed platform also for real-time measurements, we tested the DHEAS-sensitive sensor with a molecule possessing similar molar mass and chemical structure to DHEAS (Sodium deoxycholate, SDC). As shown in Figure 3.17a, SDC was added at a concentration of 1 μM and no changes were observed in the current of the DHEAS-sensitive sensor. The sample was then cleaned with DI water and exposed to a 1 μM DHEAS solution. A sharp decrease in the conductance was at this point observed as expected (Figure 3.17b), in line with the results shown in Figure 3.15. Additionally, the source-drain versus gate

voltage measurements further confirmed the high selectivity of the platform (see Figure 3.17c).

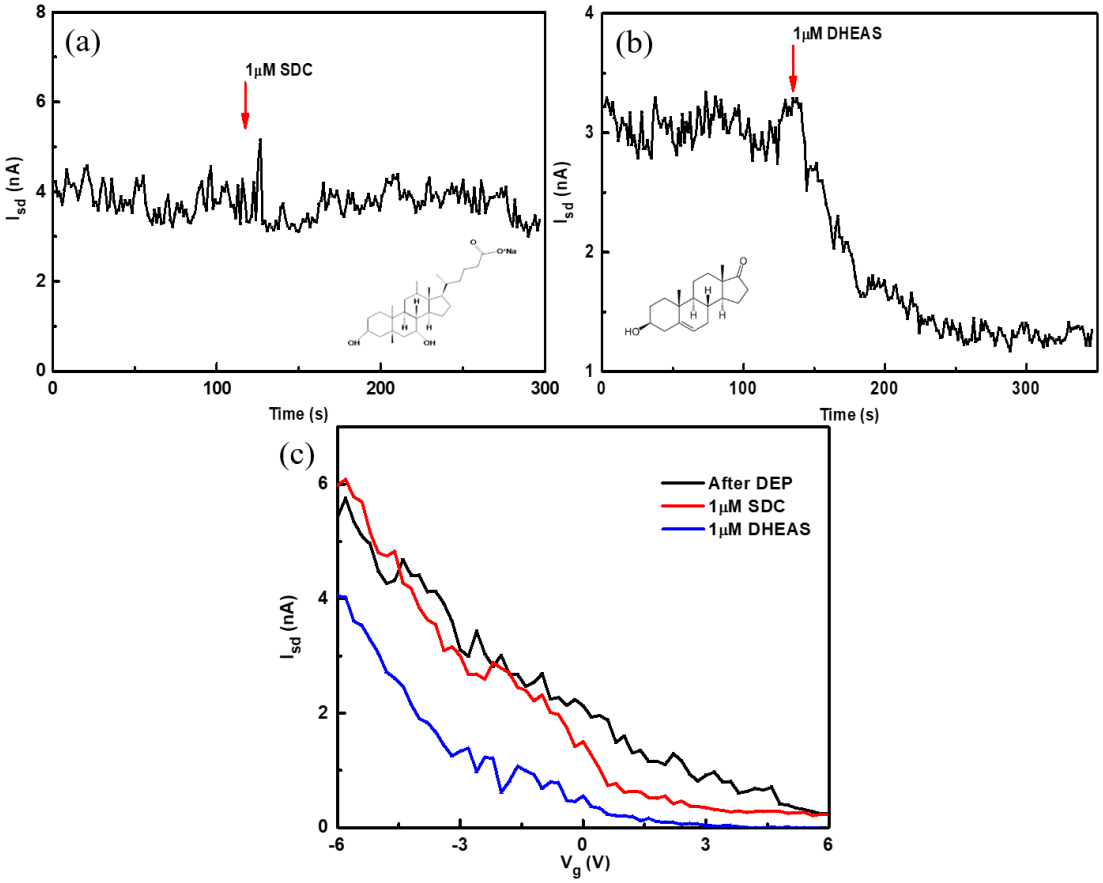


**Figure 3.17** Real time detection of (a) 1 μM SDC and (b) 1 μM DHEAS on the same device and (c) $I_{sd}$ vs $V_g$ characterization of the device before detection and after SDC and DHEAS.

## 3.5 Conclusions

In conclusion, we presented a novel solution-processable method of general applicability for the fabrication of label-free nanoscale biosensing devices, that permits the real-time and simultaneous detection of multiple analytes on the same chip. We assembled hybrids of SWCNTs and aptamers from solution to surfaces in nanoscale device configurations, where the nanotubes could act as the transducer elements, and the aptamers as the recognition components, of an electrical biosensing platform. As

proof of concept, we demonstrated the selective recognition of different biomarkers indicative of stress and neuro-trauma conditions, at various physiologically relevant concentrations, from pM to μM. The devices exhibited high selectivity and sensitivity, as well as multiplexing ability thanks to the immobilization of CNT-aptamer hybrids with distinct biorecognition elements on the same nanoscale chip via a DEP-based strategy; this grants low cost processability and low power consumption. Additionally, the devices are reconfigurable and reusable via a simple cleaning procedure. To the best of our knowledge, these results represent the first example of solution-processable and reconfigurable nanoscale multiplexing sensing devices based on the use of carbon nanostructures. Despite these promising features, issues related to electrical noise occurring during the detection remain to be solved. Although we can conclude from our experiments results that this solution-processible strategy is feasible for the fabrication of CNT devices with low cost processability and multiplexing sensing capability, it is still hard for us to provide reliable data to investigate the relationship between electrical response and analyte concentration due to the influence of electrical noise. Future work will focus on the minimisation of the influence of electrical noise through, for example, using microfluidic systems, increasing the structural purity of CNTs (even single chirality CNTs). Eventually, statistical data will be collected to fully investigate the efficiency of these devices in the field of biosensing.

By and large, the general applicability of the strategy developed, and the solution processability of the nanoscale multiplexing biosensing devices we fabricated, hold great potential for the development of the next generation of portable, point of care and home diagnostic assays for the continuous and simultaneous monitoring of different health parameters.

References

(1) DeKosky, S. T.; Marek, K. Erratum: Looking Backward to Move Forward: Early Detection of Neurodegenerative Disorders (Science (October 31) (830)). *Science (80-. ).* **2003**, *302* (5652), 1895. https://doi.org/10.1126/science.302.5652.1895.

(2) Chen, X.; Ba, Y.; Ma, L.; Cai, X.; Yin, Y.; Wang, K.; Guo, J.; Zhang, Y.; Chen, J.; Guo, X.; Li, Q.; Li, X.; Wang, W.; Zhang, Y.; Wang, J.; Jiang, X.; Xiang, Y.; Xu, C.; Zheng, P.; Zhang, J.; Li, R.; Zhang, H.; Shang, X.; Gong, T.; Ning, G.; Wang, J.; Zen, K.; Zhang, J.; Zhang, C. Y. Characterization of MicroRNAs in Serum: A Novel Class of Biomarkers for Diagnosis of Cancer and Other Diseases. *Cell Res.* **2008**, *18* (10), 997–1006. https://doi.org/10.1038/cr.2008.282.

(3) Pepe, M. S.; Etzioni, R.; Feng, Z.; Potter, J. D.; Thompson, M. Lou; Thornquist, M.; Winget, M.; Yasui, Y. Phases of Biomarker Development for Early Detection of Cancer. *J. Natl. Cancer Inst.* **2001**, *93* (14), 1054–1061. https://doi.org/10.1093/jnci/93.14.1054.

(4) Etzioni, R.; Urban, N.; Ramsey, S.; McIntosh, M.; Schwartz, S.; Reid, B.; Radich, J.; Anderson, G.; Hartwell, L. The Case for Early Detection. *Nat. Rev. Cancer* **2003**, *3* (4), 243–252. https://doi.org/10.1038/nrc1041.

(5) Keum, H.; Mccormick, M.; Liu, P.; Zhang, Y.; Omenetto, F. G. RESEARCH ARTICLES Epidermal Electronics. **2011**, *333* (September).

(6) Tsaytler, P.; Harding, H. P.; Ron, D.; Bertolotti, A. Selective Inhibition of a Regulatory Subunit of Protein Phosphatase 1 Restores Proteostasis. *Science (80-. ).* **2011**, *332* (6025), 91–94. https://doi.org/10.1126/science.1201396.

(7) Drummond, T. G.; Hill, M. G.; Barton, J. K. Electrochemical DNA Sensors. *Nat. Biotechnol.* **2003**, *21* (10), 1192–1199. https://doi.org/10.1038/nbt873.

(8) Zangar, R. C.; Daly, D. S.; White, A. M. ELISA Microarray Technology as a High-Throughput System for Cancer Biomarker Validation. *Expert Rev. Proteomics* **2006**, *3* (1), 37–44. https://doi.org/10.1586/14789450.3.1.37.

(9) Wei, F.; Patel, P.; Liao, W.; Chaudhry, K.; Zhang, L.; Arellano-Garcia, M.; Hu, S.; Elashoff, D.; Zhou, H.; Shukla, S.; Shah, F.; Ho, C. M.; Wong, D. T. Electrochemical Sensor for Multiplex Biomarkers Detection. *Clin. Cancer Res.* **2009**, *15* (13), 4446–4452. https://doi.org/10.1158/1078-0432.CCR-09-0050.

(10) Sheean et al., 2013. NIH Public Access. *Bone* **2008**, *23* (1), 1–7. https://doi.org/10.1038/jid.2014.371.

(11) Saha, K. K.; Drndić, M.; Nikolić, B. K. DNA Base-Specific Modulation of Microampere Transverse Edge Currents through a Metallic Graphene Nanoribbon with a Nanopore. *Nano Lett.* **2012**, *12* (1), 50–55. https://doi.org/10.1021/nl202870y.

(12) Diehl, K. L.; Anslyn, E. V. Array Sensing Using Optical Methods for Detection of Chemical and Biological Hazards. *Chem. Soc. Rev.* **2013**, *42* (22), 8596–8611. https://doi.org/10.1039/c3cs60136f.

(13) Landry, M. P.; Ando, H.; Chen, A. Y.; Cao, J.; Kottadiel, V. I.; Chio, L.; Yang, D.; Dong, J.; Lu, T. K.; Strano, M. S. Single-Molecule Detection of Protein Efflux from Microorganisms Using Fluorescent Single-Walled Carbon Nanotube Sensor Arrays. *Nat. Nanotechnol.* **2017**, *12* (4), 368–377. https://doi.org/10.1038/nnano.2016.284.

(14) Vo-Dinh, T.; Griffin, G.; Stokes, D. L.; Wintenberg, A. Multi-Functional Biochip for Medical Diagnostics and Pathogen Detection. *Sensors Actuators, B Chem.* **2003**, *90* (1–3), 104–111. https://doi.org/10.1016/S0925-4005(03)00048-0.

(15) Shafiee, H.; Asghar, W.; Inci, F.; Yuksekkaya, M.; Jahangir, M.; Zhang, M. H.; Durmus, N. G.; Gurkan, U. A.; Kuritzkes, D. R.; Demirci, U. Paper and Flexible Substrates as Materials for Biosensing Platforms to Detect Multiple Biotargets. *Sci. Rep.* **2015**, *5* (i), 1–9. https://doi.org/10.1038/srep08719.

(16) Ahn, S. R.; An, J. H.; Song, H. S.; Park, J. W.; Lee, S. H.; Kim, J. H.; Jang, J.; Park, T. H. Duplex Bioelectronic Tongue for Sensing Umami and Sweet Tastes Based on Human Taste Receptor Nanovesicles. *ACS Nano* **2016**, *10* (8), 7287–7296. https://doi.org/10.1021/acsnano.6b02547.

(17) Gao, W.; Emaminejad, S.; Nyein, H. Y. Y.; Challa, S.; Chen, K.; Peck, A.; Fahad, H. M.; Ota, H.; Shiraki, H.; Kiriya, D.; Lien, D. H.; Brooks, G. A.; Davis, R. W.; Javey, A. Fully Integrated Wearable Sensor Arrays for Multiplexed in Situ Perspiration Analysis. *Nature* **2016**, *529* (7587), 509–514. https://doi.org/10.1038/nature16521.

(18) Kawasaki, E. S.; Player, A. Nanotechnology, Nanomedicine, and the Development of New, Effective Therapies for Cancer. *Nanomedicine Nanotechnology, Biol. Med.* **2005**, *1* (2), 101–109. https://doi.org/10.1016/j.nano.2005.03.002.

(19) Guo, X. Single-Molecule Electrical Biosensors Based on Single-Walled Carbon Nanotubes. *Adv. Mater.* **2013**, *25* (25), 3397–3408. https://doi.org/10.1002/adma.201301219.

(20) Xu, M.; Luo, X.; Davis, J. J. The Label Free Picomolar Detection of Insulin in Blood Serum. *Biosens. Bioelectron.* **2013**, *39* (1), 21–25. https://doi.org/10.1016/j.bios.2012.06.014.

(21) Bansal, A. K.; Hou, S.; Kulyk, O.; Bowman, E. M.; Samuel, I. D. W. Wearable Organic Optoelectronic Sensors for Medicine. *Adv. Mater.* **2015**, *27* (46), 7638–

7644. https://doi.org/10.1002/adma.201403560.

(22) Luo, X.; Davis, J. J. Electrical Biosensors and the Label Free Detection of Protein Disease Biomarkers. *Chem. Soc. Rev.* **2013**, *42* (13), 5944–5962. https://doi.org/10.1039/c3cs60077g.

(23) Zhu, R.; Azzarelli, J. M.; Swager, T. M. Wireless Hazard Badges to Detect Nerve-Agent Simulants. *Angew. Chemie - Int. Ed.* **2016**, *55* (33), 9662–9666. https://doi.org/10.1002/anie.201604431.

(24) Fennell, J. F.; Liu, S. F.; Azzarelli, J. M.; Weis, J. G.; Rochat, S.; Mirica, K. A.; Ravnsbæk, J. B.; Swager, T. M. Nanowire Chemical/Biological Sensors: Status and a Roadmap for the Future. *Angew. Chemie - Int. Ed.* **2016**, *55* (4), 1266–1281. https://doi.org/10.1002/anie.201505308.

(25) Zheng, G.; Patolsky, F.; Cui, Y.; Wang, W. U.; Lieber, C. M. Multiplexed Electrical Detection of Cancer Markers with Nanowire Sensor Arrays. *Nat. Biotechnol.* **2005**, *23* (10), 1294–1301. https://doi.org/10.1038/nbt1138.

(26) Zhang, A.; Lieber, C. M. Nano-Bioelectronics. *Chem. Rev.* **2016**, *116* (1), 215–257. https://doi.org/10.1021/acs.chemrev.5b00608.

(27) Fennell, J. F.; Liu, S. F.; Azzarelli, J. M.; Weis, J. G.; Rochat, S.; Mirica, K. A.; Ravnsbæk, J. B.; Swager, T. M. Nanowire Chemical/Biological Sensors: Status and a Roadmap for the Future. *Angew. Chemie - Int. Ed.* **2016**, *55* (4), 1266–1281. https://doi.org/10.1002/anie.201505308.

(28) Chiesa, M.; Cardenas, P. P.; Otón, F.; Martinez, J.; Mas-Torrent, M.; Garcia, F.; Alonso, J. C.; Rovira, C.; Garcia, R. Detection of the Early Stage of Recombinational DNA Repair by Silicon Nanowire Transistors. *Nano Lett.* **2012**, *12* (3), 1275–1281. https://doi.org/10.1021/nl2037547.

(29) Antonucci, A.; Kupis-Rozmysłowicz, J.; Boghossian, A. A. Noncovalent Protein

and Peptide Functionalization of Single-Walled Carbon Nanotubes for Biodelivery and Optical Sensing Applications. *ACS Appl. Mater. Interfaces* **2017**, *9* (13), 11321–11331. https://doi.org/10.1021/acsami.7b00810.

(30) Wang, X.; Gao, L.; Liang, B.; Li, X.; Guo, X. Revealing the Direct Effect of Individual Intercalations on DNA Conductance toward Single-Molecule Electrical Biodetection. *J. Mater. Chem. B* **2015**, *3* (26), 5150–5154. https://doi.org/10.1039/c5tb00666j.

(31) Schnorr, J. M.; Swager, T. M. Wiring-up Catalytically Active Metals in Solution with Sulfonated Carbon Nanotubes. *J. Mater. Chem.* **2011**, *21* (13), 4768–4770. https://doi.org/10.1039/c0jm04287k.

(32) Sorgenfrei, S.; Chiu, C. Y.; Gonzalez, R. L.; Yu, Y. J.; Kim, P.; Nuckolls, C.; Shepard, K. L. Label-Free Single-Molecule Detection of DNA-Hybridization Kinetics with a Carbon Nanotube Field-Effect Transistor. *Nat. Nanotechnol.* **2011**, *6* (2), 126–132. https://doi.org/10.1038/nnano.2010.275.

(33) Rosenstein, J. K.; Lemay, S. G.; Shepard, K. L. Single-Molecule Bioelectronics. *Wiley Interdiscip. Rev. Nanomedicine Nanobiotechnology* **2015**, *7* (4), 475–493. https://doi.org/10.1002/wnan.1323.

(34) Kauffman, D. R.; Star, A. Electronically Monitoring Biological Interactions with Carbon Nanotube Field-Effect Transistors. *Chem. Soc. Rev.* **2008**, *37* (6), 1197–1206. https://doi.org/10.1039/B709567H.

(35) So, H.-M.; Won, K.; Kim, Y. H.; Kim, B.-K.; Ryu, B. H.; Na, P. S.; Kim, H.; Lee, J.-O. Single-Walled Carbon Nanotube Biosensors Using Aptamers as Molecular Recognition Elements. *J. Am. Chem. Soc.* **2005**, *127* (34), 11906–11907. https://doi.org/10.1021/ja053094r.

(36) Choi, Y.; Moody, I. S.; Sims, P. C.; Hunt, S. R.; Corso, B. L.; Persez, I.; Weiss,

G. A.; Collins, P. G. Single-Molecule Lysozyme Dynamics. *Science (80-. ).* **2012**, *335* (6066), 319–325. https://doi.org/10.1126/science.1214824.

(37) Weizmann, Y.; Chenoweth, D. M.; Swager, T. M. DNA−CNT Nanowire Networks for DNA Detection. *J. Am. Chem. Soc.* **2011**, *133* (10), 3238–3241. https://doi.org/10.1021/ja109180d.

(38) Sims, P. C.; Moody, I. S.; Choi, Y.; Dong, C.; Iftikhar, M.; Corso, B. L.; Gul, O. T.; Collins, P. G.; Weiss, G. A. Electronic Measurements of Single-Molecule Catalysis by CAMP-Dependent Protein Kinase A. *J. Am. Chem. Soc.* **2013**, *135* (21), 7861–7868. https://doi.org/10.1021/ja311604j.

(39) Pugliese, K. M.; Tolga Gul, O.; Choi, Y.; Olsen, T. J.; Sims, P. C.; Collins, P. G.; Weiss, G. A. Processive Incorporation of Deoxynucleoside Triphosphate Analogs by Single-Molecule DNA Polymerase i (Klenow Fragment) Nanocircuits. *J. Am. Chem. Soc.* **2015**, *137* (30), 9587–9594. https://doi.org/10.1021/jacs.5b02074.

(40) Allen, B. L.; Kichambare, P. D.; Star, A. Carbon Nanotube Field-Effect-Transistor-Based Biosensors. *Adv. Mater.* **2007**, *19* (11), 1439–1451. https://doi.org/10.1002/adma.200602043.

(41) Snow, E. S.; Perkins, F. K.; Robinsona, J. A. Chemical Vapor Detection Using Single-Walled Carbon Nanotubes. *Chem. Soc. Rev.* **2006**, *35* (9), 790–798. https://doi.org/10.1039/b515473c.

(42) Kim, S. N.; Rusling, J. F.; Papadimitrakopoulos, F. Carbon Nanotubes for Electronic and Electrochemical Detection of Biomolecules. *Adv. Mater.* **2007**, *19* (20), 3214–3228. https://doi.org/10.1002/adma.200700665.

(43) Salehi-Khojin, A.; Khalili-Araghi, F.; Kuroda, M. A.; Lin, K. Y.; Leburton, J. P.; Masel, R. I. On the Sensing Mechanism in Carbon Nanotube Chemiresistors.

*ACS Nano* **2011**, *5* (1), 153–158. https://doi.org/10.1021/nn101995f.

(44) Bouilly, D.; Hon, J.; Daly, N. S.; Trocchia, S.; Vernick, S.; Yu, J.; Warren, S.; Wu, Y.; Gonzalez, R. L.; Shepard, K. L.; Nuckolls, C. Single-Molecule Reaction Chemistry in Patterned Nanowells. *Nano Lett.* **2016**, *16* (7), 4679–4685. https://doi.org/10.1021/acs.nanolett.6b02149.

(45) Wang, F.; Swager, T. M. Diverse Chemiresistors Based upon Covalently Modified Multiwalled Carbon Nanotubes. *J. Am. Chem. Soc.* **2011**, *133* (29), 11181–11193. https://doi.org/10.1021/ja201860g.

(46) Chen, G.; Li, J.; Lv, H.; Wang, S.; Zuo, J.; Zhu, L. Mesoporous Coxsn(1 - x)O2 as an Efficient Oxygen Evolution Catalyst Support for Spe Water Electrolyzer. *R. Soc. Open Sci.* **2019**, *6* (4), 1–25. https://doi.org/10.6084/m9.figshare.

(47) Hamaguchi, N.; Ellington, A.; Stanton, M. Aptamer Beacons for the Direct Detection of Proteins. *Anal. Biochem.* **2001**, *294* (2), 126–131. https://doi.org/10.1006/abio.2001.5169.

(48) Hermann, T.; Patel, D. J. Adaptive Recognition by Nucleic Acid Aptamers. *Science (80-. ).* **2000**, *287* (5454), 820–825. https://doi.org/10.1126/science.287.5454.820.

(49) Khosravi, F.; Loeian, S. M.; Panchapakesan, B. Ultrasensitive Label-Free Sensing of IL-6 Based on PASE Functionalized Carbon Nanotube Micro-Arrays with RNA-Aptamers as Molecular Recognition Elements. *Biosensors* **2017**, *7* (2). https://doi.org/10.3390/bios7020017.

(50) Liu, J.; Cao, Z.; Lu, Y. *Functional Nucleic Acid Sensors*; 2009; Vol. 109. https://doi.org/10.1021/cr030183i.

(51) Liu, S.; Zhang, X.; Luo, W.; Wang, Z.; Guo, X.; Steigerwald, M. L.; Fang, X. Single-Molecule Detection of Proteins Using Aptamer-Functionalized

Molecular Electronic Devices. *Angew. Chemie - Int. Ed.* **2011**, *50* (11), 2496–2502. https://doi.org/10.1002/anie.201006469.

(52) Maehashi, K.; Katsura, T.; Kerman, K.; Takamura, Y.; Matsumoto, K.; Tamiya, E. Label-Free Protein Biosensor Based on Aptamer-Modified Carbon Nanotube Field-Effect Transistors. *Anal. Chem.* **2007**, *79* (2), 782–787. https://doi.org/10.1021/ac060830g.

(53) Ordinario, D. D.; Burke, A. M.; Phan, L.; Jocson, J. M.; Wang, H.; Dickson, M. N.; Gorodetsky, A. A. Sequence Specific Detection of Restriction Enzymes at DNA-Modified Carbon Nanotube Field Effect Transistors. *Anal. Chem.* **2014**, *86* (17), 8628–8633. https://doi.org/10.1021/ac501441d.

(54) Shangguan, D.; Meng, L.; Cao, Z. C.; Xiao, Z.; Fang, X.; Li, Y.; Cardona, D.; Witek, R. P.; Liu, C.; Tan, W. Identification of Liver Cancer-Specific Aptamers Using Whole Live Cells. *Anal. Chem.* **2008**, *80* (3), 721–728. https://doi.org/10.1021/ac701962v.

(55) So, H. M.; Park, D. W.; Jeon, E. K.; Kim, Y. H.; Kim, B. S.; Lee, C. K.; Choi, S. Y.; Kim, S. C.; Chang, H.; Lee, J. O. Detection and Titer Estimation of Escherichia Coli Using Aptamer-Functionalized Single-Walled Carbon-Nanotube Field-Effect Transistors. *Small* **2008**, *4* (2), 197–201. https://doi.org/10.1002/smll.200700664.

(56) Stojanovic, M. N.; Kolpashchikov, D. M. Modular Aptameric Sensors. *J. Am. Chem. Soc.* **2004**, *126* (30), 9266–9270. https://doi.org/10.1021/ja032013t.

(57) Zheng, M.; Jagota, A.; Semke, E. D.; Diner, B. A.; McLean, R. S.; Lustig, S. R.; Richardson, R. E.; Tassi, N. G. DNA-Assisted Dispersion and Separation of Carbon Nanotubes. *Nat. Mater.* **2003**, *2* (5), 338–342. https://doi.org/10.1038/nmat877.

(58) Martin, J. A.; Chávez, J. L.; Chushak, Y.; Chapleau, R. R.; Hagen, J.; Kelley-Loughnane, N. Tunable Stringency Aptamer Selection and Gold Nanoparticle Assay for Detection of Cortisol. *Anal. Bioanal. Chem.* **2014**, *406* (19), 4637–4647. https://doi.org/10.1007/s00216-014-7883-8.

(59) Gatti, R.; Antonelli, G.; Prearo, M.; Spinella, P.; Cappellin, E.; De Palo, E. F. Cortisol Assays and Diagnostic Laboratory Procedures in Human Biological Fluids. *Clin. Biochem.* **2009**, *42* (12), 1205–1217. https://doi.org/https://doi.org/10.1016/j.clinbiochem.2009.04.011.

(60) Mendonsa, S. D.; Bowser, M. T. In Vitro Selection of Aptamers with Affinity for Neuropeptide Y Using Capillary Electrophoresis. *J. Am. Chem. Soc.* **2005**, *127* (26), 9382–9383. https://doi.org/10.1021/ja052406n.

(61) Andrews, J. A.; Neises, K. D. Cells, Biomarkers, and Post-Traumatic Stress Disorder: Evidence for Peripheral Involvement in a Central Disease. *J. Neurochem.* **2012**, *120* (1), 26–36. https://doi.org/10.1111/j.1471-4159.2011.07545.x.

(62) Yang, K. A.; Pei, R.; Stefanovic, D.; Stojanovic, M. N. Optimizing Cross-Reactivity with Evolutionary Search for Sensors. *J. Am. Chem. Soc.* **2012**, *134* (3), 1642–1647. https://doi.org/10.1021/ja2084256.

(63) Lapchak, P. A.; Chapman, D. F.; Nunez, S. Y.; Zivin, J. A. Dehydroepiandrosterone Sulfate Is Neuroprotective in a Reversible Spinal Cord Ischemia Model: Possible Involvement of GABA(A) Receptors. *Stroke* **2000**, *31* (8), 1953–1957. https://doi.org/10.1161/01.STR.31.8.1953.

(64) Park, H.; Zhao, J.; Lu, J. P. Effects of Sidewall Functionalization on Conducting Properties of Single Wall Carbon Nanotubes. *Nano Lett.* **2006**, *6* (5), 916–919. https://doi.org/10.1021/nl052488d.

(65) Blake, R. D.; Delcourt, S. G. Thermodynamic Effects of Formamide on DNA Stability. *Nucleic Acids Res.* **1996**, *24* (11), 2095–2103. https://doi.org/10.1093/nar/24.11.2095.

(66) Martínez, M. T.; Tseng, Y. C.; González, M.; Bokor, J. Streptavidin as CNTs and DNA Linker for the Specific Electronic and Optical Detection of DNA Hybridization. *J. Phys. Chem. C* **2012**, *116* (42), 22579–22586. https://doi.org/10.1021/jp306535d.

(67) Lai, R. Y.; Plaxco, K. W.; Heeger, A. J. Aptamer-Based Electrochemical Detection of Picomolar Platelet-Derived Growth Factor Directly in Blood Serum. *Anal. Chem.* **2007**, *79* (1), 229–233. https://doi.org/10.1021/ac061592s.

(68) Baker, B. R.; Lai, R. Y.; Wood, M. S.; Doctor, E. H.; Heeger, A. J.; Plaxco, K. W. An Electronic, Aptamer-Based Small-Molecule Sensor for the Rapid, Label-Free Detection of Cocaine in Adulterated Samples and Biological Fluids. *J. Am. Chem. Soc.* **2006**, *128* (10), 3138–3139. https://doi.org/10.1021/ja056957p.

(69) Idili, A.; Ricci, F.; Vallée-Bélisle, A. Determining the Folding and Binding Free Energy of DNA-Based Nanodevices and Nanoswitches Using Urea Titration Curves. *Nucleic Acids Res.* **2017**, *45* (13), 7571–7580. https://doi.org/10.1093/nar/gkx498.

# Chapter 4 Tuning Electrostatic Gating of Semi-conducting Carbon Nanotubes by Controlling Protein Orientation in Biosensing Devices

## 4.1 Introduction

The construction of nanoscale field effect transistors (FETs) for sensing, whereby the gating voltage is replaced by a biomolecular event, offers huge potential for building high sensitivity, target-specific, miniaturized, and label-free biosensing devices.[1–7] Proteins are decorated with charged residues, whose distribution and area varies within a protein, so generating a specific electrostatic signature. Therefore, there is great interest in developing systems that can sense and importantly differentiate these surfaces. Moreover, protein-protein interactions are widespread in nature driving many important biological processes; these highly specific interactions can be used to electrostatically gate conductance so forming the basis of electrical-based biosensors.[4,5,8–10]

While various semiconducting materials have been used in FET sensing devices, one-dimensional (1D) materials offer advantages in terms of high surface area and restricted conduction pathways.[4,6] Among 1D nanomaterials for sensing, single walled carbon nanotubes (SWCNTs) have emerged as excellent candidates, due to their high aspect ratios, appropriate size compatibility with biological analytes, the different strategies available for their functionalization, and the ease of integrating them into electronic circuits.[6,9,11–17] CNTs have been interfaced to different biomolecules[4,6], with a

particular focus on nucleic acids [18–20] (e.g. DNA/aptamers) and proteins [8,21–27](e.g. antibodies); this allowed biomolecular events to be transduced into measurable changes in CNT conductance,[4,6,18,28–31] even down to the single biomolecule level.[20,27,32–34]

Despite the vast literature on FET biosensors, including CNT-based ones, the approaches developed so far for the assembly of protein hybrids in device configurations have typically been non-specific in terms of protein attachment sites, and hence lack control over protein orientation. This is particularly critical, as it does not allow us to fully take advantage of the unique surface distribution of electrostatic features of a protein, nor optimize communication between the protein(s) and the CNT. Furthermore, non-specific attachment can result in function and thus sensing capability being compromised through, for example, sterically blocking access to a binding site. The lack of geometric control is particularly important for nanoscale sensors where proteins constitute the sensing element and individual protein attachment variations can lead to major functional differences between devices. It is therefore of paramount importance to control the protein's site/residue that interfaces with the FET in order to define the unique surface electrostatic signature driving gating upon sensing protein targets.

Herein, we present the fabrication of CNT-protein FET biosensors with control over protein orientation in device configuration, focusing on the detection of a major cause of antimicrobial resistance, class A β-lactamases (BL).[35,36] We employed the BL inhibitory protein (BLIP2) that acts as a "universal antibody" specific for a wide range of class A BLs.[37–40] By placing the non-canonical amino acid (ncAA) p-azido-L-phenylalanine (AzF)[41,42] at three different positions in BLIP2, we defined the single-site attachment of BLIP2 to the CNTs, in order to sample different electrostatic surfaces of an incoming BL (TEM-1). We show that the device response (the electrostatic-

surface gating of SWCNTs conductance upon binding of BLs) is dependent on the defined orientation of the protein-protein complex with respect to the nanotubes. In particular, the device conductance increased or decreased depending on the selected BLIP2 orientation; this behavior is interpreted as due to changes of the local electrostatic surface presented within the Debye length upon binding, [3,29,43–45] and can support the identification of preferred proteins orientations for optimal sensing.

## 4.2 BLIP and TEM-1

### 4.2.1 Protein engineering and production

Figure 4.1 shows the strategy we proposed to control the orientation of BLIP2 attached to the sidewall of SWCNTs (see section 2.2.3). Pyrene-NHS was reacted with DBCO-amine in DMF to form pyrene-DBCO, which was used as linkers to attach BLIP2 to SWCNTs. Pyrene groups would bind to the sidewall of SWCNTs via π-π stacking, while DBCO groups would specifically react with phenol-azide (AzF) groups introduced in proteins via biocompatible strain-promoted azide-alkyne cycloaddition (SPAAC). We can introduce AzF groups at defined sites/residues in BLIP2 via protein engineering, thus controlling the orientation of BLIP2 attached to SWCNTs.

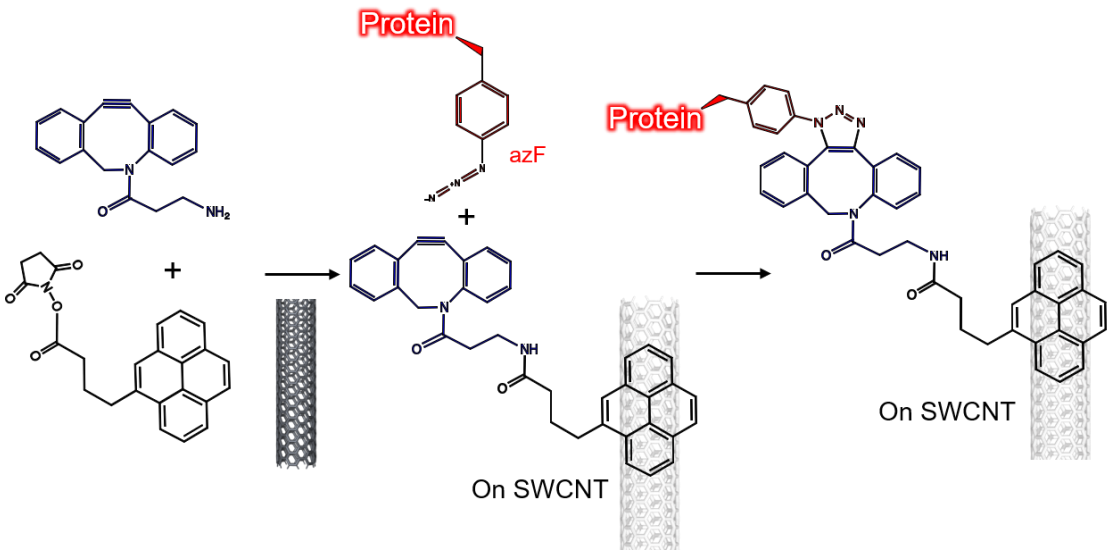

**Figure 4.1** Outline of approach for attachment of proteins to SWCNTs.

Our collaborator, the Jones group, engineered BLIP2 variants to introduce the AzF handles to BLIP2 via a reprogrammed genetic code approach. As shown in Figure 4.2, the noncanonical amino acid (ncAA) azF (p-azido-L-phenylalanine) can be incorporated at defined sites/residues in a protein of interest in response to the TAG amber stop codon (see Figure 4.2).

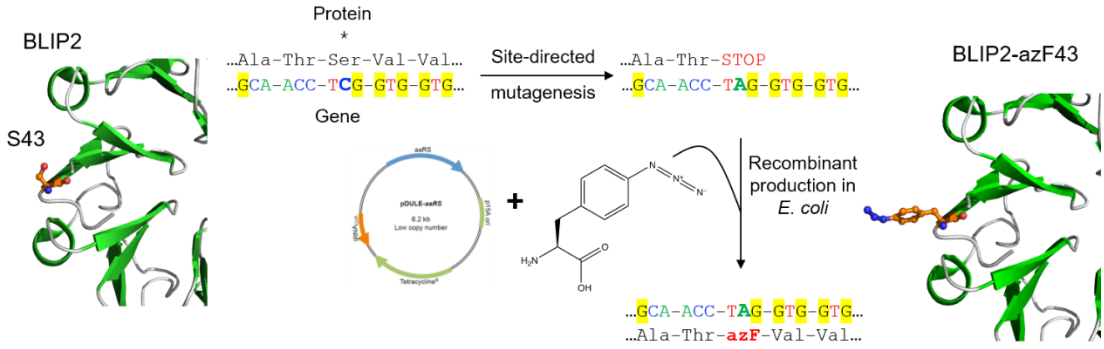


**Figure 4.2** Engineering of proteins with the noncanonical amino acid (ncAA) azF (p-azido-L-phenylalanine) at defined sites/residues via a reprogrammed genetic code approach.

Our collaborator also performed electrostatic modelling to analyse the molecular structure of BLIP2 variants and TEM-1. Based on the structural analysis, they introduced AzF handles at 4 different residues in BLIP2 to investigate different facets of the protein-interface to gate SWCNT conductance in response to the BL, TEM-1: Ala41, Ser43, Gly49 and Thr213 (Figure 6.3a). Residues 41 and 43 lie on one side of the cone-like structure, opposite to that of residue 213. Electrostatic surface modelling of BLIP2 complexed to the BL TEM-1 demonstrates that by placing AzF at residues 41/43 or 213, very distinct surface charge profiles should be sampled (Figure 4.3b). Gly49 lies at the BL binding interface so introduction of AzF and subsequent SWCNT

binding should abolish any BL-dependent conductance.

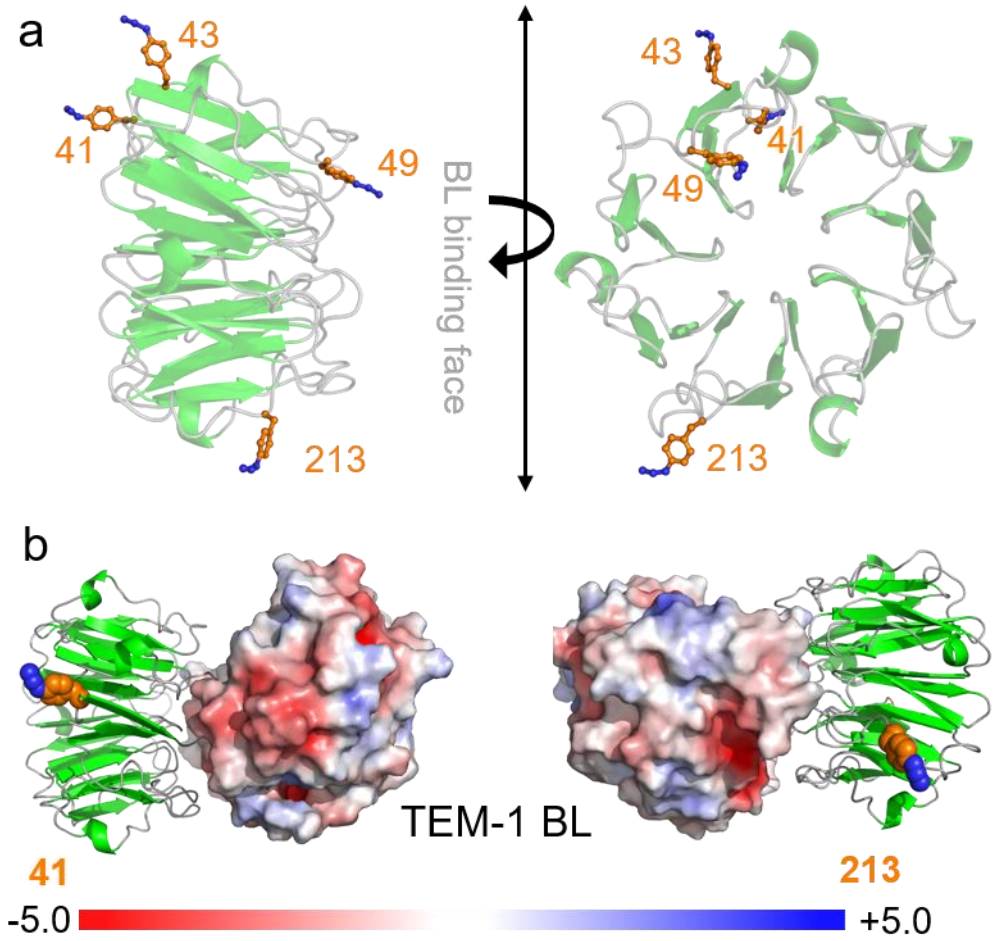


**Figure 4.3** Selected residues for replacement with AzF. (b) BLIP2-BL interaction (PDB code 1jtd). BLIP2 is shown in green with interfacing residue 41 and 213 shown as orange spheres. The electrostatic surface (calculated using APBS electrostatic software) of the BL TEM-1 is shown with a sliding scale of charge distribution. The AzF models were built as described previously.

### 4.2.2 Enzyme inhibition assay

Our collaborator performed the enzyme inhibition assay to investigate the interaction between TEM-1 and the four BLIP2 variants. The assay measured the initial rate of nitrocefin hydrolysis by TEM-1, by recording the absorbance increase on hydrolysis of the β-lactam ring amide bond. Initial rates were recorded using 0.3 nM TEM-1 with increasing concentrations of BLIP2 until full inhibition had been achieved for all BLIP2

variants. The initial rates were plotted and fitted to the Morrison Equation using GraphPad Prism software to estimate the Kiapp for each interaction. As shown in Figure 4.4, the assays revealed that BLIP2$^{41AzF}$ and BLIP2$^{213AzF}$ retained near wild type, picomolar binding affinity, while BLIP2$^{43AzF}$ and BLIP2$^{49AzF}$ had attenuated affinity in the low nanomolar range.

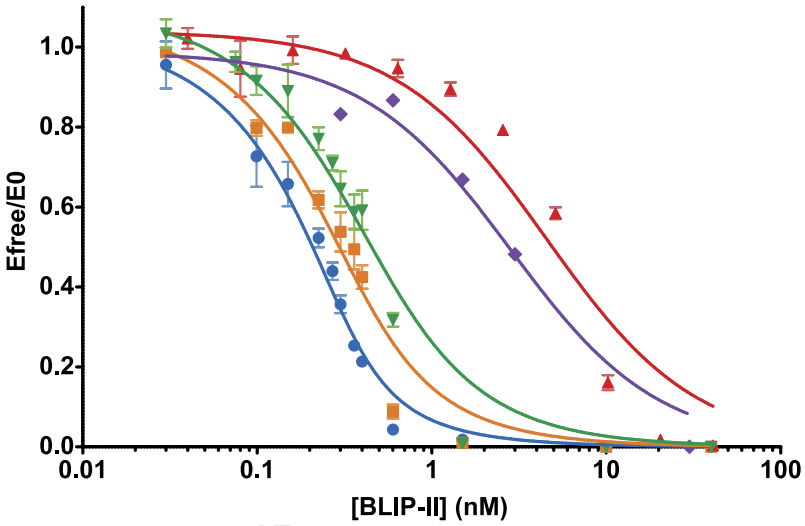


**Figure 4.4** Inhibition of TEM-1$^{WT}$ by BLIP2 variants. In order of binding affinity, left to right: Blue: BLIP2$^{WT}$. Orange: BLIP2$^{41AzF}$. Green: BLIP2$^{213AzF}$. Purple: BLIP2$^{43AzF}$. Red: BLIP2$^{49AzF}$. Values were fitted to the Morrison tight binding equation to calculate Kiapp. $E_{free}/E_0$ is the proportion of free enzyme remaining. Calculated inhibitory constant for each variant: BLIP2$^{WT}$ 32 ± 4 pM, BLIP2$^{41AzF}$ 78 ± 12 pM, BLIP2$^{43AzF}$ 1724 ± 378 pM, BLIP2$^{49AzF}$ 2839 ± 406 pM, BLIP2$^{213AzF}$ 157 ± 20 pM.

## 4.3 Attachment of BLIP to SWCNT devices

SWCNTs were immobilised between pre-patterned gold electrodes via DEP (Figure 4.5), which was confirmed by atomic force microscopy (AFM). With optimal parameters, we were able to control the assembly of SWCNTs (see section 2.3.2). Figure 4.6a shows a representative AFM image in which a small bundle of SWCNTs was immobilized between electrodes, forming FET configuration.

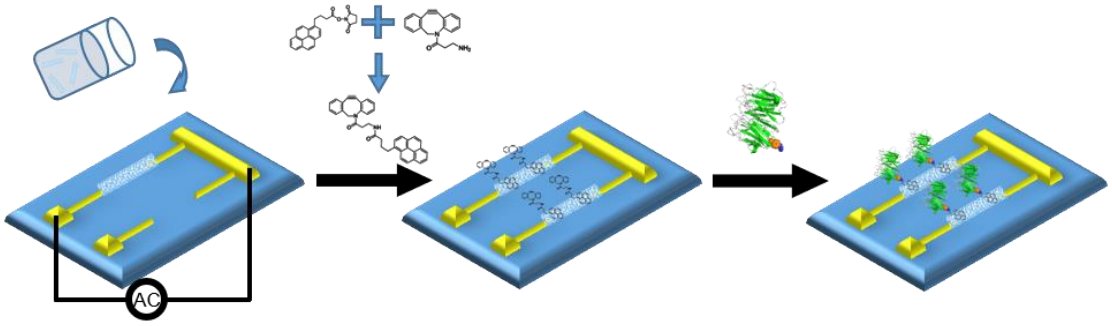


**Figure 4.5** Schematic of the fabrication of SWCNT-BLIP2 devices.

We tested the electrical properties of these devices, as shown in Figure 4.6b and Figure4.6c. The current through the devices is dependent on the gate voltage and decreases as the gate voltage increases, demonstrating the p-type nature of these SWCNT-based FETs.

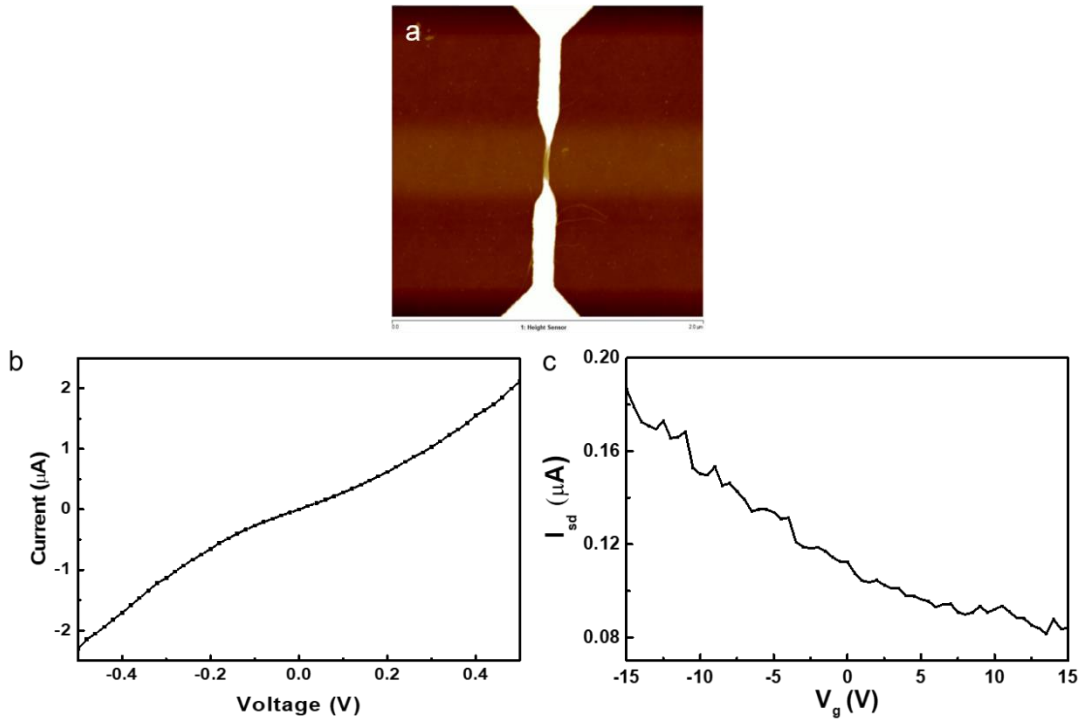


**Figure 4.6** (a)Representative AFM image of a SWCNT device and (b) representative (b) I-V curves and (c) transfer characteristics of the device ($V_{sd}$= 0.1V).

Subsequently, these devices were immersed into a mixture solution containing a 3:1

mixture of pyrene-butanol (PB) and pyrene-DBCO. PB acted as a spacer, which reduced BLIP2 density and minimized non-specific adsorption. Ethanol-amine was added to the devices to block the unreacted NHS residue to rule out the potential reaction between pyrene-NHS and proteins. On the other hand, the DBCO groups allowed attachment of BLIP2 via biocompatible strain-promoted azide-alkyne cycloaddition (SPAAC) (Figure 4.1 and Figure 4.7a) when these devices were incubated with BLIP2 variants, without altering the electronic properties of the nanotubes by direct covalent attachment. AFM was used to monitor the topographical changes before and after protein attachment. Figure 4.7b shows a representative topographical profile of the device before and after $BLIP^{241AzF}$ attachment: the transverse height profile of the same tube sector increased by ~3-4 nm, in line with the structure of BLIP2.

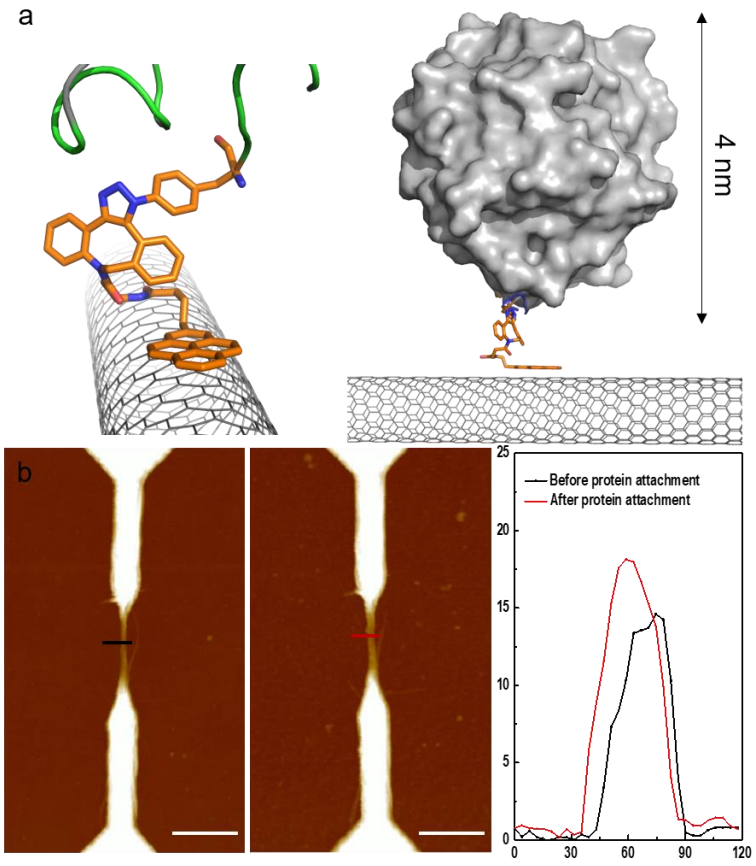


**Figure 4.7** Attachment of BLIP2 to SWCNTs. BLIP2$^{41AzF}$ is shown as a representative example. (a) Model of the BLIP2$^{41AzF}$-SWCNT interface, with a close-up of the pyrene-protein conjugation site. (b) AFM images of SWCNT devices before and after attachment of BLIP2$^{41AzF}$ and their corresponding height profile analysis.

Other BLIP2 variants (BLIP2$^{43AzF}$, BLIP2$^{49AzF}$ and BLIP2$^{213AzF}$) were also attached to the SWCNT devices, which were imaged by AFM. Figure 4.8 shows the analysis of the height profile of these devices. We observed nanotube transverse increases of 3-6 nm upon protein attachment, again in line with what was expected based on the structure of BLIP2. The height of the SWCNT bundles was controlled in the range of 10-15 nm before functionalisation, hence the SWCNT surface available for functionalisation was also limited. AFM topographical analysis allowed us to estimate the average number of proteins attached to the tubes in each device to be c.a. 40-80 proteins.

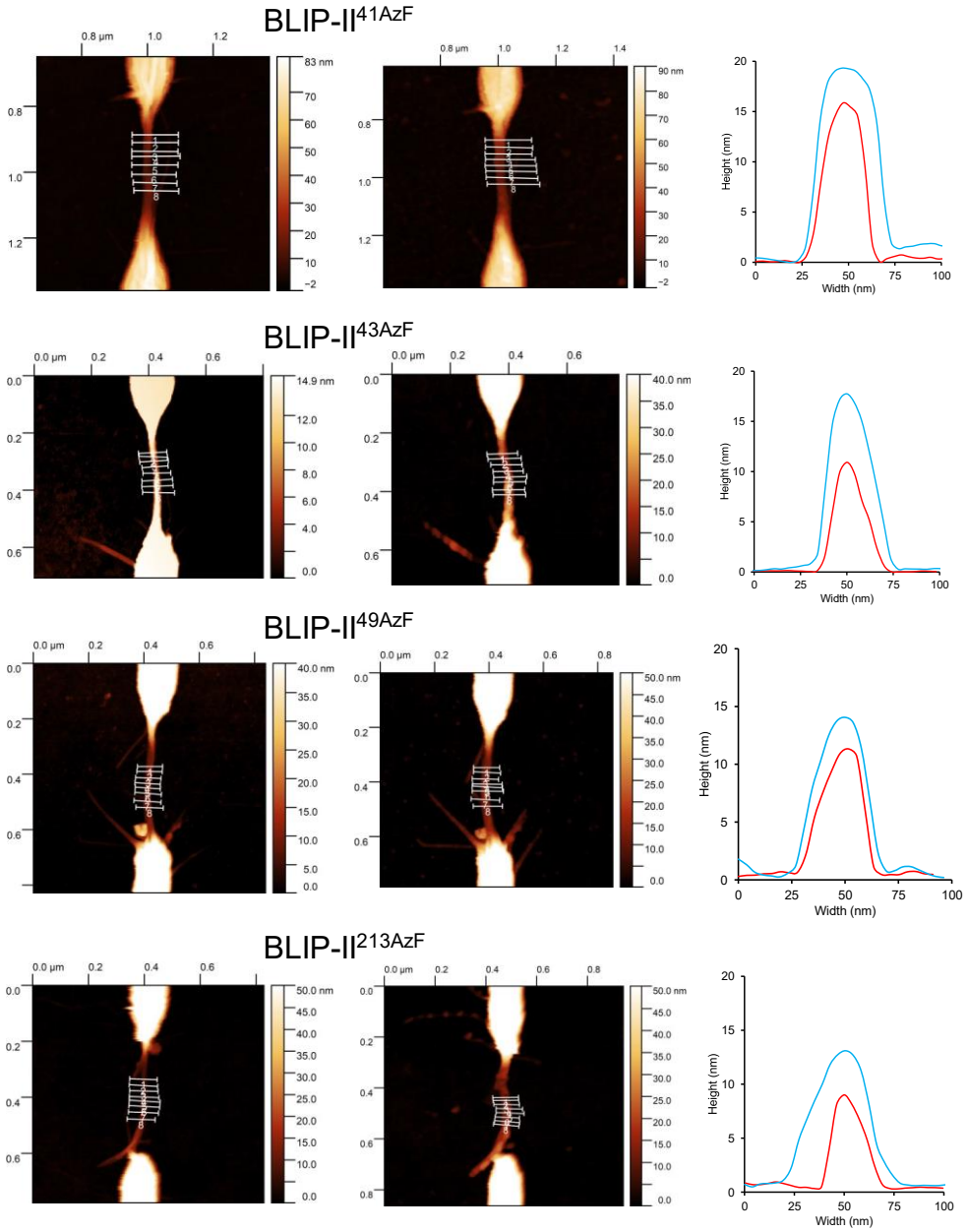


**Figure 4.8** Functionalisation of SWCNT devices with BLIP2 AzF proteins. Transverse height profiles across DBCO-pyrene functionalised SWCNT bundles before (left AFM images) and after (right AFM images) protein functionalisation. Average bundle heights increased between 3-6 nm for all variants after incubation with proteins (plots: red – before; blue – after).

Control experiments were performed to confirm the attachment of BLIP2 variants onto SWCNTs. We did not observe changes in height after SWCNT devices were immersed PB solution, suggesting that pyrene groups cannot induces changes in height (Figure

4.9a and 4.9b). The devices were subsequently incubated with BLIP2 variants. No binding of proteins was observed (Figure 4.9c), indicating that non-specific adsorption has been suppressed and that DBCO groups are essential for the protein attachment.

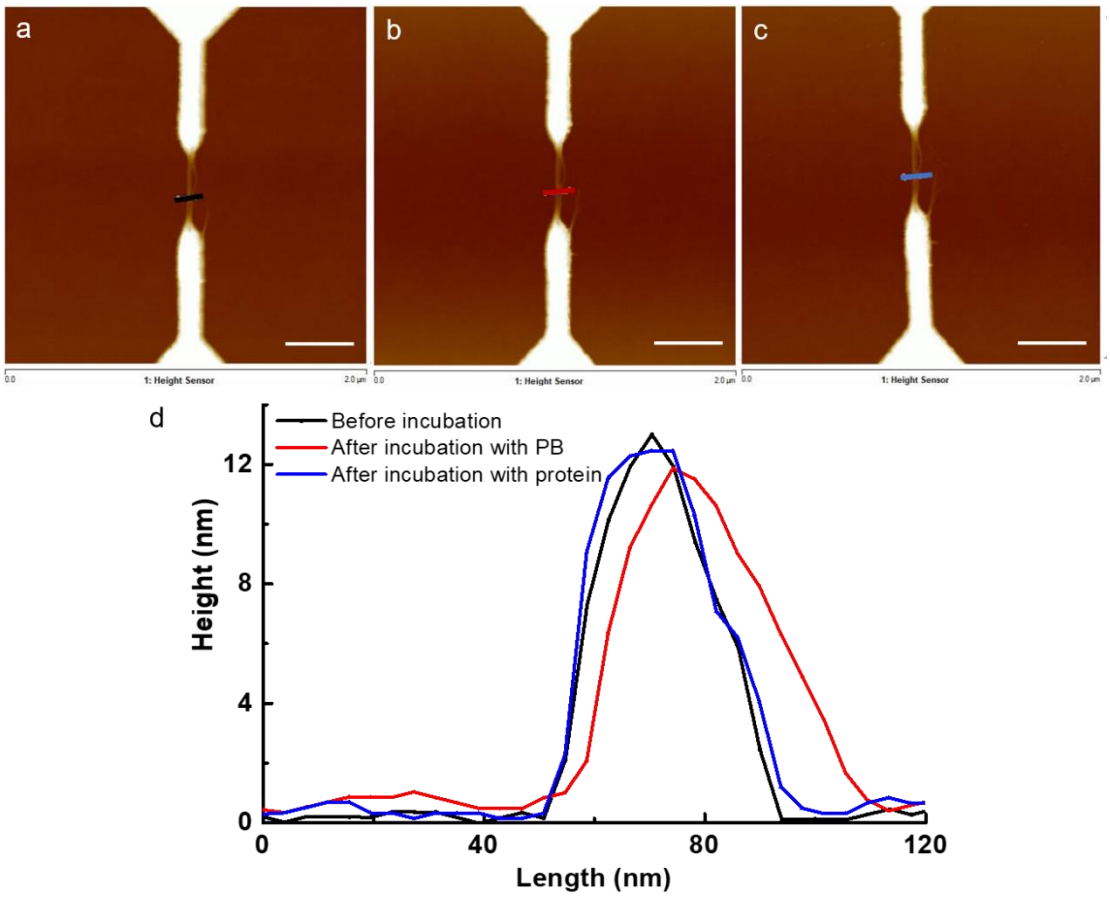


**Figure 4.9** AFM images of devices (a) before incubation with PB (12-13nm) (b) after incubation with PB (12-13nm) (c) after incubation with BLIP T213 (12-13nm) and (d) their corresponding height profile. (scale bar:400 nm)

We also incubated devices (coated with pyrene-DBCO and PB) with wild type BLIP2 (BLIP2 without AzF handles, $BLIP2^{WT}$). As shown in Figure 4.10, we did not observe changes in the height of the SWCNT bundles after incubation. These results suggest that proteins can only be attached to SWCNT devices when DBCO groups and AzF groups are available and that our AzF-containing BLIP2 variants attached to SWCNT-FETs as designed.

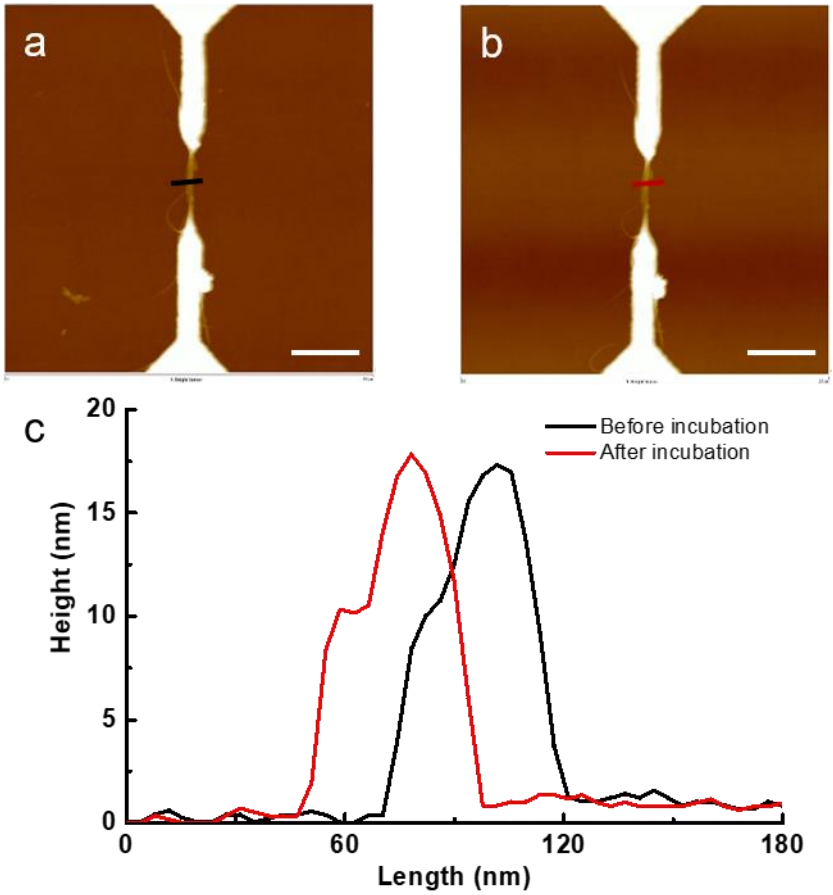


**Figure 4.10** Control experiment with BLIP$^{WT}$. AFM images of devices (a) before incubation with BLIPWT and (b) after incubation with BLIP$^{WT}$ and (c) their corresponding height profiles. (scale bar: 400nm)

## 4.4 Electrical monitoring the binding of TEM-1 to BLIP with defined orientation

We performed real-time conductance measurements by using devices functionalised with the four BLIP2 variants (and hence different protein's orientations), monitoring current dependent changes upon addition of the BL enzyme TEM-1. Dulbecco's phosphate buffered saline (DPBS) was used as the test buffer due to its high ionic strength, mainly containing 137mM sodium chloride (NaCl) and 8 mM sodium phosphate ($Na_2HPO_4$). According to Formula (1), the ionic strength ($I$) of DPBS is:

Ionic Strength: $$I = \frac{1}{2}\sum c_i \, z_i{}^2 \qquad (1)$$

where $c_i$ is the molar concentration of ion $i$ (M, mol/L), $z_i$ is the charge number of that

ion, and the sum is taken over all ions in the solution. Therefore, the ionic strength of 1×DPBS is:

$I = 0.5 \times (0.14 \times 1^2 + 0.14 \times 1^2 + 0.03 \times 12 + 0.01 \times 32)$ M

$I = 0.20$ M

Based on Formula (2), the Debye Length ($\lambda_D$) is:

Debye Length: $$\lambda_D \approx {}^{0.32}/_{\sqrt{I}} \quad (2)$$

Therefore, the Debye Length of 1×DPBS is:

$\lambda_D \approx 0.7$ nm

Therefore, the high ionic strength of DPBS restricts the Debye length ($\lambda_D$) to *circa* 0.7 nm, which is smaller than the size of TEM-1 (~2×4 nm). This indicates that only limited surfaces of TEM-1 enter the screening layer of the device, influencing the conductance of the SWCNTs.

Figure 4.11a and c shows the real time detection of TEM-1 in DPBS buffer with devices functionalised with BLIP2$^{41AzF}$. The current measured across the devices increased stepwise when TEM-1 was added at increasing concentrations. Similar results were observed when we did the detection in serum (Figure 4.11b).

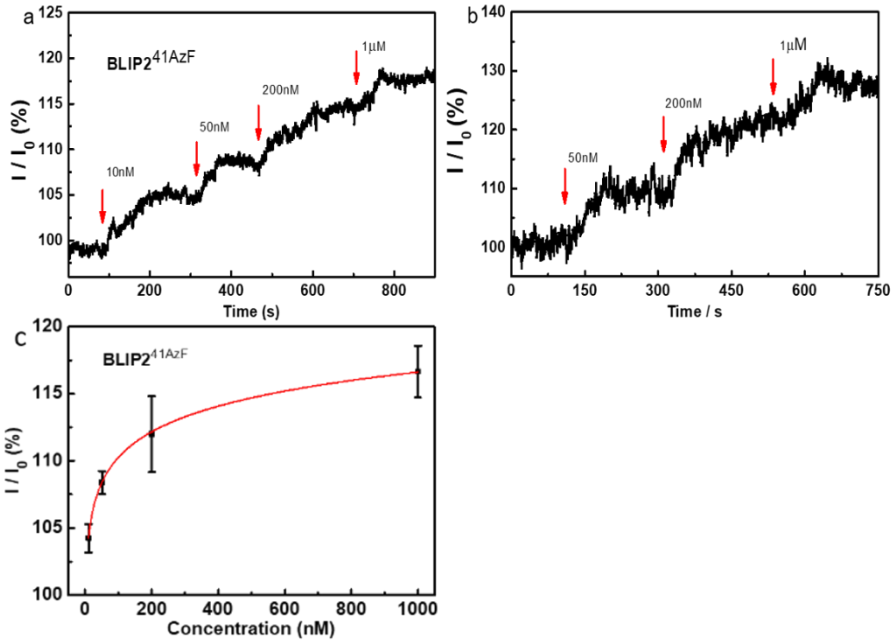


**Figure 4.11** Real-time detection of TEM-1 in (a) DPBS and (b) serum and (c) calibration curve of the detection of TEM-1 in DPBS using devices functionalised with BLIP2$^{41AzF}$. Addition of TEM-1 at different concentrations is shown on each conductance trace.

Control experiments with non-functionalised devices (i.e. without any BLIP2 variants) were performed to rule out the influence of non-specific adsorption. As shown in Figure 4.12, we did not observe any significant changes in current upon addition of DPBS buffer or TEM-1 of different concentrations. This indicates that non-specific adsorption was effectively suppressed in the SWCNT devices and that only devices functionalised with BLIP2s give an electrical response upon addition of TEM-1.

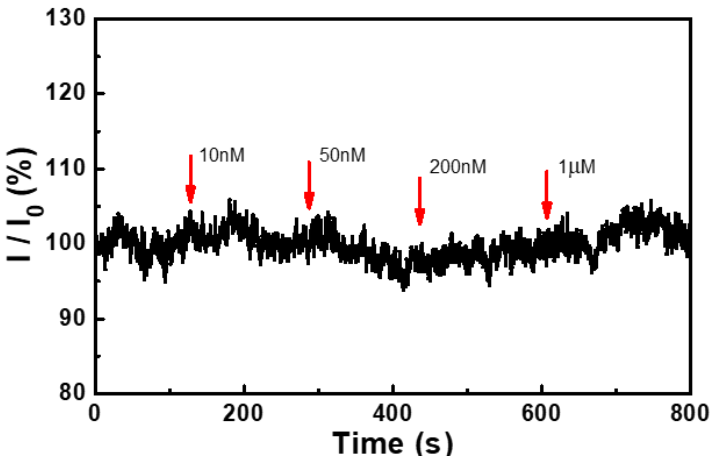

**Figure 4.12** Real time detection of TEM-1 with non-functionalised devices.

To explain the experimental results, our collaborator performed electrostatic modelling of the BLIP variants and TEM-1 (Figure 4.13). As shown in Figure 4.13a, molecular modelling of the BLIP$^{41AzF}$-pyrene adduct docked onto the surface of the SWCNT suggests that TEM-1 binding will present a negative acidic patch, comprised predominantly of residues E28, D35 and D38 within the Debye length. The observed increase in current in our p-type SWCNT-FET can therefore be rationalized as due to the higher negative charge density induced by TEM-1 binding near the nanotube surface, that stabilizes a higher concentration of positive charges in the active channel, hence acting as an additional gating mechanism.

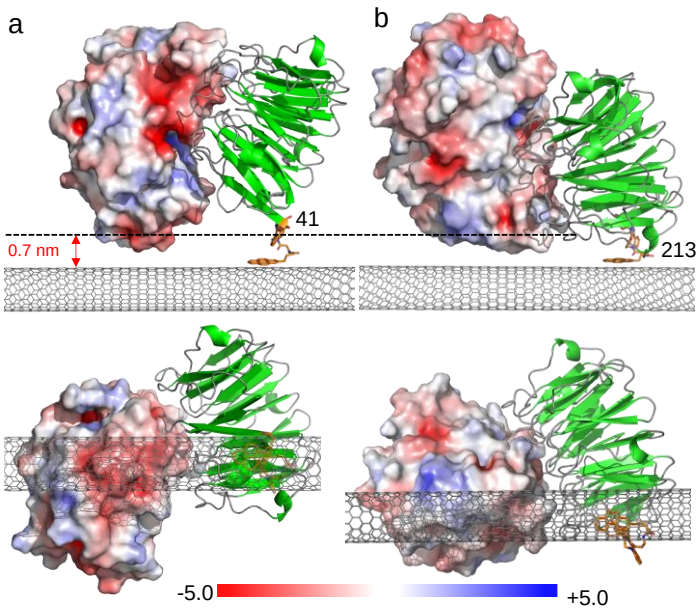


**Figure 4.13** Models of TEM-1 electrostatic surface presentation on binding (a) BLIP2$^{41AzF}$ and (b) BLIP2$^{213AzF}$. Top is a side-on view of the complex with the Debye length shown as a dashed line. The pyrene adduct is coloured orange and SWCNT grey. Bottom is the bottom up view of complex with the SWCNT in the foreground.

Devices functionalised with BLIP2$^{43AzF}$ exhibit a similar trend with increased conductance observed upon addition of TEM-1. However, the step changes on

increasing TEM-1 concentration are significantly different (Figure 4.14b and c): current increases were smaller than the those observed for BLIP2$^{41AzF}$, with little change observed at lower TEM-1 concentrations (10-50 nM). It is reasonable to assume that is due to the lower affinity of BLIP2$^{43AzF}$ for TEM-1 (Figure 4.4) making the bound state less populated compared to the BLIP2$^{41AzF}$ case. This may be impacted further by the positioning of the BL binding site of BLIP2$^{43AzF}$ relative to the nanotube surface. While BLIP2$^{43AzF}$ presents the same negative patch of TEM-1 as BLIP2$^{41AzF}$, relativity small changes in the orientation of BLIP2 on the nanotube can increase the distance between TEM-1 and the tube surface to beyond the Debye length. Thus, even small apparent changes in residue coupling position can have major impacts on biosensing capability.

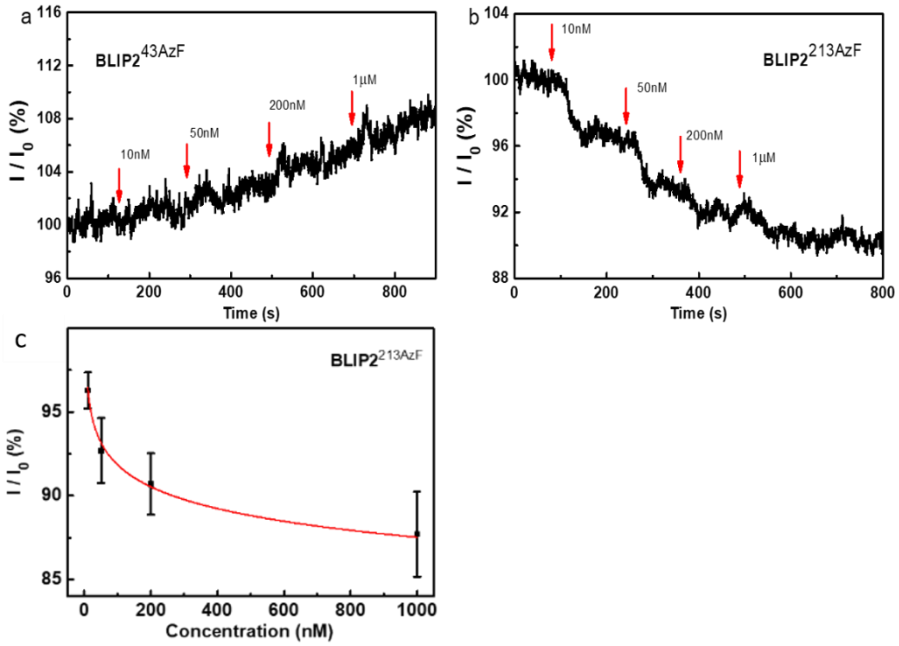


**Figure 4.14** Real-time detection of TEM-1 in DPBS using devices functionalised with (a) BLIP2$^{43AzF}$ and (b) BLIP2$^{213AzF}$; (c) Calibration curve of the detection of TEM-1 in DPBS using devices functionalised with BLIP2$^{213AzF}$. Addition of TEM-1 at different concentrations is shown on each conductance trace.

However, devices functionalised with BLIP$^{49AzF}$ did not exhibit significant changes in current response on addition of TEM-1 at various concentrations (Figure 4.15). This

behaviour was expected, and BLIP2$^{AzF49}$ acts as a secondary control: its attachment to the SWCNT prevents BL binding, with the SWCNT and the pyrene adduct blocking access to the protein's TEM-1 binding site (Figure 4.14b).

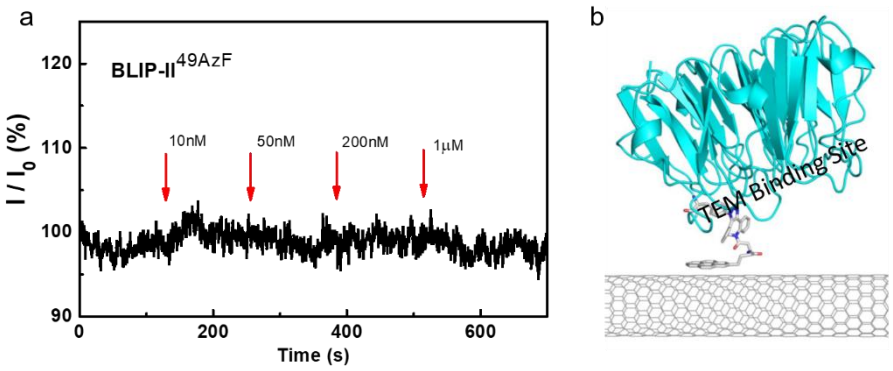


Figure 4.15 (a) Conductance across SWCNTs electrodes functionalised with BLIP2$^{49AzF}$. The red arrows indicate the time points when TEM-1 at the stated concentration was added. (b) Model of the BLIP2$^{49AzF}$-SWCNT complex. The binding site for incoming TEM-1 will be occluded by both the SWCNT and the pyrene adduct.

To test how the presentation of different electrostatic surfaces affect conductance across our devices, we assessed the behaviour of BLIP2$^{213AzF}$ functionalised FETs to TEM-1 binding. As shown in Figure 4.14b, the current through these devices decreased stepwise as the concentration of the added TEM-1 was increased, i.e. an opposite response if compared to devices functionalized with BLIP2$^{41AzF}$. Structural Modelling suggests that TEM-1 presents a positively charged basic patch (Figure 4.13b) comprised of residues R93, R94, H96 within the Debye length of BLIP2$^{213AzF}$ functionalised SWCNTs. Due to the p-type nature of our SWCNT-FETs, the positive charge of the protein complex within the Debye length of the SWCNTs increases charge carrier repulsion decreasing transconductance. The observed differences in the conductance behaviour of the SWCNT-FET devices presenting distinct protein's variants, can be interpreted as due to changes in the local electrostatic surface accessible within the Debye length upon binding, and can support the identification of preferred

proteins orientations toward optimized sensing.

## 4.5 Conclusions

In summary, we fabricated SWCNT-FETs to investigate the influence of a protein's electrostatic surface features in the electrical sensing of a β-lactamase enzyme involved in AMR. Four distinct BLIP2 variants were engineered bioorthogonal reaction handles at specific residues allowing proteins to be tethered to SWCNTs in defined orientations. Devices functionalised with different BLIP2 variants successfully detected the β-lactamase TEM-1 through changes in conductance, with device performance dependent on BLIP2 attachment site, and hence orientation. Presentation of different TEM-1 electrostatic surfaces within the Debye length led either to increase or decrease in conductance. This allowed biosensing through electrostatic surface profiling of distinct protein-protein interactions rather than just basic on/off binding events, whereby one protein may bind several different proteins. With regards to AMR detection this has significant potential as BLIP2 binds a range of BL enzymes, each with their own specific electrostatic profile. This may in turn open up new approaches for AMR-related diagnostic devices.

## References

(1) Luo, X.; Davis, J. J. Electrical Biosensors and the Label Free Detection of Protein Disease Biomarkers. *Chem. Soc. Rev.* **2013**, *42* (13), 5944. https://doi.org/10.1039/c3cs60077g.

(2) Cui, Y.; Wei, Q.; Park, H.; Lieber, C. M. Nanowire Nanosensors for Highly Sensitive and Selective Detection of Biological and Chemical Species. *Science (80-. ).* **2001**, *293* (5533), 1289–1292. https://doi.org/10.1126/science.1062711.

(3) Nakatsuka, N.; Yang, K. A.; Abendroth, J. M.; Cheung, K. M.; Xu, X.; Yang, H.; Zhao, C.; Zhu, B.; Rim, Y. S.; Yang, Y.; Weiss, P. S.; Stojanović, M. N.; Andrews, A. M. Aptamer-Field-Effect Transistors Overcome Debye Length Limitations for Small-Molecule Sensing. *Science (80-. ).* **2018**, *362* (6412), 319–324. https://doi.org/10.1126/science.aao675.

(4) Kauffman, D. R.; Star, A. Electronically Monitoring Biological Interactions with Carbon Nanotube Field-Effect Transistors. *Chem. Soc. Rev.* **2008**, *37* (6), 1197–1206. https://doi.org/10.1039/B709567H.

(5) Zhang, A.; Lieber, C. M. Nano-Bioelectronics. *Chem. Rev.* **2016**, *116* (1), 215–257. https://doi.org/10.1021/acs.chemrev.5b00608.

(6) Fennell, J. F.; Liu, S. F.; Azzarelli, J. M.; Weis, J. G.; Rochat, S.; Mirica, K. A.; Ravnsbæk, J. B.; Swager, T. M. Nanowire Chemical/Biological Sensors: Status and a Roadmap for the Future. *Angew. Chemie - Int. Ed.* **2016**, *55* (4), 1266–1281. https://doi.org/10.1002/anie.201505308.

(7) Seo, G.; Lee, G.; Kim, M. J.; Baek, S.-H.; Choi, M.; Ku, K. B.; Lee, C.-S.; Jun, S.; Park, D.; Kim, H. G.; Kim, S.-J.; Lee, J.-O.; Kim, B. T.; Park, E. C.; Kim, S. Il. Rapid Detection of COVID-19 Causative Virus (SARS-CoV-2) in Human Nasopharyngeal Swab Specimens Using Field-Effect Transistor-Based Biosensor. *ACS Nano* **2020**. https://doi.org/10.1021/acsnano.0c02823.

(8) Broza, Y. Y.; Zhou, X.; Yuan, M.; Qu, D.; Zheng, Y.; Vishinkin, R.; Khatib, M.; Wu, W.; Haick, H. Disease Detection with Molecular Biomarkers: From Chemistry of Body Fluids to Nature-Inspired Chemical Sensors. *Chem. Rev.* **2019**, *119* (22), 11761–11817. https://doi.org/10.1021/acs.chemrev.9b00437.

(9) Jariwala, D.; Sangwan, V. K.; Lauhon, L. J.; Marks, T. J.; Hersam, M. C. Carbon Nanomaterials for Electronics, Optoelectronics, Photovoltaics, and Sensing. *Chem. Soc.*

*Rev.* **2013**, *42* (7), 2824–2860. https://doi.org/10.1039/C2CS35335K.

(10) Keskin, O.; Gursoy, A.; Ma, B.; Nussinov, R. Principles of Protein−Protein Interactions: What Are the Preferred Ways For Proteins To Interact? *Chem. Rev.* **2008**, *108* (4), 1225–1244. https://doi.org/10.1021/cr040409x.

(11) Dresselhaus, M. S.; Dresselhaus, G.; Saito, R. Physics of Carbon Nanotubes. *Carbon N. Y.* **1995**, *33* (7), 883–891. https://doi.org/https://doi.org/10.1016/0008-6223(95)00017-8.

(12) Tasis, D.; Tagmatarchis, N.; Bianco, A.; Prato, M. Chemistry of Carbon Nanotubes. *Chem. Rev.* **2006**, *106* (3), 1105–1136. https://doi.org/10.1021/cr050569o.

(13) Kim, S. N.; Rusling, J. F.; Papadimitrakopoulos, F. Carbon Nanotubes for Electronic and Electrochemical Detection of Biomolecules. *Adv. Mater.* **2007**, *19* (20), 3214–3228. https://doi.org/10.1002/adma.200700665.

(14) Schnorr, J. M.; Swager, T. M. Emerging Applications of Carbon Nanotubes. *Chem. Mater.* **2011**, *23* (3), 646–657. https://doi.org/10.1021/cm102406h.

(15) Hodge, S. A.; Bayazit, M. K.; Coleman, K. S.; Shaffer, M. S. P. Unweaving the Rainbow: A Review of the Relationship between Single-Walled Carbon Nanotube Molecular Structures and Their Chemical Reactivity. *Chem. Soc. Rev.* **2012**, *41* (12), 4409–4429. https://doi.org/10.1039/C2CS15334C.

(16) Liu, L.; Han, J.; Xu, L.; Zhou, J.; Zhao, C.; Ding, S.; Shi, H.; Xiao, M.; Ding, L.; Jin, C.; Zhang, Z.; Peng, L. Aligned, High-Density Semiconducting Carbon Nanotube Arrays for High-Performance Electronics. **2020**, *1* (May), 850–856.

(17) Sun, W.; Shen, J.; Zhao, Z.; Arellano, N.; Rettner, C.; Tang, J.; Zheng, M.; Han, S.; Shih, W. M.; Maune, H. T.; Yin, P. Precise Pitch-Scaling of Carbon Nanotube Arrays within Three-Dimensional DNA Nanotrenches. **2020**, *877* (May), 874–877.

(18) Xu, X.; Clément, P.; Eklöf-Österberg, J.; Kelley-Loughnane, N.; Moth-Poulsen, K.; Chávez, J. L.; Palma, M. Reconfigurable Carbon Nanotube Multiplexed Sensing Devices. *Nano Lett.* **2018**, *18* (7), 4130–4135. https://doi.org/10.1021/acs.nanolett.8b00856.

(19) So, H.-M.; Won, K.; Kim, Y. H.; Kim, B.-K.; Ryu, B. H.; Na, P. S.; Kim, H.; Lee, J.-O. Single-Walled Carbon Nanotube Biosensors Using Aptamers as Molecular Recognition Elements. *J. Am. Chem. Soc.* **2005**, *127* (34), 11906–11907. https://doi.org/10.1021/ja053094r.

(20) Sorgenfrei, S.; Chiu, C.; Gonzalez, R. L.; Yu, Y.-J.; Kim, P.; Nuckolls, C.; Shepard, K. L. Label-Free Single-Molecule Detection of DNA-Hybridization Kinetics with a Carbon Nanotube Field-Effect Transistor. *Nat. Nanotechnol.* **2011**, *6* (2), 126–132. https://doi.org/10.1038/nnano.2010.275.

(21) Calvaresi, M.; Zerbetto, F. The Devil and Holy Water: Protein and Carbon Nanotube Hybrids. *Acc. Chem. Res.* **2013**, *46* (11), 2454–2463. https://doi.org/10.1021/ar300347d.

(22) Thomas, S. K.; Jamieson, W. D.; Gwyther, R. E. A.; Bowen, B. J.; Beachey, A.; Worthy, H. L.; Macdonald, J. E.; Elliott, M.; Castell, O. K.; Jones, D. D. Site-Specific Protein Photochemical Covalent Attachment to Carbon Nanotube Side Walls and Its Electronic Impact on Single Molecule Function. *Bioconjug. Chem.* **2020**, *31* (3), 584–594. https://doi.org/10.1021/acs.bioconjchem.9b00719.

(23) Freeley, M.; Worthy, H. L.; Ahmed, R.; Bowen, B.; Watkins, D.; Macdonald, J. E.; Zheng, M.; Jones, D. D.; Palma, M. Site-Specific One-to-One Click Coupling of Single Proteins to Individual Carbon Nanotubes: A Single-Molecule Approach. *J. Am. Chem. Soc.* **2017**, *139* (49), 17834–17840. https://doi.org/10.1021/jacs.7b07362.

(24) Goldsmith, B. R.; Mitala, J. J.; Josue, J.; Castro, A.; Lerner, M. B.; Bayburt, T. H.; Khamis, S. M.; Jones, R. A.; Brand, J. G.; Sligar, S. G.; Luetje, C. W.; Gelperin, A.;

Rhodes, P. A.; Discher, B. M.; Johnson, A. T. C. Biomimetic Chemical Sensors Using Nanoelectronic Readout of Olfactory Receptor Proteins. *ACS Nano* **2011**, *5* (7), 5408–5416. https://doi.org/10.1021/nn200489j.

(25) Choi, Y.; Moody, I. S.; Sims, P. C.; Hunt, S. R.; Corso, B. L.; Seitz, D. E.; Blaszczak, L. C.; Collins, P. G.; Weiss, G. A. Single-Molecule Dynamics of Lysozyme Processing Distinguishes Linear and Cross-Linked Peptidoglycan Substrates. *J. Am. Chem. Soc.* **2012**, *134* (4), 2032–2035. https://doi.org/10.1021/ja211540z.

(26) Antonucci, A.; Kupis-Rozmysłowicz, J.; Boghossian, A. A. Noncovalent Protein and Peptide Functionalization of Single-Walled Carbon Nanotubes for Biodelivery and Optical Sensing Applications. *ACS Appl. Mater. Interfaces* **2017**, *9* (13), 11321–11331. https://doi.org/10.1021/acsami.7b00810.

(27) Choi, Y.; Moody, I. S.; Sims, P. C.; Hunt, S. R.; Corso, B. L.; Persez, I.; Weiss, G. A.; Collins, P. G. Single-Molecule Lysozyme Dynamics. *Science (80-. ).* **2012**, *335* (6066), 319–325. https://doi.org/10.1126/science.1214824.

(28) Wylie, B. J.; Franks, W. T.; Graesser, D. T.; Rienstra, C. M. Site-Specific 13C Chemical Shift Anisotropy Measurements in a Uniformly 15N,13C-Labeled Microcrystalline Protein by 3D Magic-Angle Spinning NMR Spectroscopy. *J. Am. Chem. Soc.* **2005**, *127* (34), 11946–11947. https://doi.org/10.1021/ja053862e.

(29) Zheng, H. Y.; Alsager, O. A.; Zhu, B.; Travas-Sejdic, J.; Hodgkiss, J. M.; Plank, N. O. V. Electrostatic Gating in Carbon Nanotube Aptasensors. *Nanoscale* **2016**, *8* (28), 13659–13668. https://doi.org/10.1039/C5NR08117C.

(30) Weizmann, Y.; Chenoweth, D. M.; Swager, T. M. DNA−CNT Nanowire Networks for DNA Detection. *J. Am. Chem. Soc.* **2011**, *133* (10), 3238–3241. https://doi.org/10.1021/ja109180d.

(31) Ordinario, D. D.; Burke, A. M.; Phan, L.; Jocson, J.-M.; Wang, H.; Dickson, M. N.;

Gorodetsky, A. A. Sequence Specific Detection of Restriction Enzymes at DNA-Modified Carbon Nanotube Field Effect Transistors. *Anal. Chem.* **2014**, *86* (17), 8628–8633. https://doi.org/10.1021/ac501441d.

(32) Www.Advmat.de E. **2013**, *25* (25), 10488.

(33) Vernick, S.; Trocchia, S. M.; Warren, S. B.; Young, E. F.; Bouilly, D.; Gonzalez, R. L.; Nuckolls, C.; Shepard, K. L. Electrostatic Melting in a Single-Molecule Field-Effect Transistor with Applications in Genomic Identification. *Nat. Commun.* **2017**, *8* (May), 1–9. https://doi.org/10.1038/ncomms15450.

(34) Rosenstein, J. K.; Lemay, S. G.; Shepard, K. L. Single-Molecule Bioelectronics. *Wiley Interdiscip. Rev. Nanomedicine Nanobiotechnology* **2015**, *7* (4), 475–493. https://doi.org/10.1002/wnan.1323.

(35) Petrosino, J.; Cantu, C.; Palzkill, T. β-Lactamases: Protein Evolution in Real Time. *Trends Microbiol.* **1998**, *6* (8), 323–327. https://doi.org/https://doi.org/10.1016/S0966-842X(98)01317-1.

(36) MATAGNE, A.; LAMOTTE-BRASSEUR, J.; FRÈRE, J.-M. Catalytic Properties of Class A β-Lactamases: Efficiency and Diversity. *Biochem. J.* **1998**, *330* (2), 581–598. https://doi.org/10.1042/bj3300581.

(37) Fryszczyn, B. G.; Adamski, C. J.; Brown, N. G.; Rice, K.; Huang, W.; Palzkill, T. Role of β-Lactamase Residues in a Common Interface for Binding the Structurally Unrelated Inhibitory Proteins BLIP and BLIP-II. *Protein Sci.* **2014**, *23* (9), 1235–1246. https://doi.org/10.1002/pro.2505.

(38) Gretes, M.; Lim, D. C.; de Castro, L.; Jensen, S. E.; Kang, S. G.; Lee, K. J.; Strynadka, N. C. J. Insights into Positive and Negative Requirements for Protein–Protein Interactions by Crystallographic Analysis of the β-Lactamase Inhibitory Proteins BLIP, BLIP-I, and BLP. *J. Mol. Biol.* **2009**, *389* (2), 289–305.

https://doi.org/https://doi.org/10.1016/j.jmb.2009.03.058.

(39) Brown, N. G.; Chow, D.-C.; Sankaran, B.; Zwart, P.; Prasad, B. V. V.; Palzkill, T. Analysis of the Binding Forces Driving the Tight Interactions between β-Lactamase Inhibitory Protein-II (BLIP-II) and Class A β-Lactamases. *J. Biol. Chem.* **2011**, *286* (37), 32723–32735. https://doi.org/10.1074/jbc.M111.265058.

(40) Lim, D.; Park, H. U.; De Castro, L.; Kang, S. G.; Lee, H. S.; Jensen, S.; Lee, K. J.; Strynadka, N. C. J. Crystal Structure and Kinetic Analysis of β-Lactamase Inhibitor Protein-II in Complex with TEM-1 β-Lactamase. *Nat. Struct. Biol.* **2001**, *8* (10), 848–852. https://doi.org/10.1038/nsb1001-848.

(41) Lang, K.; Chin, J. W. Cellular Incorporation of Unnatural Amino Acids and Bioorthogonal Labeling of Proteins. *Chem. Rev.* **2014**, *114* (9), 4764–4806. https://doi.org/10.1021/cr400355w.

(42) Reddington, S.; Watson, P.; Rizkallah, P.; Tippmann, E.; Jones, D. D. Genetically Encoding Phenyl Azide Chemistry: New Uses and Ideas for Classical Biochemistry. *Biochem. Soc. Trans.* **2013**, *41* (5), 1177–1182. https://doi.org/10.1042/BST20130094.

(43) Stern, E.; Wagner, R.; Sigworth, F. J.; Breaker, R.; Fahmy, T. M.; Reed, M. A. Importance of the Debye Screening Length on Nanowire Field Effect Transistor Sensors. *Nano Lett.* **2007**, *7* (11), 3405–3409. https://doi.org/10.1021/nl071792z.

(44) Kase, H.; Negishi, R.; Arifuku, M.; Kiyoyanagi, N.; Kobayashi, Y. Biosensor Response from Target Molecules with Inhomogeneous Charge Localization. *J. Appl. Phys.* **2018**, *124* (6). https://doi.org/10.1063/1.5036538.

(45) Vacic, A.; Criscione, J. M.; Rajan, N. K.; Stern, E.; Fahmy, T. M.; Reed, M. A. Determination of Molecular Configuration by Debye Length Modulation. *J. Am. Chem. Soc.* **2011**, *133* (35), 13886–13889. https://doi.org/10.1021/ja205684a.

# Chapter 4 Tuning Electrostatic Gating of Semi-conducting Carbon Nanotubes by Controlling Protein Orientation in Biosensing Devices

# Chapter 5 Direct Synthesis of Multiplexed Metal-Nanowire Based Devices Using Carbon Nanotubes as Vector Templates

## 5.1 Introduction

The ability to control the arrangement of materials into highly oriented structures with nanoscale accuracy is of great importance, for a variety of applications including nanoelectronics, energy storage and nanomedicine. Strategies have been proposed, from top-down methods, such as lithography or reactive ion etching,[1–4] to bottom-up approaches, including wet-chemistry and chemical vapor deposition.[5–8] While successful, these methodologies suffer from various limitations: top-down strategies are typically costly and time consuming, while the most common bottom-up approaches require high temperatures and employ a metal catalyst, inducing enlarged grain size and contamination, respectively. Notably, these drawbacks have been partially overcome with the use of templates that allow the formation of low-dimensionality nanostructures of a wide range of materials.[9–12]

In this regard, SWCNTs, due to the confinement effects enabled by their nanoscopic tubular design, have been employed as 1D templates to control the position and orientation of molecules or atoms for the construction of nanoscale 1D architectures. Successful examples include the liquid and gas-phase encapsulation of molecules with subsequent nanocrystal growth,[13–17] and the use of nanotubes as nanoreactors and

templates, via solution and gas-phase chemical approaches.[18–26] Additionally, coupling between the material grown and the nanotube was demonstrated, with evidence of electron and/or energy transfer.[27–34] However, a combination of sonication and density gradient ultracentrifugation is the only approach to have successfully removed newly formed 1D nanostructures from nanotube templates, and most importantly no examples are reported which subsequently use the extracted material for nanoelectronics: it can indeed be desirable to exploit solely metal species in device configurations, for example for sensing applications.[35–37]

Here we present a strategy for the formation of metal and metal alloy nanowire-based devices employing SWCNTs as templates, where a solution processable methodology is employed for the fabrication of distinct (multiplexed) electronic devices on the same chip. Vapors of metal precursors are used to fill the SWCNTs that are then dispersed in separate aqueous solutions. Different filled SWCNTs are immobilized between distinct electrode pairs on the same substrate, via dielectrophoresis (DEP); thermal annealing is performed to grow the metal/alloy inside the tube. The nanotubes are then removed by oxygen plasma treatment, leaving only the metal nanowires on the substrate, for their electrical characterizations to be performed. This route represents a facile, scalable and environmentally friendly method for the fabrication of arrays of distinct 1D metals in device configurations and on the same chip.

## 5.2 Formation of metal-precursor filled SWCNT

Metal-precursor filled SWCNTs ($M(acac)_2$@SWCNTs) were synthesised by our collaborate, the Thomas group (see section 2.2.4). Briefly, $M(acac)_2$ (where M = Pt, Cu or a mixture of Pt:Cu in a 1:1 ratio of atomic %) was mixed with freshly opened SWCNTs, followed by incubation under vacuum at 150 °C for 3 days to ensure the

penetration of the SWCNTs by the $M(acac)_2$. After cooling down rapidly, the mixture was washed with dichloromethane and was filtrated to remove any excess material from the exterior of SWCNT. The dimensions of the internal cavity of SWCNTs is shown in Figure 5.1, which enables effective encapsulation of metal precursor into SWCNTs. Although the melting point of $M(acac)_2$ is more than 200 °C at ambient pressure,[38] it was found that $M(acac)_2$ would sublime without decomposition at 110 °C under vacuum. Therefore, gaseous metal complex would penetrate the internal channels of the nanotube when the mixture of SWCNTs and $M(acac)_2$ was heated at 150 °C under vacuum. Subsequent rapid cooling down resulted in condensation of gaseous metal complex inside the channel of SWCNT, thus forming $M(acac)_2$@SWCNT. In this method, SWCNTs act as containers for the metal precursors and vector templates imposing strict control on the confinement of the metal precursors. This is a universal sublimation method which has been reported for many transition metal complexes.[39–41]

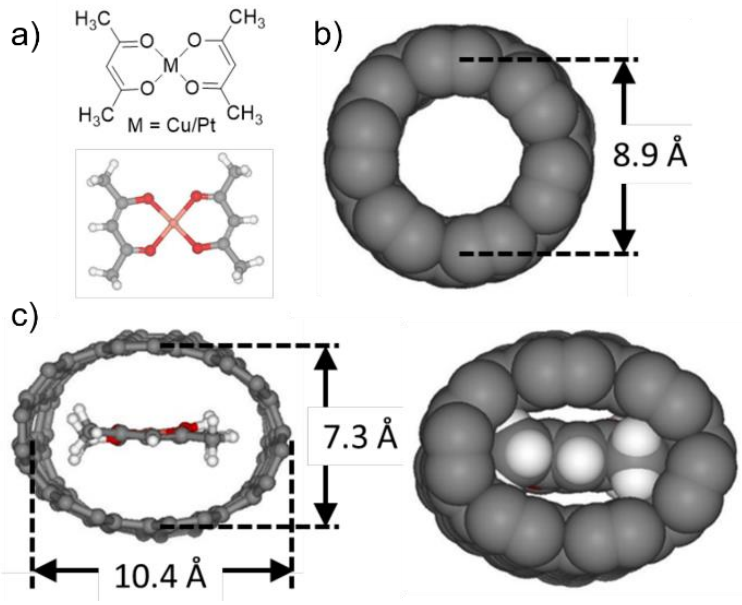


**Figure 5.1** (a) Molecular structure (top) and ball and stick (bottom) models of metal complex precursors used, (b) space filling molecular model of an empty (7,6) SWCNT, and (c) ball and stick (left) and space filling (right) molecular models of $Cu(acac)_2$@(7,6)SWCNT showing that significant distortion of the nanotube shape needs to occur to enable the Cu complex to fit.

On the other hand, $M(acac)_2$ can be easily decomposed into metal when it was heated at high temperature under vacuum. Fluorescence detected X-ray absorption spectroscopy (FD-XAS) was performed by our collaborator to confirm the decomposition of $M(acac)_2$. As shown in Figure 5.2a, the spectra show that the shape of the Cu K edge of the $Cu(acac)_2$@SWCNT (orange) is very similar to that of free $Cu(acac)_2$ powder (blue). This suggests that the $Cu(acac)_2$ remains intact during the filling process and that there is little electronic interaction between the Cu atoms and the nanotube interior after encapsulation.

Subsequently, we annealed the $Cu(acac)_2$@SWCNT at 200 °C for 1h to decompose the Cu precursor to form Cu@SWCNT. The shape of the Cu K edge of Cu@SWCNT (green) is significantly different from that of $Cu(acac)_2$@SWCNT, suggesting the decomposition of $Cu(acac)_2$@SWCNT. We also measured the spectra of Cu foil (red) as a control experiment, which is similar to that of Cu@SWCNT. This demonstrates the formation of Cu species in the internal channel of the nanotube. Similar results were observed in the spectra of [$Pt(acac)_2$ + $Cu(acac)_2$]@SWCNT before and after thermal treatment (Figure 5.2b). Therefore, results from FD-XAS confirm the decomposition of metal precurosr into metal inside the SWCNT channels.

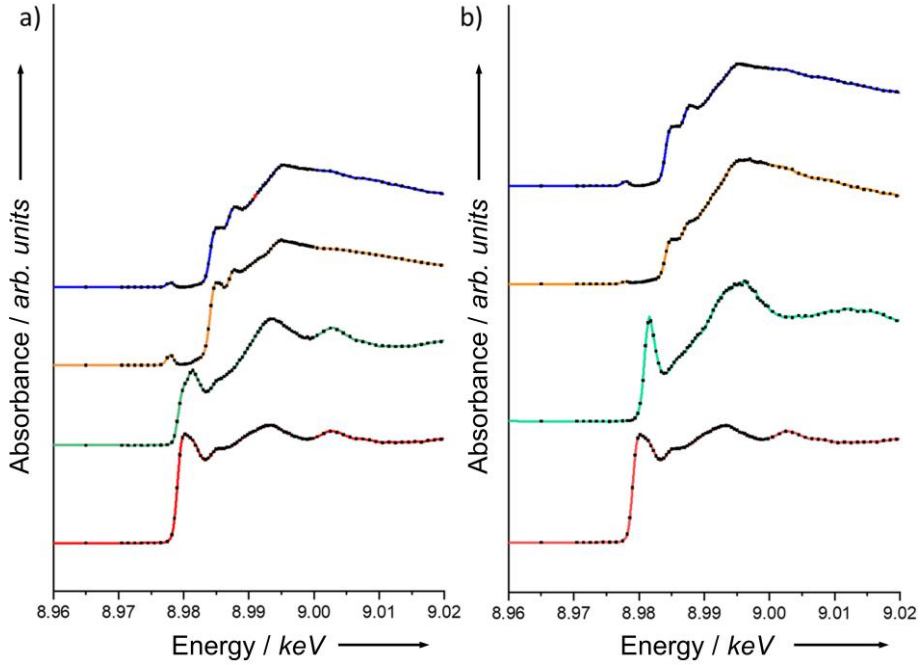


**Figure 5.2** FD-XAS spectra of the Cu K edge of (a) $Cu(acac)_2$ (blue), $Cu(acac)_2$@SWCNT (orange), Cu@SWCNT (green) and Cu foil (red); (b) $Cu(acac)_2$ (blue), [$Pt(acac)_2$ + $Cu(acac)_2$]@SWCNT (orange), Pt-Cu@SWCNT (green) and Cu foil (red). The raw data is shown in black, and the smoothed data is overlaid in colour in each case.

Our collaborator also performed time-resolved FD-XAS measurements of $Cu(acac)_2$ and $Cu(acac)_2$@SWCNT during the heating experiment. As shown in Figure 5.3 and Figure 5.4, a gradual change in the Cu K edge was observed overtime. Arrows in Figure 5.3 and Figure 5.4 show the changes in the spectra during the process, indicating the decomposition of $Cu(acac)_2$. We observed similar changes in the spectra of both $Cu(acac)_2$ and $Cu(acac)_2$@SWCNT, which indicate the decomposition of $Cu(acac)_2$ to form Cu species, further confirming the change in oxidation state after thermal treatment.

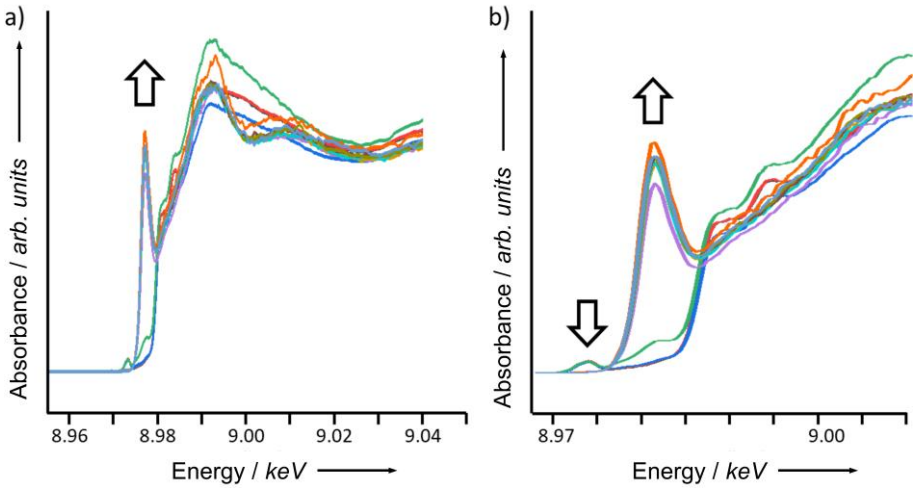


**Figure 5.3** (a) Full and (b) zoomed in region of the FD-XAS spectra of $Cu(acac)_2$ heated from 20-250 °C (red/brown) at a rate of 0.0097 °C /s, showing a gradual change in the Cu K edge overtime, indicating metal complex decomposition to form a Cu species.

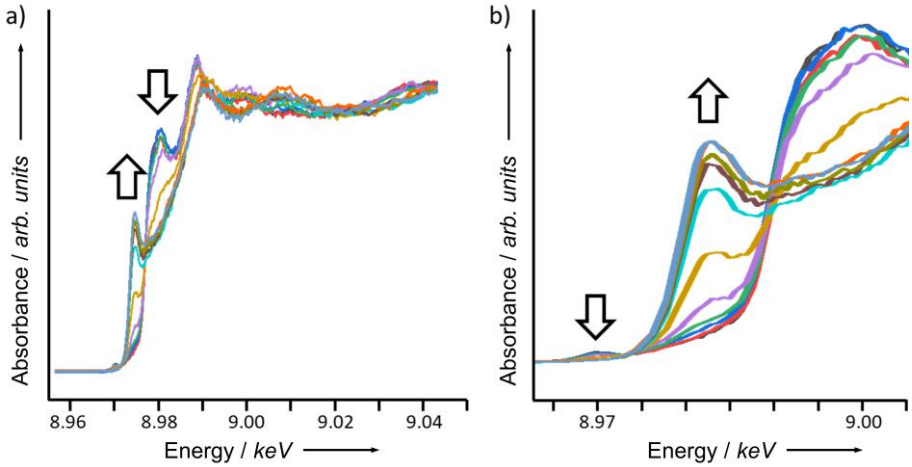


**Figure 5.4** (a) Full and (b) zoomed in region of the FD-XAS spectra of Cu(acac)2@SWCNT heated from 20-250 °C (red/brown) at a rate of 0.0097 °C/s, showing a gradual change in the Cu K edge overtime, indicating metal complex decomposition and Cu@SWCNT formation.

Transmission electron microscopy (TEM) and local energy-dispersive X-ray (EDX) spectroscopy were used by our collaborator to confirm the formation of metal species inside SWCNT channels after annealing treatment i.e. metal precursors encapsulated in SWCNTs would decompose to form Cu, Pt-Cu alloy and Pt respectively. TEM images

show the presence of metal species inside the SWCNT cavity, which is further confirmed by the EDX spectra (Figure 5.5). The observed Ni peaks in (a) and (b) and the Cu peaks in c) are from the TEM grid. Additionally, we determined that the filling yields for all samples were more than 85%.

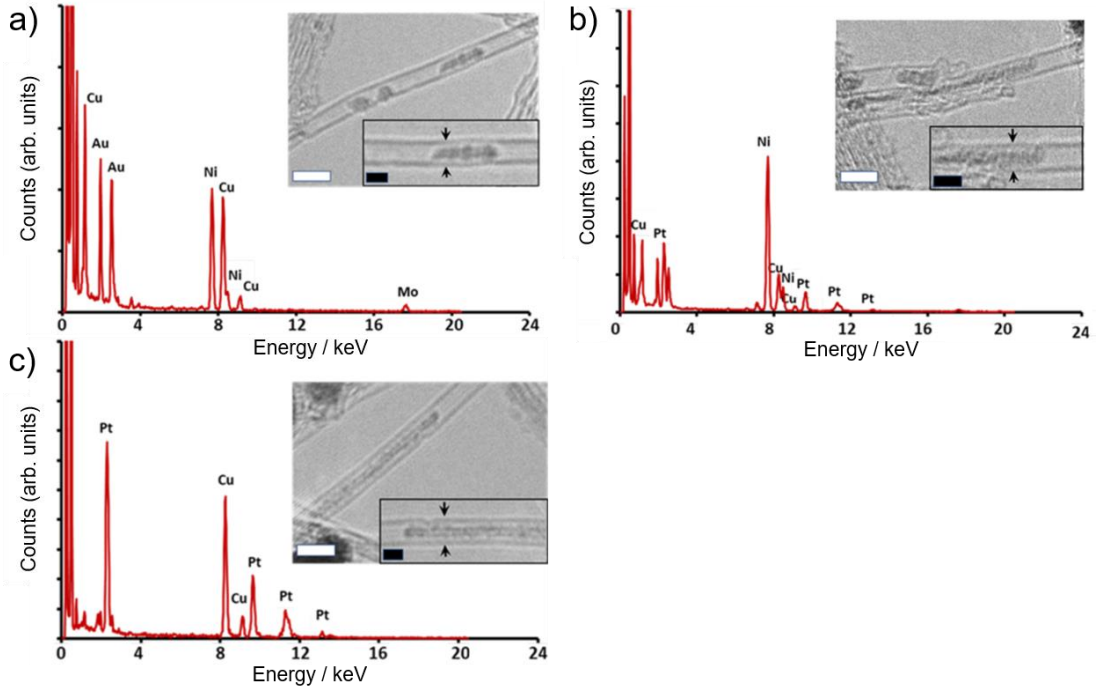


**Figure 5.5** EDX spectra recorded at 100 keV primary electron energy and integrated over a small bundle of nanotubes confirms the presence of Cu and/or Pt inside the nanotubes for; (a) Cu@SWCNT, (b) PtCu@SWCNT, and (c) Pt@SWCNT. TEM images (inset) of each material confirm the presence of the metal species inside the SWCNT cavity in each case with black arrows highlighting the diagnostic 0.3 nm van der Waals gap between the encapsulated metal species and the nanotube wall. Scale bars are 2 nm (white) and 1 nm (black) in all cases. The observed Ni peaks in (a) and (b) and the Cu peaks in c) are from the TEM grid.

## 5.3 Immobilisation of individual filled SWCNT devices

The metal-precursor filled SWCNTs were immobilised between pre-patterned electrode pairs in a device configuration to explore the potential application of nanotubes as vector templates for the fabrication of metal nanowire devices. $Cu(acac)_2$@SWCNT, $Pt(acac)_2$@SWCNT, and [$Pt(acac)_2$ + $Cu(acac)_2$]@SWCNT were

dispersed in SDS solutions and were immobilised between electrode pairs in a field effect transistor configuration via DEP, as shown in Figure 5.6 (see section 2.3.2). Since the filled SWCNT can only be immobilised between the electrodes where alternating current (AC) voltage is applied, we were able to immobilise SWCNTs encapsulated with distinct metal precursors ($M(acac)_2$, where M = Cu and/or Pt) between different electrode pairs on the same substrate surface by repeating the process of DEP with different $M(acac)_2$@SWCNT solutions. The devices were subsequently rinsed with water to remove the SDS and blow-dried with nitrogen gas for further investigation.

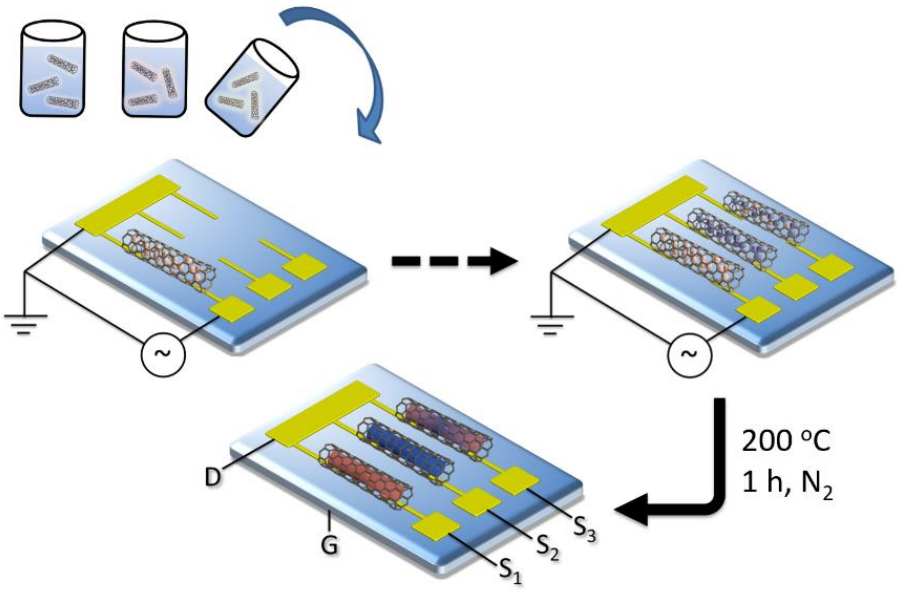


**Figure 5.6** Schematic representation of the deposition of $M(acac)_2$@SWCNT by DEP (beige for $Cu(acac)_2$, blue for $Pt(acac)_2$ and both colors for the Pt-Cu alloy), followed by decomposition of the precursor after annealing. The chip is presented in the FET configuration, where S, D and G are the source, drain and gate electrodes, respectively.

Our initial attempt was to utilise an individual metal-precursor filled SWCNT as a vector template to fabricate metal nanowire devices. With optimal parameters, we were able to immobilise a single $M(acac)_2$@SWCNT (M=Cu and/or Pt) between electrode pairs, which was confirmed via Atomic Force Microscopy (AFM) as shown in Figure 5.7a. We further investigated the electrical properties of these devices before and after

annealing treatment under nitrogen gas at 200 °C (at which temperature the precursors have been observed to decompose to form metal species), as shown in Figure 5.7b-d. We observed a significant decrease in the conductance of all devices after annealing treatment. This can be attributed to changes in the electronic structure of the nanotube caused by the formation of metal species since encapsulated guest species cannot provide a viable conduction pathway. We propose that changes in the interactions between guest and nanotubes due to the decomposition of the metal precursors ($M^{2+}$) to form nanowires ($M^0$) influence the charge density of states of the nanotube, resulting in reduction of the conductance of the nanotubes.

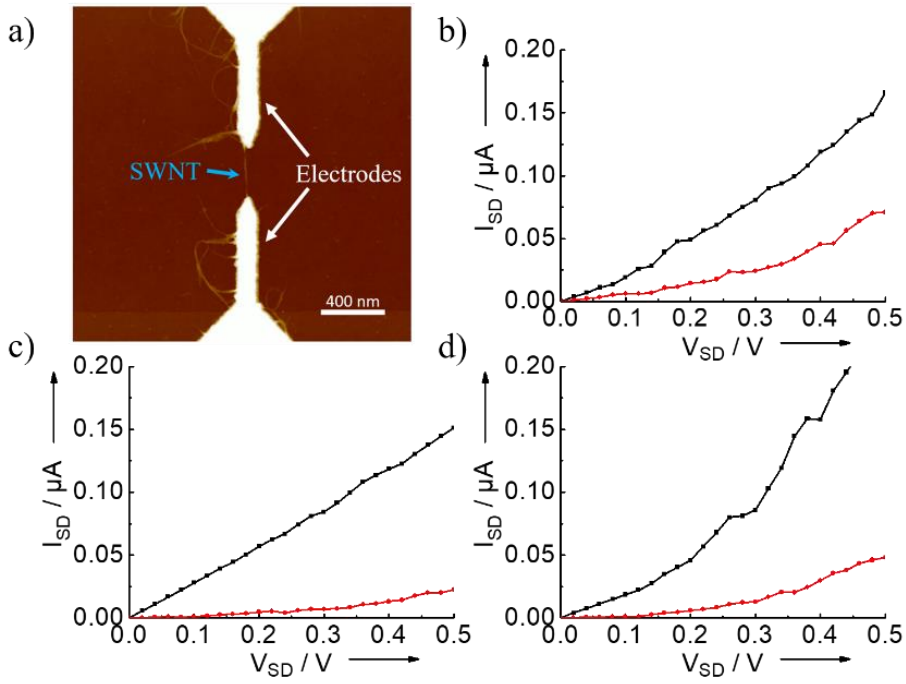


**Figure 5.7** (a) AFM topographical image of a single filled SWCNT immobilized between two electrodes; $I_{SD}$-$V_{SD}$ curve characterization of (b) $Cu(acac)_2$@SWCNT, (c) $Pt(acac)_2$@SWCNT and (d) [$Pt(acac)_2$ + $Cu(acac)_2$]SWCNT hybrids after deposition by DEP (black) and after annealing at 200 °C (red).

As a control experiment, we also measured the conductance of devices only containing a single pristine empty SWCNT before and after annealing treatment. In this case we

observed an increase in the conductivity after annealing, likely due to the improved electrical contact between the nanotube and the gold electrodes (Figure 5.8).[42] This further confirms that the decomposition of metal precursors influences the conductance of SWCNTs.

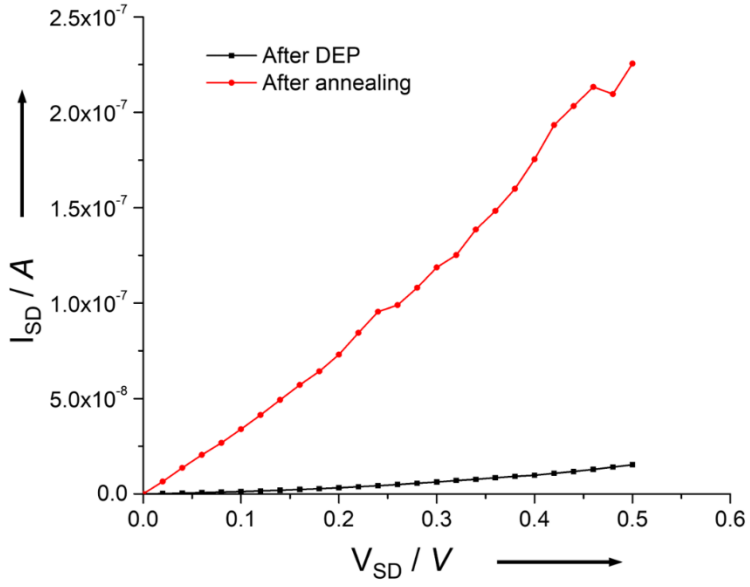


**Figure 5.8** $I_{SD}$-$V_{SD}$ curve ($V_G$=0 mV) characterization of an individual empty SWCNT.

However, as reported previously,[43] the metal does not grow uniformly inside the nanotubes during the annealing treatment as there are insufficient metal atoms to form a continuous metal wire inside an individual SWCNT (Figure 5.5). After removal of the SWCNT shell by oxygen plasma treatment,[44] we observed the formation of nanoparticles and non-continuous nanowires between the electrodes (Figure 5.9). Therefore, in order to fabricate devices with continuous metal nanowires, we need to immobilise a bundle of M(acac)$_2$@SWCNT between the electrodes, instead of an individual filled SWCNT.

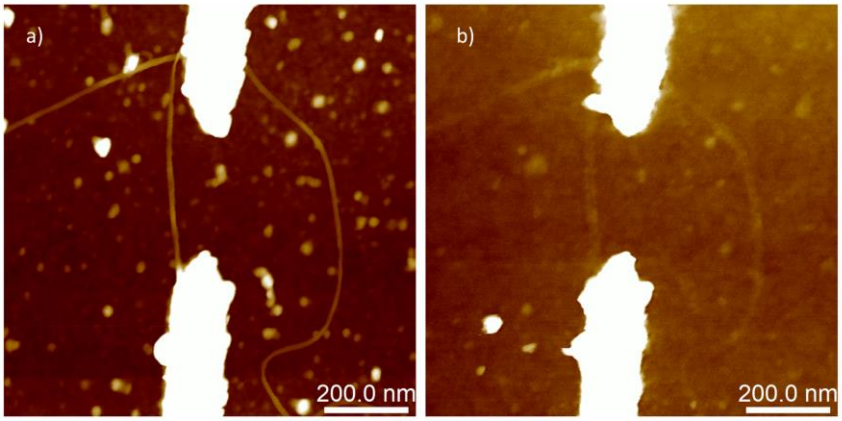


**Figure 5.9** AFM image of a single $Cu(acac)_2$@SWCNT immobilized between electrode pairs a) before and b) after oxygen plasma treatment.

## 5.4 Immobilisation of bundle SWCNT devices

In order to immobilise a bundle of $M(acac)_2$@SWCNT, we optimised the parameters of DEP, i.e. increasing the concentration of the filled SWCNT solution and the DEP time (see section 2.3.2). Figure 5.10a shows a representative AFM image of a small bundle (c.a. 100 nm in height) of $Cu(acac)_2$@SWCNT immobilized between an electrode pair. The samples were annealed at 200 °C for 1h for the formation of metal nanoparticles inside SWCNT channels. Subsequently, the devices were exposed to oxygen plasma for 60 s (see section 2.3.4), resulting in the removal of SWCNT shell while the metal remaining between electrodes (Figure 5.11).

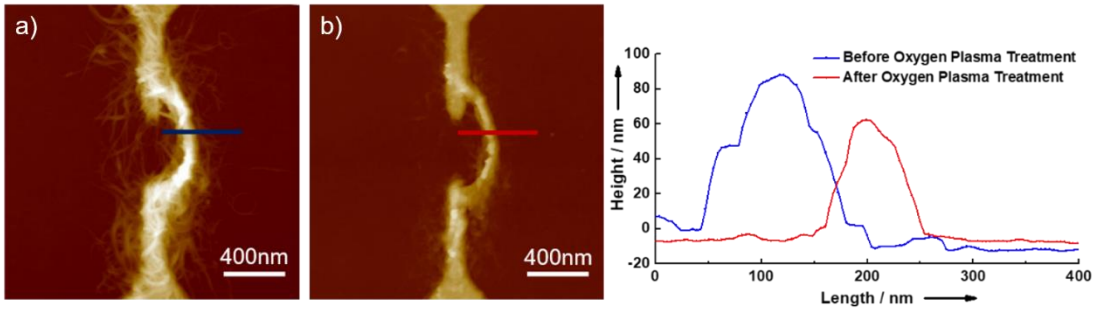


**Figure 5.10** Representative AFM images of a small bundle (c.a. 100 nm in height) of $Cu(acac)_2$@SWCNT immobilized between an electrode pair (a) before annealing treatment (b) after oxygen plasma treatment and their corresponding height profile.

Figure 5.10b shows the AFM image of the device after oxygen plasma treatment, where the height of the bundle is c.a. 70 nm. The change in height (Figure 5.10c) can be attributed to the removal of SWCNT shell caused by oxygen plasma. However, the SWCNT shell cannot be fully removed and the metal nanoparticles can be partially oxidised. Therefore, the composition of the nanoscale bundles might include metal nanoparticles, intercalated carbon fragments and metal oxide nanoparticles.

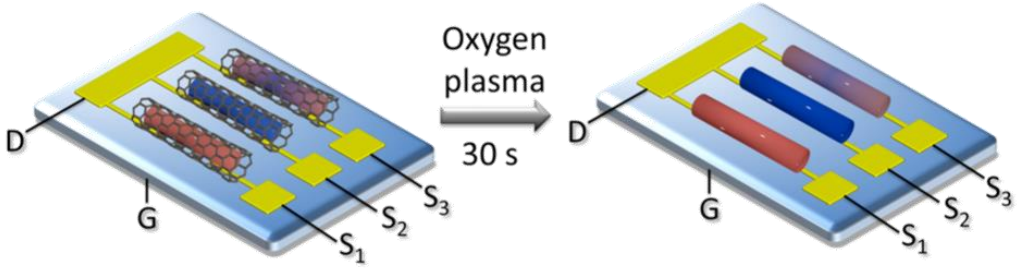


**Figure 5.11** Scheme showing the removal of the SWCNTs leaving the material grown on the substrate.

We also recorded the current as a function of voltage ($I_{SD}$ vs $V_{SD}$) curves of devices before and after annealing treatment, and after oxygen plasma treatment, as shown in Figure 5.12. A decrease in the conductivity of the device was observed after annealing, while in the control experiment with a bundle of pristine SWCNTs we observed an increase in the conductivity after annealing (Figure 5.13). Moreover, when the SWCNTs were removed via oxygen plasma, a sharp decrease in the conductivity was observed. The inhomogeneity of the metal wires, the non-optimal contact of these with the macroscopic electrode once the SWCNT is removed, and the potential presence of intercalated carbon fragments, might be reasons for the observed decrease in conductivity.

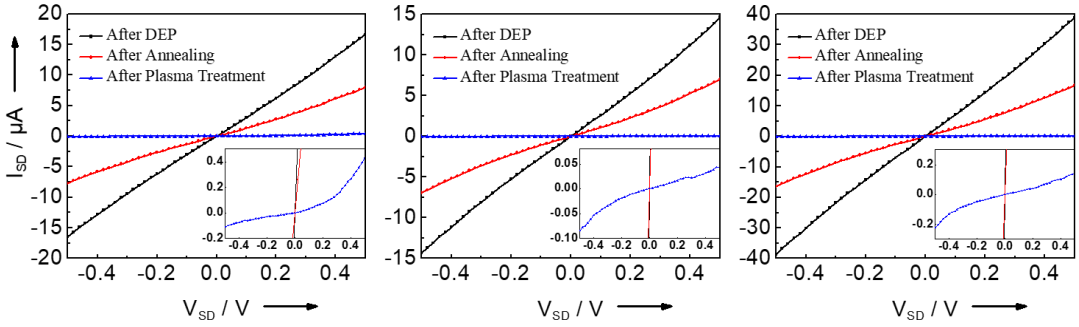


**Figure 5.12** $I_{SD}$ -$V_{SD}$ characterization of bundles of (left to right) $Cu(acac)_2$@SWCNT, $Pt(acac)_2$@SWCNT and [$Pt(acac)_2$ + $Cu(acac)_2$]@SWCNT hybrids after deposition by DEP (black), annealing at 200 °C (red) and plasma treatment (blue).

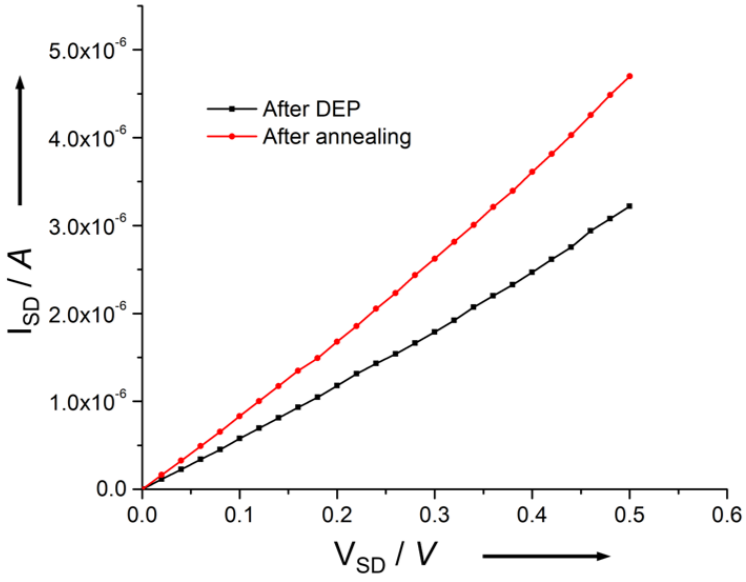


**Figure 5.13** $I_{SD}$ -$V_{SD}$ curve ($V_G$=0 mV) characterization of a bundle of SWCNTs.

To additionally demonstrate the removal of the SWCNT shell, we also performed measurements of the transfer characteristics of these devices ($I_{SD}$ vs $V_G$). With the presence of the p-type SWCNT, the device had a gate dependence for the $M(acac)_2$@SWCNT and M@SWCNT; nevertheless, this was not observed for Cu, Pt and Pt-Cu nanowires when the SWCNTs were removed (Figure 5.14).

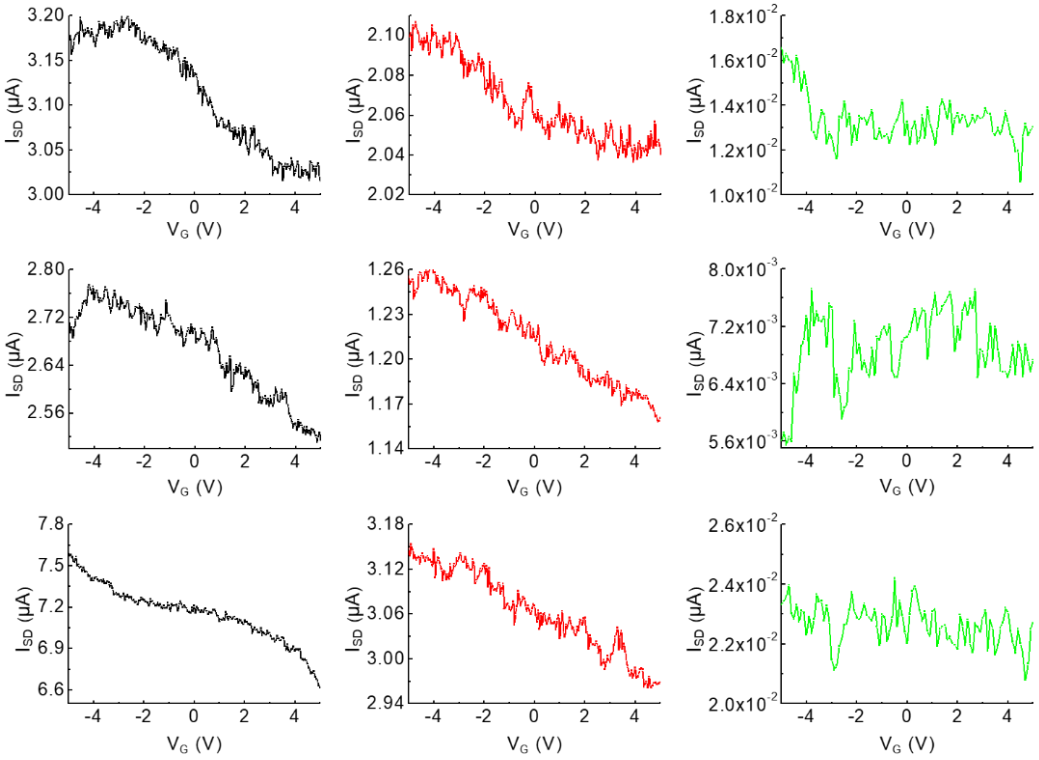


**Figure 5.14** $I_{SD}$ -$V_G$ characterization ($V_{SD}$=100 mV) with gate dependence of SWCNT hybrids after deposition by (left to right): DEP (black), annealing at 200 °C (red) and plasma treatment (green) for: a) $Cu(acac)_2$@SWCNT; b) $Pt(acac)_2$@SWCNT; and c) $PtCu(acac)_2$@SWCNT.

## 5.5 Conclusions

In summary, we presented a solution-processable method of general applicability for the direct synthesis of multiple metal nanowires on the same chip. Various $M(acac)_2$@SWCNTs were immobilized from solution onto surfaces in nanoscale device configurations, where the SWCNTs were used as reactors and vector templates. By simple annealing, metal nanowires were grown in the cavity of the nanotubes. Subsequently, SWCNT shell was removed by oxygen plasma. Distinct Cu, Pt and PtCu nanowires were successfully synthesized between different electrode pairs on the same chip as indicated by the I-V curves recorded: no gate dependence was observed upon removal of the SWCNT shell. This strategy represents a viable route to the large-scale

fabrication and detailed exploration of materials properties in controlled 1D architectures. The universal nature of the SWCNT filling method allows a broad range of individual metals and an almost infinite number of metal combinations in alloy form to be incorporated; this in turn means that our approach has the potential to impact upon a broad range of fields, from nanoelectronics applications with low power consumption such as chemical sensors or quantum information processing, to lab-on-a-chip based tunable electrocatalytic arrays.

References

(1) Anoop, G.; Kim, T. Y.; Lee, H. J.; Panwar, V.; Kwak, J. H.; Heo, Y. J.; Yang, J. H.; Lee, J. H.; Jo, J. Y. Top-Down Synthesis of Hollow Graphene Nanostructures for Use in Resistive Switching Memory Devices. *Adv. Electron. Mater*. **2017**, *3* (10), 1–11. https://doi.org/10.1002/aelm.201700264.

(2) Chen, W.; Deng, D. Sodium-Cutting: A New Top-down Approach to Cut Open Nanostructures on Nonplanar Surfaces on a Large Scale. *Chem. Commun.* **2014**, *50* (87), 13327–13330. https://doi.org/10.1039/c4cc02409e.

(3) Lee, L.; Kang, B.; Han, S.; Kim, H. eun; Lee, M. D.; Bang, J. H. A Generalizable Top-Down Nanostructuring Method of Bulk Oxides: Sequential Oxygen–Nitrogen Exchange Reaction. *Small* **2018**, *14* (25), 1–8. https://doi.org/10.1002/smll.201801124.

(4) Mondiali, V.; Lodari, M.; Borriello, M.; Chrastina, D.; Bollani, M. Top-down SiGe Nanostructures on Ge Membranes Realized by e-Beam Lithography and Wet Etching. *Microelectron. Eng.* **2016**, *153*, 88–91. https://doi.org/10.1016/j.mee.2016.02.015.

(5) Xu, H.; Ding, Z.; Nai, C. T.; Bao, Y.; Cheng, F.; Tan, S. J. R.; Loh, K. P. Controllable Synthesis of 2D and 1D MoS2 Nanostructures on Au Surface. *Adv. Funct. Mater.* **2017**, *27* (19). https://doi.org/10.1002/adfm.201603887.

(6) Attanzio, A.; Sapelkin, A.; Gesuele, F.; van der Zande, A.; Gillin, W. P.; Zheng, M.;

Palma, M. Carbon Nanotube-Quantum Dot Nanohybrids: Coupling with Single-Particle Control in Aqueous Solution. *Small* **2017**, *13* (16), 1–5. https://doi.org/10.1002/smll.201603042.

(7) Jacobberger, R. M.; Arnold, M. S. High-Performance Charge Transport in Semiconducting Armchair Graphene Nanoribbons Grown Directly on Germanium. *ACS Nano* **2017**, *11* (9), 8924–8929. https://doi.org/10.1021/acsnano.7b03220.

(8) Freeley, M.; Attanzio, A.; Cecconello, A.; Amoroso, G.; Clement, P.; Fernandez, G.; Gesuele, F.; Palma, M. Tuning the Coupling in Single-Molecule Heterostructures: DNA-Programmed and Reconfigurable Carbon Nanotube-Based Nanohybrids. *Adv. Sci.* **2018**, *5* (10). https://doi.org/10.1002/advs.201800596.

(9) Rao, A.; Long, H.; Harley-Trochimczyk, A.; Pham, T.; Zettl, A.; Carraro, C.; Maboudian, R. In Situ Localized Growth of Ordered Metal Oxide Hollow Sphere Array on Microheater Platform for Sensitive, Ultra-Fast Gas Sensing. *ACS Appl. Mater. Interfaces* **2017**, *9* (3), 2634–2641. https://doi.org/10.1021/acsami.6b12677.

(10) Bayrak, T.; Helmi, S.; Ye, J.; Kauert, D.; Kelling, J.; Schönherr, T.; Weichelt, R.; Erbe, A.; Seidel, R. DNA-Mold Templated Assembly of Conductive Gold Nanowires. *Nano Lett.* **2018**, *18* (3), 2116–2123. https://doi.org/10.1021/acs.nanolett.8b00344.

(11) Song, J. M.; Lee, J. S. Self-Assembled Nanostructured Resistive Switching Memory Devices Fabricated by Templated Bottom-up Growth. *Sci. Rep.* **2016**, *6* (December 2015), 1–7. https://doi.org/10.1038/srep18967.

(12) Sandoval, S.; Kepić, D.; Pérez Del Pino, Á.; György, E.; Gómez, A.; Pfannmoeller, M.; Tendeloo, G. Van; Ballesteros, B.; Tobias, G. Selective Laser-Assisted Synthesis of Tubular van Der Waals Heterostructures of Single-Layered PbI2within Carbon Nanotubes Exhibiting Carrier Photogeneration. *ACS Nano* **2018**, *12* (7), 6648–6656. https://doi.org/10.1021/acsnano.8b01638.

(13) Ma, X.; Cambré, S.; Wenseleers, W.; Doorn, S. K.; Htoon, H. Quasiphase Transition in a Single File of Water Molecules Encapsulated in (6,5) Carbon Nanotubes Observed by

Temperature-Dependent Photoluminescence Spectroscopy. *Phys. Rev. Lett.* **2017**, *118* (2), 1–7. https://doi.org/10.1103/PhysRevLett.118.027402.

(14) Shi, L.; Rohringer, P.; Wanko, M.; Rubio, A.; Waßerroth, S.; Reich, S.; Cambré, S.; Wenseleers, W.; Ayala, P.; Pichler, T. Electronic Band Gaps of Confined Linear Carbon Chains Ranging from Polyyne to Carbyne. **2017**, *075601*, 1–7. https://doi.org/10.1103/PhysRevMaterials.1.075601.

(15) Cambré, S.; Wenseleers, W. Separation and Diameter-Sorting of Empty (End-Capped) and Water-Filled (Open) Carbon Nanotubes by Density Gradient Ultracentrifugation. *Angew. Chemie - Int. Ed.* **2011**, *50* (12), 2764–2768. https://doi.org/10.1002/anie.201007324.

(16) Chamberlain, T. W.; Biskupek, J.; Rance, G. A.; Chuvilin, A.; Alexander, T. J.; Bichoutskaia, E.; Kaiser, U.; Khlobystov, A. N. Size, Structure, and Helical Twist of Graphene Nanoribbons Controlled by Confinement in Carbon Nanotubes. *ACS Nano* **2012**, *6* (5), 3943–3953. https://doi.org/10.1021/nn300137j.

(17) Cambré, S.; Wenseleers, W.; Goovaerts, E. Endohedral Copper(II)Acetylacetonate/Single-Walled Carbon Nanotube Hybrids Characterized by Electron Paramagnetic Resonance. *J. Phys. Chem. C* **2009**, *113* (31), 13505–13514. https://doi.org/10.1021/jp903724h.

(18) Stoppiello, C. T.; Biskupek, J.; Li, Z. Y.; Rance, G. A.; Botos, A.; Fogarty, R. M.; Bourne, R. A.; Yuan, J.; Lovelock, K. R. J.; Thompson, P.; Fay, M. W.; Kaiser, U.; Chamberlain, T. W.; Khlobystov, A. N. A One-Pot-One-Reactant Synthesis of Platinum Compounds at the Nanoscale. *Nanoscale* **2017**, *9* (38), 14385–14394. https://doi.org/10.1039/c7nr05976k.

(19) Zhang, J.; Zhao, D.; Xiao, D.; Ma, C.; Du, H.; Li, X.; Zhang, L.; Huang, J.; Huang, H.; Jia, C. L.; Tománek, D.; Niu, C. Assembly of Ring-Shaped Phosphorus within Carbon Nanotube Nanoreactors. *Angew. Chemie - Int. Ed.* **2017**, *56* (7), 1850–1854. https://doi.org/10.1002/anie.201611740.

(20) Kharlamova, M. V.; Niu, J. J. Comparison of Metallic Silver and Copper Doping Effects on Single-Walled Carbon Nanotubes. *Appl. Phys. A Mater. Sci. Process.* **2012**, *109* (1), 25–29. https://doi.org/10.1007/s00339-012-7091-3.

(21) Cui, T.; Pan, X.; Dong, J.; Miao, S.; Miao, D.; Bao, X. A Versatile Method for the Encapsulation of Various Non-Precious Metal Nanoparticles inside Single-Walled Carbon Nanotubes. *Nano Res.* **2018**, *11* (6), 3132–3144. https://doi.org/10.1007/s12274-018-1975-2.

(22) Carter, R.; Oakes, L.; Muralidharan, N.; Cohn, A. P.; Douglas, A.; Pint, C. L. Polysulfide Anchoring Mechanism Revealed by Atomic Layer Deposition of V2O5and Sulfur-Filled Carbon Nanotubes for Lithium-Sulfur Batteries. *ACS Appl. Mater. Interfaces* **2017**, *9* (8), 7185–7192. https://doi.org/10.1021/acsami.6b16155.

(23) Sandoval, S.; Pach, E.; Ballesteros, B.; Tobias, G. Encapsulation of Two-Dimensional Materials inside Carbon Nanotubes: Towards an Enhanced Synthesis of Single-Layered Metal Halides. *Carbon N. Y.* **2017**, *123*, 129–134. https://doi.org/10.1016/j.carbon.2017.07.031.

(24) Aslam, Z.; Lozano, J. G.; Nicholls, R. J.; Koos, A. A.; Dillon, F.; Sarahan, M. C.; Nellist, P. D.; Grobert, N. Direct Visualization of Electrical Transport-Induced Alloy Formation and Composition Changes in Filled Multi-Wall Carbon Nanotubes by in Situ Scanning Transmission Electron Microscopy. *J. Alloys Compd.* **2017**, *721*, 501–505. https://doi.org/10.1016/j.jallcom.2017.05.316.

(25) Shi, L.; Yanagi, K.; Cao, K.; Kaiser, U.; Ayala, P.; Pichler, T. Extraction of Linear Carbon Chains Unravels the Role of the Carbon Nanotube Host. *ACS Nano* **2018**, *12*, 8477–8484. https://doi.org/10.1021/acsnano.8b04006.

(26) Medeiros, P. V. C.; Marks, S.; Wynn, J. M.; Vasylenko, A.; Ramasse, Q. M.; Quigley, D.; Sloan, J.; Morris, A. J. Single-Atom Scale Structural Selectivity in Te Nanowires Encapsulated Inside Ultranarrow, Single-Walled Carbon Nanotubes. *ACS Nano* **2017**, *11* (6), 6178–6185. https://doi.org/10.1021/acsnano.7b02225.

(27) Marega, R.; Bonifazi, D. Filling Carbon Nanotubes for Nanobiotechnological Applications. *New J. Chem.* **2014**, *38* (1), 22–27. https://doi.org/10.1039/c3nj01008b.

(28) Martincic, M.; Tobias, G. Filled Carbon Nanotubes in Biomedical Imaging and Drug Delivery. *Expert Opin. Drug Deliv.* **2015**, *12* (4), 563–581. https://doi.org/10.1517/17425247.2015.971751.

(29) Ramachandran, K.; Raj Kumar, T.; Babu, K. J.; Gnana Kumar, G. Ni-Co Bimetal Nanowires Filled Multiwalled Carbon Nanotubes for the Highly Sensitive and Selective Non-Enzymatic Glucose Sensor Applications. *Sci. Rep.* **2016**, *6* (June), 1–12. https://doi.org/10.1038/srep36583.

(30) Brahim, S.; Colbern, S.; Gump, R.; Moser, A.; Grigorian, L. Carbon Nanotube-Based Ethanol Sensors. *Nanotechnology* **2009**, *20* (23). https://doi.org/10.1088/0957-4484/20/23/235502.

(31) Kharlamova, M. V.; Kramberger, C.; Domanov, O.; Mittelberger, A.; Yanagi, K.; Pichler, T.; Eder, D. Fermi Level Engineering of Metallicity-Sorted Metallic Single-Walled Carbon Nanotubes by Encapsulation of Few-Atom-Thick Crystals of Silver Chloride. *J. Mater. Sci.* **2018**, *53* (18), 13018–13029. https://doi.org/10.1007/s10853-018-2575-y.

(32) Tobias, G.; Ballesteros, B.; Green, M. L. H. Carbon Nanocapsules: Blocking Materials inside Carbon Nanotubes. *Phys. Status Solidi Curr. Top. Solid State Phys.* **2010**, *7* (11–12), 2739–2742. https://doi.org/10.1002/pssc.200983823.

(33) Spinato, C.; Perez Ruiz De Garibay, A.; Kierkowicz, M.; Pach, E.; Martincic, M.; Klippstein, R.; Bourgognon, M.; Wang, J. T. W.; Ménard-Moyon, C.; Al-Jamal, K. T.; Ballesteros, B.; Tobias, G.; Bianco, A. Design of Antibody-Functionalized Carbon Nanotubes Filled with Radioactivable Metals towards a Targeted Anticancer Therapy. *Nanoscale* **2016**, *8* (25), 12626–12638. https://doi.org/10.1039/c5nr07923c.

(34) Van Bezouw, S.; Arias, D. H.; Ihly, R.; Cambré, S.; Ferguson, A. J.; Campo, J.; Johnson, J. C.; Defillet, J.; Wenseleers, W.; Blackburn, J. L. Diameter-Dependent Optical

Absorption and Excitation Energy Transfer from Encapsulated Dye Molecules toward Single-Walled Carbon Nanotubes. *ACS Nano* **2018**, *12* (7), 6881–6894. https://doi.org/10.1021/acsnano.8b02213.

(35) Cao, K.; Zoberbier, T.; Biskupek, J.; Botos, A.; McSweeney, R. L.; Kurtoglu, A.; Stoppiello, C. T.; Markevich, A. V.; Besley, E.; Chamberlain, T. W.; Kaiser, U.; Khlobystov, A. N. Comparison of Atomic Scale Dynamics for the Middle and Late Transition Metal Nanocatalysts. *Nat. Commun.* **2018**, *9* (1), 1–10. https://doi.org/10.1038/s41467-018-05831-z.

(36) Zoberbier, T.; Chamberlain, T. W.; Biskupek, J.; Kuganathan, N.; Eyhusen, S.; Bichoutskaia, E.; Kaiser, U.; Khlobystov, A. N. Interactions and Reactions of Transition Metal Clusters with the Interior of Single-Walled Carbon Nanotubes Imaged at the Atomic Scale. *J. Am. Chem. Soc.* **2012**, *134* (6), 3073–3079. https://doi.org/10.1021/ja208746z.

(37) Botos, A.; Biskupek, J.; Chamberlain, T. W.; Rance, G. A.; Stoppiello, C. T.; Sloan, J.; Liu, Z.; Suenaga, K.; Kaiser, U.; Khlobystov, A. N. Carbon Nanotubes as Electrically Active Nanoreactors for Multi-Step Inorganic Synthesis: Sequential Transformations of Molecules to Nanoclusters and Nanoclusters to Nanoribbons. *J. Am. Chem. Soc.* **2016**, *138* (26), 8175–8183. https://doi.org/10.1021/jacs.6b03633.

(38) Ohfuchi, M.; Miyamoto, Y. Optical Properties of Oxidized Single-Wall Carbon Nanotubes. *Carbon N. Y.* **2017**, *114*, 418–423. https://doi.org/10.1016/j.carbon.2016.12.052.

(39) Lee, R. S.; Kim, H. J.; Fischer, J. E.; Thess, A.; Smalley, R. E. Conductivity Enhancement in Single-Walled Carbon Nanotube Bundles Doped with K and Br. *Nature* **1997**, *388* (6639), 255–257. https://doi.org/10.1038/40822.

(40) Dresselhaus, M. S.; Jorio, A.; Hofmann, M.; Dresselhaus, G.; Saito, R. Perspectives on Carbon Nanotubes and Graphene Raman Spectroscopy. *Nano Lett.* **2010**, *10* (3), 751–758. https://doi.org/10.1021/nl904286r.

(41) Buzaeva, M. V.; Dubrovina, V. V.; Davydova, O. A.; Klimov, E. S. Dissolution of Copper in the Presence of Ortho-Quinones with Electron-Acceptor Substituents. *Russ. J. Appl. Chem.* **2011**, *84* (5), 892–894. https://doi.org/10.1134/S1070427211050260.

(42) Lee, J.; Park, C.; Kim, J.; Kim, J. Formation of Low-Resistance Ohmic Contacts between Carbon Nanotube and Metal Electrodes by a Rapid. **1953**.

(43) Chamberlain, T. W.; Zoberbier, T.; Biskupek, J.; Botos, A.; Kaiser, U.; Khlobystov, A. N. Formation of Uncapped Nanometre-Sized Metal Particles by Decomposition of Metal Carbonyls in Carbon Nanotubes. *Chem. Sci.* **2012**, *3* (6), 1919–1924. https://doi.org/10.1039/c2sc01026g.

(44) Guo, X.; Small, J. P.; Klare, J. E.; Wang, Y.; Purewal, M. S.; Tam, I. W.; Hong, B. H.; Caldwell, R.; Huang, L.; Brien, S. O.; Yan, J.; Breslow, R. Covalently Bridging Gaps in with Conducting Molecules. *Science (80-. ).* **2011**, *356* (2006), 356–360. https://doi.org/10.1126/science.1120986.

# Chapter 6 Directed Assembly of Single Chirality Carbon Nanotubes: from Individual Devices to Photodetectors

## 6.1 Introduction

The use of single-walled carbon nanotubes (SWCNTs) as components in next generation nanoelectronic devices has been a major focus in the nanomaterials field for the past few decades, owing to their outstanding electrical properties.[1–6] In particular, SWCNT-based field effect transistors (FETs) can be used for many applications, and a variety of FETs, ranging from dense arrays to individual SWCNTs devices, have been made to investigate the electrical properties of SWCNTs.[7–15]

SWCNTs can be metallic or semiconducting based on their structure. These discrete structures can be defined by the chirality index (n,m) which corresponds to the direction and magnitude of the rolling vector along the hexagonal carbon lattice.[16] The chirality of a SWCNT has direct implications on its electrical and optical properties; moreover, the bandgap of semiconducting SWCNTs is inversely proportional to the tube diameter.[17–20] Consequently, it is desirable to control the chirality and hence electronic properties of SWCNTs to tailor their use for specific applications.[21–23]

Various techniques have been proposed to produce SWCNTs with highly enriched single-chirality species, through either direct controlled growth[24–32] or by separation post-synthesis.[33–38] Although SWCNTs with defined chiralities can be achieved via chemical vapor deposition,[18,25,27,39] different in-solution strategies have been developed for chirality enrichment such as chromotography,[40–42] density differentiation,[43,44] DNA

recognition,[45,46] and polymer systems.[47–51]

In particular, approaches based on polymer aqueous two-phase (ATP) systems have been demonstrated to be efficient for SWCNT separation.[48,52–54] ATP systems work on the principle that each chirality of SWCNT will vary in solvation energy due to differences in surfactant or DNA interactions with the sidewall. Consequently, SWCNTs are unevenly distributed in the two phases, resulting in spontaneous separation of SWCNTs.[48,53] By tuning the surfactants or DNA, and using modulating agents to push SWCNTs between phases, ATP systems allow the simultaneous separation of many individual species in a single experiment.[55] This strategy is advantageous as it shows potential for large scale separation of SWCNTs due to its ease of processing.[48,53]

Additionally, the electrical properties also make SWCNTs promising building blocks for optoelectronic devices. It has been demonstrated that interfacing SWCNTs with inorganic nanoparticles can achieve highly sensitive optoelectronic devices, since the presence of SWCNTs greatly improves the charge mobility and facilitates the charge transfer at the heterointerface.[56]

In this contribution, we performed the separation of single chirality SWCNTs via ATP extraction and obtained two different species with high purity: (6,5) and (7,5) species. Dielectrophoresis (DEP), which allows for precise assembly of SWCNTs from solution onto the substrate using alternating current (AC) electrical field, was used to immobilise an individual (6,5) and (7,5) between prepatterned electrodes. Furthermore, since SWCNTs can be only immobilised between electrodes where AC voltage is applied, we extended the idea and immobilised individual (6,5), (7,5) and metallic species on the same chip, forming multiplexed single chirality SWCNT devices. We also synthesised CdS-SWCNT hybrids in solution using both mixed chirality and single

chirality SWCNTs. After immobilisation of these hybrids into device configuration, we investigated the photoinduced electrical response of these devices at different wavelengths.

## 6.2 Separation of single chirality carbon nanotubes

My colleagues, Zamaan Mukadam and Giuseppe Amoroso (respectively Msci and PhD student in the Palma group) , performed the separation of DNA-wrapped SWCNTs in several polymer aqueous two-phase (ATP) systems, following a previously published strategy (see section 2.2.5).[57] Briefly, SWCNT mixture wrapped with DNA sequence ($(CCG)_2CC$) was added to a polyethylene glycol/dextran (PEG/DX) ATP system. After vortex and centrifuge, (6,5) species was enriched in the DX-rich bottom phase. the DX-rich bottom phase and SWCNTs residing in it were collected as the starting materials for further purification. A blank PEG/DX was added to the bottom phase, forming a new ATP system. Poly(vinylpyrrolidone) (PVP) serving as a modulating agent was added to the ATP system to further facilitate the separation. After repeating the purification process, highly enriched (6,5) species was obtained. The absorption spectrum of the separated (6,5) species shows the $E_{11}$ transition at 1000 nm and the $E_{22}$ transition at 590 nm, demonstrating the high enrichment of (6,5) tubes (Figure 6.1a).[48] (7,5) species was separated and purified via a similar process (see section 2.2.5). Figure 6.1b shows the shows the absorption spectrum of the separated (7,5) species, in which the $E_{11}$ transition peaks at 1050 nm and the $E_{22}$ transition at 650 nm, demonstrating the high purity of the (7,5) species.[48]

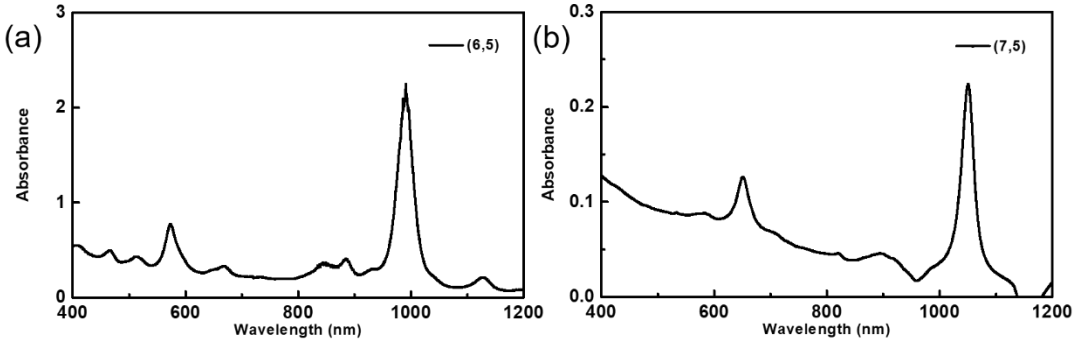


**Figure 6.1** Absorbance spectra of highly enriched (a) (6,5) and (b) (7,5) species

AFM was used to characterise the morphology of the separated (6,5) tubes (Figure 6.2). The average diameter of these SWCNTs was found to be 2.1 ± 0.3 nm, larger than the expected 0.76 nm diameter due to the presence of DNA.[58]

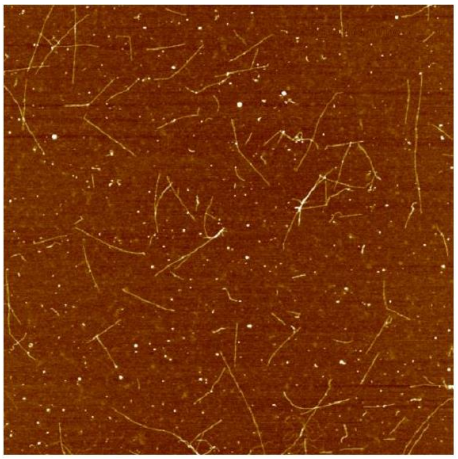

**Figure 6.2** Representative AFM image of the separated (6, 5) species

## 6.3 Fabrication of individual carbon nanotube devices

### 6.3.1 Immobilisation of individual SWCNT

To remove the polymers dissolved in aqueous solution for the separation of single chirality SWCNTs, the SWCNT solutions were centrifuged against a filter with a 100 KDa cut-off. Subsequently, dielectrophoresis (DEP) was performed to immobilise individual SWCNTs between electrodes. With optimised parameters of DEP, we were able to immobilise individual SWCNTs between electrodes. Additionally, as SWCNTs

can only be immobilised between electrodes where AC voltage is applied, we were able to immobilise individual SWCNTs of different chiralities on the same chip: in this case, we immobilised (6,5), (7,5) and metallic SWCNTs forming multiplexed single chirality devices (Figure 6.3).

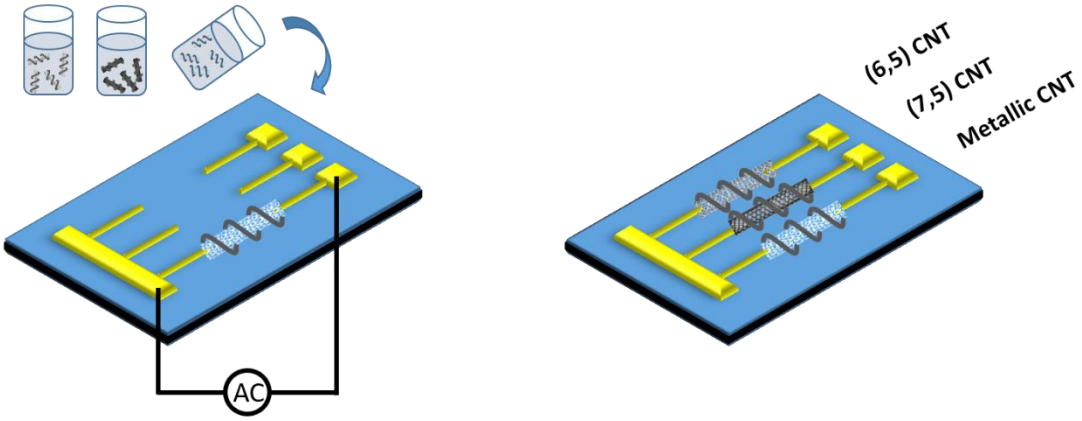


**Figure 6.3** Schematic of the fabrication of multiplexed single chirality devices

AFM was used to confirm the immobilisation of individual SWCNTs. Figure 6.4 shows representative AFM images of individual SWCNTs of different chiralities immobilised between electrodes on a single chip. The channel length of the devices is 300 nm. The diameter of the SWCNTs immobilised between electrodes is measured to be 2.5 ± 0.7 nm, in good agreement with the measured diameter of the separated SWCNTs (Figure 6.4).

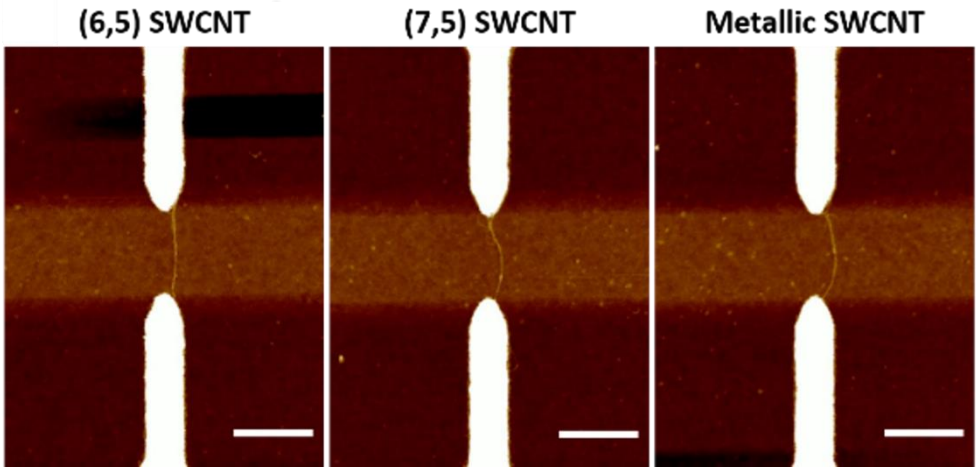


**Figure 6.4** Representative AFM images of individual single chirality SWCNTs immobilised between electrodes. Scale bar:100 nm

### 6.3.2 Electrical measurements

The conductance of these SWCNT devices cannot be measured directly after immobilisation, mainly due to the influence of DNA. Therefore, these devices were annealed at 200 $^{o}$C for 2h under nitrogen gas to minimize the presence of DNA between the SWCNTs and the metallic electrodes : annealing treatment is known to improve electrical contact between carbon nanotube and gold electrodes.[8,59]

Figure 6.5 shows I-V curves through these individual SWCNT devices in which various gate voltages were applied. The devices containing individual (6,5) and (7,5) show typically semiconducting behaviour since the current decreases as the gate voltage increases, suggesting the p-type nature of these devices (Figure 6.5a and 6.5b). The current-voltage characteristics of metallic SWCNT devices are shown in Figure 6.5c: gate voltage cannot induce changes in the current in these devices made from metallic SWCNTs.

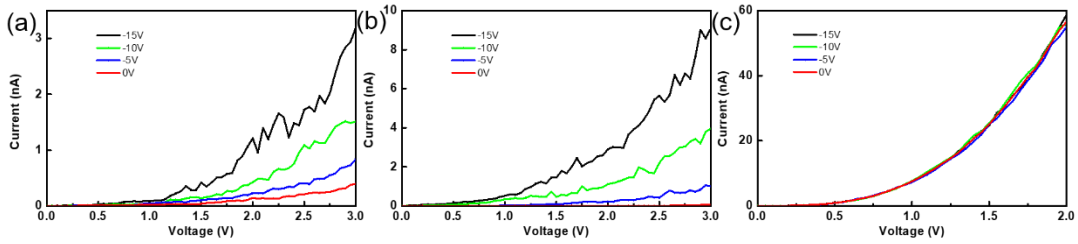


**Figure 6.5** Current-voltage characteristics of the (a) (6,5) (b) (7,5) and (c) metallic SWCNT devices at different values of gate voltage.

To further confirm the electrical properties of these devices, we measured the transfer characteristics of these devices (Figure 6.6). Figure 6.6a and 6.6b shows the transfer characteristics of (6,5) and (7,5) devices. These devices show typically p-type transport characteristics. The $I_{on}/I_{off}$ ratio of the devices is more than $10^3$, indicating good FET behaviour.[7,60]

Figure 6.6c shows the current through the devices made with metallic SWCNTs as a function of gate voltage. As expected, the current is independent on the gate voltage applied, demonstrating the metallic nature of these devices. However, the average contact resistance is on the order of magnitude of 10 MΩ, which is higher than the reported results.[7,8] This can be attributed to the remaining residues from the degraded DNA.

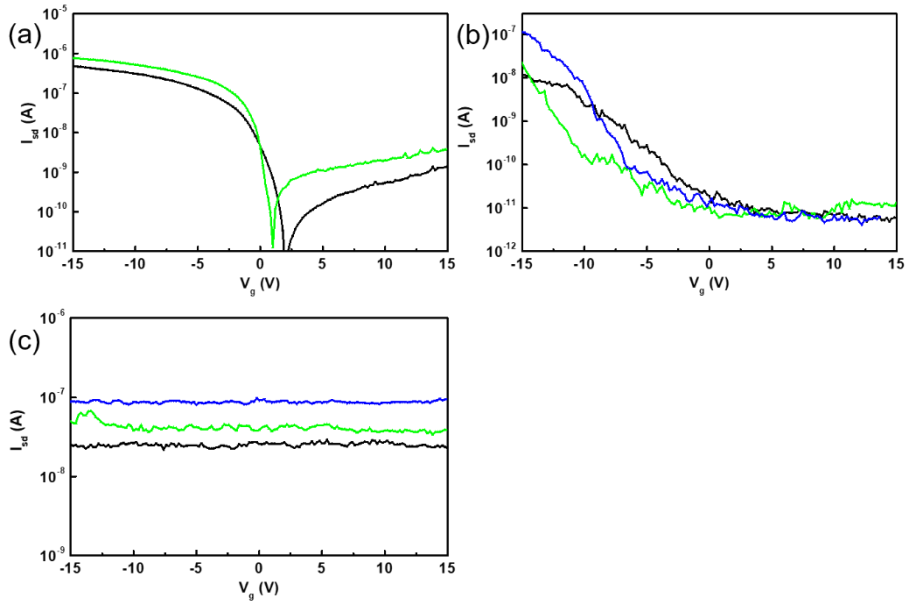


**Figure 6.6** Transfer characteristics of the (a) (6,5), (b) (7,5) and (c) metallic devices.

## 6.4 Fabrication of metal sulfide-SWCNT hybrids for photodetection

### 6.4.1 Mixed chirality SWCNT devices

My colleague, Qingyu Ye (PhD student in the Palma group) prepared metal sulfide-SWCNT hybrids. Briefly, mixed chirality SWCNTs wrapped with DNA sequences were incubated with $Cd(NO_3)_2$. Since DNA is negatively charged, $Cd^{2+}$ ions were adsorbed on the DNA. Subsequently, $Na_2S$ solution was added to the solution, resulting in the formation of nanoscale CdS particles around SWCNTs (see Figure 6.7).

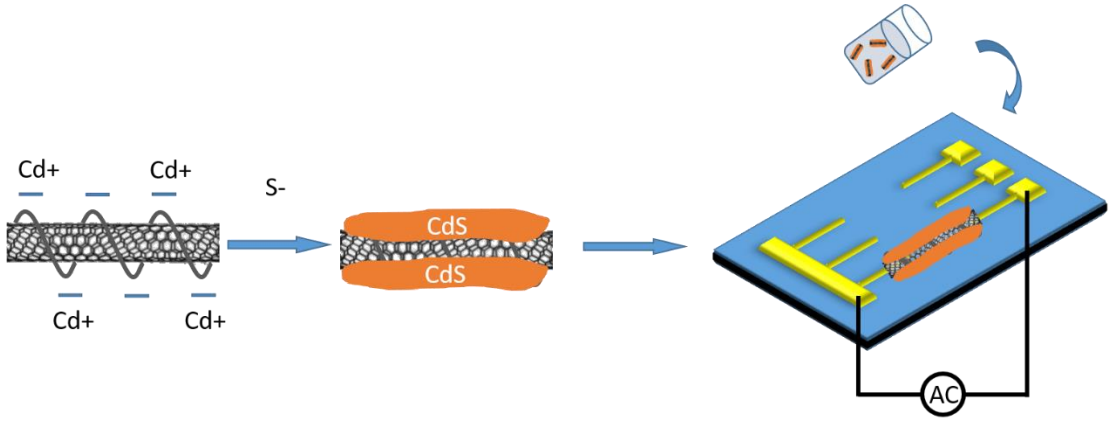

**Figure 6.7** Schematic of fabrication of CdS-SWCNT hybrids for photodetection.

Representative AFM images of CdS-SWCNT hybrids were shown in Figure 6.8a. Subsequently, These CdS-SWCNT hybrids were immobilised between electrodes via DEP, which is shown in Figure 6.8b.

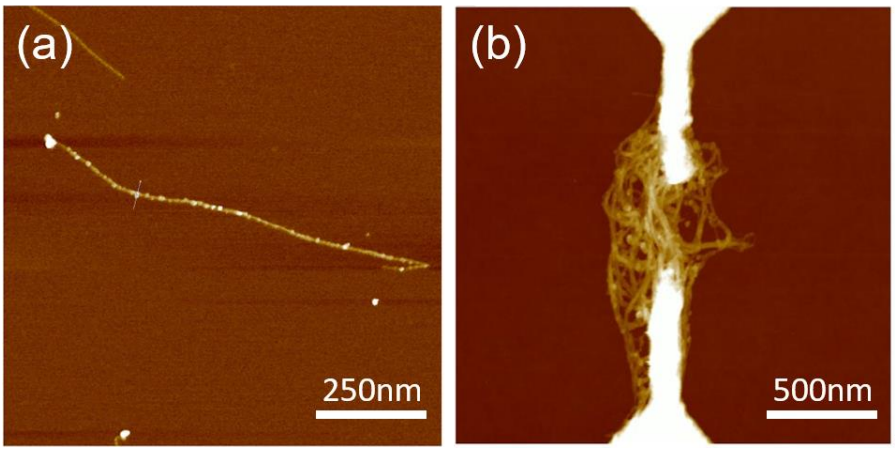


**Figure 6.8** AFM images of (a) Cd-SWCNT hybrids and (b) after immobilisation.

We investigated the photo response of the CdS-SWCNT devices. A constant voltage (1V) was applied to the source electrode while the drain electrode was grounded. Meanwhile, we shined lasers of different wavelength (red (650 nm), green (532 nm), blue (405 nm), 20 mW/cm$^2$) for 20 seconds on the device and recorded the current through it. As shown in Figure 6.9, the illumination of the red laser can barely induce change in the current while the green laser can induce a slight decrease in current. The current can recover to its initial state when the green laser is turned off. Shining the blue laser can induce a dramatic change in current and the device shows reversibility when the laser is turned on and off.

The results can be attributed to the excitation of CdS nanoparticles upon laser illumination. The energy of the red laser is not enough to activate CdS nanoparticles

considering the bandgap of CdS nanoparticles. The energy of the green laser and the blue laser can activate CdS nanoparticles, hence inducing photo response in the devices. Moreover, since the energy of the blue laser is larger than that of the green laser, the blue laser can activate more CdS nanoparticles, hence inducing larger photo response. Another possibility is that due to the diverse chiralities in the mixed SWCNTs, they show different response to the limited electron activated by the green laser, hence compromising the sensitivity.

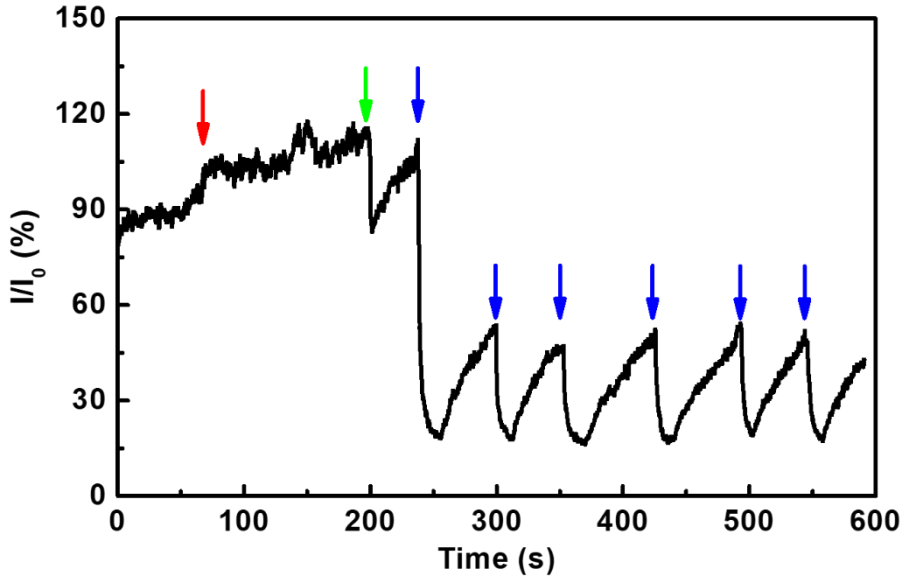


**Figure 6.9** Photo response of CdS-SWCNT devices to lasers of different wavelength (red (650 nm), green (532 nm), blue (405 nm)). The coloured arrows indicate the illumination of the lasers of corresponding colour.

Control experiments were performed using devices only containing bare SWCNTs and DNA wrapped SWCNTs. As shown in Figure 6.10a, all three lasers can barely induce any changes in current in the device containing bare SWCNT, demonstrating that SWCNTs are not sensitive to lasers. On the other hand, the device containing DNA wrapped SWCNTs showed no response to both the red and the green laser. Interestingly, the blue laser can induce a decrease in current. This can be attributed to the interaction between SWCNTs and DNA.[61] However, compared to CdS-SWCNT devices, the

response is smaller and the current takes more time to recover. Therefore, the control experiments demonstrate that the sensitivity of CdS-SWCNT devices comes from the interaction between CdS and SWCNTs.

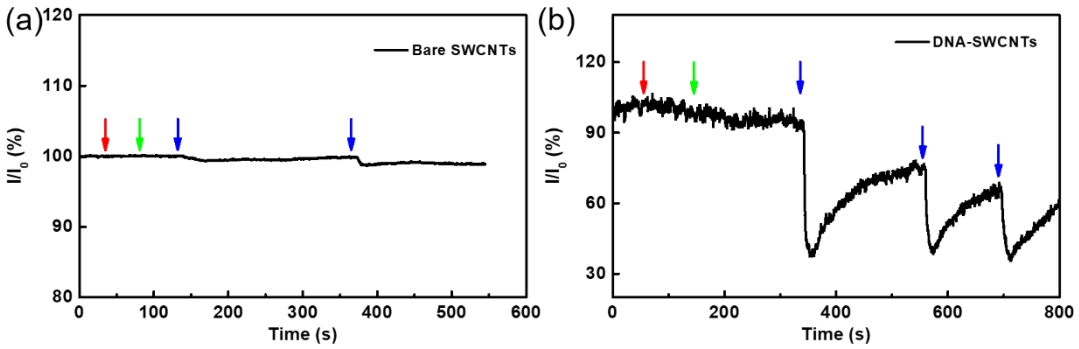


**Figure 6.10** Photo response of (a) bare SWCNT device (b) DNA wrapped SWCNT device to lasers of different wavelength (red (650 nm), green (532 nm), blue (405 nm)). The coloured arrows indicate the illumination of the lasers of corresponding colour.

To better understand the interaction between CdS nanoparticles and SWCNTs, we measured the transfer characteristics of CdS-SWCNT devices before and after the illumination of the blue laser. As shown in Figure 6.11a (black curve), the CdS-SWCNT device exhibits typical p-type behaviour, demonstrating that semiconducting SWCNTs are the main conductive paths. However, when the blue laser is turned on, although the device still shows p-type nature (Figure 6.11a, blue curve), the current through the device decreases dramatically. This suggests that there is electron transfer from CdS nanoparticles to SWCNTs, given the p-type nature of semiconducting SWCNTs. This is in line with the energy band structure of SWCNTs and CdS (Figure 6.11b). Electron transfer from CdS nanoparticles to SWCNTs under illumination leads to electron-hole recombination with the tubes. This causes reduction of carrier density, hence resulting in a decrease in currents.

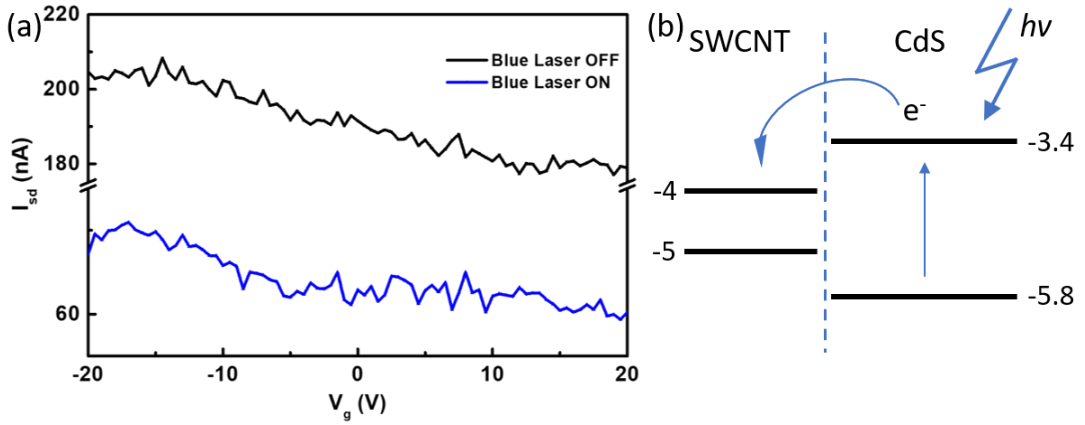


**Figure 6.11** (a) Transfer characteristics of CdS-SWCNT devices with the illumination of the blue laser on and off and (b) the energy band structure of SWCNTs and CdS. $e^-$ represents electron and *hv* is the energy of absorbed photon.

### 6.4.2 Single chirality SWCNT devices

Similarly, single chirality (6,5) tubes were applied to synthesize CdS-(6,5) hybrids by Qingyu. The CdS-(6,5) hybrids were then immobilised between electrodes. Figure 6.12 shows the photo response of CdS-(6,5) devices. The device is not sensitive to the red laser, in line with the previous observation in CdS-SWCNT devices. However, the current decreases dramatically when the green laser is turned on, which is different from the observation in CdS-SWCNT devices. This can be attributed to the uniform electronic structure of single chirality SWCNTs, suggesting the higher sensitivity of CdS-(6,5) devices. The CdS-(6,5) device is also sensitive to the blue laser, which is line in with the observation in CdS-SWCNT devices.

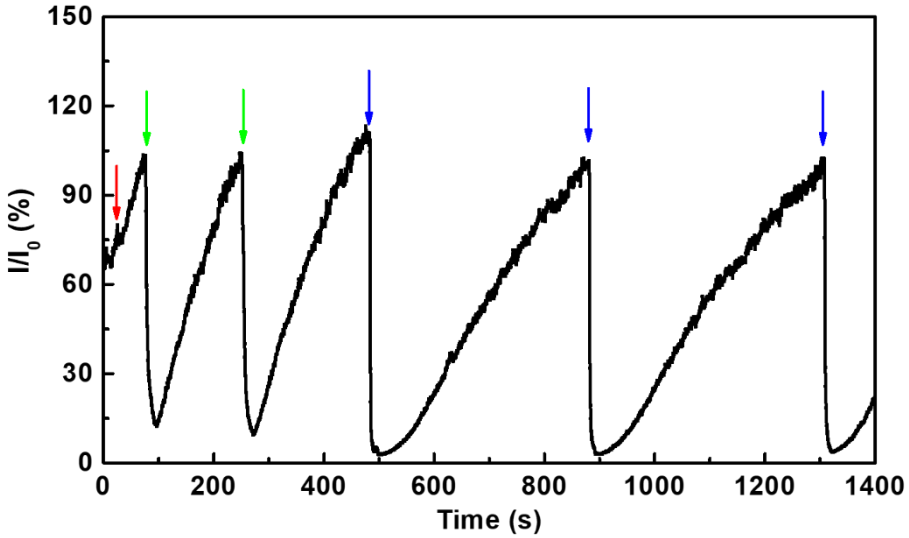


**Figure 6.12** Photo response of CdS-(6,5) devices to lasers of different wavelength (red (650 nm), green (532 nm), blue (405 nm)). The coloured arrows indicate the illumination of the lasers of corresponding colour.

Figure 6.13 shows the transfer characteristics of CdS-(6,5) devices before and after illumination of lasers of different wavelength. In all cases, the device shows typical p-type FET behaviour, suggesting that (6,5) tubes are the main conductive paths. As expected, shining the red laser cannot induce any changes in the device, while illumination of the green and the blue laser induce deceases in current. According to the energy band structure of SWCNTs and CdS nanoparticles (Figure 6.11b), laser illumination leads to electron excitation in CdS nanoparticles. Subsequently, these electrons transfer from CdS into (6,5) tubes, resulting in electron-hole recombination within (6,5) tubes. Given the p-type nature of (6,5) tubes, this recombination causes a reduction of carrier density and hence a decrease of the current (Figure 6.13).

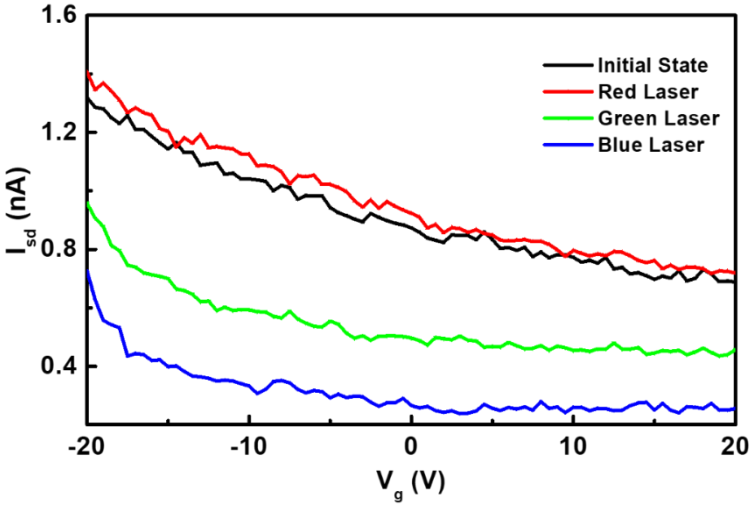


**Figure 6.13** Transfer characteristics of CdS-(6,5) devices before and after illumination of lasers of different wavelength (red (650 nm), green (532 nm), blue (405 nm)).

## 6.5 Conclusions

We demonstrated the separation of single chirality SWCNTs via ATP extraction and obtained two different species with high purity: (6,5) and (7,5) species. Since SWCNTs can be precisely positioned from solution on to substrate where AC voltage is applied, we immobilised individual (6,5), (7,5) and metallic tubes on the same chip, forming multiplexed single chirality SWCNT devices. Electrical measurement shows the (6,5) and (7,5) devices exhibit good FET behaviour while metallic tube devices show metallic behaviour. We also synthesised CdS-SWCNT hybrids in solution using both mixed chirality and single chirality SWCNT. After immobilisation of these hybrids into device configuration, we investigated the photoinduced electrical response of these devices at different wavelengths. The results suggest that CdS-(6,5) devices show higher sensitivity compared to mixed chirality devices. Our future work will focus on the separation of single chirality SWCNTs and investigation of the photo response of CdS-SWCNT devices with different chiralities.

References

(1) Yang, N.; Chen, X.; Ren, T.; Zhang, P.; Yang, D. Carbon Nanotube Based Biosensors. *Sensors Actuators, B Chem.* **2015**, *207* (PartA), 690–715. https://doi.org/10.1016/j.snb.2014.10.040.

(2) Kim, S. N.; Rusling, J. F.; Papadimitrakopoulos, F. Carbon Nanotubes for Electronic and Electrochemical Detection of Biomolecules. *Adv. Mater.* **2007**, *19* (20), 3214–3228. https://doi.org/10.1002/adma.200700665.

(3) Guo, X. Single-Molecule Electrical Biosensors Based on Single-Walled Carbon Nanotubes. *Adv. Mater.* **2013**, *25* (25), 3397–3408. https://doi.org/10.1002/adma.201301219.

(4) Otsuka, K.; Inoue, T.; Maeda, E.; Kometani, R.; Chiashi, S.; Maruyama, S. On-Chip Sorting of Long Semiconducting Carbon Nanotubes for Multiple Transistors along an Identical Array. *ACS Nano* **2017**, *11* (11), 11497–11504. https://doi.org/10.1021/acsnano.7b06282.

(5) Magnin, Y.; Amara, H.; Ducastelle, F.; Loiseau, A.; Bichara, C. Entropy-Driven Stability of Chiral Single-Walled Carbon Nanotubes. *Science (80-. ).* **2018**, *362* (6411), 212–215. https://doi.org/10.1126/science.aat6228.

(6) Jeon, I.; Matsuo, Y.; Maruyama, S. Single-Walled Carbon Nanotubes in Solar Cells. *Top. Curr. Chem.* **2018**, *376* (1), 1–28. https://doi.org/10.1007/s41061-017-0181-0.

(7) Stokes, P.; Khondaker, S. I. Directed Assembly of Solution Processed Single-Walled Carbon Nanotubes via Dielectrophoresis: From Aligned Array to Individual Nanotube Devices. *J. Vac. Sci. Technol. B Microelectron. Nanom. Struct.* **2010**, *28* (6), C6B7. https://doi.org/10.1116/1.3501347.

(8) Vijayaraghavan, A.; Oron-Carl, M.; Blatt, S.; Vijayaraghavan, A.; Blatt, S.;

Weissenberger, D.; Weissenberger, D.; Oron-Carl, M.; Hennrich, F.; Hennrich, F.; Gerthsen, D.; Hahn, H.; Gerthsen, D.; Hahn, H.; Krupke, R.; Krupke, R. Ultra-Large-Scale Directed Assembly of Single-Walled Carbon Nanotube Devices. Supporting Information. *Nano Lett.* **2007**, *7* (6), 1556–1560. https://doi.org/10.1021/nl0703727.

(9) Stokes, P.; Silbar, E.; Zayas, Y. M.; Khondaker, S. I. Solution Processed Large Area Field Effect Transistors from Dielectrophoreticly Aligned Arrays of Carbon Nanotubes. *Appl. Phys. Lett.* **2009**, *94* (11). https://doi.org/10.1063/1.3100197.

(10) Tans, S. J.; Verschueren, A. R. M.; Dekker, C. Gate Voltage (V):-3 300 K +1 +2 +4 +6 I (NA) 0. **6AD**, *672* (1989), 669–672.

(11) Franklin, A. D. 498443a. **2020**, 0–1.

(12) Zhang, S.; Kang, L.; Wang, X.; Tong, L.; Yang, L.; Wang, Z.; Qi, K.; Deng, S.; Li, Q.; Bai, X.; Ding, F.; Zhang, J. Arrays of Horizontal Carbon Nanotubes of Controlled Chirality Grown Using Designed Catalysts. *Nature* **2017**, *543* (7644), 234–238. https://doi.org/10.1038/nature21051.

(13) Kang, L.; Hu, Y.; Zhong, H.; Si, J.; Zhang, S.; Zhao, Q.; Lin, J.; Li, Q.; Zhang, Z.; Peng, L.; Zhang, J. Large-Area Growth of Ultra-High-Density Single-Walled Carbon Nanotube Arrays on Sapphire Surface. *Nano Res.* **2015**, *8* (11), 3694–3703. https://doi.org/10.1007/s12274-015-0869-9.

(14) Si, J.; Zhong, D.; Xu, H.; Xiao, M.; Yu, C.; Zhang, Z.; Peng, L. M. Scalable Preparation of High-Density Semiconducting Carbon Nanotube Arrays for High-Performance Field-Effect Transistors. *ACS Nano* **2018**, *12* (1), 627–634. https://doi.org/10.1021/acsnano.7b07665.

(15) Rao, R.; Pint, C. L.; Islam, A. E.; Weatherup, R. S.; Hofmann, S.; Meshot, E. R.;

Wu, F.; Zhou, C.; Dee, N.; Amama, P. B.; Carpena-Nuñez, J.; Shi, W.; Plata, D. L.; Penev, E. S.; Yakobson, B. I.; Balbuena, P. B.; Bichara, C.; Futaba, D. N.; Noda, S.; Shin, H.; Kim, K. S.; Simard, B.; Mirri, F.; Pasquali, M.; Fornasiero, F.; Kauppinen, E. I.; Arnold, M.; Cola, B. A.; Nikolaev, P.; Arepalli, S.; Cheng, H. M.; Zakharov, D. N.; Stach, E. A.; Zhang, J.; Wei, F.; Terrones, M.; Geohegan, D. B.; Maruyama, B.; Maruyama, S.; Li, Y.; Adams, W. W.; Hart, A. J. Carbon Nanotubes and Related Nanomaterials: Critical Advances and Challenges for Synthesis toward Mainstream Commercial Applications. *ACS Nano* **2018**, *12* (12), 11756–11784. https://doi.org/10.1021/acsnano.8b06511.

(16) Scarselli, M.; Castrucci, P.; De Crescenzi, M. Electronic and Optoelectronic Nano-Devices Based on Carbon Nanotubes. *J. Phys. Condens. Matter* **2012**, *24* (31). https://doi.org/10.1088/0953-8984/24/31/313202.

(17) Hagen, A.; Hertel, T. Quantitative Analysis of Optical Spectra from Individual Single-Wall Carbon Nanotubes. *Nano Lett.* **2003**, *3* (3), 383–388. https://doi.org/10.1021/nl020237o.

(18) Yang, F.; Wang, X.; Zhang, D.; Yang, J.; Luo, D.; Xu, Z.; Wei, J.; Wang, J. Q.; Xu, Z.; Peng, F.; Li, X.; Li, R.; Li, Y.; Li, M.; Bai, X.; Ding, F.; Li, Y. Chirality-Specific Growth of Single-Walled Carbon Nanotubes on Solid Alloy Catalysts. *Nature* **2014**, *510* (7506), 522–524. https://doi.org/10.1038/nature13434.

(19) Artyukhov, V. I.; Penev, E. S.; Yakobson, B. I. Why Nanotubes Grow Chiral. *Nat. Commun.* **2014**, *5* (May). https://doi.org/10.1038/ncomms5892.

(20) Zhu, Z.; Wei, N.; Cheng, W.; Shen, B.; Sun, S.; Gao, J.; Wen, Q.; Zhang, R.; Xu, J.; Wang, Y.; Wei, F. Rate-Selected Growth of Ultrapure Semiconducting Carbon Nanotube Arrays. *Nat. Commun.* **2019**, *10* (1), 1–8. https://doi.org/10.1038/s41467-019-12519-5.

(21) Kruss, S.; Hilmer, A. J.; Zhang, J.; Reuel, N. F.; Mu, B.; Strano, M. S. Carbon Nanotubes as Optical Biomedical Sensors. *Adv. Drug Deliv. Rev.* **2013**, *65* (15), 1933–1950. https://doi.org/10.1016/j.addr.2013.07.015.

(22) Yang, F.; Wang, M.; Zhang, D.; Yang, J.; Zheng, M.; Li, Y. Chirality Pure Carbon Nanotubes: Growth, Sorting, and Characterization. *Chem. Rev.* **2020**, *120* (5), 2693–2758. https://doi.org/10.1021/acs.chemrev.9b00835.

(23) Gaviria Rojas, W. A.; Hersam, M. C. Chirality-Enriched Carbon Nanotubes for Next-Generation Computing. *Adv. Mater.* **2020**, *32* (41), 1–28. https://doi.org/10.1002/adma.201905654.

(24) Chiang, W. H.; Sankaran, R. M. Linking Catalyst Composition to Chirality Distributions of As-Grown Single-Walled Carbon Nanotubes by Tuning Ni x Fe 1x Nanoparticles. *Nat. Mater.* **2009**, *8* (11), 882–886. https://doi.org/10.1038/nmat2531.

(25) Sanchez-Valencia, J. R.; Dienel, T.; Gröning, O.; Shorubalko, I.; Mueller, A.; Jansen, M.; Amsharov, K.; Ruffieux, P.; Fasel, R. Controlled Synthesis of Single-Chirality Carbon Nanotubes. *Nature* **2014**, *512* (1), 61–64. https://doi.org/10.1038/nature13607.

(26) Che, Y.; Wang, C.; Liu, J.; Liu, B.; Lin, X.; Parker, J.; Beasley, C.; Wong, H. S. P.; Zhou, C. Selective Synthesis and Device Applications of Semiconducting Single-Walled Carbon Nanotubes Using Isopropyl Alcohol as Feedstock. *ACS Nano* **2012**, *6* (8), 7454–7462. https://doi.org/10.1021/nn302720n.

(27) Zhang, F.; Hou, P. X.; Liu, C.; Wang, B. W.; Jiang, H.; Chen, M. L.; Sun, D. M.; Li, J. C.; Cong, H. T.; Kauppinen, E. I.; Cheng, H. M. Growth of Semiconducting Single-Wall Carbon Nanotubes with a Narrow Band-Gap Distribution. *Nat. Commun.* **2016**, *7*. https://doi.org/10.1038/ncomms11160.

(28) Hu, Y.; Kang, L.; Zhao, Q.; Zhong, H.; Zhang, S.; Yang, L.; Wang, Z.; Lin, J.; Li, Q.; Zhang, Z.; Peng, L.; Liu, Z.; Zhang, J. Growth of High-Density Horizontally Aligned SWNT Arrays Using Trojan Catalysts. *Nat. Commun.* **2015**, *6*, 1–6. https://doi.org/10.1038/ncomms7099.

(29) Tomada, J.; Dienel, T.; Hampel, F.; Fasel, R.; Amsharov, K. Combinatorial Design of Molecular Seeds for Chirality-Controlled Synthesis of Single-Walled Carbon Nanotubes. *Nat. Commun.* **2019**, *10* (1), 1–10. https://doi.org/10.1038/s41467-019-11192-y.

(30) Hussain, A.; Ding, E. X.; McLean, B.; Mustonen, K.; Ahmad, S.; Tavakkoli, M.; Page, A. J.; Zhang, Q.; Kotakoski, J.; Kauppinen, E. I. Scalable Growth of Single-Walled Carbon Nanotubes with a Highly Uniform Structure. *Nanoscale* **2020**, *12* (23), 12263–12267. https://doi.org/10.1039/d0nr01919d.

(31) Maruyama, S.; Kojima, R.; Miyauchi, Y.; Chiashi, S.; Kohno, M. Low-Temperature Synthesis of High-Purity Single-Walled Carbon Nanotubes from Alcohol. *Chem. Phys. Lett.* **2002**, *360* (3–4), 229–234. https://doi.org/10.1016/S0009-2614(02)00838-2.

(32) An, H.; Kumamoto, A.; Takezaki, H.; Ohyama, S.; Qian, Y.; Inoue, T.; Ikuhara, Y.; Chiashi, S.; Xiang, R.; Maruyama, S. Chirality Specific and Spatially Uniform Synthesis of Single-Walled Carbon Nanotubes from a Sputtered Co-W Bimetallic Catalyst. *Nanoscale* **2016**, *8* (30), 14523–14529. https://doi.org/10.1039/c6nr02749k.

(33) Liu, H.; Nishide, D.; Tanaka, T.; Kataura, H. Large-Scale Single-Chirality Separation of Single-Wall Carbon Nanotubes by Simple Gel Chromatography. *Nat. Commun.* **2011**, *2* (1). https://doi.org/10.1038/ncomms1313.

(34) Zheng, M.; Semke, E. D. Enrichment of Single Chirality Carbon Nanotubes. *J.*

*Am. Chem. Soc.* **2007**, *129* (19), 6084–6085. https://doi.org/10.1021/ja071577k.

(35) Green, A. A.; Hersam, M. C. Nearly Single-Chirality Single-Walled Carbon Nanotubes Produced via Orthogonal Iterative Density Gradient Ultracentrifugation. *Adv. Mater.* **2011**, *23* (19), 2185–2190. https://doi.org/10.1002/adma.201100034.

(36) Krupke, R.; Hennrich, F.; Löhneysen, H. v.; Kappes, M. M. Separation of Metallic from Semiconducting Single-Walled Carbon Nanotubes. *Science (80-. ).* **2003**, *301* (5631), 344–347. https://doi.org/10.1126/science.1086534.

(37) Zheng, M.; Jagota, A.; Semke, E. D.; Diner, B. A.; McLean, R. S.; Lustig, S. R.; Richardson, R. E.; Tassi, N. G. DNA-Assisted Dispersion and Separation of Carbon Nanotubes. *Nat. Mater.* **2003**, *2* (5), 338–342. https://doi.org/10.1038/nmat877.

(38) Ju, S. Y.; Doll, J.; Sharma, I.; Papadimitrakopoulos, F. Selection of Carbon Nanotubes with Specific Chiralities Using Helical Assemblies of Flavin Mononucleotide. *Nat. Nanotechnol.* **2008**, *3* (6), 356–362. https://doi.org/10.1038/nnano.2008.148.

(39) Kharlamova, M. V.; Kramberger, C.; Saito, T.; Sato, Y.; Suenaga, K.; Pichler, T.; Shiozawa, H. Chirality-Dependent Growth of Single-Wall Carbon Nanotubes as Revealed inside Nano-Test Tubes. *Nanoscale* **2017**, *9* (23), 7998–8006. https://doi.org/10.1039/c7nr01846k.

(40) Tulevski, G. S.; Franklin, A. D.; Afzali, A. High Purity Isolation and Quantification of Semiconducting Carbon Nanotubes via Column Chromatography. *ACS Nano* **2013**, *7* (4), 2971–2976. https://doi.org/10.1021/nn400053k.

(41) Flavel, B. S.; Kappes, M. M.; Krupke, R.; Hennrich, F. Separation of Single-

Walled Carbon Nanotubes by 1-Dodecanol-Mediated Size-Exclusion Chromatography. *ACS Nano* **2013**, *7* (4), 3557–3564. https://doi.org/10.1021/nn4004956.

(42) Flavel, B. S.; Moore, K. E.; Pfohl, M.; Kappes, M. M.; Hennrich, F. Separation of Single-Walled Carbon Nanotubes with a Gel Permeation Chromatography System. *ACS Nano* **2014**, *8* (2), 1817–1826. https://doi.org/10.1021/nn4062116.

(43) Arnold, M. S.; Green, A. A.; Hulvat, J. F.; Stupp, S. I.; Hersam, M. C. Sorting Carbon Nanotubes by Electronic Structure Using Density Differentiation. *Nat. Nanotechnol.* **2006**, *1* (1), 60–65. https://doi.org/10.1038/nnano.2006.52.

(44) Arnold, M. S.; Stupp, S. I.; Hersam, M. C. Enrichment of Single-Walled Carbon Nanotubes by Diameter in Density Gradients. *Nano Lett.* **2005**, *5* (4), 713–718. https://doi.org/10.1021/nl050133o.

(45) Tu, X.; Manohar, S.; Jagota, A.; Zheng, M. DNA Sequence Motifs for Structure-Specific Recognition and Separation of Carbon Nanotubes. *Nature* **2009**, *460* (7252), 250–253. https://doi.org/10.1038/nature08116.

(46) Zheng, M.; Jagota, A.; Strano, M. S.; Santos, A. P.; Barone, P.; Chou, S. G.; Diner, B. A.; Dresselhaus, M. S.; McLean, R. S.; Onoa, G. B.; Samsonidze, G. G.; Semke, E. D.; Usrey, M.; Watts, D. J. Structure-Based Carbon Nanotube Sorting by Sequence-Dependent DNA Assembly. *Science (80-. ).* **2003**, *302* (5650), 1545–1548. https://doi.org/10.1126/science.1091911.

(47) Brady, G. J.; Joo, Y.; Wu, M. Y.; Shea, M. J.; Gopalan, P.; Arnold, M. S. Polyfluorene-Sorted, Carbon Nanotube Array Field-Effect Transistors with Increased Current Density and High on/off Ratio. *ACS Nano* **2014**, *8* (11), 11614–11621. https://doi.org/10.1021/nn5048734.

(48) Ao, G.; Khripin, C. Y.; Zheng, M. DNA-Controlled Partition of Carbon

Nanotubes in Polymer Aqueous Two-Phase Systems. *J. Am. Chem. Soc.* **2014**, *136* (29), 10383–10392. https://doi.org/10.1021/ja504078b.

(49) Ding, J.; Li, Z.; Lefebvre, J.; Cheng, F.; Dubey, G.; Zou, S.; Finnie, P.; Hrdina, A.; Scoles, L.; Lopinski, G. P.; Kingston, C. T.; Simard, B.; Malenfant, P. R. L. Enrichment of Large-Diameter Semiconducting SWCNTs by Polyfluorene Extraction for High Network Density Thin Film Transistors. *Nanoscale* **2014**, *6* (4), 2328–2339. https://doi.org/10.1039/c3nr05511f.

(50) Khripin, C. Y.; Fagan, J. A.; Zheng, M. Spontaneous Partition of Carbon Nanotubes in Polymer-Modified Aqueous Phases. *J. Am. Chem. Soc.* **2013**, *135* (18), 6822–6825. https://doi.org/10.1021/ja402762e.

(51) Li, H.; Gordeev, G.; Garrity, O.; Peyyety, N. A.; Selvasundaram, P. B.; Dehm, S.; Krupke, R.; Cambré, S.; Wenseleers, W.; Reich, S.; Zheng, M.; Fagan, J. A.; Flavel, B. S. Separation of Specific Single-Enantiomer Single-Wall Carbon Nanotubes in the Large-Diameter Regime. *ACS Nano* **2020**, *14* (1), 948–963. https://doi.org/10.1021/acsnano.9b08244.

(52) Wei, L.; Flavel, B. S.; Li, W.; Krupke, R.; Chen, Y. Exploring the Upper Limit of Single-Walled Carbon Nanotube Purity by Multiple-Cycle Aqueous Two-Phase Separation. *Nanoscale* **2017**, *9* (32), 11640–11646. https://doi.org/10.1039/c7nr03302h.

(53) Lyu, M.; Meany, B.; Yang, J.; Li, Y.; Zheng, M. Toward Complete Resolution of DNA/Carbon Nanotube Hybrids by Aqueous Two-Phase Systems. *J. Am. Chem. Soc.* **2019**, *141* (51), 20177–20186. https://doi.org/10.1021/jacs.9b09953.

(54) Li, H.; Gordeev, G.; Garrity, O.; Reich, S.; Flavel, B. S. Separation of Small-Diameter Single-Walled Carbon Nanotubes in One to Three Steps with Aqueous Two-Phase Extraction. *ACS Nano* **2019**, *13* (2), 2567–2578.

https://doi.org/10.1021/acsnano.8b09579.

(55) Fagan, J. A.; Khripin, C. Y.; Silvera Batista, C. A.; Simpson, J. R.; Hároz, E. H.; Hight Walker, A. R.; Zheng, M. Isolation of Specific Small-Diameter Single-Wall Carbon Nanotube Species via Aqueous Two-Phase Extraction. *Adv. Mater.* **2014**, *26* (18), 2800–2804. https://doi.org/10.1002/adma.201304873.

(56) Li, X.; Jia, Y.; Cao, A. Tailored Single-Walled Carbon Nanotube-CdS Nanoparticle Hybrids for Tunable Optoelectronic Devices. *ACS Nano* **2010**, *4* (1), 506–512. https://doi.org/10.1021/nn901757s.

(57) Streit, J. K.; Fagan, J. A.; Zheng, M. A Low Energy Route to DNA-Wrapped Carbon Nanotubes via Replacement of Bile Salt Surfactants. *Anal. Chem.* **2017**, *89* (19), 10496–10503. https://doi.org/10.1021/acs.analchem.7b02637.

(58) Zheng, M.; Jagota, A.; Semke, E. D.; Diner, B. A.; McLean, R. S.; Lustig, S. R.; Richardson, R. E.; Tassi, N. G. DNA-Assisted Dispersion and Separation of Carbon Nanotubes. *Nat. Mater.* **2003**, *2* (5), 338–342. https://doi.org/10.1038/nmat877 M4 - Citavi.

(59) Penzo, E.; Palma, M.; Chenet, D. A.; Ao, G.; Zheng, M.; Hone, J. C.; Wind, S. J. Directed Assembly of Single Wall Carbon Nanotube Field Effect Transistors. *ACS Nano* **2016**, *10* (2), 2975–2981. https://doi.org/10.1021/acsnano.6b00353.

(60) Zhang, L.; Tu, X.; Welsher, K.; Wang, X.; Zheng, M.; Dai, H. Optical Characterizations and Electronic Devices of Nearly Pure (10,5) Single-Walled Carbon Nanotubes. *J. Am. Chem. Soc.* **2009**, *131* (7), 2454–2455. https://doi.org/10.1021/ja8096674.

(61) Strano, M. S.; Zheng, M.; Jagota, A.; Onoa, G. B.; Heller, D. A.; Barone, P. W.; Usrey, M. L. Understanding the Nature of the DNA-Assisted Separation of Single-Walled Carbon Nanotubes Using Fluorescence and Raman Spectroscopy.

*Nano Lett.* **2004**, *4* (4), 543–550. https://doi.org/10.1021/nl034937k.

# Chapter 7 Conclusions and Outlook

Nanomaterials have been promising building blocks for the next generation electronics due to the need for high performance electronics and the trend towards miniaturized devices. Various nanomaterials with different sizes, shapes and compositions have been introduced into electrical circuits to fabricate functional devices. Due to their excellent properties, nanomaterials have shown potential applications in a variety of fields, including field effect transistors, biosensing electronics and optoelectronics. While promising, it is still challenging to fabricate devices with low-cost processability and multipurpose capability.

In this work, we have focused on the fabrication and characterisation of functional devices. In particular, we controlled the interfacing of SWCNTs with either biomolecules, like DNA and proteins, or metal precursors, or semiconductors. These SWCNT hybrids were then assembled from solution onto prepatterned electrodes, into field effect transistor configurations. Atomic force microscopy has been applied to investigate the morphology of these devices. We demonstrated the potential applications of these nanoscale devices in various fields, such as biosensing and photodetection.

Distinct hybrids of SWCNTs and aptamers were synthesized in aqueous solution and were subsequently assembled from solution into nanoscale device configurations on the same chip, in which the nanotubes could act as the transducer elements, and the aptamers as the recognition components, of an electrical biosensing platform. These devices allowed the real-time and simultaneous detection of multiple analytes on the

same chip. As proof of concept, we demonstrated the selective recognition of different biomarkers indicative of stress and neuro-trauma conditions, at various physiologically relevant concentrations, from pM to μM. The results showed that these devices exhibited high selectivity and sensitivity, as well as multiplexing ability due to the immobilization of CNT-aptamer hybrids with distinct biorecognition elements on the same nanoscale chip via a DEP-based strategy. Additionally, the devices are reconfigurable and reusable via a simple cleaning procedure.

Similarly, biosensors based on SWCNT FETs were fabricated to investigate the influence of a protein's electrostatic surface features in the electrical sensing of a β-lactamase enzyme. BILP2 variants were attached to SWCNTs in defined orientations since the bioorthogonal reaction handles were engineered at specific residues in BLIP2 variants. Using these devices functionalised with different BILP2 variants, we performed electrical detection of β-lactamase TEM. The results showed that the responses of these devices were dependent on the BLIP2 variants, and hence orientation. Presentation of different TEM electrostatic surfaces within the Debye length led either to increase or decrease in conductance. This allowed biosensing through electrostatic surface profiling of distinct protein-protein interactions.

Another achievement of this work is the direct synthesis of multiple metal nanowires on the same chip. Different $M(acac)_2$@SWCNT were immobilized from solution into nanoscale device configurations on the same chip, where the SWCNTs were used as vector templates. Metal nanowires were grown in the cavity of the nanotubes after annealing treatment, and were exposed to oxygen plasma to remove the nanotube shell. Distinct Cu, Pt and PtCu nanowires were successfully synthesized between different electrode pairs on the same chip as indicated by the electrical measurement: no gate dependence was observed upon removal of the SWCNT shell. This strategy represents

a viable route to the large-scale fabrication and detailed exploration of materials properties in controlled 1D architectures.

Additionally, we separated single chirality SWCNT species from the SWCNT mixture and demonstrated the fabrication of multiplexed single chirality SWCNT devices. This allowed us to investigate the electrical properties of the SWCNTs with defined chirality. Subsequently, SWCNT-CdS hybrids were synthesized using both mixed chirality and single chirality SWCNTs and were immobilised between electrodes to fabricate photodetectors. Real time detection showed that both mixed chirality devices and single chirality devices exhibited high sensitivity to blue laser, but single chirality devices were more sensitive to green laser.

While in this thesis we have presented the fabrication and characterisation of a variety of functional nanoscale devices, there are still many challenges inhibiting the practical applications of these devices. i) Although functional devices can be easily fabricated via the techniques developed in this thesis, variation in these devices still exist. This will influence the accuracy of the experimental results. It is of importance to develop strategies for the fabrication of devices with high reproducibility. ii) The SWCNTs used in the thesis are mixed chirality, which may compromise the sensitivity and selectivity of the devices. The diversity of SWCNT chiralities may also cause high signal to noise ratio in the electrical measurement. Therefore, future work will focus on the separation of single chirality SWCNTs, and application of these single chirality SWCNTs. iii) For some reasons, most devices in thesis cannot last too long. How to increase the stability of these devices is another important research topic.

Despite these challenges, this work provides promising strategies for the fabrication of devices with multipurpose capability, easy processing and low-cost fabrication. This will help to develop next generation electronics.